216
3-16
C

2077

MASTER

DNA-1892-3
Rev. 1
(formerly DASA-1892-3)

Weapons Radiation Shielding Handbook

Chapter 3 / Methods for Calculating Neutron and Gamma-Ray Attenuation

by Paul N. Stevens and David K. Trubey

Handbook Editors

Lorraine S. Abbott, H. Clyde Claiborne, and Charles E. Clifford

APPROVED FOR PUBLIC RELEASE;
DISTRIBUTION UNLIMITED.

THIS DOCUMENT CONFIRMED AS
UNCLASSIFIED
DIVISION OF CLASSIFICATION
BY J H Kahn/amb
DATE 3/22/72

DEFENSE NUCLEAR AGENCY

Washington, D. C. 20305

DISTRIBUTION OF THIS DOCUMENT IS UNLIMITED

R3564

DISCLAIMER

This report was prepared as an account of work sponsored by an agency of the United States Government. Neither the United States Government nor any agency Thereof, nor any of their employees, makes any warranty, express or implied, or assumes any legal liability or responsibility for the accuracy, completeness, or usefulness of any information, apparatus, product, or process disclosed, or represents that its use would not infringe privately owned rights. Reference herein to any specific commercial product, process, or service by trade name, trademark, manufacturer, or otherwise does not necessarily constitute or imply its endorsement, recommendation, or favoring by the United States Government or any agency thereof. The views and opinions of authors expressed herein do not necessarily state or reflect those of the United States Government or any agency thereof.

DISCLAIMER

Portions of this document may be illegible in electronic image products. Images are produced from the best available original document.

Printed in the United States of America. Available from
National Technical Information Service
U.S. Department of Commerce
5285 Port Royal Road, Springfield, Virginia 22151
Price: Printed Copy $3.00; Microfiche $0.95

This report was prepared as an account of work sponsored by the United States Government. Neither the United States nor the United States Atomic Energy Commission, nor any of their employees, nor any of their contractors, subcontractors, or their employees, makes any warranty, express or implied, or assumes any legal liability or responsibility for the accuracy, completeness or usefulness of any information, apparatus, product or process disclosed, or represents that its use would not infringe privately owned rights.

DNA-1892-3
Rev. 1
(formerly DASA-1892-3)

WEAPONS RADIATION SHIELDING HANDBOOK

Chapter 3. Methods for Calculating Neutron and Gamma-Ray Attenuation

by

Paul N. Stevens and David K. Trubey

Approved for public release; distribution unlimited.

Handbook Editors
Lorraine S. Abbott, H. Clyde Claiborne, and Charles E. Clifford

DEFENSE NUCLEAR AGENCY
Washington, D.C. 20305

NOTICE

This report was prepared as an account of work sponsored by the United States Government. Neither the United States nor the United States Atomic Energy Commission, nor any of their employees, nor any of their contractors, subcontractors, or their employees, makes any warranty, express or implied, or assumes any legal liability or responsibility for the accuracy, completeness or usefulness of any information, apparatus, product or process disclosed, or represents that its use would not infringe privately owned rights.

MARCH 1972

Preparing Agency
OAK RIDGE NATIONAL LABORATORY
Oak Ridge, Tennessee 37830
Operated by UNION CARBIDE CORPORATION
for the U.S. ATOMIC ENERGY COMMISSION
DNA Order No. 71-804-0
RMSS Subtask PEO33-01

DISTRIBUTION OF THIS DOCUMENT IS UNLIMITED

Preface

At the request of the Defense Nuclear Agency, Oak Ridge National Laboratory has undertaken the preparation of a handbook to aid engineers charged with the responsibility of designing shields to protect military equipment and personnel in the vicinity of a nuclear weapons burst. Thus far, six chapters have been issued: Chapter 2, "Basic Concepts of Radiation Shielding Analysis"; Chapter 3, "Methods for Calculating Neutron and Gamma-Ray Attenuation"; Chapter 4, "Neutron and Gamma-Ray Albedos"; Chapter 5, "Methods for Calculating Effects of Ducts, Access Ways, and Holes in Shields"; Chapter 6, "Methods for Predicting Radiation Fields Produced by Nuclear Weapons"; and Chapter 7, "Engineering Method for Designing Initial Radiation Shields for Blast-Hardened Underground Structures." Other chapters in preparation are an introductory first chapter and Chapter 8, "Engineering Method for Designing Initial Radiation Shields for Aboveground Structures." Additional chapters are under consideration, in particular a chapter to present an engineering method for calculating dose rates, as opposed to total doses, but no definite plans to prepare such chapters have yet been made. Also, at least for the present, the plan to combine the chapters into volumes has been abandoned.

This document is a first revision of Chapter 3, which was originally issued in 1967. Since that date it has become apparent that Chapter 3 is being used both as a text and as a frequent reference in a number of colleges and universities, and in view of the recent rapid advances in adapting the various transport methods to deep-penetration shielding problems, plus the tendency of many designers to apply the methods directly, the authors and editors deemed it essential that the chapter be updated and expanded. Since this revision was undertaken immediately following the preparation of Chapter 2, the two chapters are uniquely compatible and complimentary as shielding texts.

In order to prepare this and other chapters of the Handbook, it has been necessary for Oak Ridge National Laboratory to obtain the assistance of several consultants and subcontractors. For this chapter on attenuation, Paul N. Stevens, a consultant from the University of Tennessee, together with David K. Trubey of the Laboratory prepared the first draft with which the editors worked. Other chapters similarly represent a cooperative effort of ORNL staff members and those of other organizations.

Although this revision of Chapter 3 was made wholly by the authors and editors, the character of the chapter has been retained and thus we remain indebted to the many individuals who by their extensive reviews contributed to the original version. In particular, we wish to acknowledge the help given by F. R. Mynatt, formerly of the Oak Ridge Computing Technology Center and now of the Laboratory, who was largely responsible for the original version of Section 3.3. In addition, several persons at the Laboratory served as on-the-spot authorities to help resolve problem areas as they arose. For this type of help we are especially grateful to F. H. Clark and P. H. Pitkanen, who reviewed the section on the moments method (Section 3.4), to Clark and V. R. Cain, who contributed to the section on the Monte Carlo method (Section 3.5), and to R. R. Coveyou, who reviewed the section on the invariant imbedding techniques (Section 3.7). We are also indebted to Mrs. Betty F. Maskewitz and her associates for providing the information on the computer code abstracts, both in the original version and in this revised version.

Appreciation is also expressed to Maj. F. A. Verser and to Lt. Cols. Charles D. Daniel and William A. Alfonte, who as past DNA Shielding Project Officers handled the early administration of the contract and assisted in establishing the scope of the Handbook. The work they began was continued until recently by Maj. R. W. Enz, who gave invaluable advice and assistance that aided the publication of these first six chapters. Capt. Dean Kaul is now serving as the project officer and will oversee the forthcoming chapters.

Finally, we wish to thank Mrs. Virginia M. Hamrick, who assisted in the editing of the first version of the chapter, and Mrs. Virginia Glidewell, who for this second version typed and helped proofread the many drafts which are always necessary precursors to such a publication.

Contents

3.0. Introduction

The design of shields for protection against the neutrons and gamma rays given off by a weapons burst or an operating reactor requires a detailed knowledge of the behavior of the radiation transported through the attenuating media. Numerical and, in some cases, analytical solutions of radiation transport problems can be obtained by one of several calculational techniques. Selection of the proper technique for a specific shield design problem is usually governed by the type of problem to be solved, the degree of accuracy required, and of course the costs involved. The purpose of this chapter of the Handbook is to help the shield designer choose the best method by providing him with reasonably simplified and generalized descriptions of the more commonly used techniques. As a further aid, summaries of digital computer programs which solve shielding problems by the various techniques are presented in an appendix, and other appendixes include basic data and functions of general utility.

The calculational methods covered here are those of spherical harmonics, discrete ordinates, moments, Monte Carlo, diffusion theory, invariant imbedding, and kernels, plus a method which combines a removal kernel with diffusion theory. Except for the invariant imbedding method, all these techniques are either approximate solutions to the well-known Boltzmann equation or are based on kernels obtained from solutions to the equation.* The Boltzmann equation, which is discussed in Section 3.1, is a precise mathematical description of the general behavior of uncharged radiation particles in terms of position, energy, direction, and time.

In the application of the methods to radiation shielding calculations, both neutrons and gamma rays are considered to be neutral particles that move in straight lines until they interact with an atom. These interactions result in either the scattering or the absorption of the incident particle. In a scattering interaction the incident particle is deflected in direction and degraded in energy, while in an absorption it effectively disappears, both processes thereby decreasing the number and energies of the particles penetrating the shield. (An exception is the fission reaction, usually classified as an absorption, but this process is not normally of interest in shield design.)

Most of the calculational methods presented in this chapter would in principle apply equally well to both gamma rays and neutrons. However, the differences in their interaction mechanisms as exemplified by their cross sections lead to many real differences in the implemented solutions. For example, gamma-ray cross sections are smooth functions of both the gamma-ray energy and the atomic number of the material. In contrast, neutron cross sections usually exhibit complex resonance structure, with the total and differential scattering cross sections varying irregularly with respect to energy and having little similarity for nuclides of nearly the same atomic number or atomic mass. Also, gamma-ray cross sections are relatively well known, whereas the neutron cross-section data are not complete in many regions of special interest to shield design. Most neutron cross-section work to date has been performed in support of reactor design, and because of this the work in the resonance energy regions has concentrated on neutron energies at which the cross sections are high rather than low, that is, on the peaks rather than the valleys of a plot of the cross section as a function of energy. In shield design the valleys are of more interest since neutrons with energies corresponding to the valleys tend to dominate the penetration process.

Another important difference between shielding calculations for gamma rays and those for neutrons lies in the consideration of secondary radiations produced by the interactions of the primary particles. In the case of gamma rays the secondary particles (electrons, positrons, and low-energy photons) normally do not create shielding problems and thus can be ignored. In the case of neutrons, however, the secondary particles may be the most important source, particularly if the neutron interactions are predominantly absorptions, which are always accompanied by the emission of either charged particles or "capture" gamma rays. While the

*Kernels may also be obtained from experiments.

charged particles can usually be neglected, the capture gamma rays are often highly penetrating, and the fact that they are born throughout the shield further complicates the situation. Neutron inelastic scatterings can also produce secondary gamma rays.

The recognition of secondary gamma rays as a serious shielding problem has resulted in the development of techniques to compute the neutron fluxes and the corresponding secondary gamma-ray fluxes simultaneously. In particular, several computer codes based on the discrete ordinates and Monte Carlo methods have been designed to solve the "coupled" problem.

With the availability of so many methods of varying sophistication, it is generally believed that shield designers now have the tools at hand for adaptation to most shielding problems. If this is indeed true, then the limiting factor in calculating the attenuation of neutrons and gamma rays in shields is the availability and accuracy of the basic data, that is, the interaction cross sections and the radiation source distributions. Concentrated efforts are currently underway to provide such data.

3.1. The General Boltzmann Transport Equation and Its Adjoint

The Boltzmann transport equation describes the general behavior of uncharged radiation particles (e.g., neutrons) or quanta of electromagnetic radiation (e.g., gamma rays) in terms of seven-dimensional phase space $(\bar{r},E,\bar{\Omega},t)$. This phase space consists of three spatial coordinates, the particle energy, two direction-defining angles, and time. Knowledge of the radiation particle density over all phase space for some prescribed physical situation is in fact the complete solution to the transport problem. However, experience has shown that the particle flux, which is simply related to the particle density (particle flux = particle density × particle speed), is a more convenient variable for analysis. Accordingly, the *angular flux*, $\Phi(\bar{r},E,\bar{\Omega},t)$, is used as the dependent variable in the Boltzmann equation.

When associated with differential phase space in energy and direction, the time-dependent angular flux can be interpreted as

$\Phi(\bar{r},E,\bar{\Omega},t)\,dE\,d\bar{\Omega}$ = the number of particles that cross a unit area normal to the $\bar{\Omega}$ direction per unit time at the space point $\bar{r}$ and time t with energies in dE about E and with directions that lie within the differential solid angle $d\bar{\Omega}$ about the unit vector $\bar{\Omega}$.

This function is more properly called the *particle flux density differential in energy and angle,** but the simple expression angular flux has become standard terminology. Integrating the angular flux over all directions yields the scalar flux, given by

$$\Phi(\bar{r},E,t) = \int_{4\pi} \Phi(\bar{r},E,\bar{\Omega},t)\,d\bar{\Omega}$$

and having units of particles cm^{-2} sec^{-1} MeV^{-1}. This scalar flux is sometimes referred to as the differential flux, since it is differential with respect to energy. A second integration over some specified energy range will produce $\Phi(\bar{r})$, which is a total flux (particles cm^{-2} sec^{-1}).

The derivation of the general time-dependent integro-differential form of the Boltzmann transport equation can be regarded as a bookkeeping process that sets the net storage of particles within a differential element of phase space $(d\bar{r}\,dE\,d\bar{\Omega}\,dt)$ equal to the particle gains minus particle losses in that element and leads to the following familiar form:

$$\frac{1}{v}\frac{\partial}{\partial t}\Phi(\bar{r},E,\bar{\Omega},t) = S(\bar{r},E,\bar{\Omega},t) + \iint \Sigma_s(\bar{r},E'\rightarrow E,\bar{\Omega}'\rightarrow\bar{\Omega})\,\Phi(\bar{r},E',\bar{\Omega}',t)\,dE'\,d\bar{\Omega}' - \nabla\cdot\bar{\Omega}\,\Phi(\bar{r},E,\bar{\Omega},t) - \Sigma_t(\bar{r},E)\,\Phi(\bar{r},E,\bar{\Omega},t)\,, \quad (3.1)$$

where

$\bar{r}$ = position variable,

E = the particle's kinetic energy,

v = the particle's speed corresponding to its kinetic energy E,

$\bar{\Omega}$ = a unit vector which describes the particle's direction of motion,

t = time variable,

$\Phi(\bar{r},E,\bar{\Omega},t)$ = the time-dependent angular flux,

$\frac{1}{v}\frac{\partial}{\partial t}\Phi(\bar{r},E,\bar{\Omega},t)\,dE\,d\bar{\Omega}$ = net storage (gains minus losses) per unit volume and time at the space point $\bar{r}$ and time t of particles with energies in dE about E and with directions which lie in $d\bar{\Omega}$ about $\bar{\Omega}$,

$S(\bar{r},E,\bar{\Omega},t)\,dE\,d\bar{\Omega}$ = the gain due to source particles emitted per unit volume and time at the space point $\bar{r}$ and time t with energies in dE about E and directions which lie in $d\bar{\Omega}$ about $\bar{\Omega}$,

*See Chapter 2 for a detailed discussion of flux and other basic concepts.

$\Sigma_s(\bar{r},E'\to E,\bar{\Omega}'\to\bar{\Omega})\ dE\ d\bar{\Omega}$ = the differential scattering cross section which describes the probability that a particle with an initial energy E' and an initial direction $\bar{\Omega}'$ undergoes a scattering collision at $\bar{r}$ which places it into a direction that lies in $d\bar{\Omega}$ about $\bar{\Omega}$ with a new energy in dE about E,

$\left[\iint \Sigma_s(\bar{r},E'\to E,\bar{\Omega}'\to\bar{\Omega})\ \Phi(\bar{r},E',\bar{\Omega}',t)\ dE'\ d\bar{\Omega}'\right] dE\ d\bar{\Omega}$ = inscattering gain per unit volume and time at the space point $\bar{r}$ and time t of particles with energies in dE about E and directions which lie in $d\bar{\Omega}$ about $\bar{\Omega}$,

$\bar{\Omega}\cdot\nabla\ \Phi(\bar{r},E,\bar{\Omega},t)\ dE\ d\bar{\Omega}$ = net convective loss* per unit volume and time at the space point $\bar{r}$ and time t of particles with energies in dE about E and directions which lie in $d\bar{\Omega}$ about $\bar{\Omega}$,

$\Sigma_t(\bar{r},E)$ = the total cross section at the space point $\bar{r}$ for particles of energy E,

$\Sigma_t(\bar{r},E)\ \Phi(\bar{r},E,\bar{\Omega},t)\ dE\ d\bar{\Omega}$ = collision loss per unit volume and time at the space point $\bar{r}$ and time t of particles with energies in dE about E and directions which lie in $d\bar{\Omega}$ about $\bar{\Omega}$.

One of its more familiar and useful forms is for the time-independent problem, given by

$$\bar{\Omega}\cdot\nabla\ \Phi(\bar{r},E,\bar{\Omega}) + \Sigma_t(\bar{r},E)\ \Phi(\bar{r},E,\bar{\Omega}) = S(\bar{r},E,\bar{\Omega}) + \iint \Sigma_s(\bar{r},E'\to E,\bar{\Omega}'\to\bar{\Omega})\ \Phi(\bar{r},E',\bar{\Omega}')\ dE'\ d\bar{\Omega}' \quad (3.2)$$

where the storage term is identically zero and the phase space is six-dimensional $(\bar{r},E,\bar{\Omega})$. This form is the basis for solution of steady-state radiation shielding problems such as determining the biological shield associated with a nuclear reactor operating at constant power.

The solution of the transport equation represents the average value of the particle flux or particle density. In real systems, there will be fluctuations from the average; in some cases these fluctuations will be important, but, in general, they will not have a bearing on the validity of the equation predicting the expected value.

Methods of solving the transport equation are inherently complex due to its integrodifferential form, and exact solutions are limited to a few highly specialized problems. The most practical techniques are approximate and essentially numerical in nature, the more familiar ones being the spherical harmonics method, the discrete ordinates (S_n) technique, and the moments method. It is interesting to note that diffusion theory actually corresponds to a low-order approximation of the transport equation (see Section 3.2). Also, integral forms of the transport equation may be regarded as the formal basis for the Monte Carlo method, the results of which can in principle be made to approach the exact solution. More complete descriptions of these and other approximate methods are presented in the following sections of this chapter.

The integrodifferential equation which is adjoint to Eq. 3.1 is derived in Appendix 3A and can be written as

$$-\frac{1}{v}\frac{\partial}{\partial t}\Phi^*(\bar{r},E,\bar{\Omega},t) - \bar{\Omega}\cdot\nabla\ \Phi^*(\bar{r},E,\bar{\Omega},t) + \Sigma_t(\bar{r},E)\ \Phi^*(\bar{r},E,\bar{\Omega},t) = S^*(\bar{r},E,\bar{\Omega},t) + \iint \Sigma_s(\bar{r},E\to E',\bar{\Omega}\to\bar{\Omega}')\ \Phi^*(\bar{r},E',\bar{\Omega}',t)\ dE'\ d\bar{\Omega}' \quad (3.3)$$

where

$\Phi^*(\bar{r},E,\bar{\Omega},t)$ = the adjoint flux which has the interpretation of "value function," a measure of the present and future contributions to the effect of interest by a radiation particle leaving a collision at a point whose coordinates in phase space are $(\bar{r},E,\bar{\Omega},t)$, *if*

---

*The form of the net convective loss term, $\bar{\Omega}\cdot\nabla\ \Phi(\bar{r},E,\bar{\Omega},t)$, is less obvious than the other terms which comprise the Boltzmann equation. The derivation of this term involves formulating the net outflow (loss) of particles having phase space coordinates $(\bar{r},E,\bar{\Omega},t)$ across the surface of the differential volume $d\bar{r}$,

$$\int_{\text{Surface of } d\bar{r}} \bar{J}(\bar{r},E,\bar{\Omega},t)\cdot d\bar{s}\,.$$

The desired form is obtained by transforming the above surface integral into an equivalent volume integral. This is accomplished by application of the "divergence theorem":

$$\int_{\text{Surface of } d\bar{r}} \bar{J}(\bar{r},E,\bar{\Omega},t)\cdot d\bar{s} = \int_{d\bar{r}} \nabla\cdot J(\bar{r},E,\bar{\Omega},t)\ d\bar{r}\,.$$

Evaluation of the volume integral over the differential phase space $d\bar{r}$ yields $\nabla\cdot\bar{J}(\bar{r},E,\bar{\Omega},t)\ d\bar{r}$ and on a per unit volume basis the net convective term becomes $\nabla\cdot\bar{J}(\bar{r},E,\bar{\Omega},t)$, which can be rewritten in terms of the angular flux as $\bar{\Omega}\cdot\nabla\ \Phi(\bar{r},E,\bar{\Omega},t)$.

$S^*(\bar{r},E,\bar{\Omega},t)$ = the adjoint source term, is defined as the direct contribution to the effect of interest by a unit angular flux with phase space coordinates $(\bar{r},E,\bar{\Omega},t)$.

Consistent with the above interpretations of Φ^* and S^*, the effect of interest λ (for example, flux density, current, absorption, heating, leakage, transmission, reflection, and dose) is uniquely determined if either the forward or adjoint fluxes are known; that is

$$\lambda = \int\int\int\int \Phi(\bar{r},E,\bar{\Omega},t)\, S^*(\bar{r},E,\bar{\Omega},t)\, d\bar{r}\, dE\, d\bar{\Omega}\, dt$$

or

$$\lambda = \int\int\int\int S(\bar{r},E,\bar{\Omega},t)\, \Phi^*(\bar{r},E,\bar{\Omega},t)\, d\bar{r}\, dE\, d\bar{\Omega}\, dt$$

$$- \int\int\int\int \Phi(\bar{r},E,\bar{\Omega},t)\, \Phi^*(\bar{r},E,\bar{\Omega},t)\, \bar{\Omega}\cdot d\bar{s}\, dE\, d\bar{\Omega} dt \ .$$

The *adjoint flux* does not correspond in the usual sense to a real physical quantity. Instead it is the flux associated with the adjoint equation when that equation is interpreted as describing the transport of hypothetical radiation particles, sometimes called "adjunctons." The rationale of the concept of adjunctons follows at least in part from the similarity of the adjoint equation to the Boltzmann transport equation.

The adjoint equation, which mathematically defines the characteristics of the adjunctons, has often been referred to as the "backward" equation because the movement of adjunctons is backward to that of real particles. That is, they originate at a point in phase space associated with the detector and move in the direction of phase space that corresponds to the real source. This behavior requires that in a collision the adjuncton gain energy, which contradicts the usual energy conservation principles unless *prior to the collision* the target nucleus has the kinetic energy it would have acquired in a real collision process with a particle which has the final energy of the adjuncton. This precludes the assignment of physical properties to the adjunctons that would resemble those of real particles.

The lack of physical properties is not a serious shortcoming since adjunctons are not useful as radiation particles per se. Rather, the adjoint flux which mathematically exists at some point in phase space has the precise interpretation of "value function."

The value function is used as an importance function to bias Monte Carlo analyses of the behavior of real particles (neutrons and gamma rays) (see Section 3.5). Calculation of the answer of interest through solution of the adjoint problem avoids the difficulties associated with estimation of the flux at a point, provided, of course, that the source has a more agreeable (diffuse) configuration. Further, given a flux field, an equivalent source can be constructed to which an individual particle can contribute only once. The adjoint flux can be interpreted as the estimator of the effect of interest for these source neutrons and the forward and adjoint solutions are thus combined to achieve a desired result with possibly greater calculational efficiency than would be possible by either method alone.

The adjoint concept also provides a fundamental basis for perturbation analyses which if properly implemented is a powerful tool in the study of small changes to a shield configuration.

Since the adjoint equation is very similar to the usual Boltzmann transport equation, it is not surprising that methods developed to solve the latter will also apply to the former. For example, adjoint fluxes have been calculated using the techniques of diffusion theory, Monte Carlo, and "exact" transport theory. Consequently, there should be no serious practical or fundamental difficulties in calculating the adjoint flux.

3.2. Spherical Harmonics Method

The method of "spherical harmonics" as applied to the solution of the Boltzmann transport equation (Eq. 3.2) consists of representing the various angle-dependent terms as expansions of the spherical harmonics polynomials. These polynomials, commonly called associated spherical harmonics, are described, for example, by Weinberg and Wigner[1] and are given by the following expressions:

$$P_{jm}(\bar{\Omega}) = \sum_k (-1)^{k-m} \frac{j[(j+m)!\,(j-m)!]^{1/2}}{(j-m-k)!\,(m+k)!\,k!\,(j-k)!}\, e^{im\varphi} \left(\cos\frac{1}{2}\theta\right)^{2j-m-2k} \left(\sin\frac{1}{2}\theta\right)^{2k+m}$$

$$= e^{im\varphi} \frac{(-\sin\theta)^m}{j!\,2^j} \left[\frac{(j-m)!}{(j+m)!}\right]^{1/2} \frac{d^{j+m}(\cos^2\theta - 1)^j}{(d\cos\theta)^{j+m}}, \quad (3.4)$$

where $\bar{\Omega}$ is the unit vector which for this application corresponds to specifying the direction of the particle motion, and θ and φ are the polar and azimuthal angles respectively.

Applying the spherical harmonics technique to the general transport problem is inherently complex and involves mathematical procedures and concepts beyond the scope of this handbook. However, a simplified and lucid illustration of the method can be shown for the case of a steady-state (no time dependence), one-speed (no energy dependence), one-dimensional (slab geometry with azimuthal symmetry), homogeneous (constant system parameters) neutron transport problem. Consistent with these simplifications, the general Boltzmann transport equation as given by Eq. 3.2 can be written as

$$\mu \frac{\partial \Phi(x,\mu)}{\partial x} + \Sigma_t\, \Phi(x,\mu) = S(x,\mu) + \int_{-1}^{+1} \Sigma_s(\mu,\mu')\, \Phi(x,\mu')\, d\mu', \quad (3.5)$$

where

$\Phi(x,\mu)$ = angular flux (neutron flux per unit μ) $= 2\pi\, \Phi(x,\bar{\Omega})$,

x = spatial variable in slab geometry, the direction of which is specified by the unit vector $\bar{i}$,

μ = direction cosine with respect to the x axis $= \bar{\Omega}\cdot\bar{i} = \cos\theta$,

Σ_t = total macroscopic cross section,

$\Sigma_s(\mu,\mu')\, d\mu$ = a scattering cross section which describes the probability that a neutron with an incident direction cosine μ' will be scattered such that its emergent direction has a direction cosine in $d\mu$ about μ,

$$\Sigma_s(\mu,\mu') = \int_0^{2\pi} \Sigma_s(\bar{\Omega},\bar{\Omega}')\, d\varphi,$$

$\Sigma_s(\bar{\Omega},\bar{\Omega}')$ = the macroscopic differential scattering cross section,

$\Sigma_s(\bar{\Omega},\bar{\Omega}')\, \Phi(x,\bar{\Omega}')\, d\bar{\Omega}\, d\bar{\Omega}'$ = the number of neutrons which scatter from the differential solid angle $d\bar{\Omega}'$ about $\bar{\Omega}'$ through an angle $\cos^{-1}\, \bar{\Omega}\cdot\bar{\Omega}'$ into the differential solid angle $d\bar{\Omega}$ about $\bar{\Omega}$, per unit volume and time,

$S(x,\mu)\, d\mu$ = source neutrons emitted with direction cosines in $d\mu$ about μ per unit volume and time.

The angle-dependent terms in Eq. 3.5 can each be represented as a series of spherical harmonics of the

first kind, the Legendre polynomials $P_j(\mu)$. These polynomials are the degenerate form of the associated spherical harmonics and are given by Eq. 3.4 when the index m is set equal to zero; that is,

$$P_j(\mu) \equiv P_{j,0}(\bar{\Omega}) .$$

The first few Legendre polynomials are

$$P_0(\mu) = 1 ,$$

$$P_1(\mu) = \mu ,$$

$$P_2(\mu) = \frac{1}{2}(3\mu^2 - 1) ,$$

$$P_3(\mu) = \frac{1}{2}(5\mu^2 - 3\mu) ,$$

. . . .

Expanding the angular neutron flux in terms of these polynomials yields

$$\Phi(x,\mu) = \sum_{j=0}^{\infty} \Phi_j(x) P_j(\mu) , \qquad (3.6)$$

where

$\Phi_j(x)$ = position-dependent Legendre coefficients (j = 0,1,2,...∞) corresponding to the neutron flux

$$= \frac{2j+1}{2} \int_{-1}^{+1} \Phi(x,\mu) P_j(\mu) \, d\mu .$$

In general the Legendre coefficients have no physical significance, except for $\Phi_0(x)$ and $\Phi_1(x)$, which are related to the total flux $\Phi(x)$ and net current $J(x)$ in the following manner:

$$\Phi_0(x) = \frac{1}{2} \int_{-1}^{+1} \Phi(x,\mu) \, d\mu$$

$$= \frac{1}{2} \Phi(x) ,$$

$$\Phi_1(x) = \frac{3}{2} \int_{-1}^{+1} \mu \, \Phi(x,\mu) \, d\mu$$

$$= \frac{3}{2} J(x) .$$

The source term can also be expanded in terms of Legendre polynomials, yielding the expression

$$S(x,\mu) = \sum_{j=0}^{\infty} S_j(x) P_j(\mu) , \qquad (3.7)$$

where

$S_j(x)$ = position-dependent Legendre coefficients (j = 0,1,2,...∞) corresponding to the source term

$$= \frac{2j+1}{2} \int_{-1}^{+1} S(x,\mu) P_j(\mu) \, d\mu .$$

The zeroth coefficient corresponds to the isotropically emitting component of the source term,

$$S_0(x) = \frac{1}{2} \int_{-1}^{+1} S(x,\mu) \, d\mu$$

$$= \frac{1}{2} S(x) ,$$

$S(x)$ = total source term at x,

and for an isotropic source the other coefficients (j = 1,2,...∞) are all zero.

Since for most practical situations the differential scattering cross section depends only on the change in direction as denoted by $\mu_0 = \bar{\Omega} \cdot \bar{\Omega}'$, the series expansion for $\Sigma_s(\bar{\Omega},\bar{\Omega}')$ is made in terms of the Legendre polynomials $P_i(\mu_0)$:

$$\Sigma_s(\bar{\Omega},\bar{\Omega}') = \sum_{i=0}^{\infty} \eta_i P_i(\mu_0) , \qquad (3.8)$$

where

η_i = Legendre coefficients (i = 0,1,2,...∞) corresponding to the differential scattering cross section

$$= \frac{2i+1}{2} \int_{-1}^{+1} \Sigma_s(\bar{\Omega},\bar{\Omega}') P_i(\mu_0) \, d\mu_0 .$$

Again the low-order (j = 0,1) coefficients can be related to physical parameters of the problem. In particular, η_0 is the isotropic component of the differential scattering cross section and η_1 is related to the average value of the cosine of the scattering angle:

$$\eta_0 = \frac{1}{2} \int_{-1}^{+1} \Sigma_s(\bar{\Omega},\bar{\Omega}') \, d\mu_0$$

$$= \Sigma_s / 4\pi ,$$

Σ_s = macroscopic scattering cross section

$$= 2\pi \int_{-1}^{+1} \Sigma_s(\bar{\Omega},\bar{\Omega}')\, d\mu_0 ,$$

$$\eta_1 = \frac{3}{2} \int_{-1}^{+1} \Sigma_s(\bar{\Omega},\bar{\Omega}')\, \mu_0\, d\mu_0$$

$$= \frac{3}{4\pi} \Sigma_s\, \bar{\mu}_0 ,$$

$\bar{\mu}_0$ = average value of the cosine of the scattering angle in the laboratory frame of reference

$$= \frac{\int_{-1}^{+1} \Sigma_s(\bar{\Omega},\bar{\Omega}')\, \mu_0\, d\mu_0}{\int_{-1}^{+1} \Sigma_s(\bar{\Omega},\bar{\Omega}')\, d\mu_0} .$$

The spherical harmonics form of the Boltzmann equation is obtained by introducing the above series representations for $\Phi(x,\mu)$, $S(x,\mu)$, and $\Sigma_s(\bar{\Omega},\bar{\Omega}')$ into Eq. 3.5, multiplying each term by the Legendre polynomial $P_n(\mu)$ and integrating over all μ (-1 to $+1$). When Eqs. 3.6, 3.7, and 3.8 are substituted into Eq. 3.5 and the orthogonality property of Legendre polynomials,

$$\int_{-1}^{+1} P_j(\mu)\, P_n(\mu)\, d\mu = 0 \quad \text{if } j \neq n$$

$$= \frac{2}{2n+1} \quad \text{if } j = n ,$$

is used along with the addition theorem for Legendre polynomials,*

$$P_j(\mu_0) = P_j(\mu)\, P_j(\mu')$$

$$+ 2 \sum_{m=1}^{j} \frac{(j-m)!}{(j+m)!} P_j^m(\mu) P_j^m(\mu') \cos m(\varphi - \varphi') ,$$

and with the recursion relationship

$$\mu\, P_j(\mu) = \frac{j+1}{2j+1} P_{j+1}(\mu) + \frac{j}{2j+1} P_{j-1}(\mu) ,$$

*The use of the addition theorem makes possible the evaluation of the inscattering-integral term containing $\Sigma_s(\bar{\Omega},\bar{\Omega}')$, which is necessarily expanded in terms of $P_i(\mu_0)$ rather than $P_i(\mu)$.

the following set of coupled differential equations is obtained:

$$\frac{n+1}{2n+3} \frac{d}{dx} \Phi_{n+1}(x) + \frac{n}{2n-1} \frac{d}{dx} \Phi_{n-1}(x)$$

$$= \frac{4\pi}{2n+1} \eta_n \Phi_n(x) - \Sigma_t \Phi_n(x) + S_n(x) ,$$

$$\text{for } n = 0,1,2,\ldots\infty . \quad (3.9)$$

This set of equations, which no longer involves the directional variables and therefore is more amenable to solution than Eq. 3.5, is called the second (or spherical harmonics component) form of the Boltzmann equation by Weinberg and Wigner[1] and others. Solution of this set of equations can be accomplished by rather straightforward although sometimes complex techniques.

Practical methods of solution require that the series representation of $\Phi(x,\mu)$ be limited to a finite number of terms, for example, to $(n+1)$ terms; n is commonly called the truncation number, and the corresponding calculation is referred to as the P_n approximation.

For the P_1 approximation, consider only the $n = 0$ and $n = 1$ forms of Eq. 3.9. With $n = 1$, Eq. 3.9 can be written as

$$\frac{2}{3} \Phi_1(x) = -\frac{1}{3(\Sigma_t - \bar{\mu}_0 \Sigma_s)} \frac{d}{dx} 2\Phi_0(x) . \quad (3.10)$$

Then, identifying

$$\frac{2}{3} \Phi_1(x) = J(x)$$

and

$$2\Phi_0(x) = \Phi(x)$$

and introducing the "transport-corrected" diffusion coefficient

$$D \equiv \frac{1}{3(\Sigma_t - \bar{\mu}_0 \Sigma_s)} = \frac{1}{3\Sigma_{tr}} , \quad (3.11)$$

Eq. 3.10 can be rewritten as

$$J(x) = -D \frac{d}{dx} \Phi(x) . \quad (3.12)$$

Equation 3.12 is commonly referred to as "Fick's law."

With $n = 0$, Eq. 3.9 becomes

$$\frac{d}{dx}\frac{2}{3}\Phi_1(x) = -\Sigma_a\, 2\Phi_0(x) + 2S_0(x)\,,$$

which can be rewritten as

$$\frac{d}{dx}J(x) = -\Sigma_a\,\Phi(x) + S(x)\,. \tag{3.13}$$

Equation 3.13 can be interpreted as a precise neutron balance on the one-dimensional phase space (x). The familiar "diffusion equation" is obtained by substituting Eq. 3.12 into Eq. 3.13:

$$D\frac{d^2}{dx^2}\Phi(x) - \Sigma_a\,\Phi(x) + S(x) = 0\,. \tag{3.14}$$

The P_1 approximation is equivalent to diffusion theory (see Section 3.6) and involves only a linear representation of the angular flux,

$$\Phi(x,\mu) = \Phi_0(x) + \mu\,\Phi_1(x)\,.$$

This restricts its application to situations wherein the neutron flux is nearly isotropic, a condition not characteristic of the penetrating components of neutrons that traverse a shield. It is noted that the P_1 approximation did not require isotropic scattering in the laboratory frame of reference (an assumption required in the derivation of Fick's law).

In a similar fashion, the accuracy of the spherical harmonics calculation is also influenced by the number of terms used to represent the differential scattering cross section. Only a few terms are necessary for nearly isotropic scattering, but a large number of terms are required for adequate treatment of anisotropic scattering, and in the past this has limited the use of the spherical harmonics treatment. However, recent advances in cross-section technology and increased computer capacity have for all practical considerations removed this limitation.

It has been shown[1] that the accuracy of the spherical harmonics method is improved when the truncation number n is equal to or greater than 3. This is demonstrated in Table 3.1, in which the results obtained with P_1, P_3, P_5, and P_{15} approximations are compared with those obtained from a rigorous calculation by the Wiener-Hopf method for the well-known

Table 3.1. Comparison of Normalized Total Fluxes Obtained with Various P_n Approximations and with a Rigorous Solution by the Wiener-Hopf Method[a]

Scattering (mfp)	Total Flux				
	P_1	P_3	P_5	P_{15}	Wiener-Hopf Method
0.0	1.0000	1.0000	1.0000	1.0000	1.0000
0.1	1.1732	1.2094	1.2263	1.2528	1.2608
0.2	1.3464	1.4123	1.4389	1.4680	1.4714
0.3	1.5196	1.6099	1.6414	1.6664	1.6685
0.4	1.6928	1.8031	1.8365	1.8564	1.8587
0.5	1.8660	1.9927	2.0261	2.0417	2.0443
0.6	2.0392	2.1794	2.2117	2.2241	2.2271
0.7	2.2124	2.3637	2.3944	2.4045	2.4077
0.8	2.3856	2.5460	2.5749	2.5834	2.5868
0.9	2.5589	2.7267	2.7537	2.7613	2.7652
1.0	2.7321	2.9060	2.9312	2.9382	2.9419
2.0	4.4641	4.6623	4.6792	4.6853	4.6902

[a]From ref. 1.

Milne problem with spherically symmetric scattering and no absorption. These results indicate that the P_3 approximation is a vast improvement over diffusion theory (P_1 approximation) and that computer implementation of the P_3 approximation is reasonable.

Shure[2] found that a multigroup P_3 approach in one dimension for calculating spatial and spectral neutron distributions in metal-hydrogenous reactor shields yielded satisfactory estimates of neutron attenuation for reasonable amounts of computer time. Further, it was recognized by Lanning[3] that for some design problems the low-order approximations were sufficiently accurate. He successfully calculated the spatial distribution of the gamma-ray energy flux in one-dimensional slab geometry.

3.3. The Discrete Ordinates S_n Method*

The discrete ordinates S_n method is a means of effecting a numerical solution of the energy-dependent linear Boltzmann transport equation. The most recent versions of the method permit anisotropic scattering to be included, thus making it suitable for both neutron and gamma-ray deep-penetration calculations in a wide variety of shielding problems. Since the method is fundamentally formulated as a finite difference equation (rather than as finite differencing of an analytic approximation), a minimum number of limiting assumptions is required, and the solutions apparently approach the exact solution of the Boltzmann equation as the space, energy, and angle meshes approach differential size. The method can be applied without significant restrictions to the general core criticality problem, and it can be used for both homogeneous and laminated shields with a variety of source configurations, including surface- and volume-distributed sources.

The original method of discrete ordinates is attributed to Wick[4] and to Chandrasekhar.[5] Early applications were limited to simple problems such as the transport of monoenergetic neutrons isotropically scattered in one-dimensional slabs. The fundamental assumption in the method was that the integral in the Boltzmann equation could be approximated by a Gaussian quadrature formula; consequently, functions involved in the integral had to be evaluated only at the angles corresponding to the Gaussian zeros. Although this original discrete ordinates method could be extended to anisotropic scattering, it was limited to slab geometry.

A discrete ordinates technique which could be extended to spherical and cylindrical geometries was introduced by Carlson,[6] and it is this method that is commonly referred to as the discrete ordinates S_n method. The S_n technique serves as the basis for several widely used codes, such as the one-dimensional codes DTF II,[7] DTF IV,[8] ANISN,[9] and DSN[10] and the two-dimensional codes TDC[10] and DOT.[11,12]

Other approaches that can also be classified as discrete ordinates methods are the direct numerical integration techniques employed by the NIOBE[13] and BIGGI-3P† computer programs, but these techniques have not been utilized to a large extent for shielding problems in the United States.

Early versions of the S_n method assumed that the angular flux varies with angle as connected line segments in an even number of equally spaced angular increments. This representation, although reasonably accurate for homogeneous one-dimensional systems, was found to be unsuitable for the general problem because it fails to preserve optical reciprocity (i.e., the method consists of a nonsymmetric angular quadrature). Also, recursions involving many terms are required, and an extension of the method to multidimensional geometries is most difficult. These shortcomings are largely alleviated by the use of the "diamond difference" technique,[10] which relates in a more general fashion the angular flux within each particular angular increment to the endpoint values of the increment. With the diamond difference method the Boltzmann equation can be integrated over an angular increment, yielding, for the derivative terms, a two-point difference equation involving the angular flux evaluated at the increment endpoints.

The linear Boltzmann equation of transport theory is not derived from first principles of physics but is a flow balance for a differential phase space cell, treating in a phenomenological manner the events causing an increase or a decrease in the number of particles contained in the cell. The discrete ordinates difference equations can be formulated in an equivalent manner but by considering a finite-difference cell – the way it is presented in most references. For some time it was not clear that the difference equations would in general approach the analytic

*The description of the discrete ordinates method which appeared in the first edition of this chapter was primarily the work of F. R. Mynatt of the Computing Technology Center, Oak Ridge, Tennessee. The revisions for this edition have been made by one of the chapter authors (P.N.S.).

†See Appendix 3B.

form of the Boltzmann equation as the finite-difference phase space cell approached differential size. Lathrop[8] showed that they would for the one-dimensional geometries, and this is established implicitly in the following paragraphs in which the difference equations for spherical geometry are derived directly from the analytic Boltzmann equation. Spherical geometry, although simple, serves to illustrate all the characteristics of the discrete ordinates equations except for discrete ray streaming, which occurs only in two- or three-dimensional geometry.

Transport Equation and Phase Space Geometry. – In the following paragraphs the derivation of the discrete ordinates equations will be performed for the special case of spherically symmetric, spherical geometry and the steady-state condition. With only slight modification this derivation can be made to apply to other one-dimensional configurations, namely slab and infinite-cylinder geometries. The derivation also embodies the essential features of two-dimensional derivations while avoiding much of the complexity. However, it does not adequately reflect the unique complexities of the time-dependent discrete ordinates analysis. Therefore a derivation of the discrete ordinates equations for the time-dependent problem and a brief description of their use are presented in Appendix 3C.

Phase space for this special case consists of three variables: the radius of the sphere (r), the energy of the particle (E), and the cosine of the angle of the particle direction relative to the radius (μ). A differential phase space cell is given by

$$\text{differential phase space cell} = dV\, dE\, d\mu$$

$$= 4\pi r^2\, dr\, dE\, d\mu\ , \qquad (3.15)$$

and the finite-difference cell is obtained by integrating Eq. 3.15 over any particular finite intervals of radius, energy and angle. It is given by

$$\text{finite-difference cell} = V_I\, \Delta E_G\, \Delta\mu_D$$

$$= \frac{4\pi}{3}(r_{i+1}^3 - r_i^3)(E_g - E_{g+1})(\mu_{d+1} - \mu_d)^*\ .$$

For the one-dimensional spherical geometry problem, the following two analytic forms of the Boltzmann transport equation can be considered:

$$\mu \frac{\partial}{\partial r}\Phi(r,E,\mu) + \frac{(1-\mu^2)}{r}\frac{\partial}{\partial \mu}\Phi(r,E,\mu) + \Sigma_t(r,E)\,\Phi(r,E,\mu) = S(r,E,\mu) + \int_0^\infty \int_{-1}^{+1} \Sigma_s(r, E' \to E, \mu_0) \times \Phi(r,E',\mu')\, dE'\, d\mu'\ , \qquad (3.16)$$

and

$$\frac{\mu}{r^2}\frac{\partial}{\partial r}[r^2\,\Phi(r,E,\mu)] + \frac{1}{r}\frac{\partial}{\partial \mu}[(1-\mu^2)\,\Phi(r,E,\mu)] + \Sigma_t(r,E)\,\Phi(r,E,\mu) = S(r,E,\mu) + \int_0^\infty \int_{-1}^{+1} \Sigma_s(r, E' \to E, \mu_0) \times \Phi(r,E',\mu')\, dE'\, d\mu'\ , \qquad (3.17)$$

where

$\Phi(r,E,\mu)$ = the angular flux, which can be interpreted as the particle track length per unit time per unit volume about r per unit energy about E and per unit direction cosine about μ,

$\Sigma_t(r,E)$ = position- and energy-dependent macroscopic total cross section,

$\Sigma_s(r, E' \to E, \mu_0)\, dE\, d\mu$ = differential scattering cross section describing the probability that a particle with an initial energy E' and direction cosine μ' undergoes a collision at r, resulting in a change of flight direction de-

*The following subscript notation is used throughout this section: subscripts I, G, and D denote functions whose values are associated with the Ith space interval, Gth energy group, and Dth angular interval, respectively; i and $i+1$ refer to a function evaluated at the lower and upper limits of the Ith space interval; $g+1$ and g refer to a function evaluated at the lower and upper limits of the Gth energy group; and $d+1$ and d refer to a function evaluated at the lower and upper limits of the Dth angular interval. Therefore since the μ-integration will be performed in the direction of decreasing μ, i.e. $\mu_d \to \mu_{d+1}$, the interval $\Delta\mu_D = \mu_{d+1} - \mu_d$ will be negative.

scribed by the cosine of the scattering angle μ_0, which places it into a new direction which lies in $d\mu$ about μ with a new energy in dE about E,

μ_0 = cosine of the scattering angle = $\overline{\Omega}\cdot\overline{\Omega}'$,

$\overline{\Omega}, \overline{\Omega}'$ = final and initial flight direction unit vectors respectively,

$S(r,E,\mu)$ = source particles per unit time per unit volume about r per unit energy about E and per unit direction cosine about μ.

Integration of both Eq. 3.16 and Eq. 3.17 would yield particle balance equations; however, the same would not be true for the numerical approximation of Eq. 3.16. Equation 3.17 is called the "conservative" form of the transport equation, and its integration over any phase space volume results in interface terms, which may be identified as leakage terms that satisfy the divergence theorem exactly. As a consequence, the "conservative" equation (Eq. 3.17) is the preferred formal basis for numerical analyses.

Derivation of Finite-Difference Equation. — The discrete ordinates difference equation is obtained by applying the following simple integral operator to the transport equation (Eq. 3.17) in a manner consistent with the classical technique for obtaining difference equations:

$$\text{integral operator} = \int_{r\epsilon V_I} \int_{E\epsilon\Delta E_G} \int_{\mu\epsilon\Delta\mu_D} \times 4\pi r^2 \, dr \, dE \, d\mu \, . \qquad (3.18)$$

This operator integrates* each term of the transport equation over the difference cell. Application of the operator to the first term of Eq. 3.17 gives

$$T_1 = \int_{r\epsilon V_I} \int_{E\epsilon\Delta E_G} \int_{\mu\epsilon\Delta\mu_D} \frac{\mu}{r^2} \times \frac{\partial}{\partial r}[r^2 \, \Phi(r,E,\mu)] \, 4\pi r^2 \, dr \, dE \, d\mu \, ,$$

which on rearranging becomes

$$T_1 = 4\pi \int_{r\epsilon V_I} \int_{\mu\epsilon\Delta\mu_D} \mu \times \frac{\partial}{\partial r}\left[r^2 \int_{E\epsilon\Delta E_G} \Phi(r,E,\mu)\, dE\right] dr \, d\mu \, . \qquad (3.19)$$

The integral of the flux over the energy group G may be identified as the group angular flux

$$\Phi_G(r,\mu) \equiv \int_{E\epsilon\Delta E_G} \Phi(r, E, \mu)\, dE \, , \qquad (3.20)$$

in which case Eq. 3.19 becomes

$$T_1 = 4\pi \int_{\mu\epsilon\Delta\mu_D} \mu d\mu \times \int_{r\epsilon V_I} \frac{\partial}{\partial r}[\, r^2 \, \Phi_G(r,\mu)\,]\, dr \, . \qquad (3.21)$$

The volume integral in Eq. 3.21 can be modified and evaluated in the following manner,

$$\int_{r\epsilon V_I} \frac{\partial}{\partial r}[r^2 \, \Phi_G(r,\mu)]\, dr = \int_{r\epsilon V_I} d[r^2 \, \Phi_G(r,\mu)] = r_{i+1}^2 \, \Phi_{i+1,G}(\mu) - r_i^2 \, \Phi_{i,G}(\mu) \, , \qquad (3.22)$$

where $\Phi_{i+1,G}(\mu) = \Phi_G(r_{i+1}, \mu)$ and $\Phi_{i,G}(\mu) = \Phi_G(r_i,\mu)$. Substitution of Eq. 3.22 into Eq. 3.21 yields the following expression for the first term:

$$T_1 = 4\pi \int_{\mu\epsilon\Delta\mu_D} \mu r_{i+1}^2 \, \Phi_{i+1,G}(\mu)\, d\mu - 4\pi \int_{\mu\epsilon\Delta\mu_D} \mu r_i^2 \, \Phi_{i,G}(\mu)\, d\mu \, . \qquad (3.23)$$

It follows from the mean value theorem that any integral can be approximated by

$$\int_{x_1}^{x_2} x \, f(x)\, dx \cong \bar{x} \, f(\bar{x}) \, \Delta x \, , \qquad (3.24)$$

where $\Delta x = x_2 - x_1$ and $x_1 < \bar{x} < x_2$. The parameter $\bar{x}$ may be adjusted to give the equality; for well-behaved functions the closer $\bar{x}$ is to the true mean, the better the approximation. Applying the mean value theorem to Eq. 3.23 to evaluate the angular integrals results in

*The integration limits are expressed symbolically by $x\epsilon X$, which implies a definite integral with respect to the variable x over the interval X.

$$T_1 = 4\pi (\bar{\mu}_D\, r_{i+1}^2\, \Phi_{i+1,G,D}\, \Delta\mu_D - \bar{\mu}_D\, r_i^2\, \Phi_{i,G,D}\, \Delta\mu_D) ,$$

where $\Phi_{i,G,D} \equiv \Phi_{i,G}(\bar{\mu}_D)$ and $\bar{\mu}_D$ is a mean value approximation for the direction cosine over the direction increment $\Delta\mu_D$. Identifying the surface areas of the volume increment by

$$A_i = 4\pi r_i^2 , \quad A_{i+1} = 4\pi r_{i+1}^2 \tag{3.25}$$

yields the final form for the first term:

$$T_1 = \bar{\mu}_D\, \Delta\mu_D\, (A_{i+1}\, \Phi_{i+1,G,D} - A_i\, \Phi_{i,G,D}) . \tag{3.26}$$

The integral operator (Eq. 3.18) is next applied to the second term in Eq. 3.17 and the result rearranged:

$$T_2 = 4\pi \int_{r\epsilon V_I} \int_{\mu\epsilon\Delta\mu_D} r \frac{\partial}{\partial\mu} \left[(1-\mu^2) \times \int_{E\epsilon\Delta E_G} \Phi(r,E,\mu)\, dE \right] dr\, d\mu . \tag{3.27}$$

Defining the group angular flux as before, Eq. 3.27 becomes

$$T_2 = 4\pi \int_{r\epsilon V_I} r\, dr \int_{\mu\epsilon\Delta\mu_D} \frac{\partial}{\partial\mu} [(1-\mu^2) \times \Phi_G(r,\mu)]\, d\mu . \tag{3.28}$$

The integration over μ is accomplished according to the procedure suggested by Eq. 3.22 with the following result:

$$T_2 = 4\pi \left[\int_{r\epsilon V_I} (1-\mu_{d+1}^2)\, \Phi_{G,d+1}(r)\, r\, dr - \int_{r\epsilon V_I} (1-\mu_d^2)\, \Phi_{G,d}(r)\, r\, dr \right] . \tag{3.29}$$

The remaining integration over the radius variable is performed by using the mean value approximation (Eq. 3.24):

$$T_2 = 4\pi [(1-\mu_{d+1}^2)\, \Phi_{I,G,d+1}\, \bar{r}_I\, \Delta r_I - (1-\mu_d^2)\, \Phi_{I,G,d}\, \bar{r}_I\, \Delta r_I] , \tag{3.30}$$

where $\bar{r}_I$ is a mean value within the spatial increment $\Delta r_I = r_{i+1} - r_i$.

Equation 3.30 reduces to a two-point difference in the angle index

$$T_2 = B_{I,d+1}\, \Phi_{I,G,d+1} - B_{I,d}\, \Phi_{I,G,d} \tag{3.31}$$

if the curvature coefficient $B_{I,d}$ is defined by the expression

$$B_{I,d} \equiv 4\pi r_I\, \Delta r_I (1-\mu_d^2) . \tag{3.32}$$

Consistent with the conservation property of the technique, Eq. 3.30 or Eq. 3.31 gives an overall neutron balance. This is apparent since a summation of Eq. 3.30 over (NOA) direction increments $\Delta\mu_D$ yields

$$[(1-\mu_{NOA+1}^2)\, \Phi_{I,G,NOA+1} - (1-\mu_1^2)\, \Phi_{I,G,1}]$$

which, because $\mu_{NOA+1} = -1$ and $\mu_1 = +1$, is identically zero.

Equation 3.32, which defines the curvature coefficients, can be recast in the form of a recursion relation which involves the coefficients $B_{I,d+1}$ and $B_{I,d}$. First, $B_{I,d}$ is subtracted from $B_{I,d+1}$, where $B_{I,d}$ and $B_{I,d+1}$ are given by Eq. 3.32, yielding

$$B_{I,d+1} - B_{I,d} = -4\pi \bar{r}_I\, \Delta r_I (\mu_{d+1}^2 - \mu_d^2) . \tag{3.33}$$

It is assumed that $\bar{r}_I$ in Eq. 3.33 is the arithmetic mean, that is, that

$$\bar{r}_I = \frac{r_{i+1} + r_i}{2} .$$

Then it follows that

$$\bar{r}_I\, \Delta r_I = \frac{(r_{i+1}^2 - r_i^2)}{2} . \tag{3.34}$$

Following similar arguments, the factor $(\mu_{d+1}^2 - \mu_d^2)$ can be expressed as

$$(\mu_{d+1}^2 - \mu_d^2) = 2\bar{\mu}_D\, \Delta\mu_d . \tag{3.35}$$

Introducing Eqs. 3.34 and 3.35 into Eq. 3.33 yields the following recursion relation:

$$B_{I,d+1} - B_{I,d} = -4\pi (r_{i+1}^2 - r_i^2)\, \bar{\mu}_D\, \Delta\mu_D . \tag{3.36}$$

The final form for the recursion relation is obtained by introducing the cell areas A_{i+1} and A_i (see Eq. 3.25) and rearranging, with the result that

$$B_{I,d+1} = B_{I,d} - \bar{\mu}_D \, \Delta\mu_D (A_{i+1} - A_i) \, , \qquad (3.37)$$

where $B_{I,NOA+1} = B_{I,1} = 0$. Equation 3.37 is the form of the curvature coefficient found in the literature. The only approximation made in the preceding derivation is in the definition of mean values.

When the integral operator, Eq. 3.18, is applied to the fifth term of Eq. 3.17 (which is called the inscattering integral), the result is

$$T_5 = \int_{r \in V_I} \int_{E \in \Delta E_G} \int_{\mu \in \Delta\mu_D} \int_0^\infty \times \int_{-1}^{+1} \Sigma_s(r, E' \to E, \mu_0) \times \Phi(r, E', \mu') \, dE' \, d\mu' \, 4\pi r^2 \, dr \, dE \, d\mu \, . \qquad (3.38)$$

The differential scattering cross section can be approximated by a truncated Legendre polynomial expansion in the cosine of the scattering angle:

$$\Sigma_s(r, E' \to E, \mu_0) = \frac{1}{2} \sum_{n=0}^{N} \Sigma^n(r, E' \to E) \, P_n(\mu_0) \, , \qquad (3.39)$$

where the Σ^n's are Legendre coefficients of the expansion.

The Legendre polynomial $P_n(\mu_0)$ can be expressed in terms of the initial and final direction cosines by the addition theorem for Legendre polynomials, which for spherically symmetric geometry is simply

$$P_n(\mu_0) = P_n(\mu) \, P_n(\mu') \, . \qquad (3.40)$$

In adapting Eq. 3.38 to a multigroup calculation, the integrals over all incident energies and all incident angles are replaced by sums of integrals over the primed phase space cell. Symbolically this is denoted by

$$\int_0^\infty f(E') \, dE' = \sum_{G'=1}^{NOG} \int_{E' \in \Delta E_{G'}} f(E') \, dE' \, ,$$

$$\int_{-1}^{+1} f(\mu') \, d\mu' = \sum_{D'=1}^{NOA} \int_{\mu' \in \Delta\mu_{D'}} f(\mu') \, d\mu' \, , \qquad (3.41)$$

where NOG and NOA signify the number of energy groups and number of angular increments respectively.

Combining Eqs. 3.39 and 3.40 with Eq. 3.38, approximating the incident energy and angle integrals by Eq. 3.41, and evaluating all remaining integrals by the mean value approximation yields (after considerable rearrangement of terms) the following forms for the inscattering integral:

$$T_5 = \frac{V_I \, \Delta\mu_D}{2} \sum_{G'=1}^{NOG} \sum_{n=0}^{N} P_n(\bar{\mu}_D) \, \Sigma^{n,I}_{G' \to G} \sum_{D'=1}^{NOA} \Phi_{I,G',D'} \, P_n(\bar{\mu}_{D'}) \, \Delta\mu_{D'}$$

$$= \frac{V_I \, \Delta\mu_D}{2} \sum_{G'=1}^{NOG} \sum_{n=0}^{N} P_n(\bar{\mu}_D) \, \Sigma^{n,I}_{G' \to G} \, j^n_{I,G'} \, , \qquad (3.42)$$

where $\Sigma^{n,I}_{G' \to G}$ is the nth Legendre moment of the multigroup scattering cross section (multigroup macroscopic transfer coefficient), defined by

$$\Sigma^{n,I}_{G' \to G} \equiv \frac{\int_{r \in V_I} \int_{E \in \Delta E_G} \int_{E' \in \Delta E_{G'}} \Sigma^n(r, E' \to E) \int_{-1}^{+1} \Phi(r, E', \mu') \, P_n(\mu') \, dE' \, d\mu' \, r^2 \, dr \, dE}{\int_{r \in V_I} \int_{E' \in \Delta E_{G'}} \int_{-1}^{+1} \Phi(r, E', \mu') \, P_n(\mu') \, dE' \, d\mu' \, r^2 \, dr} \, , \qquad (3.43)$$

and $j^n_{I,G'}$ is the nth Legendre coefficient of the angular dependence of the flux, calculated from

$$j^n_{I,G'} = \sum_{D'=1}^{NOA} \Phi_{I,G',D'} P_n(\bar{\mu}_{D'}) \Delta\mu_{D'} . \quad (3.44)$$

Application of the integral operator (Eq. 3.18) to the removal term (third term) of Eq. 3.17 gives

$$T_3 = \int_{r\in V_I} \int_{E\in\Delta E_G} \int_{\mu\in\Delta\mu_D} \Sigma_t(r,E) \times \Phi(r,E,\mu)\, 4\pi r^2\, dr\, dE\, d\mu . \quad (3.45)$$

The evaluation of Eq. 3.45 requires some effort in order to avoid the assumption of angle-energy separability in the weighting of the multigroup cross sections. As the first step in evaluating Eq. 3.45 in terms of a cross section that is independent of angle, the energy integral of Eq. 3.45 is written as

$$T_3^E = \int_{E\in\Delta E_G} \Sigma_t(r,E)\, \Phi(r,E,\mu)\, dE = \Sigma_G^t(r)\, \Phi_G(r,\mu) - R , \quad (3.46)$$

where

R = correction factor that is to be determined,

$\Sigma_G^t(r)$ = flux-weighted group-G total cross section defined by

$$\Sigma_G^t(r) \equiv \frac{\int_{E\in\Delta E_G} \Sigma_t(r,E)\, j^0(r,E)\, dE}{\int j^0(r,E)\, dE} , \quad (3.47)$$

in which $j^0(r,E)$ is the zeroth Legendre coefficient of the angular dependence of the flux, which is identical to the differential flux $\Phi(r,E)$.

Rearrangement of Eq. 3.46 provides an explicit expression for R:

$$R = \Sigma_G^t(r)\, \Phi_G(r,\mu) - \int_{E\in\Delta E_G} \Sigma_t(r,E)\, \Phi(r,E,\mu)\, dE , \quad (3.48)$$

which has only a small effect when the energy group structure is reasonably fine.

The correction factor R is determined by expressing the angular fluxes as truncated Legendre series and then combining the two terms which comprise Eq. 3.48. The truncated Legendre series representation of the flux is

$$\Phi(r,E,\mu) \cong \sum_{n=0}^{N} \frac{2n+1}{2} j^n(r,E)\, P_n(\mu) . \quad (3.49)$$

When Eq. 3.49 is substituted into Eq. 3.48, the result is

$$R = \Sigma_G^t(r) \sum_{n=0}^{N} \frac{2n+1}{2} j^n_G(r)\, P_n(\mu) - \int_{E\in\Delta E_G} \Sigma_t(r,E) \times \sum_{n=0}^{N} \frac{2n+1}{2} j^n(r,E)\, P_n(\mu)\, dE ,$$

which can be written as

$$R = \sum_{n=0}^{N} \frac{2n+1}{2} \left[\Sigma_G^t(r) - \Sigma_G^{tn}(r) \right] j^n_G(r)\, P_n(\mu) , \quad (3.50)$$

where

$$j^n_G(r) = \int_{E\in\Delta E_G} j^n_G(r,E)\, dE ,$$

and the moments of the cross section are defined by

$$\Sigma_G^{tn}(r) \equiv \frac{\int_{E\in\Delta E_G} \Sigma_t(r,E)\, j^n(r,E)\, dE}{j^n_G(r)} . \quad (3.51)$$

Substitution of Eqs. 3.49 and 3.50 into Eq. 3.46 yields the final form for the energy integral:

$$T_3^E = \Sigma_G^t(r) \sum_{n=0}^{N} \frac{2n+1}{2} j^n_G(r)\, P_n(\mu) - \sum_{n=0}^{N} \frac{2n+1}{2} \left[\Sigma_G^t(r) - \Sigma_G^{tn}(r) \right] j^n_G(r)\, P_n(\mu) . \quad (3.52)$$

Using this form for the energy integral in Eq. 3.45, the remaining integrals are evaluated by the

mean value approximation, yielding

$$T_3 = V_I \Delta\mu_D \left[\Sigma^t_{I,G} \Phi_{I,G,D} - \sum_{n=0}^{N} \frac{2n+1}{2} \left(\Sigma^t_{I,G} - \Sigma^{tn}_{I,G} \right) j^n_{I,G} P_n(\bar{\mu}_D) \right] . \quad (3.53)$$

The series in Eq. 3.53 is very similar in form to the inscattering integral term (T_5) and may be included there by replacing $\Sigma^{n,I}_{G' \to G}$ in Eq. 3.42 with

$$\Sigma^{n,I\,(\mathrm{mod})}_{G' \to G} = \Sigma^{n,I}_{G' \to G} + (2n+1) \left(\Sigma^t_{I,G} - \Sigma^{tn}_{I,G} \right) \delta_{G,G'} , \quad (3.54)$$

where $\delta_{G,G'} = 1$ if $G' = G$ and $= 0$ if $G' \neq G$. The modified removal term then has the desired form

$$T_3 = V_I \Delta\mu_D \Sigma^t_{I,G} \Phi_{I,G,D} . \quad (3.55)$$

Application of the integral operator to the source term of Eq. 3.17 is straightforward since, with the exception of defining multigroup constants, the mean value approximation is used for all variables. The final result for a general fixed source is

$$T_4 = V_I \Delta\mu_D S_{I,G,D} . \quad (3.56)$$

If multiplication is present (eigenvalue problem),

$$S(r,E,\mu) = \frac{1}{k_{\mathrm{eff}}} \chi(E) \times \int_0^\infty \nu\Sigma_f(r,E') j^0(r,E') \, dE' , \quad (3.57)$$

which gives

$$T_4 = V_I \Delta\mu_D \frac{\chi_G}{k_{\mathrm{eff}}} \sum_{G'=1}^{NOG} \nu\Sigma^f_{I,G'} j^0_{I,G'} , \quad (3.58)$$

where

k_{eff} = effective multiplication constant of the system,

$\Sigma^f_{I,G'}$ = macroscopic fission cross section at energy G', within the spatial interval V_I,

ν = number of neutrons per fission by neutrons of energy G',

χ_G = fission spectrum defined by

$$\chi_G \equiv \int_{E \in \Delta E_G} \chi(E) \, dE ,$$

$$\nu\Sigma^f_{I,G'} = \frac{\int_{E' \in \Delta E_{G'}} \nu\Sigma^f_I(E') \, j^0_I(E') \, dE'}{j^0_{I,G'}} .$$

The discrete ordinates difference equation is obtained by substituting the derived expressions for each of the five terms into Eq. 3.17 and then dividing through by $\Delta\mu_D$. The result is

$$\bar{\mu}_D (A_{i+1} \Phi_{i+1,G,D} - A_i \Phi_{i,G,D}) + \frac{1}{\Delta\mu_D} (B_{I,d+1} \Phi_{I,G,d+1} - B_{I,d} \Phi_{I,G,d}) + V_I \Sigma^t_{I,G} \Phi_{I,G,D} = V_I S_{I,G,D} + \frac{V_I}{2} \times \sum_{n=0}^{N} P_n(\bar{\mu}_D) \sum_{G'=1}^{NOG} \Sigma^{n,I\,(\mathrm{mod})}_{G' \to G} \times \sum_{D'=1}^{NOA} \Phi_{I,G',D'} P_n(\bar{\mu}_{D'}) \Delta\mu_{D'} . \quad (3.59)$$

Although derived for spherical geometry, that is, for

$$A_i = 4\pi r_i^2 \text{ and } V_I = \frac{4\pi}{3} (r^3_{i+1} - r^3_i) ,$$

Eq. 3.59 is the general discrete ordinates difference equation for the one-dimensional geometries. The equations for the other geometries are obtained from Eq. 3.59 with $A_i = 1.0$ and $V_I = \Delta r_I$ for a slab and with $A_i = 2\pi r_i$ and $V_I = \pi(r^2_{i+1} - r^2_i)$ for a cylinder.

Numerical Solution of the Discrete Ordinates Equation. – Equation 3.59 contains discrete-flux variables having both centered and endpoint subscripts. This in effect increases the number of unknowns such that an insufficient number of determining relations are available for their solution. This difficulty can be resolved by relating the "centered" and "endpoint" fluxes in some consistent fashion. The diamond difference technique is the most widely used method for this purpose and includes two relationships for the spatial variable,

$$\Phi_{I,G,D} = A\Phi_{i+1,G,D} + (1 - A) \Phi_{i,G,D} , \quad \mu > 0 , \quad (3.60a)$$

and

$$\Phi_{I,G,D} = (1 - A)\ \Phi_{i+1,G,D} + A\Phi_{i,G,D}\ ,$$

$$\mu < 0\ , \quad (3.60b)$$

and a single expression for the angular variable,

$$\Phi_{I,G,D} = B\Phi_{I,G,d+1} + (1 - B)\ \Phi_{I,G,d}\ , \quad (3.61)$$

where A and B are constants which can be assigned values of the interval ($\frac{1}{2}$,1). When $A = B = \frac{1}{2}$, Eqs. 3.60*a* and 3.60*b* are the same for all values of μ and together with Eq. 3.61 are known as the "ordinary" diamond difference equations which can be rewritten as:

$$\Phi_{i+1,G,D} = 2\Phi_{I,G,D} - \Phi_{i,G,D},\ \bar{\mu}_D > 0\ , \quad (3.62a)$$

or

$$\Phi_{i,G,D} = 2\Phi_{I,G,D} - \Phi_{i+1,G,D},\ \bar{\mu}_D < 0\ , \quad (3.62b)$$

and

$$\Phi_{I,G,d+1} = 2\Phi_{I,G,D} - \Phi_{I,G,d}\ . \quad (3.63)$$

These equations form the basis for most current computer solutions. For a spatial sweep when $\bar{\mu}_D > 0$, Eqs. 3.59, 3.62*a*, and 3.63 are combined to provide the following explicit expression for the "centered" discrete ordinate flux, $\Phi_{I,G,D}$:

$$\Phi_{I,G,D} = \frac{\bar{\mu}_D(A_{i+1} + A_i)\,\Phi_{i,G,D} + \dfrac{1}{\Delta\mu_D}(B_{I,d+1} + B_{I,d})\,\Phi_{I,G,d} + V_I\,S'_{I,G,D}}{\bar{\mu}_D(2A_{i+1}) + \dfrac{2B_{I,d+1}}{\Delta\mu_D} + V_I\,\Sigma^t_{I,G}}\ , \quad (3.64)$$

where the source term $S'_{I,G,D}$ includes the fixed source and all inscattering sources. For a typical spatial mesh sweep ($\bar{\mu}_D > 0$), Eq. 3.64 would be used to solve for the centered flux $\Phi_{I,G,D}$. Then the endpoint fluxes $\Phi_{i+1,G,D}$ and $\Phi_{I,G,d+1}$ would be calculated by Eqs. 3.62*a* and 3.63 respectively. The next centered flux $\Phi_{I+1,G,D}$ is then calculated again using Eq. 3.64 and so on. If the flux is decreasing so rapidly that the centered flux $\Phi_{I,G,D}$ is less than one-half of either previous endpoint flux $\Phi_{i,G,D}$ or $\Phi_{I,G,d}$, then the newly calculated endpoint flux, $\Phi_{i+1,G,D}$ or $\Phi_{I,G,d+1}$, will be negative. This phenomenon is called "diamond difference breakdown" and will result in a meaningless positive-negative oscillation of the calculated fluxes. To remedy this, the calculation may be modified by refining the space and/or angle mesh, which would necessarily increase the computational time. However, most problems are reasonably well behaved except possibly for a few points. For this condition, a technique called "negative flux fix-up" could be employed. The troublesome fluxes are immediately recalculated using the "step" difference equations which always yield positive fluxes.

If $A = B = 1$ in Eq. 3.60*a*, 3.60*b*, and 3.61, the step function relationship is obtained which equates the centered fluxes to the appropriate endpoint fluxes. The "step" difference equations are:

$$\Phi_{i+1,G,D} = \Phi_{I,G,D}\ , \quad \bar{\mu}_D > 0, \quad (3.65a)$$

or

$$\Phi_{i,G,D} = \Phi_{I,G,D}\ , \quad \bar{\mu}_D < 0\ . \quad (3.65b)$$

and

$$\Phi_{I,G,d+1} = \Phi_{I,G,D}\ . \quad (3.66)$$

An explicit expression for the centered flux, $\Phi_{I,G,D}$ is obtained for the $\mu_D > 0$ spatial mesh sweep by substituting Eqs. 3.65*a* and 3.66 into Eq. 3.59, yielding

$$\Phi_{I,G,D} = \frac{\bar{\mu}_D\,A_i\,\Phi_{i,G,D} + \dfrac{1}{\Delta\mu_D}B_{I,d}\,\Phi_{I,G,d} + V_I\,S'_{I,G,D}}{\bar{\mu}_D\,A_{i+1} + \dfrac{B_{I,d+1}}{\Delta\mu_D} + V_I\,\Sigma^t_{I,G}}\ . \quad (3.67)$$

These difference equations would be solved by the same calculational sequence described earlier for the "ordinary" diamond difference equations. The step-function relationship is less accurate than the ordinary diamond difference scheme for the same mesh; however, it has the advantage of always giving positive fluxes for

positive sources and is used for the correction of negative fluxes, which occasionally occur with other diamond difference schemes.

The choice of the discrete directions plays an important role in the discrete ordinates or S_n method. It does not appear that a most accurate (or best) quadrature scheme for a specific problem can be selected *a priori*. The efficiency of a given set of discrete directions (quadrature set) depends on problem parameters such as geometry, optical thickness, energy group structure, spatial mesh size, etc., and a generalization of these dependencies is not possible.

The discrete directions and associated weights (which represent solid angle) define the quadrature used in the inscattering integral; the directions define the mean values for the angles, such as $\bar{\mu}_D'$, and thus affect the approximations in the convection term. In all S_n codes, the discrete directions are represented as points on the surface of a unit sphere located at the point in space for which the flux is to be defined and oriented in a fixed manner with respect to the coordinate system. The points or directions are located on the sphere in a reflective manner with respect to the three planes defining an octant such that the point description of one octant defines the whole sphere. This is not an absolute necessity but is usually required because of reflecting boundaries.

The more recent S_n codes allow specification of direction weights as well as the directions themselves. Carlson *et al.*[10] developed a rather elegant method of areas which computes directions and direction weights that are symmetric with respect to rotational interchange of the axes of the unit sphere. Although the directions and weights in the area method are somewhat adjustable, the best results occur with the recommended values, which satisfy various approximate moment conditions and asymptotic theories. The area method has the advantage of rotation symmetry and the important advantage of all positive weights for any order of S_n.

Although rotation reflection symmetry has desirable qualities, only three-dimensional calculations would benefit from full symmetry; two-dimensional problems thus require twofold symmetry, and one-dimensional problems require no symmetry conditions within the octant. Thus for one- and two-dimensional geometries and especially for problems in which other conditions outweigh the symmetry considerations, some liberty in choosing directions may be exercised.

Two commonly used angular segmentation methods, the Gauss-Legendre (P_{n-1}) method and the double Gauss-Legendre ($DP_{n/2-1}$) method are based on Gaussian quadrature. The directions for the P_{n-1} method are the n zeros of the Legendre polynomials of the first kind,

$$P_{n-1}(\mu_j) = 0 , \quad j = 1, 2, \ldots n ,$$

and the directions for the $DP_{n/2-1}$ quadrature are given by

$$\mu_k = \frac{\mu_j + 1}{2} , \quad \mu_k > 0 ,$$

$$\mu_k = \frac{\mu_j - 1}{2} , \quad \mu_k < 0 ,$$

where the μ_j's are the $n/2$ zeros of $P_{n/2-1}(\mu_j) = 0$. The directions defined by the $DP_{n/2-1}$ method are characteristically more dense about $\mu = 0$ than those of the P_{n-1} method.

For one-dimensional plane and spherical geometry, experience has shown that the P_{n-1} quadrature is well suited for deep-penetration problems. For thin shields involving isotropic plane or spherical shell sources, the double Gauss-Legendre quadrature is preferable. For specific problems, increased accuracy is usually obtained by using a higher-order Gaussian quadrature rather than by developing a special biased quadrature to exploit special characteristics of the problem.

In two-dimensional geometries or one-dimensional cylindrical geometry less experience is available on which to base the selection of the quadrature scheme. Good results have been obtained using quadratures that are designed to integrate specified orders of a spherical harmonic. In this method the direction set is left to be specified, and is often based on Gaussian zeroes or complete symmetry requirements. For specific problems increased accuracy is gained by using a proven quadrature to a higher order rather than by developing special biased sets. It is usually more expensive to develop and test a biased quadrature than to use the standard quadrature with a higher order.

A typical computer solution of the discrete ordinates problem is basically one of iterating the solution to some prescribed degree of convergence. The sweep of the mesh points is carefully ordered to "follow" the neutrons (or gamma rays). For shielding problems, all particles undergoing scattering will always degrade in energy. Therefore, the calculation will begin with the highest energy group (G = 1) and progress sequentially through the lower energy

groups. The angular sweep is performed in the direction of increasing D (decreasing $\bar{\mu}_D$) beginning with $D = 1$, which for most penetration problems corresponds to the most important direction. The spatial sweep begins at a boundary along which the inwardly directed flux values are specified and the sweep is made to the other boundary and then repeated for the next angle. The spatial sweep for negative $\bar{\mu}_D$ begins at the other boundary at which point the re-entrant fluxes are usually specified as zero and proceeds to the source boundary. After progressing through all angles at one energy, the next lower energy group is treated in a similar manner and so on.

In solving Eq. 3.64 or Eq. 3.67 for the centered flux $\Phi_{I,G,D}$ some of the required discrete ordinate fluxes have not yet been calculated; namely the "within group" scattering involves some as yet undetermined fluxes – those which correspond to angles $\bar{\mu}_{D'}$, where $D' \geqslant D$. Therefore the solution is obtained through the process of "inner iteration" whereby values for the unknown fluxes are taken as their previous iterate estimates. Details of the various iteration schemes and of the related convergence problem are omitted here but can be found in the descriptions of codes DTF IV,[8] ANISN,[9] and DOT.[11,12]

Advantages and Disadvantages. – From the results of calculations made with S_n codes, it appears that for shielding applications the discrete ordinates methods have the following advantages:

1. Depending somewhat on the sophistication desired, the S_n calculations are easy to prepare.

2. The method is not stochastic, and flux errors at deep penetration are systematic rather than statistical.

3. Production problems having similar characteristics benefit from knowledge of fluxes calculated in a similar case.

4. Secondary gamma rays may be calculated by the same method, either as a second calculation or simultaneously with the neutrons. The gamma-ray yield distribution may also be made a function of the energy of the captured neutron.

5. The range of neutron energies from highest fission energies to thermal, including upscattering, may be calculated by the same method.

6. The one-dimensional calculations are much faster (in computer time) than similar Monte Carlo calculations (see Section 3.5). In two dimensions the type of problem and the desired answers determine whether S_n or Monte Carlo is better.

The following disadvantages are evident, but additional development can alleviate or eliminate them:

1. Convergence of the iterative method is not always uniform and well defined. The best method currently used is to determine from each iteration the maximum error in the scalar flux at any point in space relative to the previous iterate value. Iterations proceed until the error falls below a specified limit.

2. Flux aberrations are frequently observed in two dimensions due to localized sources and the propagation of neutrons in discrete directions (the "ray" effect).

3. No basic ground rules exist which define for a particular problem the best direction set, space mesh, multigroup structure, and polynomial expansion limit.

3.4. Moments Method

Another technique that can be used to solve the Boltzmann transport equation is the moments method. This method has some important advantages not shared by other methods, one being that foreknowledge about the behavior of the solution can be incorporated analytically in a very natural way, thereby often reducing the effort required to achieve a specific result and/or a desired accuracy. Another is that the type of recursion relation developed precludes a truncation at a crucial part of the calculation; that is, a finite number of moments may be calculated exactly (ignoring errors due to the numerical solution) without considering the influence of higher moments.

In a discussion of the moments method it is perhaps most instructive to first consider the formal definition for the moments and the manner in which they relate to a system parameter of interest, $f(x)$. If $f(x)$ is defined for all x within the interval $A \leqslant x \leqslant B$, then the nth moment of $f(x)$ is

$$M_n = \int_A^B x^n f(x)\, dx \,, \tag{3.68}$$

provided that the integral exists. Only nonnegative integral values of n are considered in practical applications.

Definite interpretations may be associated with the various moments. For example, the zeroth moment is a normalizing number, and the first, second, third, and fourth moments are closely related to the mean value, variance, skewness, and kurtosis respectively. In the physics of statics and dynamics the first moment of the mass is the center of gravity and the second is the moment of inertia.

No such particular meanings are given to the moments as they are used in the solution of radiation transport problems (except for the second moment which is proportional to the Fermi age). Rather, they may be regarded as a transform, much the same as Laplace, Fourier, or finite trigonometric transforms. The major portion of the calculation is performed in terms of the transform (moments) space; then, by an appropriate inversion, the desired answer of interest is reconstructed from the moments.

The application of the moments method to the solution of the Boltzmann transport equation is limited with respect to the geometrical configuration of the problem. It is usually applied only to infinite homogeneous media with plane, line, or point sources. The method as applied to gamma rays has been described by Goldstein and Wilkins,[14] and by Fano *et al.*,[15] and as applied to neutrons by Goldstein,[16] Certaine,[17] and Aronson *et al.*[18,19] A summary of neutron results has been given by Krumbein.[20] Applications of moments method results to fallout shelter design have been developed by Spencer, Eisenhauer *et al.*[21,22] The technique is basically the same for both neutrons and gamma rays and a description for one should suffice for the other. The most significant differences lie in the treatment of the scattering integral and in the more complex nature of the neutron cross sections. The description presented below is for slab geometry in terms of the simpler gamma-ray problem, in which the dependent variable is the angular energy flux $I(x,\lambda,\omega)$, and the Compton wavelength is taken as the energy variable.

Consider the following specialized form of the Boltzmann equation:

$$\omega \frac{\partial I}{\partial x} + \mu(\lambda)\, I(x,\lambda,\omega) = \int_{\lambda_0}^{\lambda} \int_{4\pi} I(x,\lambda',\omega')\, Nk(\lambda',\lambda)\, \frac{\delta(1+\lambda'-\lambda-\bar{\Omega}\cdot\bar{\Omega}')}{2\pi}\, d\bar{\Omega}'\, d\lambda' + S(\lambda,\omega)\, \delta(x) \,, \tag{3.69}$$

where

$I(x,\lambda,\omega)\, dE\, d\omega$ = energy flux (MeV per unit area and time) due to gamma rays with energies in dE about E and direction cosines which lie in $d\omega$ about ω,

x = spatial coordinate in slab geometry,

λ = gamma-ray wavelength after scattering expressed in Compton wavelength units,

λ' = gamma-ray wavelength prior to scattering,

λ_0 = gamma-ray wavelength corresponding to the source energy E_0,

ω = direction cosine with respect to x axis,*

$\mu(\lambda)$ = total macroscopic cross section evaluated at the energy corresponding to the gamma-ray wavelength λ,

$\overline{\Omega}\cdot\overline{\Omega}'$ = cos θ, cosine of the scattering angle between initial and final gamma-ray directions, where $\overline{\Omega}'$ and $\overline{\Omega}$ are the initial and final unit direction vectors respectively,

N = electron density,

$k(\lambda',\lambda) = 2\pi \frac{\lambda}{\lambda'} \sigma(\lambda',\theta)$,

$\sigma(\lambda',\theta)$ = cross section per electron for Compton scattering given by the well-known Klein-Nishina formula (see Chapt. 2, Sect. 2.7.3),

$\delta(x)$ = Dirac delta function, which has the property

$$\int_a^b f(x)\ \delta(x - X)\ dx = f(X)$$

for $a < X < b$ and locates the plane source at $x = 0$,

$\delta(1 + \lambda' - \lambda - \overline{\Omega}\cdot\overline{\Omega}')$ = Dirac delta function which prescribes that the angular change $(\overline{\Omega}' \to \overline{\Omega})$ be consistent with the change in wavelength $(\lambda - \lambda')$ as given by the Compton scattering equation, $\lambda - \lambda' = 1 - \overline{\Omega}\cdot\overline{\Omega}'$,

$S(\lambda,\omega)\ dE\ d\omega$ = plane source of gamma rays (energy emission per unit area and time of gamma rays with energies in dE about E and direction cosines which lie in $d\omega$ about ω).

Solving Eq. 3.69 by the moments method is similar to the spherical harmonics treatment (see Section 3.2) in that the angular energy flux is first expanded as a Legendre polynomial series:

$$I(x,\lambda,\omega) = \sum_{j=0}^{\infty} \frac{2j+1}{2} I_j(x,\lambda)\ P_j(\omega)\ , \quad (3.70)$$

where the $P_j(\omega)$'s are the Legendre polynomials and the coefficients of the expansion are given by

$$I_j(x,\lambda) = \int_{-1}^{+1} I(x,\lambda,\omega)\ P_j(\omega)\ d\omega\ . \quad (3.71)$$

It can be shown that $I_0(x,\lambda)$ is the energy flux and that $I_1(x,\lambda)$ is the energy current.

With this series representation for the angular energy flux, the integrodifferential equation (Eq. 3.69) with the dependent variable $I(x,\lambda,\omega)$ and three continuous independent variables can be transformed into a sequence of integrodifferential equations for the variables $I_j(x,\lambda)$, which are dependent on only two independent variables. This desired result is obtained by multiplying Eq. 3.69 by $P_j(\omega)\,d\omega$ and integrating with respect to ω over the interval $(-1,+1)$, yielding (after some manipulation) the following sequence of equations:

$$\frac{j+1}{2j+1}\frac{\partial I_{j+1}}{\partial x} + \frac{j}{2j+1}\frac{\partial I_{j-1}}{\partial x} + \mu(\lambda)\ I_j(x,\lambda)$$

$$= S_j(\lambda)\ \delta(x) + \int_{\lambda_0}^{\lambda} P_j(1 + \lambda' - \lambda) N k(\lambda',\lambda)\ I_j(x,\lambda')\ d\lambda'\ , \quad j = 0,1,2,\ldots\infty\ . \quad (3.72)$$

*The cosine of the polar angle is denoted by the symbol ω rather than by μ as is the general practice throughout the chapter. This was done to allow the use of the standard notation $\mu(\lambda)$ for the total macroscopic cross section for gamma rays of wavelength λ.

In the actual calculation, the number of Legendre coefficients will be determined by the accuracy requirements for the calculation of the moments of the Legendre coefficients and the exactness in the angular representation as implied by Eq. 3.70 will not be preserved.

Elimination of the spatial variable in this sequence of equations is accomplished by the generation of the moments of the Legendre coefficients of the angular energy flux, which are defined as

$$b_{nj}(\lambda) \equiv \frac{\mu_0^{n+1}}{n!} \int_{-\infty}^{+\infty} I_j(x,\lambda)\, x^n\, dx\ , \quad (3.73)$$

or

$$b_{nj}(\lambda) \equiv \frac{1}{n!} \int_{-\infty}^{+\infty} I_j(\rho,\lambda)\, \rho^n d\rho\ ,$$

where μ_0 is the total macroscopic cross section evaluated at the source energy and $\rho = \mu_0 x$ is the number of mean free paths. The equations satisfied by $b_{nj}(\lambda)$ are obtained by multiplying Eq. 3.72 by $\mu_0^{n+1}\, x^n/n!\, dx$ and integrating with respect to x from $-\infty$ to $+\infty$. It is because of this integration over all space that the application of the moments method to the transport problem becomes inextricably restricted to the infinite-medium geometry. Using Eq. 3.73 permits the original Boltzmann equation to be reduced to the following doubly indexed sequence of linear integral equations of the Volterra type:

$$\mu(\lambda)\, b_{nj}(\lambda) = \int_{\lambda_0}^{\lambda} N\, k(\lambda',\lambda)\, P_j(1+\lambda'-\lambda)\, b_{nj}(\lambda')\, d\lambda' + \frac{\mu_0}{2j+1}\left[(j+1)\, b_{n-1,j+1} + j b_{n-1,j-1}\right] + \mu_0\, S_j(\lambda)\, \delta_{n0}\ , \quad (3.74)$$

where $j = 0,1,2,\ldots\infty$, and $n = 0,1,2,\ldots\infty$. The Kronecker delta function $\delta_{n0} = 1$ if $n = 0$ and $= 0$ if $n \neq 0$.

The evaluation of the moments for a given problem can be accomplished by a rather straightforward numerical solution of Eq. 3.74. The ease of numerical calculation depends on the form of the source function $S_j(\lambda)$. Many problems involve monoenergetic sources and the $S_j(\lambda)$'s are given by $\lambda_0 S_j\, \delta(\lambda - \lambda_0)$. Since the presence of the delta function is undesirable for machine calculation, the following transformation is made:

$$b_{nj}(\lambda) = B_{nj}(\lambda) + \lambda_0 \delta(\lambda - \lambda_0) C_{nj}\ . \quad (3.75)$$

Introducing the transformation defined by Eq. 3.75 into Eq. 3.74 yields the defining equations for B_{nj} and C_{nj}:

$$\mu B_{nj} = \int_{\lambda_0}^{\lambda} N k(\lambda',\lambda)\, P_j(1+\lambda'-\lambda)\, B_{nj}(\lambda')\, d\lambda' + \frac{\mu_0}{2j+1}\left[(j+1)\, B_{n-1,j+1} + j B_{n-1,j-1}\right] + \lambda_0 k(\lambda_0,\lambda)\, P_j(1+\lambda_0-\lambda)\, C_{nj}\ , \quad (3.76)$$

and

$$\mu C_{nj} = \mu_0 \left(\frac{j+1}{2j+1} C_{n-1,j+1} + \frac{j}{2j+1} C_{n-1,j-1}\right) + \mu_0 S_j\, \delta_{n0}\ . \quad (3.77)$$

The equations that define C_{nj} are similar in form to the equations that define b_{nj} and B_{nj} except that the inscattering integral does not appear, which suggests that all collisions are considered to be removals. It follows that $\lambda_0\, \delta(\lambda - \lambda_0)\, C_{nj}$ must be the moments for the unscattered energy flux. Therefore the transformation given by Eq. 3.75 separates the unscattered energy flux (energy flux corresponding to C_{nj}) from the total energy flux (energy flux corresponding to b_{nj}). The solution to Eq. 3.76 requires values of C_{nj} as input and the calculated moments B_{nj} are associated only with the scattered energy flux. This is convenient since the uncollided angular energy flux $I^0(x,\lambda,\omega)$ is easily calculated and values of C_{nj} are then uniquely determined.

For a typical calculation, the quantity of greatest interest is the total, or scalar, energy flux $I_0(x,\lambda)$. Therefore for this case only the moments B_{n0} ($n = 0,1,2,\ldots N$) are required. However, the calculation of a given B_{nj} requires the prior calculation of $B_{n-1,j+1}$ and $B_{n-1,j-1}$; therefore moments other than B_{n0} moments must be calculated. In general the moments B_{0j} ($j = 0,1,2,\ldots J$) can be calculated directly, while a B_{nj} moment cannot be calculated until calculations have been made of all the $B_{n'j'}$'s for which $(n+j)-(n'+j')$ is a nonnegative even integer (including zero) and $n' < n$. Table 3.2 illustrates a typical calculation sequence (for $N = 5$). It is noted that all the moments shown in the table must be calculated in order to determine the B_{n0}'s for $n \leq 5$.

Table 3.2. Sequence of Moments Calculation for $N = 5$

n	B_{nj}					
	$j = 0$	$j = 1$	$j = 2$	$j = 3$	$j = 4$	$j = 5$
0	B_{00}	B_{01}	B_{02}	B_{03}	B_{04}	B_{05}
1	B_{10}	B_{11}	B_{12}	B_{13}	B_{14}	
2	B_{20}	B_{21}	B_{22}	B_{23}		
3	B_{30}	B_{31}	B_{32}			
4	B_{40}	B_{41}				
5	B_{50}					

Since Eq. 3.76 is a Volterra type of integral equation, it can be written as

$$\mu(\lambda_i)\, v(\lambda_i) = \int_{\lambda_0}^{\lambda_i} H(\lambda_i,\lambda')\, v(\lambda')\, d\lambda' + T(\lambda_i)\,, \qquad (3.78)$$

where

$$\lambda_i = \lambda_0 + i\Delta\lambda\,,$$

$\Delta\lambda$ = arbitrary increment of wavelength,

$$v(\lambda_i) = B_{nj}(\lambda_i)\,,$$

$$H(\lambda_i,\lambda') = Nk(\lambda',\lambda_i)\, P_j(1 + \lambda' - \lambda_i)\,,$$

$$T(\lambda_i) = \frac{\mu_0}{2j+1}\left[(j+1)\, B_{n-1,j+1} + jB_{n-1,j-1}\right] + \lambda_0 H(\lambda_i,\lambda_0)\, C_{nj}\,.$$

The Volterra equation is characterized by (1) the limit of integration being the independent variable λ_i, (2) the value of the dependent variable $v(\lambda_i)$ depending on the values of $v(\lambda')$ if $\lambda' < \lambda_i$ but not for $\lambda' > \lambda_i$, and (3) $T(\lambda_i)$ involving only known or previously calculated quantities. A numerical evaluation of the integral is required, for which several schemes are available. Regardless of which scheme is employed, there are coefficients M_{ik} such that Eq. 3.78 can be rewritten as

$$\mu(\lambda_i)\, v(\lambda_i) = \sum_{k=0}^{i-1} H(\lambda_i,\lambda_k)\, v(\lambda_k)\, M_{ik} + H(\lambda_i,\lambda_i)\, v(\lambda_i)\, M_{ii} + T(\lambda_i)\,, \qquad (3.79)$$

where

$$H(\lambda_i,\lambda_i) = k(\lambda_i,\lambda_i)\, P_j(1 + \lambda_i - \lambda_i) = {}^3\!/_4\,. \qquad (3.80)$$

The trapezoidal rule is used for the $(i = 1)$ interval in which $M_{ii} = \Delta\lambda/2$ and the following explicit expression for $v(\lambda_1)$ is obtained:

$$v(\lambda_1) = \frac{T(\lambda_1) + H(\lambda_1,\lambda_0)\, v(\lambda_0)\,(\Delta\lambda/2)}{\mu(\lambda_1) - (3\Delta\lambda/8)}\,. \qquad (3.81)$$

For $i > 1, M_{ii} = \Delta\lambda/3$ and Eq. 3.79 can be rewritten as

$$v(\lambda_i) = \frac{T(\lambda_i) + \sum_{k=0}^{i-1} H(\lambda_i,\lambda_k)\, v(\lambda_k)\, M_{ik}}{\mu(\lambda_i) - (\Delta\lambda/4)}\,. \qquad (3.82)$$

The coefficients M_{ik} for i even are determined by Simpson's rule; for $i = 3$, the coefficients used are $M_{30} = {}^5\!/_{16}, M_{31} = 1$, and $M_{32} = {}^5\!/_4$ and for i odd but greater than three, the integral from λ_0 to λ_3 is evaluated using the special $(i = 3)$ coefficients, and the integral from λ_3 to λ_i is evaluated by Simpson's rule.

The gamma-ray scattering process is such that

$$H(\lambda_i,\lambda_k) = 0 \text{ when } \lambda_i > \lambda_k + 2 . \quad (3.83)$$

Therefore the sums on the index k involve only a fixed number of terms. Also,

$$H(\lambda_i,\lambda_0) = 0 \text{ when } \lambda_i > \lambda_0 + 2 , \quad (3.84)$$

and the second term in $T(\lambda_i > \lambda_0 + 2)$ vanishes. The $H(\lambda_i,\lambda_k)$ can be calculated directly, since only the Klein-Nishina formula and the Legendre polynomials are involved.

At this point it is presumed that the required moments for a given problem can be calculated, and the reconstruction of the fluxes from the moments is desired. It should be emphasized that the calculation to this point can be performed with very few approximations, excluding the approximations involved in the numerical procedures. The major source of error will lie in the subsequent reconstruction process since only a finite number of moments are available. In fact, for a finite number of moments there is an infinite number of allowable functions. The problem is basically one of choice: the selection of a functional form that will come as close as possible to describing the spatial dependence of $I_j(x,\lambda)$ while possessing a reasonably simple relationship to the available moments.

Two methods have been used to reconstruct the fluxes: the polynomial expansion method and the method of undetermined parameters. The polynomial expansion method assumes that $I_j(\rho,\lambda)$ behaves roughly as some trial function $f(\rho)$, where ρ is measured in mean free paths at the initial energy; i.e., $\rho \equiv \mu_0 x$. Then

$$I_j(\rho,\lambda) = f(\rho)\, g_j(\rho,\lambda) , \quad (3.85)$$

where $g_j(\rho,\lambda)$ contains the λ dependence of the jth coefficient and provides a correction for the ρ dependence. If a reasonable choice of $f(\rho)$ can be made, then $g_j(\rho,\lambda)$ need be only a gently varying smooth function of ρ, for example, a polynomial of degree N in ρ when $(N + 1)$ moments are available. The $g_j(\rho,\lambda)$ could be represented as an infinite series with respect to a set of orthogonal polynomials of degree n:

$$g_j(\rho,\lambda) = \sum_{n=0}^{\infty} A_{nj}(\lambda)\, p_n(\rho) . \quad (3.86)$$

The orthogonality relationship is given by

$$\int_{-\infty}^{+\infty} p_n(x)\, p_m(x)\, f(x)\, dx = \delta_{nm} , \quad (3.87)$$

where $f(x)$ is a weighting function as well as the trial function $f(\rho)$.

In practice, the representation of $g_j(\rho,\lambda)$ is limited to a finite number of terms since only $(N + 1)$ values of A_{nj} can be evaluated, given $(N + 1)$ moments. The approximation for $I_j^s(\rho,\lambda)$ can then be written as

$$I_j^s(\rho,\lambda) = f(\rho) \sum_{n=0}^{N} A_{nj}(\lambda)\, p_n(\rho) , \quad (3.88)$$

where $I_j^s(\rho,\lambda)$ is the jth Legendre coefficient of the scattered component of the angular flux. This assumes that values of $(N + 1)$ moments B_{nj} are available for the reconstruction of $I_j^s(\rho,\lambda)$.

The reconstruction is accomplished by evaluating the $(N + 1)$ coefficient A_{nj} in terms of the known $(N + 1)$ moments B_{nj} for a given value of j. To this end, $I_j^s(\rho,\lambda)$ is multiplied by $p_n(\rho)\, d\rho$ and the product is integrated from $-\infty$ to $+\infty$ yielding:

$$A_{nj}(\lambda) = \int_{-\infty}^{+\infty} I_j^s(\rho,\lambda)\, p_n(\rho)\, d\rho . \quad (3.89)$$

The polynomial $p_n(\rho)$ can be written as

$$p_n(\rho) = \sum_{i=0}^{n} a_i \rho^i , \quad (3.90)$$

where the a_i's are known parameters for a given type of polynomial. The expression for $A_{nj}(\lambda)$ then becomes

$$A_{nj}(\lambda) = \sum_{i=0}^{n} a_i \int_{-\infty}^{+\infty} I_j^s(\rho,\lambda)\, \rho^i\, d\rho . \quad (3.91)$$

The moments B_{ij} are defined as

$$B_{ij}(\lambda) \equiv \frac{1}{i!} \int_{-\infty}^{+\infty} I_j^s(\rho,\lambda)\, \rho^i\, d\rho . \quad (3.92)$$

Elimination of the integrals between the above expressions for $A_{nj}(\lambda)$ and $B_{ij}(\lambda)$ provides the desired relationship

$$A_{nj}(\lambda) = \sum_{i=0}^{n} (i!)\, a_i B_{ij} . \quad (3.93)$$

Practical considerations will usually restrict accurate calculation to the differential energy flux, $I_0^s(\rho,\lambda)$, and then only the $A_{n0}(\lambda)$'s are required; that is

$$I_0^s(\rho,\lambda) = f(\rho) \sum_{n=0}^{N} A_{n0}(\lambda)\, p_n(\rho) , \quad (3.94)$$

where

$$A_{n0}(\lambda) = \sum_{i=0}^{n} (i!)\, A_i B_{i0} \ .$$

In principle, $A_{nj}(\lambda)$ for $j > 0$ can be calculated. However, since the angular flux $I(\rho,\lambda,\omega)$ is usually highly peaked in the forward direction, the series

$$I^s(\rho,\lambda,\omega) = \sum_{j=0}^{J} \frac{2j+1}{2} I_j^s(\rho,\lambda)\, p_j(\omega) \qquad (3.95)$$

converges slowly, thereby requiring a large number of values of $I_j^s(\rho,\lambda)$, which in turn would require an unreasonably large number of moments. Finally, the scattered and unscattered energy fluxes are easily combined for most simple geometries:

$$I_0(\rho,\lambda) = I_0^0(\rho,\lambda) + I_0^s(\rho,\lambda) \ . \qquad (3.96)$$

The polynomial expansion method described above is most often used for reconstructing the energy flux of the gamma-ray problem. This is partly for historical reasons and partly due to the ability of the method to make full use of large numbers of moments within the same systematic framework of analysis. For the neutron problem the selection of a suitable weighting (or test) function is not obvious and the method loses much of its flexibility.

In using the method of undetermined parameters to reconstruct the fluxes, $I_j(\rho,\lambda)$ is represented as

$$I_j(\rho,\lambda) = \sum_i a_{ij}(\lambda)\, h_{ij}(\rho) \ , \qquad (3.97)$$

where $h_{ij}(\rho)$ is a function having the general expected behavior of $I_j(\rho,\lambda)$ but containing one or more undetermined parameters, and a_{ij} is an undetermined parameter which includes the λ dependence. In particular, let $j = 0$ and assume that $(N + 1)$ values of the $B_{n0}(\lambda)$ moments are known; then

$$I_0^s(\rho,\lambda) = \sum_i a_{i0}(\lambda)\, h_{i0}(\rho) \ . \qquad (3.98)$$

The moments corresponding to $j = 0$ can be written as

$$B_{n0}(\lambda) = \frac{1}{n!} \int_{-\infty}^{+\infty} I_0^s(\rho,\lambda)\, \rho^n \, d\rho \ ,$$

$$n = 0, 1, 2, \ldots N \ . \qquad (3.99)$$

Substituting Eq. 3.98 into 3.99 yields the following set of $(N+1)$ equations:

$$B_{n0}(\lambda) = \frac{1}{n!} \sum_i a_{i0}(\lambda) \int_{-\infty}^{+\infty} h_{i0}(\rho)\, \rho^n \, d\rho \ ,$$

$$n = 0,1,2,\ldots N \ . \qquad (3.100)$$

The $h_{i0}(\rho)$'s should be selected so that the above integration can be evaluated either analytically or numerically, and if $(N + 1)$ moments are available, then a total of $(N+1)$ undetermined parameters are allowed.

Problems not amenable to other methods can sometimes be solved by the method of undetermined parameters because of the much greater choice that can be made in the $h_{ij}(\rho)$'s. As a result this method has been more widely applied to the neutron penetration problem. A characteristic of the method is that when it fails it usually fails catastrophically, leaving no doubt about its applicability. Usually not all of the moments available are needed to obtain a satisfactory solution. The surplus moments can be used to check the accuracy by constructing moments corresponding to the unused moments, a feature not so easily accomplished by the other method.

3.5. Monte Carlo Method

A fourth technique which can be applied to the solution of the Boltzmann transport equation is the Monte Carlo method. The Monte Carlo method is a mathematical technique used to estimate a desired average quantity by random sampling from the probabilities describing the true stochastic processes. The "stochastic process" refers to those phenomena in which quantities assume different values at different times and may be represented as a family of "random variables" which fluctuate in time.

Many types of problems in physics and mathematics can be solved successfully by random sampling or stochastic techniques.[23-26] For the radiation transport problem, this normally involves a simulation of the behavior (random walk) of individual radiation particles. With sufficient sampling it is assumed that the average value obtained is an accurate estimate of the quantity being calculated.

Random Variable. – Consider some independent variable, x, which assumes values over the interval $(-\infty, +\infty)$ or (a,b). Let ξ designate any particular value of the independent variable; this quantity will be referred to as the random variable of the independent variable x. The physical situation will determine the probability that ξ assumes some particular value, x_i, or that ξ lies within some interval Δx_i.

Random Number. – A set of numbers over some interval such as (0,1) constitutes a set of random numbers if they are uniformly distributed over the interval and if no correlation exists within a randomly selected sequence of these numbers. A rigorous definition of the random number is that the probability of it (the random number) being selected from an interval y contained in the interval (0,1) is simply y.

In actual practice there are computational algorithms adapted to digital computers that generate random numbers. However, these numbers are not truly random and are therefore more descriptively called pseudo-random numbers. Consider for example the mixed congruential method in which the sequence of random numbers is generated according to the algorithm

$$x_i \equiv (a\,x_{i-1} + c)\ (\text{modulo } m)^* , \qquad (3.101)$$

where

m = a large integer which is 2^y for a binary machine and 10^x for a decimal computer,

a,c = integers between 0 and $m-1$,

x_{i-1} = previously calculated random number.

With $c \equiv 0$, the following special form, called the multiplicative congruential method, is obtained:

$$x_i = a\,x_{i-1}\ (\text{modulo } m) . \qquad (3.102)$$

For the latter method, typical values for a and m are 5^{15} and 2^{35} respectively, and the resulting equation, $x_i = 5^{15}\,x_{i-1}$ (modulo 2^{35}), has been used by the Oak Ridge National Laboratory to generate random numbers. The number 2^{35} came into use since the computer being used had 36 binary bits in the machine word.

It is most important to ensure that the period of the pseudo-random number sequence is longer than the total number of random numbers required for a given calculation. If the mixed congruential method is used, a full period of m pseudo random numbers can always be achieved with the proper choice of a, c, and m. Using the multiplicative congruential method, the period will always be less than m; however, with the proper choices for a and m, a useful period of $m/4$ can be achieved.

Probability Distributions. – If ξ is a random variable of the independent variable x, then $F(x) = P(\xi \leqslant x)$ is defined for every x and can be interpreted as the probability that ξ assumes a value less than or equal to x. This function is commonly referred to as the cumulative distribution function (cdf) and it possesses the following properties:

1. $F(x)$ is a nondecreasing function of x.
2. $F(x)$ is continuous from the right at a discontinuity.

*The notation $x \equiv y$ (mod m) is read "x is congruent to y modulo m" and means x is the remainder of y upon division by m, $0 \leqslant x < m$.

3. If the variable x is a real number, then $F(-\infty) = 0$ and $F(+\infty) = 1$.

4. The probability that the random variable assumes a value within a finite interval (x_1, x_2) is given by

$$P(x_1 < \xi \leqslant x_2) = F(x_2) - F(x_1) .$$

5. If the derivative $dF(x)/dx$ exists at x, then for a small interval Δx about x, the probability that the random variable assumes a value within Δx is approximated by

$$\lim_{\Delta x \to 0} P\left(x - \frac{\Delta x}{2} < \xi \leqslant x + \frac{\Delta x}{2}\right) \cong \frac{dF(x)}{dx} \Delta x .$$

The derivative of the cdf is denoted as $f(x)$ and is equal to the relative frequency of the random variable ξ per unit x about x. This function is usually called the "probability density function" (pdf) of the independent variable x. The pdf is related to its corresponding cdf by

$$f(x) = \frac{dF(x)}{dx} \tag{3.103}$$

or

$$F(x) = \int_{-\infty}^{x} f(x')\, dx' . \tag{3.104}$$

If $f(x) = 0$ for $x < a$ and $x > b$, then $f(x)$ must be a normalized function over the interval (a,b):

$$\int_a^b f(x')\, dx' = 1 , \tag{3.105}$$

where

$$F(a) = 0,$$
$$F(b) = 1 .$$

Also, since $F(x)$ is nondecreasing, $f(x)$ must be nonnegative over the (a,b) interval:

$$f(x) \geqslant 0 \text{ for } a \leqslant x \leqslant b .$$

For more than one independent variable (for example, two variables) the joint cumulative distribution function is given by

$$F(x,y) \equiv P(\xi \leqslant x,\ \eta \leqslant y) , \tag{3.106}$$

which is the probability that the random variables ξ and η are less than or equal to x and y respectively. The corresponding joint probability density function is defined as

$$f(x,y) \equiv \frac{\partial^2 F(x,y)}{\partial x\, \partial y} , \tag{3.107}$$

where $f(x,y)\ \Delta x\ \Delta y$ approximates the probability that the event

$$\left(x - \frac{\Delta x}{2} < \xi \leqslant x + \frac{\Delta x}{2}, y - \frac{\Delta y}{2} < \eta \leqslant y + \frac{\Delta y}{2}\right)$$

occurs.

Sampling Techniques. – A very important phase of a Monte Carlo calculation is the selection of random variables according to the appropriate pdf or related cdf. Consider two independent variables x and y and their corresponding distributions $F(x)$ and $G(y)$. If the two cdf's assume the same values, that is, if

$$F(x) = G(y) ,$$

then $\xi \leqslant x$ only if $\eta \leqslant y$. This follows since the cdf's are, among other things, monotonically increasing functions. Therefore a distribution of random variables can be determined which conform to the cdf $F(x)$ given a realization of another cdf $G(y)$:

$$F(x_i) = G(y_i), \quad i = 1,2,...N .$$

Since random numbers can be generated with ease by a computer, a convenient choice for $G(y)$ is

$$G(y) = 0,\ y \leqslant 0 ,$$

$$G(y) = y,\ 0 \leqslant y \leqslant 1 ,$$

$$G(y) = 1,\ y \geqslant 1 .$$

The distribution $G(y)$ is realized by the generation of numbers R_i uniform over the interval (0,1) and the desired random variables x_i calculated from

$$F(x_i) = \int_{-\infty}^{x_i} f(x')\, dx' = R_i,\ i = 1,2 \ldots N . \tag{3.108}$$

In principle, the previous method of sampling yields a random variable x_i for each random number R_i. However some difficulties may arise in the execution of the inverse process, $x_i = F^{-1}(R_i)$. As an alternative it is always possible to use the "rejection" method, which, although a direct approach, involves a less efficient procedure since not all samples are used. Consider the pdf $f(x)$ which is bounded over the interval (a,b); that is, it assumes some maximum value $f(x_m)$ at $x = x_m$ as

shown in the upper portion of Fig. 3.1. Define a modified distribution $f_1(x)$ such that $f_1(x_m) = 1$,

$$f_1(x) = \frac{f(x)}{f(x_m)}, \tag{3.109}$$

and express the independent variable as $x = a + R(b - a)$ where R is a random number. The procedure is to generate random numbers in pairs (R_{2i-1}, R_{2i}) for each sample attempted. The combination (R_{2i-1}, R_{2i}) is interpreted as defining a point $[a + R_{2i-1}(b - a), R_{2i}]$ with uniform probability of occurrence anywhere within the rectangle which circumscribes $f_1(x)$, as shown in Fig. 3.1*b*. If the point (x_i, R_{2i}) falls under the curve $f_1(x)$, the random variable x_i is generated. If it falls above the curve (shaded area), the sample is rejected. The procedure for the ith sample is

1. Select two random numbers (R_{2i-1}, R_{2i}).
2. Calculate x_i; $x_i = a + R_{2i-1}(b - a)$.
3. Evaluate $f_1(x_i)$.
4. Test $f_1(x_i) \geq R_{2i}$; if yes, accept sample; if no, reject sample.

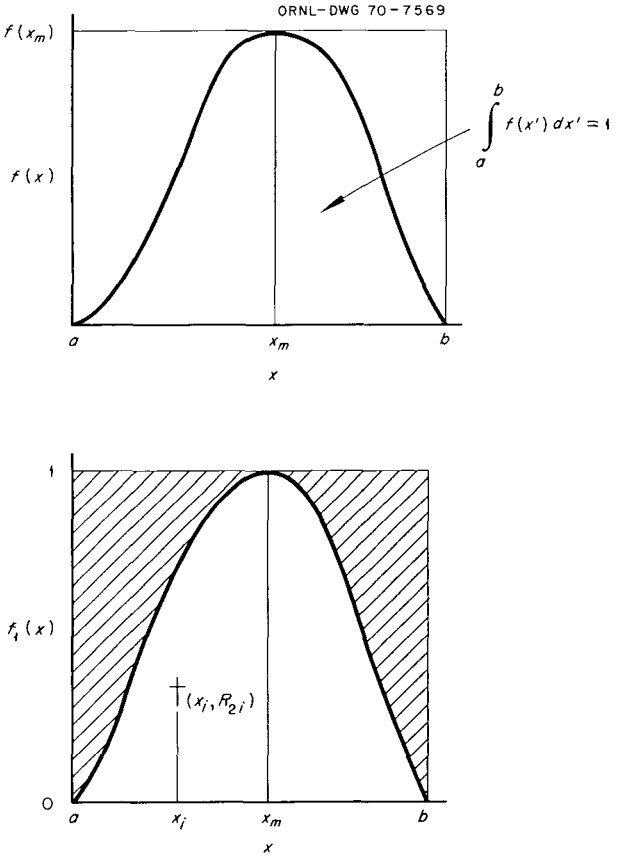

Fig. 3.1. The Probability Density Function $f(x)$. (*a*) Unmodified Distribution; (*b*) Modified Distribution $f_1(x) = f(x)/f(x_m)$.

Examples of Sampling Particle Transport Processes. – The following examples of sampling procedures are typical of those performed during the course of generating a particle history:

1. Select a nuclide from N kinds of nuclides in a mixture. (The scattering kernel will, in general, depend on the particular nuclide. Hence it is simpler to select a scattering angle and energy for a particular nuclide than for a mixture.)

Each kind of nuclide has a total macroscopic cross section Σ_n, and the total macroscopic cross section for the medium, Σ_t, is given by

$$\Sigma_t = \sum_{n=1}^{N} \Sigma_n .$$

Nuclide 1 is selected if a random number R is less than Σ_1/Σ_t, and the ith nuclide is selected if

$$\sum_{n=1}^{i-1} \frac{\Sigma_n}{\Sigma_t} \leq R < \sum_{n=1}^{i} \frac{\Sigma_n}{\Sigma_t}.$$

Once the nuclide has been selected, a choice may be made between an absorption or a scattering reaction. If another random number R is less than Σ_s/Σ_t, where Σ_s is the scattering cross section, a scattering reaction will occur; otherwise, it will be an absorption.

2. Select the azimuthal scattering angle ϕ, where its pdf is given by $f(\phi) = 1/2\pi$. Its corresponding cdf is $F(\phi) = \int_0^{\phi} f(\phi')\, d\phi' = \phi/2\pi$ and a value for ϕ is obtained by setting $F(\phi) = R$ and solving for ϕ:

$$\phi = 2\pi R ,$$

where R is a new random number.

3. Pick the distance from one collision site to the next. The pdf is given by*

$$f(x) = \Sigma_t e^{-\Sigma_t x}$$

and the cdf by

*$f(x)dx$ is the probability that the next collision site will occur within dx about x. The pdf $f(x)$ consists of two parts: $e^{-\Sigma_t x}$, the probability that a particle moves the distance x without suffering a collision, and $\Sigma_t dx$, the reaction probability associated with the differential distance of travel dx.

$$F(x) = \Sigma_t \int_0^x e^{-\Sigma_t x'} \, dx' = 1 - e^{-\Sigma_t x} .$$

Let

$$R = 1 - e^{-\Sigma_t x} ;$$

then

$$x = -\frac{1}{\Sigma_t} \ln (1 - R) .$$

Often it is difficult or impossible to solve for x explicitly, as was done in this example. A table can be constructed with $F(x)$ inverted; that is, x can be regarded as the dependent variable and $F(x)$ (or R) as the independent variable. Thus a value of x can be obtained from the table for any given value of R.

Many prescriptions for picking from various distributions have been given by Kahn.[27] Cashwell and Everett[28] and Spanier and Gelbard[29] also give many procedures useful in radiation transport applications.

Evaluation of Integrals. – For the evaluation of single or double integrals, the usual numerical integration schemes will give accurate results with less effort, but for higher order multiple integrals, Monte Carlo becomes a practical tool.[25]

The method can be demonstrated by considering the Monte Carlo evaluation of a single integral, for example, the integral

$$J = \int_a^b g(x) \, f(x) \, dx , \qquad (3.110)$$

which generates the average of the function $g(x)$ weighted by the pdf $f(x)$. The integral can be rewritten as

$$J = \int_0^1 g(x) \, dF(x) ,$$

with

$$F(x) = \int_a^x f(x') \, dx' .$$

The function $F(x)$ is the cdf corresponding to $f(x)$. With this transformation a selection of values of $F(x)$ with uniform probability over the interval (0,1) is equivalent to the selection of values of x according to $f(x)$ over the interval (a,b). The values of the random variable x are sampled from $f(x)$ and for the ith random number, R_i, the ith selection of the random variable is given by $x_i = F^{-1}(R_i)$. There is a corresponding value $g(x_i)$, and an estimation of the value of J is given by

$$\bar{J} = \frac{1}{N} \sum_{i=1}^{N} g(x_i) ,$$

where $\bar{J}$ is the Monte Carlo estimate of J, and N is the arbitrary number of samples.

When generalized to multidimensional integrals Q, the above procedure gives

$$Q = \int g(P) \, f(P) \, dP ,$$

where P denotes the multidimensional phase space. Then the Monte Carlo estimate of Q is given by

$$\bar{Q} = \frac{1}{N} \sum_{i=1}^{N} g(P_i) ,$$

where the samples having phase space coordinates P_i are selected according to a complicated set of probabilities giving rise to the probability density function $f(P)$.

Integral Forms of the Boltzmann Equation and the Random Walk. – The application of this technique to radiation transport becomes clear if the Boltzmann equation is written as an integral equation. Following Goertzel and Kalos,[26] the phase space coordinates of a particle will be denoted by (P) or for the general six-dimensional phase space by $(\bar{r},E,\bar{\Omega})$ where $\bar{r}$ is the position variable, E the particle's kinetic energy, and the unit vector $\bar{\Omega}$ its flight direction.

The motion of the particle may be completely described in terms of the flux density $\Phi(P)$, the collision density $\psi(P)$, or the density of particles leaving collisions $\chi(P)$. The collision density is so defined that the expected number of collisions of the particle within the medium in the volume of phase space V is given by the integral

$$\int_V \psi(P) \, dP .$$

The flux density may be defined as the collision density divided by the total cross section $\Sigma_t(\bar{r},E)$; then

$$\Phi(P) = \psi(P)/\Sigma_t(\bar{r},E) . \qquad (3.111)$$

The density of particles leaving collisions is defined so that the expected number of particles appearing in the volume V of phase space either as a result of a collision or directly from a particle source is given by

$$\int_V \chi(P) \, dP .$$

The source term in general phase space notation is given by $S(P)$ where $S(P)\,dP$ represent the source particles emitted in dP about P. The "transport integral operator" $T(\bar{r}' \rightarrow \bar{r},E,\bar{\Omega})$ incorporates the transport kernel,

$$\exp\left[-\int_0^{R'} \Sigma(\bar{r}-R''\bar{\Omega},E)dR''\right] .$$

That is,

$$T(\bar{r}' \rightarrow \bar{r},E,\bar{\Omega}) = \int_0^{\infty} dR'\, \Sigma_t(\bar{r},E) \times e^{-\int_0^{R'} \Sigma_t(\bar{r}-R''\bar{\Omega},E)dR''} , \quad (3.112)$$

where R' is measured from the space point $\bar{r}$ along the $(-\bar{\Omega})$ direction and corresponds to the space point $\bar{r}' = \bar{r} - R'\bar{\Omega}$. The transport operator is so defined that $T(\bar{r}' \rightarrow \bar{r},E,\bar{\Omega})\ S(\bar{r}',E,\bar{\Omega})\ d\bar{r}$ is the number of first collisions experienced by $\bar{\Omega}$-directed particles of energy E within $d\bar{r}$ about the space point $\bar{r}$. Similarly, the collision integral operator $C(\bar{r},E' \rightarrow E,\bar{\Omega}' \rightarrow \bar{\Omega})$ is defined by

$$C(\bar{r},E' \rightarrow E,\bar{\Omega}' \rightarrow \bar{\Omega}) = \int_{E'}\int_{4\pi} dE'\, d\bar{\Omega}' \times \frac{\Sigma_s(\bar{r},E' \rightarrow E,\bar{\Omega}' \rightarrow \bar{\Omega})}{\Sigma_s(\bar{r},E')} \frac{\Sigma_s(\bar{r},E')}{\Sigma_t(\bar{r},E')} \quad (3.113)$$

and the collision operator is so defined that $C(\bar{r},E' \rightarrow E,\bar{\Omega}' \rightarrow \bar{\Omega})\ dE\ d\bar{\Omega}$ represents the probability that a particle which suffers a scattering collision at $\bar{r}$ will emerge from the collision with an energy in dE about E and a direction which lies in $d\bar{\Omega}$ about $\bar{\Omega}$.

Integral forms of the Boltzmann equation can be obtained by appropriate transformations of the integro-differential form, Eq. 3.2, or they can be formulated directly from the definitions and a particle balance on the differential phase space dP. The latter procedure is used here and will be implicit in the descriptions to follow.

The event density for particles which have phase space coordinates in dP about P is given by

$$\psi(P)\,dP = \int_0^{\infty} dR'\, \Sigma_t(\bar{r},E)\, e^{-\int_0^{R'} \Sigma_t(\bar{r}-R''\bar{\Omega},E)dR''} \times \chi(\bar{r}',E,\bar{\Omega})\, d\bar{r}\, dE\, d\bar{\Omega} = T(\bar{r}' \rightarrow \bar{r},E,\bar{\Omega})\, \chi(\bar{r}',E,\bar{\Omega})\, d\bar{r}\, dE\, d\bar{\Omega} , \quad (3.114)$$

where the emergent particle density for particles which have phase space coordinates in dP about P can be expressed as

$$\chi(P)\,dP = S(P)\,dP + \int_{E'}\int_{4\pi} dE'\, d\bar{\Omega}' \times \frac{\Sigma_s(\bar{r},E' \rightarrow E,\bar{\Omega}' \rightarrow \bar{\Omega})}{\Sigma_s(\bar{r},E')} \frac{\Sigma_s(\bar{r},E')}{\Sigma_t(\bar{r},E')} \times \psi(\bar{r},E',\bar{\Omega}')\, d\bar{r}\, dE\, d\bar{\Omega} = S(P)\,dP + C(\bar{r},E' \rightarrow E,\bar{\Omega}' \rightarrow \bar{\Omega}) \times \psi(r,E',\Omega')\, dr\, dE\, d\Omega . \quad (3.115)$$

The "integral event density equation" is obtained by combining Eqs. 3.114 and 3.115 and can be written as

$$\psi(P) = T(\bar{r}' \rightarrow \bar{r},E,\bar{\Omega})\ [S(\bar{r}',E,\bar{\Omega}) + C(\bar{r}',E' \rightarrow E,\bar{\Omega}' \rightarrow \bar{\Omega})\ \psi(P')] . \quad (3.116)$$

Further, Eq. 3.115 can be interpreted as the defining equation for the emergent partial density $\chi(P)$, and if Eq. 3.114 is substituted into Eq. 3.115, the usual form of the "integral emergent particle density equation" is obtained:

$$\chi(P) = S(P) + C(\bar{r},E' \rightarrow E,\bar{\Omega}' \rightarrow \bar{\Omega}) \times T(\bar{r}' \rightarrow \bar{r},E',\bar{\Omega}')\, \chi(P') . \quad (3.117)$$

According to Eq. 3.111, knowledge of the event density $\psi(P)$ also specifies the flux density $\Phi(P)$. Therefore Eq. 3.114 also serves as the defining equation for the flux density and with $\psi(P) \equiv \Phi(P)/\Sigma_t$, the "integral flux density equation" is obtained:

$$\Phi(P) = T(\bar{r}' \rightarrow \bar{r},E,\bar{\Omega}) \left[\frac{S(\bar{r}',E,\bar{\Omega})}{\Sigma_t(\bar{r},E)} + C(\bar{r}',E' \rightarrow E,\bar{\Omega}' \rightarrow \bar{\Omega}) \frac{\Sigma_t(\bar{r}',E')}{\Sigma_t(\bar{r},E)} \Phi(P')\right] . \quad (3.118)$$

An examination of Eqs. 3.116, 3.117, or 3.118 reveals that either the integral event density equation or the integral emergent particle density equation would provide a reasonable basis for a Monte Carlo random walk. However, Eq. 3.117, the integral emergent particle density equation, is preferred since the source particles would be introduced according to the natural distribution, $S(P)$, rather than according to the distribution of first collisions, $T(\bar{r}' \rightarrow \bar{r},E,\bar{\Omega})\ S(\bar{r}',E,\bar{\Omega})$.

An important point is that the future behavior of a particle is independent of its past history and is determined only by its position in phase space. Nevertheless, it is convenient to indicate the number of collisions (n) that a particle has undergone since the

actual implementation of the random walk procedure is accomplished by approximating the integrals implied in the collision and transport operators by the sum

$$\chi(P) = \sum_{n=0}^{\infty} \chi^n(P) , \tag{3.119}$$

where

$\chi^n(P)$ = the emergent particle density of particles that have undergone exactly n collisions and have phase space coordinates (P),

$$\chi^0(P) = S(P),$$

$$\chi^n(P) = C(\bar{r},E' \rightarrow E,\bar{\Omega}' \rightarrow \bar{\Omega}) T(\bar{r}' \rightarrow \bar{r},E',\bar{\Omega}')\, \chi^{n-1}(P') . \tag{3.120}$$

Similarly,

$$\psi(P) = \sum_{n=1}^{\infty} \psi^n(P) , \tag{3.121}$$

and

$$\Phi(P) = \sum_{n=1}^{\infty} \Phi^n(P) , \tag{3.122}$$

where

$\psi^n(P)$ = the event density of particles which have undergone exactly $n - 1$ collisions and are thus entering their nth collisions and have the phase space coordinates (P)

$$= T(\bar{r}' \rightarrow \bar{r},E,\bar{\Omega})\, \chi^{n-1}(\bar{r}',E,\bar{\Omega}) , \tag{3.123}$$

and

$$\Phi^n(P) = \psi^n(P)/\Sigma_t(\bar{r},E) . \tag{3.124}$$

Substitution of Eq. 3.123 into Eq. 3.120 yields the following relationship between χ^n and ψ^n:

$$\chi^n(P) = C(\bar{r},E' \rightarrow E,\bar{\Omega}' \rightarrow \bar{\Omega})\, \psi^n(\bar{r},E',\bar{\Omega}') . \tag{3.125}$$

In solving for the basic quantities mentioned above or for others determined by these quantities, the sampling in phase space is accomplished by following particle case histories from birth [sampling from $S(P)$] to death by absorption or leakage. This analogy to real particles has led some to call Monte Carlo a theoretical experiment. For adequate numbers of case histories to be traced, a computing machine is necessary; so it is no coincidence that the development of Monte Carlo methods has closely paralleled the development of high-speed computers.

When generating the sequence of events in the life of a case history, certain quantities of interest are selected or computed at each step of the random walk. Each step may be regarded as a collision or as a flight. The quantities associated with the collision, called "collision parameters," are the phase-space coordinates such as x, y, and z (spatial coordinates), α, β, and γ (directional coordinates before or after the collision at x, y, z), the energy E (before or after the collision), and other quantities deemed useful, such as $\Sigma_t(x,y,z,E)$. The steps proceed as follows:

1. Select the initial position, energy, and direction from the source function $S(P)$.

2. Select the next collision site from $e^{-\Sigma t l}$, which is the distribution of flight lengths in units of the mean free path.

3. Force the particle to scatter* with its statistical weight modified by the probability of scattering $\Sigma_s(\bar{r},E)/\Sigma_t(\bar{r},E)$; *or* performing a collision survival test with a survival probability of $\Sigma_s(\bar{r},E)/\Sigma_t(\bar{r},E)$. In the latter case, the particle's statistical weight remains unchanged if it survives a collision and is set equal to zero if it is absorbed.

4. Select the emergent energy and change in direction of a scattered particle from the appropriate collision kernel. The energy loss and change in direction are usually related. That is, if the polar scattering angle is selected, the energy loss is then determined by the kinematics. For example, in treating gamma-ray Compton scattering, the scattering angle θ is often picked from the pdf

$$\frac{\dfrac{d\sigma(\theta,E')}{d\bar{\Omega}}}{\displaystyle\int_{4\pi} \frac{d\sigma(\theta,E')}{d\bar{\Omega}}\, d\bar{\Omega}} ,$$

where $d\sigma/d\bar{\Omega}$ is the differential Compton scattering cross section which describes the probability that a gamma ray of energy E' will scatter through an angle θ per unit solid angle. The new energy E is then determined from the Compton formula

$$E = \frac{E'}{1 + E'(1 - \cos\theta)} ,$$

where the energies are given in electron rest-mass units (m_0c^2).

In the case of neutrons, the scattering angle is generally selected in the center-of-mass system, since the scattering laws in the center-of-mass system are relatively simple, and then the angle is converted to the

*This alteration of the analog sampling scheme is a form of importance sampling and will be described more completely later in this section.

laboratory system. The kinematics of the collision usually determine the new energy except in cases such as fission and inelastic scattering when the energy of the emitted neutrons must be picked from an independent distribution.

Unless polarization effects are taken into account, the azimuthal scattering angle distribution is assumed to be uniform.

Termination of a history generally takes place when the particle is absorbed, reaches a portion of phase space not allowed, or is killed according to some prescription based on the particle's weight (see, for example, the discussion of Russian roulette given below). The most common areas of phase space not allowed are spatial regions exterior to the system considered or energy regions below an arbitrary cutoff.

Solution of the adjoint transport equation, Eq. 3.3, by the Monte Carlo method is for many problems the only practical method. As for the forward case, integral forms of the adjoint Boltzmann equation are the formal basis for the random walk logic. A detailed and interpretive derivation of these integral forms is presented in Appendix 3A along with a discussion of how they relate to a Monte Carlo solution of an adjoint problem.

Importance Sampling. – In any numerical integration scheme it is essential for accuracy to process a sufficient number of points in the phase-space regions where large contributions are made by the integrand. In many Monte Carlo problems adequate sampling becomes a crucial problem. For example, in deep-penetration shielding problems analog sampling may not within a reasonable period of time yield any histories for particles traveling through the regions of interest. Even when a few histories that make important contributions are obtained, the probable error may be too large, and increasing the number of histories decreases the error only slowly (inversely to the square root of the number of histories). A possible solution to the problem is to alter the sampling scheme to one which samples primarily from the important regions.

In importance-sampling techniques, the basic stochastic process is so modified that the event density of the basic process is multiplied by a chosen function (importance function) which measures the importance of an event at (P) on the quite reasonable basis that important regions of the phase space should be sampled most frequently. Important regions are those in which events contribute, directly or potentially, most heavily to the desired answer, the consideration of which provides some insight to the selection of the importance function.

When the sampling schemes are altered, the concept of statistical weight is introduced to correct for the altered or biased probability, so that the expected value of the mean will not be affected. For example, the information obtained from a case history is increased (and thus the probable error is decreased), generally, by not permitting absorption. Absorption is accounted for by reducing the weight of each particle by the factor Σ_s/Σ_t or, to be more general, by the ratio of the average number of particles emerging from a collision to the number entering a collision. The weighted particle whose history is being traced may be thought of as a bundle consisting of a number of subparticles, the number being proportional to the weight. At each collision some of the subparticles in the bundle are absorbed, resulting in a decrease in the weight.

Russian roulette and splitting can be used to decrease or increase (respectively) the sampling in any region of phase space and as such constitute forms of importance sampling. Thus when the weight becomes lower than some arbitrary value, a game (Russian roulette) is played in which a particle is killed if $R > C$, where C is the survival probability ($0 \leqslant C \leqslant 1$). If $R \leqslant C$, the particle survives and the weight is increased by the factor $1/C$. The surviving particle then represents all those particles killed in the game. When the particle's weight exceeds some arbitrary value, the particle is split into two or more particles with the appropriate weight reduction. These tests may be performed when a particle crosses into an important region of phase space or at the first collision site in such a region.

Importance sampling can be considered in a general way by referring back to Eq. 3.110, which can be rewritten as

$$J = \int_a^b g^*(x)\, f^*(x)\, dx ,$$

where

$$g^*(x)\, f^*(x) = g(x)\, f(x) ,$$

with the restrictions that $f^*(x) = 0$ only when $f(x) = 0$ and that

$$\int_a^b f^*(x)\, dx = 1 .$$

The expected value of J remains the same in a Monte Carlo solution involving sampling from $f^*(x)$ and evaluating $g^*(x_i)$. However, it can be shown that the variance is not the same, making it possible to improve the variance if $f^*(x)$ is selected properly. It is obvious that

$$g^*(x) = g(x)\, \frac{f(x)}{f^*(x)} ,$$

which shows that the statistical weight correction factor $f(x)/f^*(x)$ is to be used when sampling from $f^*(x)$ and evaluating $g(x)$.

For example, it is well known that in shielding problems the high-energy neutrons from a fission source dominate the penetration. In sampling from the Watt fission spectrum,[30] however, less than 1% of the samples have energies greater than 7.5 MeV. Obviously, importance sampling is needed. One way is to pick from a uniform distribution bounded by the energies E_1 and E_2. If it is assumed that the fission spectrum is given by the pdf $f(E)$, the pdf can be modified (without changing the expected means) by the pdf $f^*(E) = (E_2 - E_1)^{-1}$ in the following manner:

$$f(E) = f(E)\frac{f^*(E)}{f^*(E)} = f^*(E)\frac{f(E)}{f^*(E)} .$$

The selection of energy is made from $f^*(E)$, and the particle weight is corrected by the factor $f(E)/f^*(E)$. The cdf corresponding to $f^*(E)$ is given by

$$F^*(E) = \int_{E_1}^{E} f^*(E)\, dE = \frac{E - E_1}{E_2 - E_1} .$$

The selection of an energy E is accomplished by setting $F^*(E)$ equal to a random number R and solving the resulting equation for E, which yields

$$E = E_1 + R(E_2 - E_1) .$$

Further discussions of importance sampling can be found in refs. 23–29. In many cases the importance function is selected arbitrarily and intuitively. A more systematic (and generally successful) approach is to use the value function,[31] a solution of the equation adjoint to the Boltzmann transport equation. The value function has been shown to be a very good and sometimes optimum importance function for biasing the original Monte Carlo procedure. In most cases, a reasonable approximation to the actual value function will produce quite good results. A useful specialization of these techniques is the exponential transformation, which can be quite helpful if parameters for its use are obtained from a value function approximation.[32,33]

Scoring. – Thus far, only the generation of histories has been considered. At some point with each history a score must be evaluated, a score being the contribution to the quantity of interest. (Typical quantities of interest are flux density, current, absorption, heating, leakage, transmission, reflection, and dose.) For example, suppose that it is desired to estimate the flux averaged over a volume V of phase space. The number of collisions scored in the volume is an estimate of the collision density integrated over the phase space volume and is given by

$$\psi_V \cong \int_V \Sigma_t(P)\, \Phi(P)\, dP ,$$

and since $\Phi(P) = \psi(P)/\Sigma_t(P)$, an estimate of the flux averaged over the phase space volume V, per particle history, is

$$\bar{\Phi} = \frac{N}{V n \Sigma_t} ,$$

where

N = the number of collisions recorded in V,

Σ_t = total cross section, assumed to be constant over the phase space volume V,

n = number of particle histories.

Another commonly used estimator records d_i for every flight of length d_i in the phase space volume of interest. Then the estimate of the flux is the average track length per unit volume:

$$\bar{\Phi} = \frac{1}{V n}\sum_{i=1}^{M} d_i ,$$

where M is the number of flights during the n case histories. It is possible to reduce the variance of the estimate by using computed means in connection with the basic collision data. An example of this is the next-event estimator, which records at each collision site the probability that the next event is a score. There are many other possible means of combining analytical computation with random sampling, but they will not be discussed here.

Statistical Accuracy. – The mean is usually the quantity of most interest in a Monte Carlo problem, but in a study of the statistical properties of the problem, higher moments are often calculated. One often calculated is the second moment, which is related to the mean square error in an individual sample, the expected value of which is called the variance and is defined as

$$\sigma^2 \equiv \frac{1}{n}\sum_{i=1}^{n} (x_i - \mu)^2 , \qquad (3.126)$$

where

n = number of samples,

x_i = value of a sample,

μ = true mean (limiting value with an infinite number of samples).

In a Monte Carlo analysis, the true mean is generally not known and the variance cannot be calculated directly. However, a related quantity, called sample variance, can be determined and is given by

$$s^2 = \frac{1}{n} \sum_{i=1}^{n} (x_i - \bar{x})^2$$

$$= \frac{1}{n} \left[\sum x_i^2 - \frac{(\sum x_i)^2}{n} \right], \tag{3.127}$$

where

$$\bar{x} = \frac{1}{n} \sum_{i=1}^{n} x_i = \text{mean value of } n \text{ samples.}$$

The Gauss estimate for the variance is

$$\sigma^2 \cong \frac{n}{n-1} s^2 ,$$

which will be denoted as $\mathrm{Var}(x_i)$ and written as

$$\mathrm{Var}(x_i) = \frac{1}{n-1} \sum_{i=1}^{n} (x_i - \bar{x})^2$$

$$= \frac{1}{n-1} \left[\sum_{i=1}^{n} x_i^2 - \frac{\left(\sum_{i=1}^{n} x_i \right)^2}{n} \right]. \tag{3.128}$$

According to the "laws of large numbers," the variance of the mean, $\sigma_{\bar{x}}^2$, is related to the variance by

$$\sigma_{\bar{x}}^2 = \frac{1}{n} \sigma^2 ,$$

and its estimate, denoted by $\mathrm{Var}(\bar{x})$, is given by

$$\mathrm{Var}(\bar{x}) = \frac{\mathrm{Var}(x_i)}{n} . \tag{3.129}$$

The sample x_i may also be regarded as the mean of many histories taken as a batch and the variance of the mean can be calculated by considering a reasonably large number of such batches. Only in the limit of many histories will the estimate of the variance be the same for a particular set of case histories when divided into different arbitrary batches.

The standard deviation of the mean, $\sigma_{\bar{x}}$, is equal to the square root of the variance of the mean,

$$\sigma_{\bar{x}} = [\sigma_{\bar{x}}^2]^{1/2} , \tag{3.130}$$

and can be approximated by

$$\sigma_{\bar{x}} \cong [\mathrm{Var}(\bar{x})]^{1/2} .$$

The standard deviation is usually reported as a fractional standard deviation, defined as

$$FSD \equiv \frac{\sqrt{\mathrm{Var}(\bar{x})}}{\bar{x}} . \tag{3.131}$$

For a normal distribution, the standard deviation has the following properties: When many samples are taken and the true mean is known, the probability that the estimate of the mean will be within one standard deviation of the true mean is about 67%, within two standard deviations about 95%, and within three standard deviations about 99%. If the true mean is not known, the standard deviation is an indication of the repeatability of a given estimate of the mean; that is, there is a 67% probability that a new estimate of the mean would be within one standard deviation of the previous estimate. Thus one generally computes the sum x_i^2 as well as the sum x_i during a Monte Carlo calculation so that $\mathrm{Var}(\bar{x})$ can be calculated as well as $\bar{x}$.

There are some principles that should be kept in mind at this point. With adequate sampling of the important regions of phase space in shielding problems the distribution of the mean might be expected to be close to the normal distribution, but there is a good possibility that it will be skewed, and the above interpretation of the sample variance will be far from correct. From a practical standpoint the above interpretations of the variance are overly optimistic. In many cases (especially in deep-penetration problems) it is typical to undersample important regions of phase space and to obtain an underestimate of the mean. Then the estimate of the variance is likely to be even worse (frequently much worse[34]) and hence completely unreliable. If the standard deviation approaches 30 to 50% of the mean, the mean itself should be regarded as very unreliable.

Use of Monte Carlo Methods Today. – Monte Carlo techniques may be designed to reproduce a physical model in as much detail as is necessary, and so provide a powerful tool to solve problems with very few compromises with the physics. The Monte Carlo method is capable of incorporating any geometry. To use Monte Carlo successfully, however, generally requires a considerable investment in analysis, programming, and computer machine time. The importance of machine time is often overemphasized, with analysis and programming being underemphasized. It is important for the user to keep in mind that a well-developed theory exists which specifies, in principle, a near-optimum procedure for solving a given problem. This procedure consists of obtaining the best possible approximation to the value function for the problem and then using this function to obtain parameters for importance-sampling techniques or to guide development of new sampling techniques.

As an aid to the programmer, the concept of a Monte Carlo programming system was developed. For ex-

ample, the 05R system[35] and its updated version 06R[36] can in principle be utilized to solve any neutron transport problem. The framework is there (cross-section handling, geometry-solving routines, random-walk procedures, etc.), but the programmer must incorporate the special features he desires by adding subroutines to the framework.

Traditionally, Monte Carlo codes for solving neutron and gamma-ray transport problems have frequently been separate codes. This has been due to the physics of the interaction processes and the corresponding cross-section information required. However, when multigroup cross sections are employed, the energy group-to-group transfers contain the cross sections for all processes. Also, for anisotropic scattering each group-to-group transfer has an associated angular distribution which is a weighted average over the various cross sections involved in the energy transfer process. Thus, these multigroup cross sections have the same format for both neutrons and gamma rays. In addition, the generation of secondary gamma rays may be considered as just another group-to-group transfer. Therefore using multigroup cross sections, the logic of the random walk process (the process of being transported from one collision to another) is identical for both neutrons and gamma rays.

The use of multigroup cross sections in a Monte Carlo code means that the effort required to produce cross-section libraries is reduced. [Note: A set of multigroup neutron cross sections (99 group, P_8) based on the ENDF/B file is available from the Radiation Shielding Information Center; some coupled neutron-gamma-ray sets are also available from RSIC.]

Recently, a highly versatile and easy to use multipurpose neutron and gamma-ray transport code, the MORSE code,[37] has been developed at the Oak Ridge National Laboratory. Some of its features include the ability to treat the transport of either neutrons or gamma rays or to simultaneously treat the transport of neutrons and secondary gamma rays; the incorporation of multigroup cross sections; an option of solving either the forward or adjoint problem; modular input-output; cross section, analysis, and geometry modules; debugging routines; time dependence for both shielding and criticality problems, an albedo option at any material boundary; one-, two-, and three-dimensional geometry packages; and several types of optional importance sampling.

In general, the Monte Carlo method is not the best method for one-dimensional problems, since discrete ordinates codes are likely to be much faster than Monte Carlo codes. For two-dimensional problems, Monte Carlo and discrete ordinates methods are somewhat comparable, but for three-dimensional or two-dimensional time-dependent problems there is no competitor to Monte Carlo for a rigorous solution of transport problems.

3.6. Application of Diffusion Theory

An approach to the particle transport problem that neglects the detailed directional aspects of particle motion is that of diffusion theory. A neutron balance in the four-dimensional phase space $(\bar{r},t)$ leads to the following equation of continuity for the one-speed neutron transport problem:

$$\frac{\partial n(\bar{r},t)}{\partial t} = S(\bar{r},t) - \Sigma_a \Phi(\bar{r},t) - \nabla \cdot J(\bar{r},t), \quad (3.132)$$

where

$n(\bar{r},t)$ = neutron density (neutrons cm^{-3}),

Σ_a = macroscopic absorption cross section (cm^{-1}),

$S(\bar{r},t)$ = general source term (neutrons cm^{-3} sec^{-1}),

$\Phi(\bar{r},t)$ = total neutron flux (neutrons cm^{-2} sec^{-1}),

$\bar{J}(\bar{r},t)$ = net neutron current (neutrons cm^{-2} sec^{-1}),

$\frac{\partial n}{\partial t}$ = time rate of change of the neutron density (neutrons cm^{-3} sec^{-1}),

$\Sigma_a \Phi(\bar{r},t)$ = loss of neutrons due to absorption (neutrons cm^{-3} sec^{-1}),

$\nabla \cdot \bar{J}(\bar{r},t)$ = loss of neutrons due to convection (neutrons cm^{-3} sec^{-1}).

Equation 3.132 can be regarded as a precise relationship that can be applied without restriction to the general problem of particle transport. However, a basic limitation in its use is that except for certain very restricted situations a tractable form of the net neutron current $\bar{J}(\bar{r},t)$ does not exist. Diffusion theory in its usual form is based on the following time-independent expression for the net current:

$$\bar{J}(\bar{r}) = -D \nabla \Phi(\bar{r}) , \quad (3.133)$$

where D is the position-independent diffusion coefficient (cm), and $\nabla\Phi(\bar{r})$ is the gradient of the total neutron flux. It is noted that with the steady-state assumption, phase space has been reduced to three position variables as denoted in general vector notation by $(\bar{r})$. Equation 3.133 is identical in form with Fick's law, which simply states that the net diffusion of the particles (or molecules) in liquids and gases will be from regions of high particle density to regions of low particle density, with the gradient of the particle flux as the driving potential. The derivation of Eq. 3.133 can be found in any nuclear reactor theory textbook, for example, in the text by Weinberg and Wigner.[1]

Substitution of Eq. 3.133 into the steady-state form of Eq. 3.132 leads to the "diffusion equation"

$$D\nabla^2 \Phi(\bar{r}) - \Sigma_a \Phi(\bar{r}) + S(\bar{r}) = 0 . \quad (3.134)$$

Equation 3.134 has the same form as the steady-state form of the P_1 approximation to the spherical harmonics treatment of the Boltzmann equation (see Section 3.2).

Certain limitations are inherent to diffusion theory: (1) the scattering process is assumed to be isotropic in the laboratory frame of reference, but using a "transport-corrected" diffusion coefficient,

$$D = \frac{1}{3\Sigma_{tr}(1 - 4\Sigma_a/5\Sigma_t + \ldots)} ,$$

mitigates this limitation; (2) the directional distribution of the particle flux must be nearly isotropic; (3) the diffusing medium must be a poor absorber (i.e., $\Sigma_a \ll \Sigma_s$); and (4) the results are invalid for regions within 2 to 3 mean free paths of boundaries, strong sources, and strong sinks. The existence of these limitations is a clear indication of the approximate nature of diffusion theory insofar as the physical situation is concerned. In reality the above conditions of applicability for diffusion theory are seldom satisfied by shielding problems. However, with the judicious selection of system parameters the diffusion theory solutions of certain problems* compare favorably with solutions obtained

*For example, diffusion theory has been used in fast reactor shielding design since the leakage spectrum peaks below 0.5 MeV and the materials involved are nonhydrogenous (sodium and graphite). Also, the small source (reactor core) requires two-dimensional calculations, which are much simpler with diffusion theory.

with more exact theories or with the physical situation itself.

A neutron shielding problem would involve neutrons having a continuous energy spectrum over a wide energy range (typically from a low keV region to 10 MeV) so that a "group" approach is required to adequately describe the diffusion process.

The derivation of the group-diffusion equations is performed here beginning with the following lethargy-dependent* form of the diffusion equation:

$$-D(u)\nabla^2\Phi(\bar{r},u) + \Sigma_a(u)\Phi(\bar{r},u) + \Sigma_s(u)\Phi(\bar{r},u)\int_u^{u_T} h(u';u)\,du' = \int_0^u h(u;u')\,\Sigma_s(u')\,\Phi(\bar{r},u')\,du' + S(\bar{r},u)\,, \quad (3.135)$$

where

$\Phi(\bar{r},u)$ = a differential neutron flux that is differential with respect to the lethargy variable

$= \Phi(\bar{r},E)\left|\frac{dE}{du}\right| = \Phi(\bar{r},E)\,E\,,$

u = the lethargy (a variable which describes the kinetic energy of the neutron)

$= \ln E_0/E,$

E_0 = datum energy (frequently 10 MeV, the assumed maximum energy of fission neutrons), which corresponds to the minimum value of lethargy, $u_1 = 0$,

u_T = the lethargy which corresponds to an arbitrary limit to the slowing-down process (neutrons with lethargies greater than u_T would be within the "thermal" group and are usually referred to as thermal neutrons),

$-D(u)\nabla^2\Phi(\bar{r},u)$ = net convective loss per unit lethargy,

$\Sigma_a(u)\,\Phi(\bar{r},u)$ = absorption loss per unit lethargy,

$\Sigma_s(u)\,\Phi(\bar{r},u)\int_u^{u_T} h(u';u)\,du'$ = outscattering loss per unit lethargy,

$\int_0^u h(u;u')\,\Sigma_s(\mu')\,\Phi(\bar{r},u')\,du'$ = inscattering gain per unit lethargy,

$h(u;u')\,du$ = the probability that a scattering at the lethargy u' will result in a neutron with a lethargy in the interval du about u,

$\Sigma_s(u)$ = macroscopic scattering cross section at the lethargy u,

$S(\bar{r},u)$ = general source term per unit lethargy.

The slowing-down range in lethargy ($u_T - u_1 = u_T$) is divided into NOG intervals of arbitrary size, where

$$\Delta u_G = u_{g+1} - u_g\,, \qquad G = 1,2,\ldots NOG$$
$$u_1 = 0\,,$$
$$u_{NOG+1} = u_T\,.$$

The size of the individual lethargy intervals Δu_G would be determined by the nature of a given problem but would in any event correspond to the group structure of the available group-averaged cross-section compilations.

The standard group treatment of the energy or lethargy variable can be described as follows. Define the integral operator,†

$$I \equiv \int_{u\epsilon\Delta u_G} du\,,$$

and apply it to each term of Eq. 3.135, obtaining

$$-\nabla^2\int_{u\epsilon\Delta u_G} D(u)\,\Phi(\bar{r},u)\,du + \int_{u\epsilon\Delta u_G}\Sigma_a(u)\,\Phi(\bar{r},u)\,du + \int_{u\epsilon\Delta u_G} du\int_{u_g}^{u_T} h(u';u)\,du'\,\Sigma_s(u)\,\Phi(\bar{r},u) = \int_{u\epsilon\Delta u_G} du\int_0^{u_{g+1}} h(u;u')\,\Sigma_s(u')\,\Phi(\bar{r},u')\,du' + \int_{u\epsilon\Delta u_G} S(\bar{r},u)\,du\,. \quad (3.136)$$

*The lethargy-dependent form of the differential flux is preferred for this analysis because of the extreme range in the neutron's kinetic energy encountered in the usual shielding problem (thermal energies up to and over 10 MeV) and to illustrate the use of the lethargy variable. It should be noted that the final group-diffusion equation would have exactly the same form regardless of which energy variable (kinetic energy E or lethargy u) is used in its derivation.

†The integration limits are expressed symbolically by $u\epsilon\Delta u_G$, which implies a definite integral with respect to the lethargy variable u over the lethargy group Δu_G.

Next, define the group flux for the Gth group as

$$\Phi_G(\bar{r}) \equiv \int_{u \in \Delta u_G} \Phi(\bar{r},u)\, du ,$$

introduce group-averaged parameters, and represent the outscattering and inscattering integrals as appropriate summations over the lethargy groups:

$$-D_G \nabla^2 \Phi_G(\bar{r}) + \Sigma_G^a \Phi_G(\bar{r}) + \sum_{G'=G}^{NOG+1} \Sigma^s_{G\to G'} \Phi_G(\bar{r}) = \sum_{G'=1}^{G} \Sigma^s_{G'\to G} \Phi_{G'}(\bar{r}) + S_G(\bar{r}) , \qquad (3.137)$$

$$G = 1,2,..NOG+1 ,$$

where

$$D_G = \frac{\int_{u\in\Delta u_G} D(u)\, \Phi(\bar{r},u)\, du}{\Phi_G(\bar{r})} ,$$

$$\Sigma_G^a = \frac{\int_{u\in\Delta u_G} \Sigma_a(u)\, \Phi(\bar{r},u)\, du}{\Phi_G(\bar{r})} ,$$

$$\Sigma^s_{G'\to G} = \frac{\int_{u'\in\Delta u_{G'}} \int_{u\in\Delta u_G} h(u;u')\, \Sigma_s(u')\, \Phi(\bar{r},u')\, du\, du'}{\Phi_{G'}(\bar{r})} ,$$

$$S_G(\bar{r}) = \int_{u\in\Delta u_G} S(\bar{r},u)\, du ,$$

$G = NOG + 1$ corresponds to the thermal group.

Equation 3.137 is used to derive the difference equation for numerical solution of a particular problem. Consider, for example, a one-dimensional problem in slab geometry and divide the $\bar{r}$ space into NOS uniform segments Δx (uniform within a given homogeneous region) and designate a particular spatial meshpoint as x_i and point (discrete) values of $\Phi_G(x_i)$ and $S_G(x_i)$ as $\Phi_{i,G}$ and $S_{i,G}$ respectively. A three-point difference equation is obtained by representing the convective loss term as

$$-D_G \nabla^2 \Phi_G(\bar{r}) \cong -D_G \left[\frac{\Phi_{i+1,G} - 2\Phi_{i,G} + \Phi_{i-1,G}}{(\Delta x)^2}\right] ,$$

and Eq. 3.137 becomes

$$-D_G \left[\frac{\Phi_{i+1,G} - 2\Phi_{i,G} + \Phi_{i-1,G}}{(\Delta x)^2}\right] + \Sigma_G^a \Phi_{i,G} + \sum_{G'=G}^{NOG+1} \Sigma^s_{G\to G'} \Phi_{i,G} = \sum_{G'=1}^{G} \Sigma^s_{G'\to G} \Phi_{i,G'} + S_{i,G} . \qquad (3.138)$$

A numerical solution of Eq. 3.138 can be performed if the group-averaged cross sections are known and if the problem-defining boundary conditions are specified. Equation 3.138 can be viewed as describing the flow of neutrons downward in energy (or upward in lethargy), starting from a given initial "fixed-source" distribution of neutrons. A typical calculation would begin with the difference equation corresponding to $G = 1$. The spatial sweep is initiated at the inner boundary, at which point the inward flow of source neutrons is specified by a positive partial current, and proceeds in a stepwise fashion through the shield with additional neutrons being introduced according to the general source term, $S_{i,G}$, and finally terminates at the outer (or external) boundary where a zero re-entrant partial-current boundary condition must be satisfied. The nature of the calculation is such that the latter boundary condition will not be satisfied exactly and the solution is achieved by the process of iteration whereby the spatial sweep is repeated. This procedure as applied to a particular group is commonly referred to as "inner iteration" and is discontinued when the flux is sufficiently converged as specified by a convergence criterion such as

$$\frac{\Phi^n - \Phi^{n-1}}{\Phi^n} < \epsilon ,$$

where Φ^n is the nth iterate estimate of the flux and ϵ is the fractional change experienced by the Φ^n in a single iteration (usually ranges in value from 10^{-3} down to 10^{-5}).

The calculation then advances to the next lower energy group ($G = 2$) and the above procedure (inner iterations) is repeated. Source neutrons for group 2 include the downscattering loss from group 1 into group 2 in addition to the fixed-source component. The calculation proceeds sequentially down through all ($NOG + 1$) groups, the process comprising a single "outer iteration." This completes the numerical portion of the solution of a typical fixed-source (shielding) problem. Additional outer iterations would be required for a core-criticality problem because of the feedback effect of the fission neutrons. For the criticality problem, the outer iterations would be continued until a reasonably stable (from one outer iteration to the next) set of iterate flux values is obtained.

It must be emphasized that the typical neutron shielding problem is not amenable to solution by the straightforward application of diffusion theory, because the neutrons are on the average very energetic and possess a strong forward directional bias. The limita-

tions of diffusion theory under these conditions are clearly violated and results thus obtained would be meaningless. But when applied to certain special problems in combination with other methods, diffusion theory has proved useful. Applications of diffusion theory to the neutron shielding problem are discussed further in Section 3.9.

The use of diffusion theory to predict gamma-ray energy fluxes seems to be unjustified on superficial examination of the gamma-ray transport phenomenon. Certainly deep penetration by gamma radiation cannot be described by diffusion theory, because the resultant gamma-ray flux is due to photons that have maintained a strong directional correlation. But diffusion theory seems to be adequate for small-to-moderate penetrations relatively near the source under conditions where the low-energy end of the spectrum predominates and the scattering is more nearly isotropic. These restricted conditions exist, for example, for gamma-ray heating calculations.[38]

3.7. Invariant Imbedding Method

The method of "invariant imbedding" is not another technique for solving the Boltzmann transport equation. Rather it is a different fundamental approach to the mathematical description of particle transport. The method has for its historical basis the early works of a Russian astrophysicist, V. A. Ambarzumian, who confined his interest to the transport problems of astrophysics.[39] Recent investigations[40,41] have shown that the invariant imbedding approach can be applied to a much broader class of problems, including the neutron and gamma-ray transport problems encountered in radiation shielding.

The dependent variables of the invariant imbedding formulation are the reflection and transmission functions, with the region dimensions (shield thickness) and the energy and direction of the particle comprising the six-dimensional phase space. In this context a particular shielding problem is viewed as being "imbedded" in a more general class of shields having different dimensions. Characteristically, and in contrast with solutions of the Boltzmann transport equation, the invariant imbedding method provides transmission and reflection information for a large variety of shields, as well as for the specific problem of interest. However, the detailed behavior of the radiation during transport through the shield is not explicit during the analysis and for that reason is unavailable, a not too serious shortcoming – if not frequently a real advantage – for the typical shielding problem.

The reflection and transmission functions of invariant imbedding are each defined by an integrodifferential equation. These equations can be derived by applying the usual conservation principles of radiation transport to a shield system, the dimensions of which are allowed to vary by differential amounts. For simplicity and greater clarity, the derivations are performed in slab geometry with azimuthal symmetry. Phase space becomes three-dimensional: the shield thickness X, the energy variable E, and the direction variable μ (cosine of the polar angle θ). A schematic representation of this configuration is shown in Fig. 3.2.

The reflection of particles is denoted by $R(X;\mu,E;\mu_0,E_0)\, d\mu\, dE$ and is defined as the number of particles that are reflected from a slab of thickness X with energies in dE about E and directions that lie in $d\mu$ about μ per incident particle with energy E_0 and direction μ_0; the reflection function $R(X;\mu,E;\mu_0,E_0)$ can be regarded as an angular flux within the differential slab thickness dX. The reflection equation describes the change in the reflection function due to

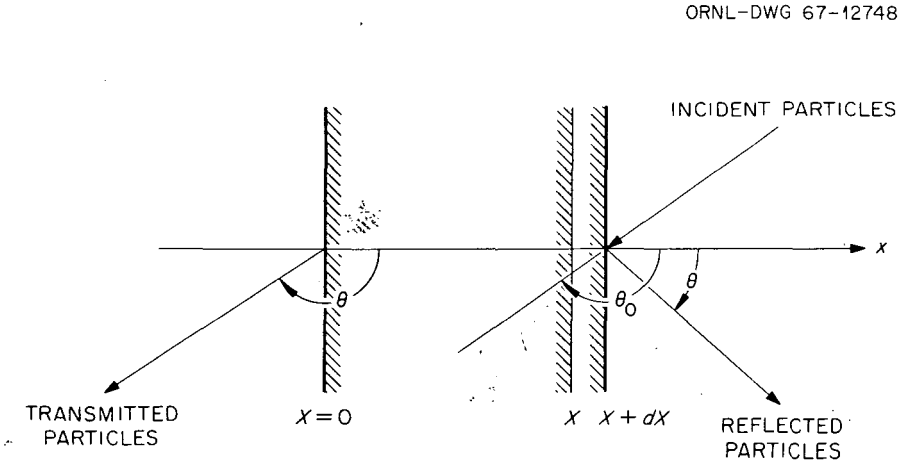

Fig. 3.2. Geometry for Invariant Imbedding Technique.

changes in the shield thickness and is formulated without involving the transmission function. The derivation is accomplished by equating the difference in the reflection functions for slabs of thicknesses $X + dX$ and X with the net change in the reflection function which results from collisions suffered by the particles within the differential slab dX:

$$R(X + dX; \mu, E; \mu_0, E_0)\, d\mu\, dE - R(X; \mu, E; \mu_0, E_0)\, d\mu\, dE = -\Sigma_t(X, E_0)\, R(X; \mu, E; \mu_0, E_0)\, \frac{dX}{\mu_0}\, d\mu\, dE$$

$$- \Sigma_t(X, E)\, R(X; \mu, E; \mu_0, E_0)\, \frac{dX}{\mu}\, d\mu\, dE + \Sigma_s(X, E_0 \to E, \mu_0 \to \mu)\, \frac{dX}{\mu_0}\, d\mu\, dE$$

$$+ \int_{-1}^{0} d\mu' \int_{0}^{\infty} dE'\, \Sigma_s(X, E_0 \to E', \mu_0 \to \mu')\, R(X; \mu, E; \mu', E')\, \frac{dX}{\mu_0}\, d\mu\, dE$$

$$+ \int_{0}^{1} \frac{d\mu'}{\mu'} \int_{0}^{\infty} dE'\, R(X; \mu', E'; \mu_0, E_0)\, \Sigma_s(X, E' \to E, \mu' \to \mu)\, dX\, d\mu\, dE$$

$$+ \int_{0}^{1} \frac{d\mu'}{\mu'} \int_{-1}^{0} d\mu'' \int_{0}^{\infty} dE' \int_{0}^{\infty} dE''\, R(X; \mu', E'; \mu_0, E_0)\, \Sigma_s(X, E' \to E'', \mu' \to \mu'')$$

$$\times R(X; \mu, E; \mu'', E'')\, dX\, d\mu\, dE\,, \quad (3.139)$$

where $\Sigma_t(X,E_0)$ is the position-dependent total macroscopic cross section evaluated at the particle energy E_0, and $\Sigma_s(X,E_0 \to E', \mu_0 \to \mu')\, d\mu'\, dE'$ represents the position-dependent differential scattering cross section which describes the probability that a particle with an initial energy E_0 and an initial direction μ_0 undergoes a scattering collision that places it into a direction which lies in $d\mu'$ about μ' with a new energy in dE' about E'.

The first and second terms on the right-hand side of Eq. 3.139 represent the particle losses due to collisions within dX (any collision is presumed to alter the particle's energy and direction). The flight paths within the volume element dX are dX/μ_0 and dX/μ for the first and second terms respectively. The first term is the loss of incident particles which collide within dX, and the second term is the loss of reflected particles due to collisions within dX. The third, fourth, fifth, and sixth terms represent the inscattering gains due to scattering collisions within dX. The third term represents those particles that are scattered directly into $d\mu$ about μ and dE about E. The fourth term is the gain from particles that scatter from dX into the slab of thickness X with energies in dE' about E' and directions $d\mu'$ about μ', and then are reflected from the slab of thickness X with the proper emergent angle and direction. The fifth term is the gain from particles that scatter from the slab of thickness X into dX with energies in dE' about E' and direction $d\mu'$ about μ' and then are scattered within dX with the proper emergent energy and direction. The sixth term is the gain from particles that scatter from the slab of thickness X into dX with energies in dE' about E' and direction $d\mu'$ about μ', are scattered back into the slab of thickness X with energies in dE'' about E'' and directions $d\mu''$ about μ'', and are finally reflected from the slab of thickness X with the proper emergent energy and direction. A rearrangement of terms leads to the usual form of the reflection equation:

$$\frac{d}{dX} R(X;\mu,E;\mu_0,E_0) = -\left[\frac{\Sigma_t(X,E_0)}{\mu_0} + \frac{\Sigma_t(X,E)}{\mu}\right] R(X;\mu,E;\mu_0,E_0) + \frac{1}{\mu_0}\Sigma_s(X,E_0\to E,\mu_0\to\mu)$$

$$+ \int_{-1}^{0} d\mu' \int_0^{\infty} dE' \Sigma_s(X,E_0\to E',\mu_0\to\mu') R(X;\mu,E;\mu',E') \frac{1}{\mu_0}$$

$$+ \int_0^1 \frac{d\mu'}{\mu'} \int_0^{\infty} dE' R(X;\mu',E';\mu_0,E_0) \Sigma_s(X,E'\to E,\mu'\to\mu)$$

$$+ \int_0^1 \frac{d\mu'}{\mu'} \int_{-1}^{0} d\mu'' \int_0^{\infty} dE' \int_0^{\infty} dE'' R(X;\mu',E';\mu_0,E_0) \Sigma_s(X,E'\to E'',\mu'\to\mu'')$$

$$\times R(X;\mu,E;\mu'',E'') , \qquad (3.140)$$

with the initial condition that

$$R(0;\mu,E;\mu_0,E_0) = 0 . \qquad (3.141)$$

The transmission of particles is denoted by $T(X;\mu,E;\mu_0,E_0)\, d\mu\, dE$ and is defined as the number of particles that are transmitted through a slab of thickness X, emerging with energies in dE about E and directions in $d\mu$ about μ per incident particle with energy E_0 and direction μ_0. The derivation of the transmission equation is accomplished in a manner similar to that used to derive the reflection equation and follows the argument that the difference in the transmission functions for slabs of thicknesses $X + dX$ and X is due to collisions suffered by the particles within the differential slab dX. A familiar form of the transmission equation is

$$\frac{d}{dX} T(X;\mu,E;\mu_0,E_0) = -\frac{\Sigma_t(X,E_0)}{\mu_0} T(X;\mu,E;\mu_0,E_0)$$

$$+ \int_{-1}^{0} \frac{d\mu'}{\mu_0} \int_0^{\infty} dE' \Sigma_s(X,E_0\to E',\mu_0\to\mu') T(X;\mu,E;\mu',E')$$

$$+ \int_0^1 \frac{d\mu'}{\mu'} \int_{-1}^{0} d\mu'' \int_0^{\infty} dE' \int_0^{\infty} dE'' R(X;\mu',E';\mu_0,E_0) \Sigma_s(X,E'\to E'',\mu'\to\mu'')$$

$$\times T(X;\mu,E;\mu'',E'') , \qquad (3.142)$$

with the initial condition that

$$T(0;\mu,E;\mu_0,E_0) = \delta(\mu-\mu_0)\,\delta(E-E_0) , \qquad (3.143)$$

where the Dirac functions $\delta(\mu - \mu_0)\,\delta(E - E_0)$ mathematically represent the monoenergetic monodirectional incident particles.

The first term in the right-hand side of Eq. 3.142 represents the decrease in the transmission function due to collisions suffered within dX (any collision is presumed to alter the particle energy and direction). The second and third terms represent the inscattering gains due to scattering collisions within dX. The second term is the gain from particles that scatter from dX into the slab of thickness X with energies in dE' about E' and directions in $d\mu'$ about μ', finally emerging with energies in dE about E and directions in $d\mu$ about μ. The third term is the gain from particles that are reflected from the slab of thickness X into dX and are then scattered back into

the slab of thickness X, finally emerging with energies in dE about E and directions in $d\mu$ about μ.

The reflection equation (Eq. 3.140) and the transmission equation (Eq. 3.142) are both nonlinear integrodifferential equations which for the radiation transport problems of nuclear engineering form problems of the "initial-value" type. The reflection equation involves only the reflection function as the dependent variable, thereby allowing its solution without consideration of the transmission equation. The transmission equation appears simpler in form (fewer terms) but contains the reflection function, which must be known before a solution can be effected. Therefore a typical shielding transmission problem (initial-value) would involve the solution of a coupled pair of nonlinear intergrodifferential equations. This is in contrast to the Boltzmann equation (Eq. 3.2), which is a linear integrodifferential equation and for the same application forms a "boundary-value" type problem.

Analytical solutions of the reflection and transmission equations for practical problems are not possible because of their integrodifferential form; the nonlinearities are a further complication. As a consequence, all useful solutions are numerical in nature and are accomplished through the use of digital computers. The numerical techniques are similar to those used to solve the Boltzmann equation by the discrete ordinates technique, in which a specific combination of the independent variables defines discrete values of the neutron flux $\Phi_{I,G,D}$ (see Section 3.3 for a more complete description).

In invariant imbedding, specific combinations of the energy and direction of the particle define the particle's state "i." In this context, the discrete reflection variable $R_{ij}(X)$ is the number of particles in state i reflected by a slab of thickness X due to a unit source of particles in state j that are incident on the slab. The discrete transmission variable $T_{ij}(X)$ is the number of particles in state i that penetrate a slab of thickness X due to a unit source of particles in state j that are incident on the slab.

More detailed derivations of the defining equations for the reflection and transmission functions in slab geometry and a description of the numerical procedures are presented by Shimizu and Mizuta.[42,43] The multigroup approximation was used for the energy variable and the direction cosines were discretized according to the Gaussian zeros. Solutions for the gamma-ray transport problem are presented for slabs of iron, water, lead, and concrete and also include comparisons of these results with experimental data and with moments method and Monte Carlo calculations.

A paper by Mathews, Hansen, and Mason[44] describes the application of invariant imbedding to practical energy-dependent neutron shielding problems, such as for a thick water shield and a thinner heterogeneous iron-polyethylene-iron shield. The reflection and transmission equations in discrete variable notation, along with a general description of numerical techniques used in their solution, are also included.

A detailed set of reflection, transmission, and escape function* equations in particle-state notation for the monoenergetic neutron transport problem in slab geometry is given by Mingle,[45] who includes applications of the method of escape probabilities, blackness coefficients, and critical size determinations.

The application of the invariant embedding method to a nonsteady energy-dependent transmission and reflection problem in slab geometry is described by Mockel.[46,47] The time-dependent invariant imbedding equations include time derivatives which are eliminated by a Laplace transform (0^- to ∞). Results are presented for the time-dependent asymptotic neutron flux in a "pulsed" experiment, and for the thermal utilization in an infinite slab lattice.

A review of previous and related work in invariant embedding is presented by Pfeiffer and Shapiro.[48] This includes the concepts of transmission and reflection matrices (response matrices); adding, doubling, and halving relations; and response functions. The use of response functions in shielding and criticality problems is described and some related experimental work is also presented – in particular a demonstration of the feasibility of obtaining cross sections from experimentally determined response functions.

The advantages and disadvantages of the invariant imbedding method relative to other techniques should strongly influence the extent and directions of future shielding applications. The advantages of the method are that it yields very detailed solutions (gives energy and angular distributions), it is efficient for deep penetrations with reasonably short computer times, it is well suited for heterogeneous shield configurations, the effects of boundaries are implicitly and exactly included in the solution, and it has the computational advantages of being an initial-value problem. The

*When internal sources are present, it is necessary to introduce the "escape function," defined as the contribution to the surface current due to a particular volumetric source. The theory and derivation of the defining equations for the escape function are very similar to that presented in this section for the reflection and transmission functions.

disadvantages of the method are that it is inefficient for thin shields (the method is very slow during initial phases of solution), it is difficult to apply to other than slab geometries, it does not generate detailed particle-state information within the shield (actually an advantage from a computational point of view), the basic equations are nonlinear (not too serious if solution is obtained numerically), and the calculational techniques and "user" computer programs are not as advanced as those for the solutions of the Boltzmann equation.

3.8. Kernel Methods

The relative value of kernel methods in modern shielding calculations is a matter of widely varying opinion. Those accustomed to using the more sophisticated methods may hold kernel methods in low regard; however, they are still often the method of choice for many engineers in design work. Experience has shown that these methods are useful but that they cannot solve all shielding problems.*

The basic idea of a kernel is obvious enough physically. The field associated with a distributed source may be determined by evaluating and summing the effects of each elementary portion of the source. If the kernel $K(P' \rightarrow P)$ is the effect of interest at the *observer's point* P caused by a unit point source at the *source point* P', then the effect of interest at P due to a source distribution $S(P')\,dP'$ is the integral of $K(P' \rightarrow P)\,S(P')\,dP'$ over the whole range of P' occupied by the source. Note that P in general defines a point in phase space, which includes spatial, energy, direction, and time coordinates. In the terminology of mathematical physics the function $K(P' \rightarrow P)$ is called Green's function; however, it is more commonly referred to as an attenuation kernel, a point-to-point kernel, a point kernel, or simply as a kernel. It may be used to calculate any of several effects of interest such as dose rate, flux density, energy absorption, or energy spectra. For example, the differential dose rate at P may be evaluated from

$$D(P) = \int K_r(P' \rightarrow P)\, S(P')\, dP' , \qquad (3.144)$$

which merely states that the solution of the general problem can be obtained by integrating over all sources if the point source solution of the dose rate, $K_r(P' \rightarrow P)$, is known. The underlying assumption is that the problem is linear; that is, the sources do not interact with each other.

The requirement that the general solution for the point source be known greatly limits the practical usefulness of Eq. 3.144. The general point source kernel depends on geometry, and, for practical reasons, only data for simple cases such as infinite homogeneous media have been compiled. Solving Eq. 3.144 can be a practical procedure if the kernel for the dose is a simple function of distance between source and detector, that is, given by $K_r(|\bar{r} - \bar{r}'|)$, which implies simple ray tracing† from the point at $\bar{r}'$ to the point at $\bar{r}$. Then, for example, the flux density due to a surface source is given by

$$\Phi(r) = \int K_p(R)\, S(R)\, dA(R) , \qquad (3.145)$$

where

$K_p(R)$ = kernel for particle flux,

$R = |\bar{r} - \bar{r}'|$,

$dA(R)$ = a differential area selected so that the product $[S(R)\ dA(R)]$ gives the strength of an equivalent point source located at a distance R from the detector.

The application of such point-to-point kernels for radiation transport has a history which is synonymous to much of the history of shielding technology and will be reviewed briefly in the following sections.

3.8.1. ELEMENTARY GAMMA-RAY KERNELS AND BUILDUP FACTORS

In the analysis of gamma-ray transport problems, the uncollided flux (i.e., the flux due to source gamma rays that arrive at the point of interest without suffering an interaction) is usually easily calculated. For example, for the case of a monoenergetic point isotropic source in a homogeneous medium, the uncollided flux (gamma rays cm^{-2} sec^{-1}) is given by

$$\Phi^0(R) = S\, \frac{e^{-\mu(E)R}}{4\pi R^2} , \qquad (3.146)$$

*Brief descriptions of several computer codes based on the kernel technique are given in Appendix 3B.

†Although all ray-tracing kernels are applied as though the radiation proceeds straight ahead, there is a method called the "straightahead approximation" which assumes that the important radiation continues straight ahead in spite of suffering interactions. This model has been used for treating neutron and gamma-ray transport but its best application is for charged particles, especially protons. Most of the energy loss is by ionization and excitation, and the assumption is a rather good one that the charged particle undergoes continuous slowing down in a straight line at a rate given by the stopping power.

where

S = source strength (gamma rays/sec),

$\mu(E)$ = macroscopic total cross section (cm^{-1}) evaluated at the initial gamma-ray energy E,

$e^{-\mu(E)R}$ = material attenuation factor, which is the probability that a gamma ray of energy E travels a distance R (cm) without suffering a collision,

$\frac{1}{4\pi R^2}$ = geometric attenuation for a point source (cm^{-2}).

Calculation of the scattered flux is in general much more complex. The scattered component is handled by introducing a buildup factor, which accounts for the increase (i.e., buildup) in the flux at some point $\bar{r}$ that is due to the scattered gamma rays. It is this buildup factor, defined for an infinite medium as

$$B = \frac{\text{some desired property (particle flux, energy flux, dose, etc.) of the total gamma-ray flux at } R}{\text{same property due to the uncollided flux at } R}, \quad (3.147)$$

that serves as the basis for formulating the point kernels required for gamma-ray shield analysis. For the calculation of dose, the kernel is given by

$$K_r(R) = \frac{\mu_{at}(E)\, E\, \Phi^0(R)}{S\rho_t} B_r = \frac{\mu_{at}(E)\, E\, e^{-\mu(E)R}}{4\pi R^2 \rho_t} B_r, \quad (3.148)$$

where $\mu_{at}(E)$ is the macroscopic energy absorption cross section for a material such as tissue evaluated at the initial gamma-ray energy E, ρ_t is the density of tissue, and B_r is the dose buildup factor, or, in keeping with the newer nomenclature,[49,50]* the exposure buildup factor, which is the ratio of the actual dose to the dose from uncollided photons at R. Similarly, if the desired property is the energy absorbed per unit mass, the kernel is given by

$$K_a(R) = \frac{\mu_a(E)\, E\, \Phi^0(R)}{S\rho} B_a = \frac{\mu_a(E)\, E\, e^{-\mu(E)R}}{4\pi R^2 \rho} B_a, \quad (3.149)$$

where $\mu_a(E)$ is the macroscopic energy absorption cross section evaluated at the initial gamma-ray energy E for the material in which the energy is absorbed, ρ is the density of the material, and B_a is the energy absorption (or energy deposition) buildup factor, which is the ratio of the actual energy absorbed at R to the uncollided energy absorbed at R.

Most buildup factors for gamma rays are those published in 1954 by Goldstein and Wilkins,[14] who give the results of infinite-medium calculations for six elements and water and up to nine source energies, covering the range of interest for reactor and weapons shielding. Results for other elements and energies may be obtained by interpolation of the data for the elements given since the buildup factors are smooth functions of energy and atomic number.

Although Goldstein and Wilkins obtained their buildup factors for water from a moments method calculation, they recommend an interpolation method to determine buildup factors for other homogeneous or near-homogeneous mixtures (media in which the particle sizes are significantly smaller than a mean free path). They suggest that buildup factors for such materials can be derived from those for the elements by the so-called equivalent or effective Z (atomic number) method. In this method, the equivalent atomic number for the mixture is obtained by a recipe with a sound theoretical basis: it involves plotting, as a function of energy, the ratio of the energy-dependent total attenuation coefficient to the total attenuation coefficient for the source energy and comparing the results on a per electron basis with corresponding curves for individual elements until a reasonable match is found over the region of interest. To be completely equivalent requires that the element and mixture also have the same ratio of the total cross section to the scattering cross section, which usually occurs to a good approximation when the shapes are matched except for very low-energy photons. Walker and Grotenhuis[51] used this technique to determine the buildup factors for four types of concrete: ordinary, ferrophosphorus, magnetite, and barytes. The results should be better than some determined earlier,[52,53] since more realistic effective atomic numbers were assumed.

More recently buildup factors for homogeneous materials have been calculated directly rather than obtained by the effective Z method, most of them by Clark *et al.*,[54-56] who applied the moments method to three of the aforementioned concretes (excluding ferrophosphorus concrete), as well as to air, wood, sand, and LiH. Similar buildup factors were obtained for ordinary concrete by Chilton.[57]

*See also Chapter 2 of this Handbook.

Extension of the buildup factor concept to laminated or multilayered shields leans rather heavily on rules of thumb and physical intuition. It is always possible to bracket the answer by alternately using the smallest and largest buildup factors (evaluated for the total number of mean free paths through the shield) of the individual materials present in the composite shield. Typical multilayered shields involve alternate layers of materials with high and low atomic numbers, for example, lead and water. In such cases the sequence of the materials is important. The buildup factor in lead alone is low compared to water because of the large photoelectric cross section of lead at the lower energies. Consequently a layer of lead following the water will rapidly absorb the low-energy scattered photons which were produced in the water. On the other hand, when the water follows the lead there is relatively little absorption of the low-energy photons and the overall buildup factor will be greater than in the former case. After 2 or 3 mean free paths of the second layer, the gamma-ray spectrum tends to readjust to the new medium and approaches the spectrum that would exist if the whole structure consisted of the outermost material. All this is clearly demonstrated in Figs. 3.3*a* and *b*, which compare the individual infinite-medium buildup factors for lead and water with buildup factors calculated by Bowman and Trubey[58,59] for lead-water and water-lead shields respectively. Although the two shields have the same thicknesses of lead and water, the buildup factor for the water-lead shield (case *b*) is lower than that for the lead-water shield, with both approaching the infinite-medium buildup factor for the outermost material. The rapid decrease of the slope of the stratified slab curve is the result of end leakage and is more pronounced in Fig. 3.3*a* because the low-energy photons are back-scattered more readily by water than by lead, which tends to absorb them.

It is apparent from the preceding discussion that infinite-medium buildup factors will apply for most shields, including laminated shields. However, if the outer layer of a laminated shield is less than about 2 mean free paths thick, the substitution of an infinite-

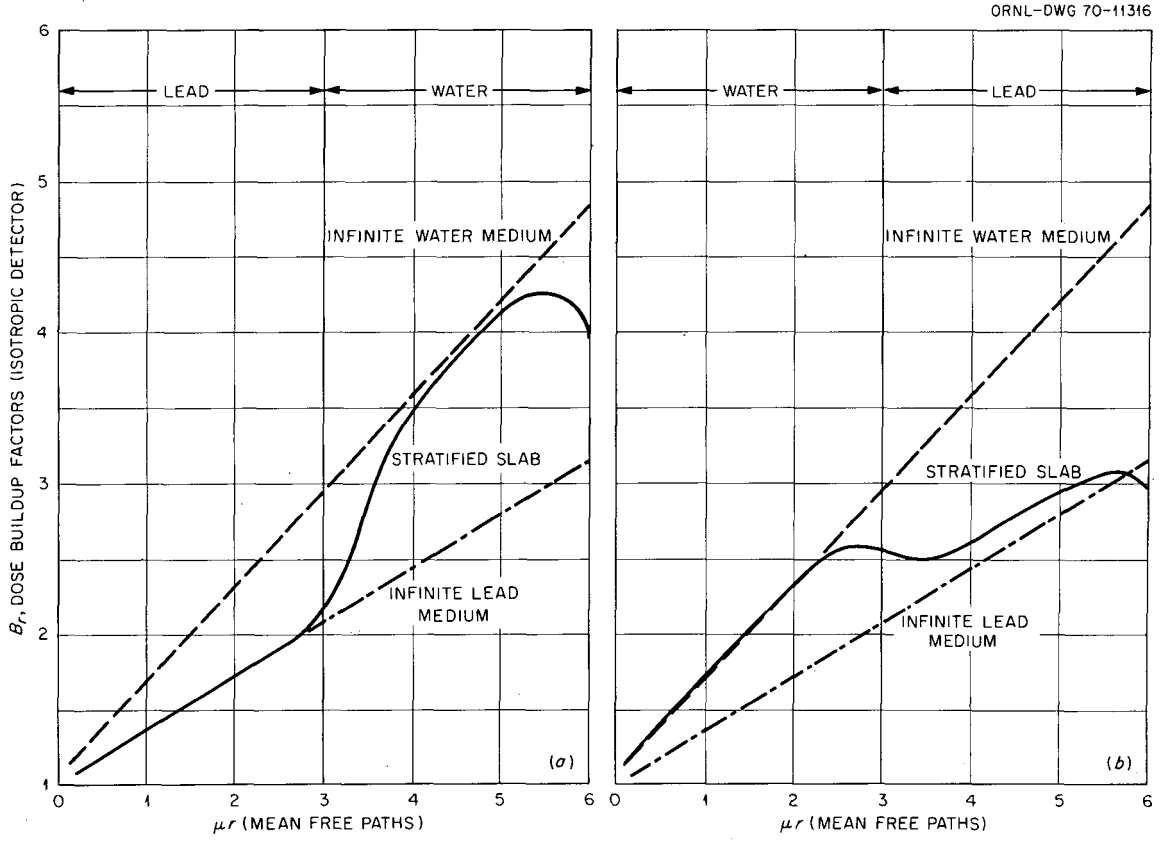

Fig. 3.3. Comparison of Infinite-Medium Buildup Factors with Stratified-Slab Buildup Factors: (*a*) Lead-Water Slab; (*b*) Water-Lead Slab. Source is normally incident plane monodirectional gamma rays. (From refs. 58 and 59.)

medium buildup factor may be inadvisable, and other techniques should be applied (see next page).

Formulas for Homogeneous Materials

Several formulas have been developed to represent the infinite-medium buildup factors determined for various elements and homogeneous materials, with the coefficients usually calculated by a best fit of the available data. Some of the more widely used functions are discussed below. There are many other possible forms of buildup factors, some of which are cited by Hubbell,[60] but they are generally more complicated and less useful than the forms given here.

Linear Form. – Probably the oldest formulas used for a buildup factor are the simple linear forms given by

$$B(E,\mu R) = 1 + \mu R \tag{3.150}$$

and

$$B(E,\mu R) = 1 + \frac{\mu - \mu_a}{\mu_a}\mu R\ , \tag{3.151}$$

where

E = source energy,

μ = linear attenuation coefficient, evaluated at the source energy E,

μ_a = energy deposition coefficient, calculated at the source energy E,

R = distance to source,

$(\mu - \mu_a)/\mu_a$ = a fitting parameter determined by Goldstein[61] from conservation of energy considerations.

These particular linear forms of the buildup factor have the advantage of being simple, but they are not very good over a significant range.

Taylor Form. – A frequently used form of the buildup factor is that of Taylor,[62] written as

$$B(E,\mu R) = A\ e^{-\alpha_1(E)\mu R} + (1 - A)\ e^{-\alpha_2(E)\mu R}\ . \tag{3.152}$$

It is apparent that substitution of Eq. 3.152 into 3.149 does not change the form of the kernel but merely generates two terms. Consequently, all available analytical solutions for the uncollided flux can be corrected for the scattered flux by simply using modified attenuation coefficients represented by $(1 + \alpha_1)\mu$ and $(1 + \alpha_2)\mu$ and multiplying the respective terms by A and $(1 - A)$. Addition of these two terms then gives the total dose.

Values of A, α_1, and α_2 were given in Taylor's original report for a number of materials, and subsequently coefficients for the energy absorption buildup factor for aluminum, tungsten, and lead and coefficients for the dose buildup factor for uranium were published by Strobel.[63]

Later Buscaglione and Manzini[64] published a rather complete set of coefficients for dose buildup factors, including those for ordinary, barytes, ferrophosphorous, and magnetite concretes. The values for concrete are based on the buildup factors published by Walker and Grotenhuis.[51] Since the Buscaglione-Manzini data are so complete, covering all the point sources used by Goldstein and Wilkins,[14] the dose coefficients are reprinted in Table 3D.1 in Appendix 3D.

Polynomial Form. – The use of a buildup factor given by a four-term polynomial capable of good accuracy became feasible when in 1958 Capo[65] published a rather complete set of coefficients for many materials. The form of the buildup factor is

$$B(E,\mu R) = \sum_{n=0}^{3} \beta_n(E)\ (\mu R)^n\ , \tag{3.153}$$

and Capo gives the coefficients β for several sets of energies, as well as coefficients for a bivariant fit which allows a set of β values to be generated for any energy. Unlike all other formulations considered here, Capo's coefficients result in an expression that does not reduce to exactly unity for $\mu R = 0$; however, the values of the β_0's are extremely close to 1.

A later set of coefficients for this form of the dose buildup factor was published by Buscaglione and Manzini[66] for various concretes. Their values, based on the data of Walker and Grotenhuis,[51] are reproduced in Table 3D.2 in Appendix 3D.

Empirical Linear and Quadratic Forms. – By least-squares fits to the data of Goldstein and Wilkins[14] for various materials and to the data of Walker and Grotenhuis[51] for four types of concrete, Trubey[67] determined values of the dose coefficient A_1 in the linear form of the exposure buildup factor given by

$$B(E,\mu R) = 1 + A_1(E)\ \mu R\ , \tag{3.154}$$

and the coefficients A_2 and b in the quadratic form given by

$$B(E,\mu R) = 1 + A_2(E)\ \mu R + b(E)(\mu R)^2. \tag{3.155}$$

Two sets of data were used, one for $\mu R \leqslant 7$ mean free paths, and another for $\mu R \leqslant 20$ mean free paths. In the fitting procedure used, the results obtained for large values of the argument were better than those obtained for small values. With heavy elements, when the fit is from 0 to 20 or more mean free paths, a large error occurs in the fitting function at small distances such that the value of B as determined by Eq. 3.155 goes to zero or is negative. This limits the use of the quadratic form with these parameters to deep-penetration calculations.

Values of the coefficients A_1, A_2, and b are presented in columns 2, 4, and 5 in Tables 3D.3 and 3D.4 in Appendix 3D. The maximum errors shown in columns 3 and 6 are those encountered over the fitted range. The error is reported either in percentage or as a factor indicated by the letter F.

Berger Form. – A two-parameter dose buildup formula proposed by Berger[68] and reintroduced by Chilton *et al.*[69] has the simplicity of the linear form but fits the buildup factor data well over a long range. This formula is

$$B(E,\mu R) = 1 + C(E)\,\mu R\, e^{D(E)\mu R} . \quad (3.156)$$

In an effort to investigate the adequacy of the formula and to make it generally useful, Trubey[67] used a least-squares procedure to obtain values of C and D for all the materials included by Goldstein and Wilkins[14] and the four types of concrete covered by Walker and Grotenhuis,[51] again using two sets of data corresponding to $\mu R \leqslant 7$ and 20 mean free paths. These values are given in columns 7 and 8 of Tables 3D.3 and 3D.4 of Appendix 3D, with the maximum error encountered over the fitted range given in column 9. It was found that this formula could reproduce the calculated buildup factor functions extremely well and had the advantages of being easily integrable over the various source regions and (unlike the Taylor form) resulting in two terms (unscattered and scattered) which have physical significance. Consequently, this form was highly recommended.[67] Other values for C and D were published by Rudloff[70] and by Chilton[71] for $\mu R \leqslant 15$ and 10 mean free paths respectively. Chilton's values are reproduced in Figs. 3.4 and 3.5 as functions of energy for various materials. It can be seen in Fig. 3.5 that for several materials and certain energies the value of D is zero, which means that the Berger formula reduces to the linear form.

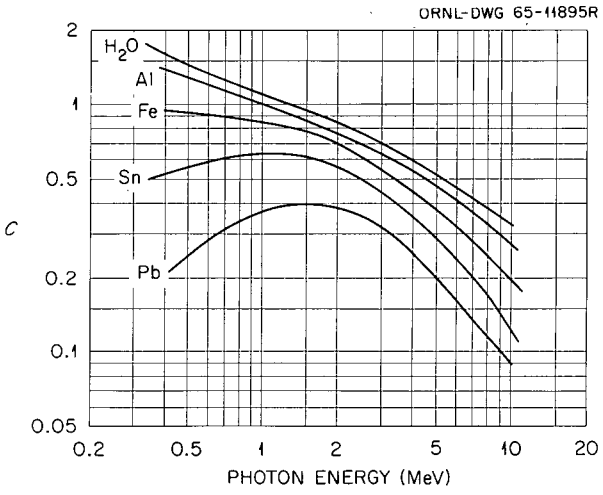

Fig. 3.4. The Coefficient C for the Berger Form of the Gamma-Ray Dose Buildup Factor. (From ref. 71.)

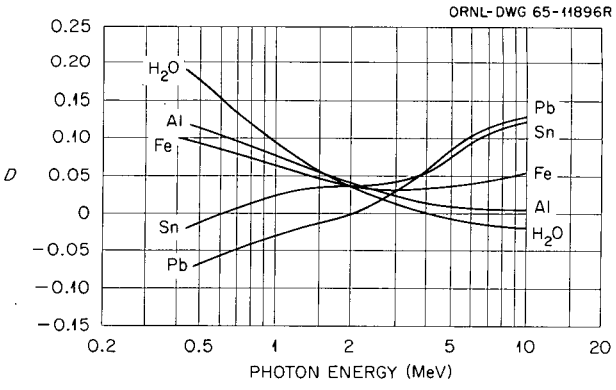

Fig. 3.5. The Coefficient D for the Berger Form of the Gamma-Ray Dose Buildup Factor. (From ref. 71.)

Formulas for Laminated Materials

As pointed out above, buildup factors for laminated shields can usually be represented by the buildup factor for the outer medium alone unless the outer layer is less than about 2 mean free paths thick, in which case a "laminated" buildup factor may be necessary. Several buildup factor formulas for such shields have been developed in recent years, some of which are discussed below. In all cases B_a and B refer to energy deposition (or absorption in the old nomenclature) and exposure buildup factors respectively. Subscripts 1 and 2 refer to the first and second layers respectively and i to the ith material. Thicknesses that are given in mean free paths are denoted by x and those given in centimeters by t.

Bowman-Trubey Formula. – Based on their Monte Carlo studies of heat deposition in one- and two-layer lead slabs in water by a plane monodirectional beam, Bowman and Trubey[58,72] suggested that combinations of the Goldstein-Wilkins energy absorption buildup factors could be used in a relation representing the buildup factor for stratified slabs. This effective buildup factor is expressed by

$$B_a(x_1,x_2) = B_{a1}(x_1 \sec\theta, E_0) \times B_{a2}(x_2 \sec\theta, E_0) \exp(-x_2 \sec\theta) + B_{a2}[(x_1+x_2)\sec\theta, E_0]\,[1-\exp(-x_2\sec\theta)]\,, \quad (3.157)$$

where θ is the angle between the direction of the incident gamma ray and the normal to the slab.

Kalos Formulas. – Kalos[73] gives the following empirical formula for normally incident gamma rays on a layer of lead followed by a thick layer of water:

$$B(x_1,x_2) = B_2(x_2) + \frac{B_1(x_1)-1}{B_2(x_1)-1}\,[B_2(x_1+x_2)-B_2(x_2)]\,. \quad (3.158)$$

For water followed by lead, he gives the formula:

$$B(x_1,x_2) = B_2(x_2) + \left[\frac{B_1(x_1)-1}{B_2(x_1)-1}\,e^{-1.7x_2} + \frac{(\mu_c/\mu)_1}{(\mu_c/\mu)_2}\,(1-e^{-x_2})\right] \times [B_2(x_1+x_2)-B_2(x_2)]\,, \quad (3.159)$$

where μ_c/μ is the ratio of the Compton scattering cross section to the total linear attenuation coefficient or total cross section.

Broder Formula. – Broder *et al.*[74] proposed the following formula for the effective buildup factor that takes all layers into account:

$$B\left(\sum_{i=1}^{N} x_i\right) = B\left(\sum_{i=1}^{N-1} x_i\right) + \left\{B_N\left(\sum_{i=1}^{N} x_i\right) - B_N\left(\sum_{i=1}^{N-1} x_i\right)\right\}, \quad (3.160)$$

where the index N corresponds to the outer layer of the laminated shield. Equation 3.160 is a recurrence formula which expresses the buildup factor for N layers in terms of the buildup factor for $N-1$ layers and a difference term in buildup for the Nth layer. By a procedure of successive substitution, the following useful expression for the buildup is obtained:

$$B\left(\sum_{i=1}^{N} x_i\right) = \sum_{n=1}^{N} B_n\left(\sum_{i=1}^{n} x_i\right) - \sum_{n=2}^{N} B_n\left(\sum_{i=1}^{n-1} x_i\right), \quad (3.161)$$

where the index n denotes the individual stratified slabs.

Kitazume Formula. – Since Broder's formula does not take into account the final saturating buildup in the last layer, which should be approximately that of the last layer alone, Kitazume[75] proposed that the difference term in Broder's formula be multiplied by $\exp(-\alpha z_n)$, where z_n is the thickness of the shield following the nth layer measured in mean free paths and α is an empirical parameter that has to be determined either by exact calculation or by experiment. With this, the Broder effective buildup factor for an intermediate slab denoted by the index n is given by

$$B\left(\sum_{i=1}^{n} x_i\right) = B\left(\sum_{i=1}^{n-1} x_i\right) + \left\{B_n\left(\sum_{i=1}^{n} x_i\right) - B_n\left(\sum_{i=1}^{n-1} x_i\right)\right\} e^{-\alpha z_n}\,, \quad (3.162)$$

where

$$z_n = \sum_{r=n+1}^{N} x_r\,.$$

Again by successive substitution, Eq. 3.162 can be transformed into an explicit expression for the overall buildup factor for the laminated shield:

$$B\left(\sum_{i=1}^{N} x_i\right) = \sum_{n=1}^{N} B_n\left(\sum_{i=1}^{n} x_i\right) \exp\left(-\alpha \sum_{r=n+1}^{N} x_r\right) - \sum_{n=2}^{N} B_n\left(\sum_{i=1}^{n-1} x_i\right) \exp\left(-\alpha \sum_{r=n}^{N} x_r\right). \quad (3.163)$$

Harima-Nishiwaki Formula. – Harima and Nishiwaki[76] recently proposed a formula that is physically justifiable, does not require determination of empirical parameters and is easy to use. The effective exposure buildup factor (for either plane or point sources) formula is

$$B(E_0,x_1+x_2) = B_2(E_0,x_1+x_2) + [B_1(E_0,x_1) - B_2(E_0,x_1)]\exp[-2(\bar{\mu}-\mu_0)x_2]\,B_2(\bar{E},\bar{\mu}x_2)\,, \quad (3.164)$$

where E_0 refers to the initial energy, $\bar{E}$ is the energy corresponding to $\bar{\mu}$, and $\bar{\mu}$ is defined by

$$\int_0^{E_0} e^{-\mu(E)x_2}\,dE = E_0\,e^{-\bar{\mu}x_2}\,, \quad (3.165)$$

Table 3.3. Deviations of Exposure Doses Obtained with Various Buildup Factors from Those Obtained with Monte Carlo Buildup Factors[a]

E_0 (MeV)	T (mfp)	t_{Pb}/T	Percent Deviation							
			Lead-Water Shield			Water-Lead Shield				
			Harima-Nishiwaki	Broder	Kalos	Harima-Nishiwaki	Broder	Kalos	Kitazume	
									$\alpha = 1.7$	$\alpha = 1.0$
1	1	0.25	+0.6	−0.6	0.0	−1.3	+9.8	0.0	+2.6	+5.2
		0.50	−2.4	−1.2	−1.8	0.0	+7.0	−1.4	+0.7	+2.8
		0.75	−5.9	−3.9	−4.6	−1.4	+0.7	−1.4	−1.4	−0.7
	2	0.25	−2.4	−2.4	−2.8	−4.1	+17.8	−1.3	−3.1	+3.6
		0.50	−6.4	−5.2	−6.4	+1.7	+18.8	−1.8	−0.6	+3.5
		0.75	−8.9	−5.5	−6.4	+1.9	+9.9	+0.6	0.0	+1.9
	4	0.25	+1.1	−1.3	−4.9	+2.4	+26.7	−6.4	−5.2	+8.4
		0.50	+1.3	+1.0	−10.3	+3.2	+41.3	0.0	−4.2	+0.9
		0.75	−3.9	+1.0	−21.3	+1.9	+18.9	+2.4	−1.0	0.0
	6	0.25	−0.6	−1.9	−8.6	−1.2	+142.0	−13.9	−16.9	−1.2
		0.50	−1.0	−3.2	−19.5	+1.1	+57.2	−1.1	−8.5	−5.2
		0.75	−6.7	−6.7	−25.2	+0.4	+26.1	+2.4	−2.0	−1.6
3	1	0.25	−1.3	−2.0	−2.0	−1.4	+0.7	−4.8	−2.7	−1.4
		0.50	−2.7	−3.3	−8.0	−1.4	0.0	−4.3	−3.6	−2.9
		0.75	−3.5	−3.5	−10.5	−0.7	0.0	−2.2	−2.2	−1.5
	2	0.25	+1.0	−0.5	−1.4	−0.5	+5.4	−8.0	−7.0	−3.2
		0.50	+0.5	−2.0	−3.6	−1.2	+3.5	−6.4	−7.5	−5.2
		0.75	−1.1	−2.8	−2.9	−1.2	+1.2	−2.5	−3.7	−3.1
	4	0.25	−2.1	−5.2	−5.8	−3.0	+8.2	−14.7	−19.7	−13.6
		0.50	−6.3	−12.7	−13.6	−0.4	+11.3	−6.7	−12.9	−10.4
		0.75	−7.8	−14.6	−11.8	+0.9	+6.5	+1.9	−4.2	−3.7
	6	0.25	−2.6	−7.8	−5.8	+1.2	+48.7	−12.8	−20.0	−13.7
		0.50	−6.2	−16.5	−13.0	+2.4	+19.3	−2.7	−13.2	−11.5
		0.75	−6.5	−18.6	−16.1	+3.0	+10.0	+0.4	−5.2	−5.2
6	1	0.25	−0.7	−1.5	−2.2	−3.7	−2.2	−3.7	−5.9	−4.4
		0.50	0.0	−1.5	−2.3	−2.3	−1.0	−3.1	−5.4	−3.9
		0.75	+0.8	0.0	−0.8	−1.6	0.0	−0.8	−3.3	−3.3
	2	0.25	+3.6	+1.2	+0.6	−1.2	+3.0	−2.4	−9.7	−5.5
		0.50	+3.7	0.0	−1.9	−2.6	−0.6	−5.1	−11.5	−9.0
		0.75	+1.3	−2.0	−2.7	−2.1	0.0	−2.1	−6.9	−6.2
	4	0.25	0.0	−4.4	−4.4	−4.9	+4.1	−7.4	−22.5	−17.6
		0.50	−0.8	−9.8	−8.5	−7.1	0.0	−2.2	−20.4	−18.6
		0.75	0.0	−9.0	−8.5	−4.0	−1.5	−1.0	−11.9	−11.4
	6	0.25	−0.4	−9.0	+2.2	+3.3	+12.1	+14.3	−15.1	−11.4
		0.50	−2.8	−16.9	−2.4	+3.4	+12.2	+16.8	−13.7	−12.6
		0.75	−5.0	−16.3	−3.3	+0.9	+5.6	−2.4	−8.9	−8.9
10	1	0.25	+2.4	0.0	0.0	−3.2	−0.8	−4.0	−7.6	−4.0
		0.50	−0.8	−3.3	−1.7	−0.8	0.0	0.0	−5.8	−4.1
		0.75	+0.9	−0.9	−0.9	−0.9	0.0	−1.8	−3.5	−3.5
	2	0.25	−0.7	−4.0	−1.3	+0.6	−0.8	−5.0	−7.6	−5.0
		0.50	−1.4	−5.6	−2.8	−1.4	+2.9	−3.6	−10.8	−7.9
		0.75	−2.3	−6.0	−3.0	−0.8	+1.5	0.0	−7.6	−6.1
	4	0.25	0.0	−6.3	−2.1	−4.2	+3.6	+5.2	−18.4	−14.3
		0.50	+1.1	−7.8	−3.4	−4.5	+2.2	+7.8	−17.9	−17.3
		0.75	+1.2	−7.3	−3.1	−1.8	+3.1	+4.3	−11.0	−10.4
	6	0.25	−2.8	−12.3	0.0	0.0	+8.4	+24.2	−16.3	−12.6
		0.50	−6.3	−18.5	−4.9	+0.5	+8.6	+25.0	−15.9	−13.9
		0.75	−5.2	−17.5	−7.2	+0.5	+5.1	+13.2	−11.2	−11.2

[a]From ref. 76.

with the energy spectrum presumed to be distributed uniformly from zero to source energy E_0.

Table 3.3, which was prepared by Harima and Nishiwaki, shows the deviation of the exposures calculated with buildup factors from the various formulas compared with the Bowman-Trubey Monte Carlo results for monoenergetic gamma rays incident on lead-water and water-lead shields. It can be seen that the Harima-Nishiwaki formula gives the best agreement with the Monte Carlo results.

3.8.2. NEUTRON REMOVAL CROSS SECTIONS

The use of buildup factors in the attenuation function, or kernel, for neutrons has not developed to a large extent in the United States, primarily because neutron interactions are much more complex than gamma-ray interactions, and consequently the uncollided neutron flux is not as easily determined as the uncollided gamma-ray flux. However, measurements at the Oak Ridge National Laboratory Lid Tank Shielding Facility (LTSF) led to the concept of a *removal* cross section averaged over source energies which can be used in a simple neutron kernel developed by Albert and Welton[77] (see Section 3.8.3) to determine the attenuation of fission neutrons through shields that have a hydrogen density of at least about 6 g/cm^2 in the outermost layer. Reactor shields nearly always contain an outer-layer hydrogen density that is large and for many years neutron attenuation in such shields was predicted with the Albert-Welton kernel utilizing LTSF-type removal cross sections. In recent years the usefulness of removal cross sections which could be applied to shields that contain less hydrogen than 6 g/cm^2 in the outer layer has been recognized, and values for a few materials have been determined. Both types of removal cross sections are discussed below.

Traditional Removal Cross Sections

The LTSF measurements[78] showed that the insertion of relatively thin slabs of material between a fission source and a thick water shield gives an effect which can be correlated by a simple exponential attenuation factor that is characteristic of absorption processes alone. This behavior might not be expected since nonabsorption effects predominate in fast-neutron attenuation. However, the large thickness of water filters out the neutrons deflected by the sample, thereby effecting their complete removal. Therefore the effect of slabs of shield materials when followed by large thicknesses of hydrogenous material can be described by an equivalent absorption cross section, called the "removal cross section."

An ideal way to experimentally determine the validity of the concept would be to use a plane monodirectional source of fission neutrons incident on a tank of water. For such a configuration the removal cross-section concept would be valid if the doses measured at the source distance z in water could be correlated by

$$D_2(z) = D_1(z)\, e^{-\Sigma_R t}\,, \qquad (3.166)$$

where

$D_1(z)$ = observed neutron dose attenuated through a distance z of water,

$D_2(z)$ = observed neutron dose attenuated through a slab of material of thickness t (inserted between source and water) plus water of thickness z,

Σ_R = macroscopic removal cross section.

In the actual experimental shielding facility where this concept was originally tested, the source was a finite isotropic disk rather than a plane monodirectional source. However, by making a few simple assumptions about the behavior of neutron penetration, an analog to Eq. 3.166 was derived and used in obtaining removal cross sections from experimental data.[79]

Values of microscopic removal cross sections (σ_R) determined from the LTSF measurements for several elements and compounds are shown in Table 3.4.[78,80-82] Empirical functions useful for interpolation in the experimental data have been derived by Zoller:[83]

$$\Sigma_R/\rho = 0.19Z^{-0.743}\ \text{cm}^2/\text{g, for } Z \leq 8\,,$$
$$= 0.125Z^{-0.565}\ \text{cm}^2/\text{g, for } Z > 8\,; \qquad (3.167)$$

$$\Sigma_R/\rho = 0.206A^{-1/3}\, Z^{-0.294} \approx 0.206\,(AZ)^{-1/3}\,, \qquad (3.168)$$

where Z is the atomic number. Most of the macroscopic removal cross sections given in Table 3.5 were obtained with Eq. 3.167.

It must be emphasized that the removal cross sections determined from LTSF experiments do not have a precise theoretical basis and should be viewed with a certain degree of suspicion. It has been demonstrated, for example, that in a homogeneous medium the removal cross section for oxygen[84] is (0.75 ± 0.05) barn rather than (0.99 ± 0.10) barn as shown in Table 3.4. It is also pointed out that the removal cross section

Table 3.4. Microscopic Removal Cross Sections of Various Elements and Compounds Measured at the ORNL Lid Tank Shielding Facility[a,b]

Material	σ_R (barns/atom)
Aluminum	1.31 ± 0.05
Beryllium	1.07 ± 0.06
Bismuth	3.49 ± 0.35
Boron[c]	0.97 ± 0.10
Carbon	0.81 ± 0.05
Chlorine[c]	1.2 ± 0.8
Copper	2.04 ± 0.11
Fluorine[c]	1.29 ± 0.06
Iron	1.98 ± 0.08
Lead	3.53 ± 0.30
Lithium	1.01 ± 0.05
Nickel	1.89 ± 0.10
Oxygen[c]	0.99 ± 0.10
Tungsten	3.36[d]
Zirconium	2.36 ± 0.12[e]
Uranium	3.6 ± 0.4
Boric oxide, B_2O_3	4.30 ± 0.41
Boron carbide, B_4C	4.7 ± 0.3[f]
Fluorothene, C_2F_3Cl	6.66 ± 0.8
Heavy water, D_2O	2.76 ± 0.11
Hevimet (90 wt % W, 6 wt % Ni, 4 wt % Cu)	3.22 ± 0.18
Lithium fluoride, LiF	2.43 ± 0.34
Oil, CH_2	2.84 ± 0.11
Paraffin, $C_{30}H_{62}$	80.5 ± 5.2
Perfluoroheptane, C_7F_{16}	26.3 ± 0.8

[a]Except where noted these values were taken from ref. 78.
[b]A measurement not included here yielded a removal cross-section value of 0.036 ± 0.002 cm^2/g for concrete (ref. 80).
[c]Cross-section value determined from measurements behind compounds of the elements.
[d]Weighted average of two values, 3.5 ± 0.2 and 3.13 ± 0.25 barns/atom (ref. 81).
[e]From ref. 82.
[f]Average of two reported values, 4.3 ± 0.4 and 5.1 ± 0.4 barns/atom.

may vary with sample thickness (the value for oxygen[85] obtained from the homogeneous-medium measurements increased from 0.72 barn at a distance 90 cm from the source to 0.79 barn at a distance 140 cm from the source). There is really no reason to expect the removal cross section to remain constant with sample thickness; however, the variation should not be very great up to about 5 relaxation lengths. Another point that should be emphasized is that the traditional removal cross section for a material described here can be applied only when that material is used in conjunction with a hydrogenous shield since hydrogen is required to moderate and absorb the scattered neutrons, as occurred in the experiments from which the removal cross sections were determined.

It follows from the removal cross-section concept that the removal cross sections of elements in a series of slabs or mixed together should be additive; that is, the number of relaxation lengths becomes

$$\sum_i \Sigma_{R_i} t_i ,$$

where the index i refers to the various elements. This additive property has been generally accepted, even though some discrepancies have been noted, particularly in regard to compounds.

Removal cross sections can be predicted by theory. Phenomenologically, the removal process can be considered to be equivalent to the total reaction rate minus the forward component of the scattering process. This suggests that an estimate of the removal cross section could be obtained from the transport cross section. As it turns out, $\Sigma_R \cong \Sigma_{tr}$ for neutrons between 6 and 8 MeV; therefore

$$\Sigma_R = \Sigma_{tr} = \Sigma_t - \Sigma_s \overline{\cos}\,\theta , \qquad (3.169)$$

where θ is the scattering angle in the laboratory frame of reference.

Removal cross sections may also be estimated from

$$\Sigma_R \tilde{=} \frac{2}{3}\Sigma_t , \qquad (3.170)$$

where Σ_t is the average total macroscopic cross section between 6 and 8 MeV, and from

$$\Sigma_R/\rho = 0.21\, A^{-0.58} , \qquad (3.171)$$

where ρ is the density and A is the atomic weight. Figure 3.6 compares plots of measured values of Σ_R/ρ

and Σ_t/ρ at 8 MeV as a function of atomic weight. It can be seen that a reasonably good fit to the curve for $A > 10$ is obtained by Eq. 3.171.

Removal Cross Sections for Hydrogen-Deficient Shields

The traditional removal cross section as discussed above is limited in application to a shield configuration that has a hydrogen density of at least 6 g/cm^2 in its outer layer. Recognizing the usefulness of a removal cross section that could be applied for shields that contain less hydrogen, Dudziak and Schmucker[86] performed a series of calculations to investigate the effect on the removal cross section of varying the surface density of the hydrogen. Using a simplified P_3 approximation to the transport equation (as incorporated in the P3MG1 code[87]), they calculated the transport of neutrons from a Po-Be source through lead followed by varying amounts of polyethylene in spherical geometry. They showed that removal cross sections for large polyethylene thicknesses approached the

Table 3.5. Fast-Neutron Removal Cross Sections and Mass Attenuation Coefficients[a]

Element	Atomic Number	ρ (g/cm^3)	Σ_R/ρ (Calc.) (cm^2/g)	Σ_R (cm^{-1})	Σ_R/ρ (Exp.) (cm^2/g)	Element	Atomic Number	ρ (g/cm^3)	Σ_R/ρ (Calc.) (cm^2/g)	Σ_R (cm^{-1})	Σ_R/ρ (Exp.) (cm^2/g)
Aluminum	13	2.699	0.0293	0.0792	0.0292 ± 0.0012	Neodymium	60	6.960	0.0124	0.0861	
Antimony	51	6.691	0.0136	0.0907		Neon	10		0.0340		
Argon	18		0.0244			Nickel	28	8.900	0.0190	0.1693	0.0190 ± 0.0010
Arsenic	33	5.730	0.0173	0.0993		Niobium	41	8.400	0.0153	0.1288	
Barium	56	3.500	0.0129	0.0450		Nitrogen	7		0.0448		
Beryllium	4	9.013	0.0678	0.1248	0.0717 ± 0.0043	Osmium	76	22.480	0.0108	0.2432	
Bismuth	83	9.747	0.0103	0.1003	0.010 ± 0.0010	Oxygen	8		0.0405		0.031 ± 0.002
Boron	5	3.330	0.0575	0.1914	0.0540 ± 0.0054	Palladium	46	12.160	0.0144	0.1747	
Bromine	35	3.120	0.0168	0.0523		Phosphorus	15	1.820	0.0271	0.0493	
Cadmium	48	8.648	0.0140	0.1213		Platinum	78	21.370	0.0107	0.2279	
Calcium	20	1.540	0.0230	0.0354		Potassium	19	6.475	0.0237	0.1533	
Carbon	6	1.670	0.0502	0.0838	0.0407 ± 0.0024	Praseodymium	59	6.500	0.0125	0.0812	
Cerium	58	6.900	0.0126	0.0870		Radium	88	5.000	0.0100	0.0498	
Cesium	55	1.873	0.0130	0.0243		Rhenium	75	20.530	0.0109	0.2238	
Chlorine	17		0.0252		0.020 ± 0.014	Rhodium	45	12.440	0.0145	0.1810	
Chromium	24	6.920	0.0208	0.1436		Rubidium	37	1.532	0.0163	0.0249	
Cobalt	27	8.900	0.0194	0.1728		Ruthenium	44	12.060	0.0147	0.1777	
Copper	29	8.940	0.0186	0.1667	0.0194 ± 0.0011	Samarium	62	7.750	0.0121	0.0941	
Dysprosium	66	8.562	0.0117	0.1003		Scandium	21	3.020	0.0224	0.0676	
Erbium	68	4.770	0.0115	0.0550		Selenium	34	4.800	0.0170	0.0818	
Europium	63	5.166	0.0120	0.0621		Silicon	14	2.420	0.0281	0.0681	
Fluorine	9		0.0361		0.0409 ± 0.0020	Silver	47	10.503	0.0142	0.1491	
Gadolinium	64	7.868	0.0119	0.0938		Sodium	11	0.971	0.0322	0.0313	
Gallium	31	5.903	0.0180	0.1060		Stronium	38	2.540	0.0160	0.0407	
Germanium	32	5.460	0.0176	0.0963		Sulfur	16	2.070	0.0261	0.0540	
Gold	79	19.320	0.0106	0.2045		Tantalum	73	16.600	0.0111	0.1838	
Hafnium	72	13.300	0.0112	0.1484		Tellurium	52	6.240	0.0134	0.0837	
Helium	2		0.1135			Terbium	65		0.0118		
Holmium	67		0.0116			Thallium	81	11.860	0.0104	0.1238	
Indium	49	7.280	0.0139	0.1009		Thorium	90	11.300	0.0098	0.1111	
Iodine	53	4.930	0.0133	0.0654		Thulium	69		0.0114		
Iridium	77	22.420	0.0107	0.2408		Tin	50	6.550	0.0137	0.0898	
Iron	26	7.865	0.0198	0.1560	0.0214 ± 0.0009	Titanium	22	4.500	0.0218	0.0981	
Krypton	36		0.0165			Tungsten	74	19.300	0.0110	0.2120	0.0082 ± 0.0018
Lanthanum	57	6.150	0.0127	0.0783		Uranium	92	18.700	0.0097	0.1816	0.0091 ± 0.0010
Lead	82	11.347	0.0104	0.1176	0.0103 ± 0.0009	Vanadium	23	5.960	0.0213	0.1267	
Lithium	3	0.534	0.0840	0.0449	0.094 ± 0.007	Xenon	54		0.0131		
Lutetium	71		0.0112			Ytterbium	70		0.0113		
Magnesium	12	1.741	0.0307	0.0535		Yttrium	39	3.800	0.0158	0.0599	
Manganese	25	7.420	0.0203	0.1505		Zinc	30	7.140	0.0183	0.130	
Mercury	80	13.546	0.0105	0.1424		Zirconium	40	6.440	0.0156	0.1001	
Molybdenum	42	10.200	0.0151	0.1543							

[a]From ref. 83.

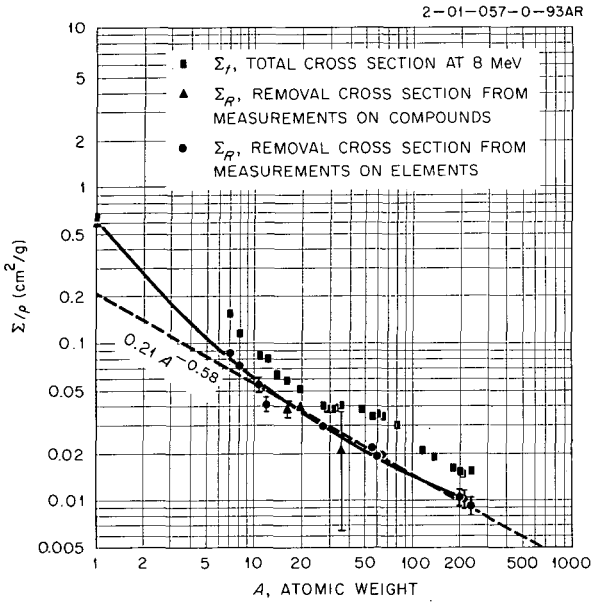

Fig. 3.6. Removal Cross Sections per Unit Mass for Fission Neutrons as a Function of Atomic Weight. (From ref. 78.)

asymptotic value of 0.116 ± 0.01 cm^{-1} (3.53 ± 0.30 b) reported from Lid Tank Shielding Facility measurements with a fission source. It was also found that extrapolating the cross section curve back to a zero polyethylene thickness yielded a value that was very close to the value of 0.0128 cm^{-1} for lead alone reported by Price and Dunn[88] on the basis of experiments with Po-Be neutrons.

Dudziak performed later calculations[89] with better cross sections, more neutron energy groups and an S_8P_3 approximation and reached essentially the same conclusions. The results of these later calculations are shown in Table 3.6. The macroscopic removal cross sections given in the table were fit to within 1.4% by a least-squares procedure to an analytical expression given by

$$\Sigma_R(t) = 0.1106\,[1 - 0.9836\exp(-0.109t)]\ , \quad (3.172)$$

where t is the polyethylene thickness in centimeters.

The Dudziak and Schmucker study[86] included some calculations for an Ra-Be source so that the sensitivity of the removal cross section to the source spectrum could be investigated. For comparable configurations the doses in the polyethylene differed by less than 9%, which indicates that the removal cross sections obtained with the Po-Be source could be applied for an Ra-Be source also.

Table 3.6. Effective Macroscopic Removal Cross Sections for Lead Followed by Various Thicknesses of Polyethylene (Po-Be Source)[a]

Polyethylene Thickness (cm)	Lead Removal Cross Section (cm^{-1})
3	0.0328
5	0.0473
7	0.0597
9	0.0701
15	0.0901
21	0.0999
25	0.1036
31	0.1069
35	0.1081
41	0.1093

[a]From ref. 89.

In similar P3MG1 calculations for a fission source, Shure *et al.*[90] determined removal cross sections for both iron and lead followed by polyethylene thicknesses up to 50 cm. They used two cutoff energies, 3.02 keV and 0.625 eV, in their dose calculations. The resulting microscopic removal cross sections, shown in Table 3.7, indicate that except for small polyethelene thicknesses the removal cross sections are relatively insensitive to the cutoff energy chosen. Shure *et al.* also found that the asymptotic values for iron and lead are in very good agreement with the experimental values of 1.98 ± 0.08 b and 3.53 ± 0.30 b respectively obtained from Lid Tank measurements.[78] For the case of no polyethylene present, the value for lead of 0.74 b (0.0243 cm^{-1}) obtained for the fission source is nearly twice that for the Po-Be source, which could be expected since the Po-Be spectrum is harder. The fact that the asymptotic removal cross sections are in agreement for the two different sources shows that the inelastic scattering in the lead apparently degrades the high-energy part of the spectra sufficiently to produce spectra that equilibrate about equally after traversing approximately 10 cm of polyethylene.

As a secondary result, Shure *et al.*[90] found that for polyethylene thicknesses > 30 cm, the fast ($E > 302$ keV), epithermal (302 keV $> E > 0.625$ eV), and thermal ($E < 0.625$ eV) neutrons contribute 83, 6, and 11% respectively to the neutron biological dose.

Shure *et al.* also investigated the use of these removal cross sections for hydrogen-deficient shields in the technique that is normally employed in application of removal cross sections for large thicknesses of hydrogenous shielding following the laminations of non-

hydrogenous material. The normal expression used to estimate the neutron dose transmitted through t cm of hydrogenous material and several slabs of nonhydrogenous materials is

$$D_{\text{lam}}(x,t) = D_{\text{calc}}(0,t) \exp\left[-\sum_i N_i \sigma_i t_i \right], \quad (3.173)$$

where D_{calc} is the calculated dose for the hydrogenous material alone and N_i is the density, σ_i the removal cross section, and t_i the thickness of the ith nonhydrogenous material. Equation 3.173 was applied to three different shield configurations utilizing lead and iron followed by various thicknesses of polyethylene. Values of D_{calc} were obtained from P3MG1 calculations and values of σ_i are those listed in Table 3.7. A comparison of the resulting dose rates with dose rates obtained with a complete P3MG1 transport calculation (see Table 3.8) showed that the frequently used design technique exemplified by Eq. 3.173 can provide good estimates of the dose rates when the removal cross sections for hydrogen-deficient shields are used.

Table 3.7. Effective Microscopic Removal Cross Sections for Iron and Lead Followed by Various Polyethylene Thicknesses (Fission Source)[a]

Polyethylene Thickness (cm)	Removal Cross Section (barn)			
	Iron		Lead	
	E_c = 302 keV	E_c = 0.625 eV	E_c = 302 keV	E_c = 0.625 eV
0	0.76	0.61	0.88	0.74
1	0.94	0.78	1.17	1.00
2	1.08	0.91	1.41	1.22
5	1.37	1.24	1.92	1.74
10	1.66	1.60	2.47	2.36
15	1.84	1.79	2.83	2.77
20	1.91	1.89	3.06	3.03
25	1.95	1.95	3.20	3.19
30	1.97	1.97	3.29	3.28
40	1.99	1.99	3.37	3.37
50	1.99	1.99	3.41	3.41

[a]From ref. 90.

Table 3.8. Comparison of Dose Rates Obtained with Transport Calculation and Removal Cross Sections (Fission Source)[a]

Polyethylene Thickness (cm)	Ratio: $(\text{Dose Rate})_{tr}/(\text{Dose Rate})_{\sigma}$					
	0.5 in. Fe 4.0 in. Pb 0.5 in. Fe		2 in. Fe 6.0 in. Pb 0.5 in. Fe		1.375 in. Fe 8.0 in. Pb	
	E_c = 302 keV	E_c = 0.625 eV	E_c = 302 keV	E_c =0.625 eV	E_c = 302 keV	E_c = 0.625 eV
0	0.92	0.95	0.92	0.82	0.94	0.96
5	1.08	1.13	1.05	0.91	1.02	1.07
10	1.08	1.12	1.05	0.98	1.02	1.07
15	1.06	1.09	1.03	0.99	1.03	1.06
20	1.04	1.06	1.03	1.01	1.03	1.05
25	1.03	1.03	1.03	1.01	1.03	1.03
30	1.02	1.03	1.03	1.02	1.03	1.03
35	1.03	1.03	1.03	1.03	1.04	1.03
40	1.02	1.02	1.03	1.03	1.04	1.03
45	1.02	1.02	1.03	1.02	1.03	1.03
50	1.03	1.04	1.03	1.03	1.03	1.04

[a]From ref. 90.

3.8.3. ALBERT-WELTON NEUTRON KERNEL

The preceding section discusses how removal cross sections can be used to determine the attenuation of neutrons through the nonhydrogenous inner layer of a shield providing the outer layer is hydrogenous. Albert and Welton[77] developed a semi-empirical theory of neutron attenuation based on removal cross sections which provides a simple method for calculating the attenuation of fission neutrons through the complete shield. Basic to the Albert-Welton model is the assumption that any neutron collision with hydrogen has the effect of an absorption. This, in effect, neglects the buildup of scattered neutrons which have undergone only small-angle scatterings by hydrogen. Inelastic scatterings with heavier nuclei are also regarded as absorptions because of the characteristically large energy loss. Other collisions are mainly small-angle elastic scatterings within the forward peak of the angular distribution, which amount to virtually no collisions. Attenuation through the materials in the shield are described in terms of removal cross sections, with the removal cross section for hydrogen taken to be its energy-dependent total cross section. The removal cross sections for the heavier nuclides are taken to be empirical energy-averaged removal cross sections such as the traditional removal cross sections described above.*

The Albert-Welton formulation for fission neutrons from a plane monodirectional source that penetrate through a mixture of water and heavy materials is given by

$$\Phi(r) \propto \exp\left(-\sum_i f_i \Sigma_{R_i} r\right) \times \int_0^\infty S(E)\, e^{-\Sigma_H(E) r}\, dE\,, \quad (3.174)$$

where

$\Phi(r)$ = number flux at a distance r from the source,

Σ_{R_i} = macroscopic removal cross section of ith element (other than hydrogen),

f_i = volume fraction of ith nonhydrogenous material,

$S(E)\,dE$ = fraction of fission neutrons at E in interval dE for a total source of 1 fission cm^{-2} sec^{-1},

$\Sigma_H(E)$ = energy-dependent total macroscopic cross section for hydrogen.

The proportionality constant included in the original Albert-Welton derivation has been removed from the inequality 3.174 to avoid the implication that the actual number flux can be computed from this.

Integration of the inequality 3.174 yields the original Albert-Welton kernel for the hydrogenous portion of the shield, which is included in the first set of brackets of the following equation:

$$\Phi(r) \propto \left[(f_w r)^{0.29}\, e^{-0.928(f_w r)^{0.58}}\right] \times \exp\left[-f_w r \Sigma_{R_O} - (1 - f_w) r \sum_i f_i \Sigma_{R_i}\right]\,, \quad (3.175)$$

where

f_w = volume fraction of water,

Σ_{R_O} = removal cross section of oxygen,

Σ_{R_i} = removal cross section of nonhydrogenous materials other than the oxygen in the water.

Although the derivation was for a plane source, Eq. 3.175 holds for a point source when multiplied by the geometric attenuation factor $1/4\pi r^2$ and the integral of $S(E)$ is normalized to 1 fission/sec. The equation is also valid when slabs of heavy material are laminated with the water. A minimum of about 50 or 60 cm of water is usually required between the dose point and the last of the heavy materials (whether as slabs or in a mixture) in order to comply with the limitations of the removal cross-section concept.

Based on more recent experimental results, Casper[91] evaluated new constants for the Albert-Welton kernel. The result for a point fission spectrum source is

$$4\pi r^2\, D(r) = 2.78 \times 10^{-5} \left[(f_w r)^{0.349} \times e^{-0.422(f_w r)^{0.58}}\right] e^{-0.0308 f_w r}\,, \quad (3.176)$$

where $D(r)$ is the neutron dose r cm from the source in (rads/hr)/(neutron/sec). When shield materials are in-

*In recent years, other kernels similar to the Albert-Welton kernel have been developed to use the removal cross sections for hydrogen-deficient shields.

serted between the water and the fission source, Eq. 3.190 is multiplied by

$$\exp\left[-(1-f_w)\sum_i \Sigma_{R_i} f_i\right]$$

to obtain the neutron dose at the shield surface.*

The Albert-Welton kernel is especially useful in the following two applications:

1. It can be used to correct measured or calculated data when small changes are made in the heavy elements of a shield. For example, suppose that a lead layer and a water layer surround a point source. If the lead layer is increased and the water thickness remains the same, the new dose rate will be given by

$$4\pi r_2^2 D_2(r_2) = 4\pi r_1^2 D_1(r_1) e^{-\Sigma_R t}, \quad (3.177)$$

where

Σ_R = removal cross section for lead,
t = change in lead thickness,
r_2 = new distance from source = $r_1 + t$,
$D_2(r_2)$ = new dose rate,
r_1 = original distance,
$D_1(r_1)$ = original dose rate.

It will be noticed that the assumption is made that the water thickness (and its effect) remains unchanged. Consequently, the dose rates are evaluated at different positions.

2. It can be used to correct results obtained for one hydrogenous medium so that they apply for another hydrogenous medium. The basic assumption is that the hydrogen effect remains constant for a given "hydrogen length," with the effects of other elements accounted for on the basis of removal cross sections. Thus the hydrogen attenuation kernel in one medium is set equal to the hydrogen attenuation in the other, giving

$$4\pi r_2^2 D_2(r_2) e^{\Sigma_{R_2} r_2} = 4\pi r_1^2 D_1(r_1) e^{\Sigma_{R_1} r_1}, \quad (3.178)$$

with the constraint, to ensure the equivalence of the hydrogen effect, of

$$\rho_2 r_2 = \rho_1 r_1, \quad (3.179)$$

where

ρ_2 = hydrogen density in medium for which $D_2(r_2)$ is unknown,
ρ_1 = hydrogen density in reference medium for which $D_1(r_1)$ is known,
Σ_{R_2} = removal cross section for all elements except hydrogen in the medium being analyzed,
Σ_{R_1} = density-corrected removal cross section for all elements except hydrogen in the reference medium.

Combining the above equations yields

$$D_2(r_2) = D_1(\rho_2 r_2/\rho_1)\,[\rho_2/\rho_1]^2 \times \exp\left(\Sigma_{R_1}\frac{\rho_2 r_2}{\rho_1} - \Sigma_R r_2\right). \quad (3.180)$$

A word of caution is appropriate here. The above equations represent a simple model of rather complex phenomena, and rather large errors are possible.

3.8.4. METHODS FOR OBTAINING KERNELS

Kernels have been obtained by a variety of techniques. Some insight in their interpretation and use is obtained if they are classified according to the method used in their determination, namely: experiments, transport calculations, and analytical models.

Experimental Kernels

The experimental (empirical) kernel may be tabulated data from an experiment or it may be implicit in a semiempirical model such as the Albert-Welton formulation, which involves the use of an experimentally determined removal cross section.

Many empirical kernels have been based on the dose rates measured in the ORNL Lid Tank Shielding Facility or similar experimental facilities. Since such data are obtained for a finite source, in the case of the LTSF a disk source, the need arose to develop techniques for converting the measured attenuation functions to more basic data such as point source kernels. Assuming that all effects are additive (that is,

*A serious shortcoming of this method is that the dose due to secondary gamma rays produced by neutron captures in the shield cannot be calculated. A significant extension of removal theory was effected by Spinney and others when the energy-dependent removal cross section concept was combined with diffusion theory. This technique is far more powerful than the removal concept alone since in addition to the neutron dose, detailed flux distributions can be calculated throughout the shield, thereby providing the source information for the secondary gamma-ray problem. A separate section is devoted to this combination removal-diffusion method (see Section 3.9).

that the problem is linear), it was possible to derive certain source geometry transformations for homogeneous media without specifying the form of the attenuation kernels. The applicability of the transformations depends upon the existence of a unique kernel, which is assured only for a truly homogeneous medium but which is nearly satisfied for many problems. The applicability also depends in most cases on the availability of sufficient data to enable evaluation of infinite series. Blizard[92,93] derived many of the most commonly used transformations, some of which are reproduced in Appendix 3E.

Kernels from Transport Calculations

Kernels have been obtained from transport calculations employing several techniques. Moments method codes, for example, have been used to produce not only gamma-ray buildup factors but also neutron attenuation kernels. Such kernels for many materials have been tabulated by Krumbein[94] as the differential energy flux or dose rate as a function of distance from a point fission or monoenergetic source in an infinite medium. These and similar kernels can be incorporated in point-kernel codes such as the QAD code,[95] which is used in space reactor shield designs (see Appendix 3B for description of code).

Neutron kernels for concrete are available from Monte Carlo transport calculations performed by Clark *et al.*[96] for monoenergetic beams of neutrons normally incident on slabs of ordinary concrete and also on a semi-infinite medium (half-space) of concrete. The neutron energies used were 0.7, 1.2, 2, 3, 4, 6, 8, 10, 12, and 14 MeV. The density of the concrete was assumed to be 2.43 g/cm^3, and its composition, other than its water content, was representative of that given for ordinary concrete 01 in ANL-5800 (ref. 97). The resulting dose attenuation curves are shown in Figs. 3F.1 through 3F.10 in Appendix 3F.

In addition to being useful directly, these results can be helpful in adjusting neutron attenuation data[98] that have been obtained for an infinite concrete medium so that the infinite-medium data can be applied to finite systems. A simple adjustment is possible since after 1 or 2 relaxation lengths the penetrating characteristics, i.e., the relaxation length, of neutrons in an infinite medium of concrete should differ very little from those of neutrons in a semi-infinite medium. Therefore such data, which in all other respects appear to be appropriate for application to a particular situation, might be fairly well adapted to a finite system by correcting the data in proportion to the ratio of the curve for the semi-infinite medium (dashed curve) to the curve for the slab configuration (solid curve) at the proper penetration distance and energy.

Discrete ordinates transport calculations which produced neutron attenuation data for concrete as a function of both incident neutron energy and incident angle were made by Schmidt and Roussin[99] with the adjoint mode of the ANISN code. Their results, reproduced in Appendix 3G, include the secondary gamma-ray dose. The importance of the secondary gamma rays can be seen from the figures. The results are given as dose equivalent, which is the quantity needed in radiation protection calculations.

Other useful neutron results were calculated by Allen and Futterer,[100] who determined by Monte Carlo methods the attenuation of the multicollision dose in the materials listed in Table 3.9 due to monoenergetic neutron beams incident at various angles. The neutron energies assumed were 5, 3, 2, 1, and 0.5 MeV, and the results are plotted in Figs. 3F.11 through 3F.15 in Appendix 3F. In order to use these curves, the multicollision dose (rate) must be known at the inner surface of a slab of one of these materials due to neutrons incident in a broad beam at an angle (or angle band) and energy (or energy band) close to the angle and energy for which the attenuation data are given. The attenuation factor appropriate to the material, thickness, energy, and angle is read from the curve, and the incident dose multiplied by that factor should approximate the dose from neutrons which have penetrated the slab.

Analytical Kernels

Analytical kernels, those which can be identified directly from relatively simple models and used in Eq. 3.145 to obtain solutions to more complex problems, can exist in many forms. For example, in computing the uncollided flux, the analytical kernel is simply $(e^{-\Sigma t R}/4\pi R^2)$ for a homogeneous medium. The paragraphs which follow present a few additional examples.

Single-Scattering Model. – The Boltzmann equation may be formulated in a Neumann series with the angular flux given for a one-velocity problem as:

$$\Phi(\bar{r},\bar{\Omega}) = \sum_{m=0}^{\infty} \Phi_m(\bar{r},\bar{\Omega}) , \tag{3.181}$$

$$\Phi_m(\bar{r},\bar{\Omega}) = \int \Phi_{m-1}(\bar{r}',\bar{\Omega}') \times \Sigma_s(\bar{r}',\bar{\Omega}' \rightarrow \bar{\Omega})\, e^{-\Sigma|\bar{r}-\bar{r}'|}\, dr' , \tag{3.182}$$

$$\Phi_0(\bar{r},\bar{\Omega}) = \int S(\bar{r}',\bar{\Omega})\, e^{-\Sigma|\bar{r}-\bar{r}'|}\, dr' , \tag{3.183}$$

Table 3.9. Compositions of Materials Used for Neutron Transmission Calculations[a]

Material	Density (g/cm^3)	Composition	
		Element	Atoms/cm^3
			$\times 10^{21}$
Borated polyethylene (8 wt % B_4C)[b]	0.97	H	76.80
		C	39.20
		^{10}B	0.658
		^{11}B	2.67
Water	1.00	H	66.90
		O	33.45
Concrete	2.26	H	13.75
		O	45.87
		Al	1.743
		Si	20.15
Nevada Test Site soil (dry)	1.15	H	8.553
		O	22.68
		Al	2.014
		Si	9.533
Nevada Test Site soil (100% saturated)	1.25	H	16.87
		O	27.00
		Al	1.976
		Si	8.963

[a]From ref. 100.

[b]Several calculations made for pure polyethylene slabs (ρ = 0.925 g/cm^3) up to 6 in. thick yielded approximately the same neutron transmission results as those for the borated polyethylene.

where $S(\bar{r},\bar{\Omega})$ is the source density, Φ_0 is the uncollided angular flux, Φ_1 is the singly scattered angular flux, and Φ_m is the angular flux of particles which have suffered exactly m collisions. There are a few situations when the series converges in just a few terms, usually when the important scattering region is a fraction of a mean free path thick. However, the full implementation of the technique is rarely attempted with most practical applications involving only the uncollided flux Φ_0 and/or the singly scattered flux Φ_1. Calculations of single scattering in air for short distances have been particularly useful.[101]

Variations on this method include the extended single scatter model which treats $\Sigma_s\Phi_1$ as the source and further scattering by a buildup factor.[102,103] Computed values of $\Sigma_s\Phi_0$ may also be used as a first-collision source in Monte Carlo calculations to reduce the variance by eliminating the randomness in the first-collision distribution and in small-source two-dimensional discrete ordinates calculations[12] to cope with the ray effects. In the latter case the source becomes distributed throughout space rather than being located at a point. The particle flow from this source is distributed in angle, which is easier to treat.

Last-Flight Kernels. – Another useful technique is to compute the transport across a void by treating the leakage from a surface as a source. A "last-flight" kernel is used to describe the point-to-detector transport across the void, and the total answer is obtained by integration over the entire surface. Thus the flux density may be computed at the center of a duct, room, or crew compartment by integrating over the walls and computing the transport from the walls to the point of interest. Moteff used this technique in his "two-component" method.[104,105] With this model there is a narrow beam component, much like a removal flux density, to be integrated over the source region, and a wide beam or diffusion component to be integrated over the shield surface, and the two components are summed to obtain the flux density at a distant point.

Integrations of the shield leakage calculated by one- and two-dimensional discrete ordinates codes have been described by Cramer and Solomito[106] and by Lindstrom and Wilcox.[107]

Monte Carlo Variance Reduction. – Analytical kernels may be used to reduce the variance of Monte Carlo calculations in several ways. The variance per case history can be reduced by replacing any randomly sampled quantity by the "expected value." For example, a computed expected value, often called statistical or next-event estimation, is a common technique. Amster and Gast[108] applied it by computing the neutron spatial distribution analytically for about four collisions in their Monte Carlo code. Berger and Doggett[109] computed all the spatial portion analytically and the rest by Monte Carlo in their solution for a gamma-ray transport problem. Cramer *et al.*[110] used analytical kernels for the neutron transport in air of keV neutrons to replace the time-consuming Monte Carlo treatment. This technique has also been implemented in the AIRTRANS code[111] which uses a kernel from 150-keV to thermal energy.

Another example of the use of analytical kernels in Monte Carlo calculations is in the choice of importance function. It is generally necessary in solving shielding problems by Monte Carlo to use importance sampling (see Section 3.5). This permits computer machine time to be used efficiently by sampling the portions of phase space which contribute significantly to the answer sought. A systematic approach is to use an appropriate

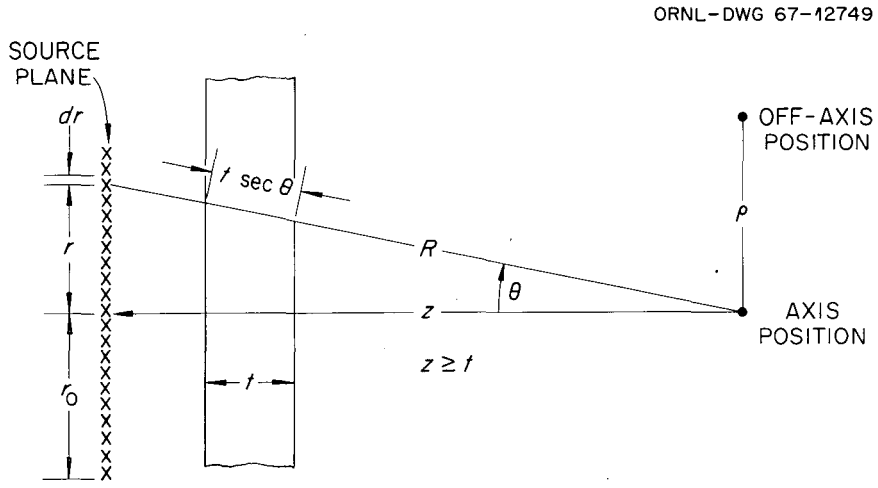

Fig. 3.7. Schematic of Disk Source.

analytical function as the importance function.[31] Bendall and McCracken[112] used the Spinney method adjoint kernel for this purpose. Armstrong and Stevens[113] used the first term of a Neumann series representation of the value function. That is, their V^0 importance function is the expected contribution to the desired answer made by a particle emerging from a collision.

3.8.5. APPLICATION OF POINT KERNELS TO DISK AND RECTANGULAR SOURCES

Sometimes solutions to shielding problems can be reasonably approximated from attenuation data for a disk or rectangular source and a slab shield. These simple plane source problems are amenable to analytic or numerical solution by integrating a point kernel over the source area as illustrated by Eq. 3.145. The results when tabulated or plotted are directly usable in practical applications.

In the examples given below it is assumed that the problems are gamma-ray problems, but the same techniques would apply for neutron problems if the buildup factors are set equal to 1 and the macroscopic neutron removal cross section Σ_R is substituted for the gamma-ray linear attenuation coefficient μ. When applied to neutrons, it is assumed that the outer layer of the shield contains an adequate amount of hydrogen and that the attenuating effect of the hydrogenous material is properly included.

Disk Source. – Consider, for example, a detector shielded from a plane disk source that is uniformly emitting S photons cm^{-2} sec^{-1} isotropically in 4π steradians (see Fig. 3.7). Applying the point kernel as given by Eq. 3.146 except for the inclusion of the uncollided flux-to-dose (rads/hr) conversion factor $G(E) = 5.767 \times 10^{-5}\ \mu_{a_t}(E)\, E/\rho_t$, the unscattered dose rate along the disk axis is

$$\Gamma(\mu t, r_0/z) = S\, G(E) \int_0^{r_0} \frac{e^{-\mu t \sec\theta}\,(2\pi r)\,dr}{4\pi(r^2 + z^2)}, \tag{3.184}$$

where z is the distance from the disk to the detector. Equation 3.184 can be transformed to

$$\Gamma(\mu t,\ r_0/z) = \frac{S\, G(E)}{2} \int_{\mu t}^{\mu t\sqrt{1+(r_0/z)^2}} \frac{e^{-y}}{y}\,dy\ , \tag{3.185}$$

where $y \equiv \mu t \sec\theta$. When integrated, Eq. 3.185 becomes

$$\Gamma(\mu t,\ r_0/z) = \frac{S\, G(E)}{2} \times \left\{E_1(\mu t) - E_1\left(\mu t\sqrt{1 + [r_0/z]^2}\right)\right\}, \tag{3.186}$$

where E_1 is the exponential integral function* of the first order and is defined by

$$E_1(x) \equiv \int_x^\infty \frac{e^{-y}}{y}\,dy\ . \tag{3.187}$$

[Equation 3.186, as well as the equations given below for computing uncollided doses, can be used to determine the total dose (uncollided + scattered) by using the Taylor form of the buildup factor (see Section 3.8.1 for a description of this procedure)].

*Plots of this function are given in Appendix 3H.

For the case of an isotropic flux Φ_0 at the source plane, which is equivalent to the angular flux

$$\Phi(\bar{\Omega}) = \frac{\Phi_0}{4\pi},^{*}$$

the unscattered dose is

$$\Gamma(\mu t, r_0/z) = G(E) \int \Phi(\bar{\Omega}) e^{-\mu t \sec\theta} \, d\bar{\Omega}_s , \qquad (3.188)$$

where $d\bar{\Omega}_s$ is the solid angle subtended by the differential area $(2\pi r dr)$. This expression can be rewritten as

$$\Gamma(\mu t, r_0/z) = \Phi_0 \, G(E) \int_0^{r_0} \frac{e^{-\mu t \sec\theta} \cos\theta (2\pi r) \, dr}{4\pi(r^2 + z^2)},$$

which integrates to

$$\Gamma(\mu t, r_0/z) = \frac{\Phi_0 \, G(E)}{2} \left\{ E_2(\mu t) - \frac{1}{\sqrt{1 + (r_0/z)^2}} E_2(\mu t \sqrt{1 + [r_0/z]^2}) \right\}, \quad (3.189)$$

where E_2 is the exponential integral function of the second order. In general,

$$E_n(x) = x^{n-1} \int_x^{\infty} e^{-y} y^{-n} \, dy .$$

The positive partial current J_n^+ at the source plane corresponding to the isotropic flux condition is given by

$$J_n^+ = \int_{\bar{\Omega}\cdot\bar{n}>0} \Phi(\bar{\Omega}) \bar{\Omega}\cdot\bar{n} \, d\bar{\Omega} = \int_0^1 \frac{\Phi_0}{4\pi} \cos\theta \, 2\pi \, d(\cos\theta) = \frac{\Phi_0}{4}, \qquad (3.190)$$

where $\bar{n}$ is a unit vector normal to the source plane. Therefore if the positive partial current is known, $4J_n^+$ must be substituted for Φ_0 in Eq. 1.89.

In general, for the $\cos^n\theta$ angular distribution in the forward direction,

$$\Phi(\bar{\Omega}) = \frac{(n+1) \, \Phi_0^{2\pi} \cos^n\theta}{2\pi}, \qquad (3.191)$$

where $\Phi_0^{2\pi} = \int_{2\pi} \Phi(\bar{\Omega}) d\bar{\Omega}$ is the 2π total flux and $n = 0$ corresponds to the isotropic flux field. Equation 3.191 is substituted into Eq. 3.188 and the integral is evaluated, yielding the following expression for the unscattered dose:

$$\Gamma(\mu t, r_0/z) = (n+1) \, \Phi_0^{2\pi} \, G(E) \left\{ E_{n+2}(\mu t) - \frac{E_{n+2}(\mu t \sqrt{1 + [r_0/z]^2})}{(\sqrt{1 + [r_0/z]^2})^{n+1}} \right\}. \quad (3.192)$$

For the off-axis position at a distance ρ measured perpendicularly to the disk axis (see Fig. 3.7), integrations must be done numerically. Hubbell *et al.*[114] integrated an expression similar to Eq. 3.184, the isotropic source case, for off-axis positions and tabulated the results in terms of the parameters μt, r_0/z, and ρ/r_0. These results are shown in Table 3I.1 of Appendix 3I. The quantity tabulated is $4\pi\Gamma(\mu t, r_0/z, \rho/r_0)/S \, G(E)$, which is the same as $4\pi\Phi^0(\rho/r_0)/S$, where $\Phi^0(\rho/r_0)$ is the uncollided flux at ρ/r_0.

In a similar manner Trubey[115] determined the data for an isotropic flux. The results are given in Table 3I.2 of Appendix 3I as $2\Gamma(\mu t, r_0/z, \rho/r_0)/\Phi_0 \, G(E)$, which is the same as $2\Phi^0(\rho/r_0)/\Phi_0$.

Certain circular aperture and disk source configurations to which these results might be applied are shown in Fig. 3.8.

Rectangular Sources. – A solution was developed by Hubbell *et al.*[116] for the uncollided flux a distance z from a plane isotropic rectangular source.† Expressed as the product of separable source and geometry functions, the uncollided flux is given by

$$\Phi^0(a,b) = \sum_{n=0}^{\infty} \frac{2n+1}{2} g_n \, p_n(a,b) , \qquad (3.193)$$

where g_n and $p_n(a,b)$ are Legendre coefficients of the source and geometry functions respectively.

If $a = H/z$ and $b = W/z$, where H and W are the height and width of the source plane (see Fig. 3.9), then Eq. 3.193 gives the flux at the corner position, that is, the flux at a distance z along the normal to the corner of the rectangular source. It follows that using the half-height and half-width gives one-fourth of the flux

*See Section 5.1.1 in Chapter 5 and Section 2.1 of Chapter 2 for a discussion of fluxes, currents, and sources.

†The application of the work of Hubbell *et al.* to rectangular ducts, which is the special case of a zero shield thickness, is described in Section 5.1.1 in Chapter 5.

at z along a normal to the center of the source plane. The Legendre coefficient of the source function is

$$g_n = \int_{-1}^{1} g(\mu t, \cos\theta)\, P_n(\cos\theta)\, d(\cos\theta)\,, \quad (3.194)$$

where $g(\mu t, \cos\theta)$ represents the angular flux at the source plane for the case of a slab shield of thickness $t(z \geq t)$ located between the source and the detector at a distance z from the source; that is,

$$g(\mu t, \cos\theta) = \frac{S\, e^{-\mu t/\cos\theta}}{4\pi \cos\theta}\,. \quad (3.195)$$

Substituting Eq. 3.195 into Eq. 3.194, Hubbell *et al.* evaluated g_n and p_n numerically and solved Eq. 3.193. The results for a corner position ($a = H/z$, $b = W/z$) are given in Table 31.1 of Appendix 3I as $4\pi\Gamma/S\ G(E)$, or $4\Phi^0/S$, in terms of the parameters μt, a, and b.

In a similar manner Trubey[115] numerically evaluated the equivalent of Eq. 3.193 for an isotropic flux (cosine distribution of the angular current), that is, for

$$g(\mu t, \cos\theta) = \frac{\Phi_0\, e^{-\mu t/\cos\theta}}{4\pi} \quad (3.196)$$

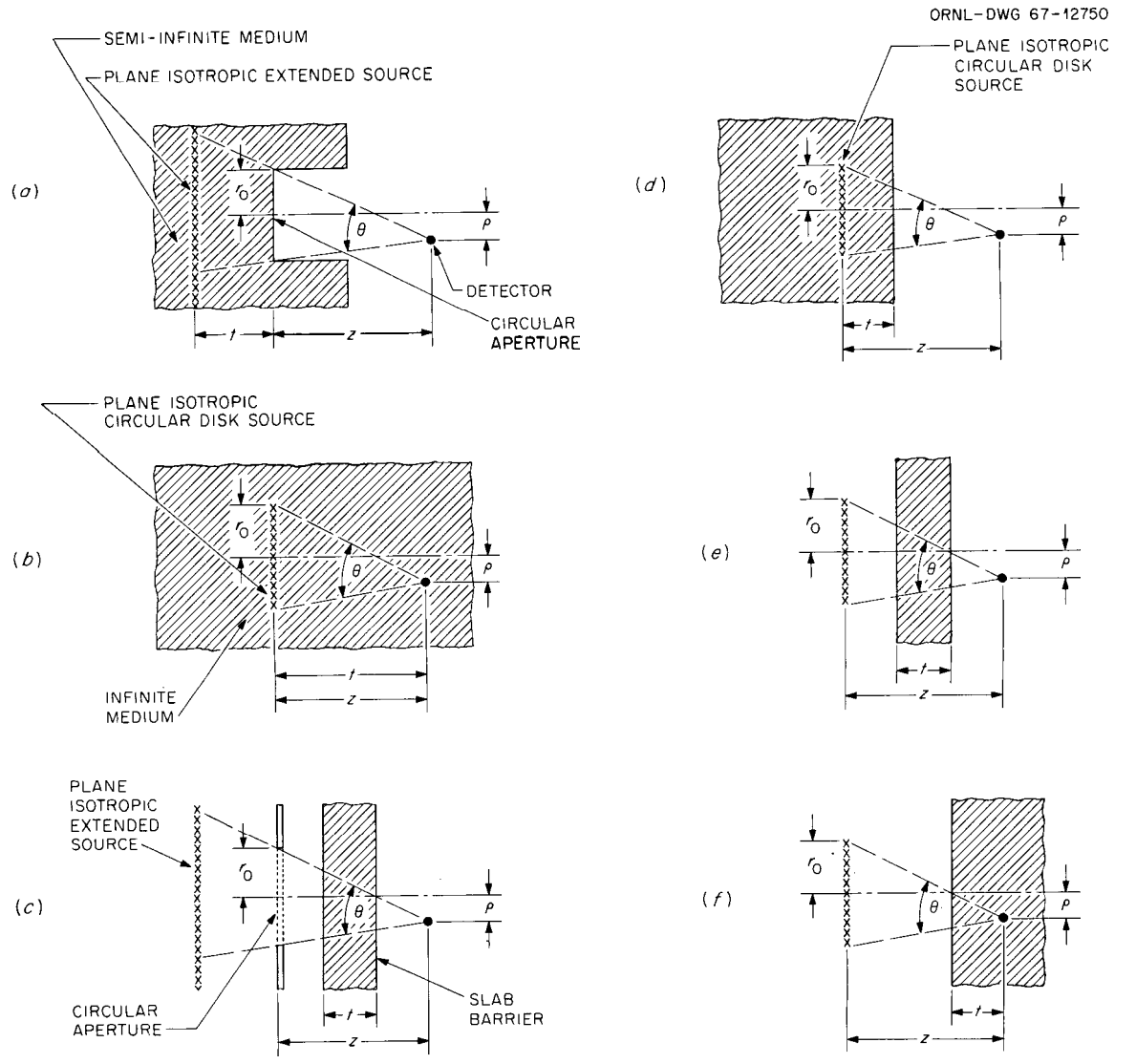

Fig. 3.8. Some Circular Aperture or Disk Source-Shield Configurations to Which Point Kernels Are Applicable. (From ref. 114.)

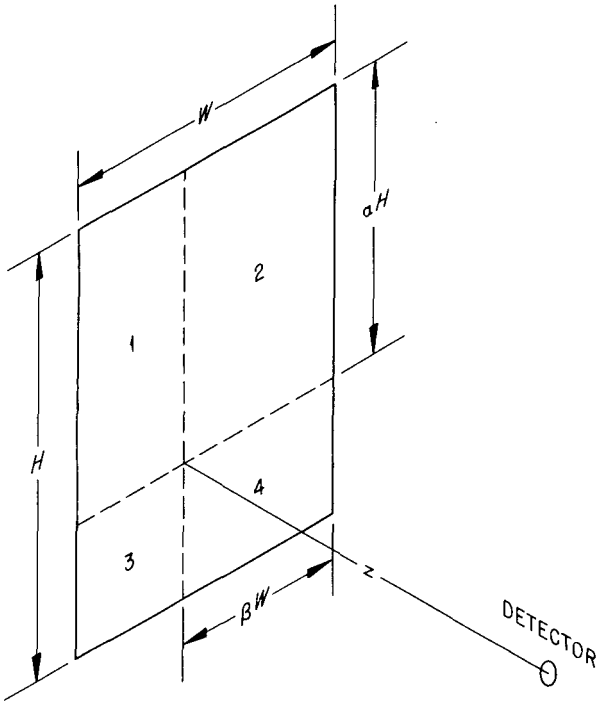

Fig. 3.9. Schematic Demonstrating Use of Corner Position of a Rectangular Source to Calculate Dose at an Arbitrary Position by Point Kernel Techniques.

These results for a corner position are given in Table 3I.4 of Appendix 3I as $2\Gamma/\Phi_0\ G(E)$, or $2\Phi^0/\Phi_0$, which is the same quantity tabulated for the disk source in Table 3I.2. For the case of a square the dose will be slightly greater than that from a disk of radius W.

Although these results relate directly to the response of a detector in a corner position, they are also applicable to any arbitrary position lying within the projection of the source plane. It is obvious from Fig. 3.9 that the dose at the detector is

$$\Gamma(H/z, W/z) = \Gamma_1\left(\frac{\alpha H}{z}, \frac{[1-\beta]\,W}{z}\right) + \Gamma_2\left(\frac{\alpha H}{z}, \frac{\beta W}{z}\right) + \Gamma_3\left(\frac{[1-\alpha]\,H}{z}, \frac{[1-\beta]\,W}{z}\right) + \Gamma_4\left(\frac{[1-\alpha]\,H}{z}, \frac{\beta W}{z}\right). \quad (3.197)$$

3.8.6. ADVANTAGES AND LIMITATIONS OF KERNEL METHODS

Clearly kernel methods remain important in shielding technology. With them results are usually obtained cheaper and faster than by full-blown transport calculations and consequently they will continue to be used for quick estimates, for checks of transport code results, and for engineering parametric studies. However, Monte Carlo or the other sophisticated transport codes should be used in the final design stages.

The danger in using a kernel method arises when the problem has complexities which cannot be accounted for by the kernel. The kernel, basically, is the solution for a differential source under prescribed conditions such as an infinite homogeneous medium and when the application departs significantly from the specified conditions, great errors are possible. It must be kept in mind that a kernel technique is intrinsically a ray-analysis technique, and if the radiation has streaming or short-circuiting paths, the kernel result may be a serious underestimate. In addition to the obvious breakdown of the simple kernel methods when applied to multi-layered geometries and irregular configurations (unless very special kernels are used), breakdown of the method will occur when dose rates away from a surface are desired or when scattering off external surfaces or from lateral shields become important.

The breakdown of kernel methods when applied to the complicated geometries of nuclear rocket designs, such as the design shown in Fig. 3.10 (ref. 117), has been experienced by several groups. Capo, Stephenson, and Magaw,[118] for example, used their KAP-V kernel code to predict the gamma-ray dose rate for the NRX series reactors and found that in some locations the predictions were a factor of 10 lower than corresponding measurements. On the other hand, Soltesz *et al.*,[119] using the same code for calculations of a rocket reactor assembly and internal shield tested at the PAX-E5 critical assembly, found that the code gave results that were in good agreement both with the measurements and with discrete ordinates and Monte Carlo calculations.

Kernel codes using the extended single-scattering model have been applied with success for rocket geometries having large hydrogen volumes (both liquid and gaseous) and shadow shields. Warman[120] used such a code for a lightly shielded engine and obtained a value of 13,500 rem at the top of the tank, which compares favorably with a value of 10,000 rem computed by the Monte Carlo method. From these examples it must be concluded that while kernel methods may give good

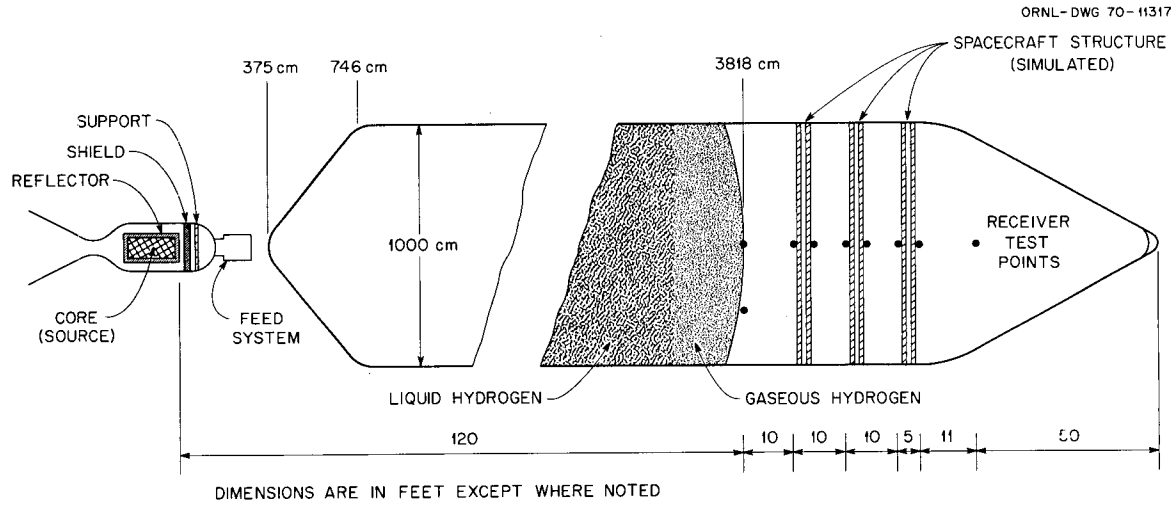

Fig. 3.10. Nuclear Rocket Geometry. (From ref. 117.)

results for a complicated geometry, underestimates or overestimates of shielding requirements are possible and the use of kernel techniques in complex situations should in general be avoided.

As pointed out above, kernel methods also tend to break down when dose rates away from a shield surface are desired. This type of difficulty can be experienced when a kernel method is used to calculate the gamma-ray dose from the surface of a lead shipping cask for spent fuel elements. Near the surface, the configuration is fairly representative of an infinite medium, and thus good answers for the dose should be obtained there. But for a point further removed, the detector views a truly finite configuration and the use of infinite-medium buildup factors will overestimate the dose.

Table 3.10 shows a comparison by Solomito and Claiborne[121] between the simple kernel method (QAD code) and a two-dimensional discrete ordinates calculation (DOT and SPACETRAN codes) at various points off the surface of a typical shipping cask (7.6-in.-thick lead shield). The column identified as "Kernel" gives the kernel method results normalized to the discrete ordinates results at the surface. The comparison shows that good answers were obtained by the kernel method near the surface (less than about 3 ft away), but that at a point 25 ft away, the kernel calculation overestimated the dose by more than a factor of two.

In general, the degree to which the kernel method results will vary from discrete ordinates or other transport methods will depend on the angular distribution of the leakage current from the surface. Unfortunately, this distribution cannot be easily determined and will depend on the source configuration and the

Table 3.10. Comparison of Gamma-Ray Doses Calculated by Kernel and Discrete Ordinates Methods for Points Off the Surface of a Lead Shipping Cask[a]

Distance from Surface (ft)	Gamma-Ray Dose (Arbitrary Units)	
	Kernel	Discrete Ordinates
0.1	0.81	0.76
0.4	0.65	0.65
0.8	0.51	0.49
1.0	0.46	0.44
1.5	0.36	0.35
3.0	0.23	0.20
25.	0.016	0.0072

[a]From ref. 121.

geometry and scattering properties of the attenuating medium. Consider, for example, the simple case of a shielded volumetric source giving rise to leakage from a plane surface but within a cone bounded by θ_0 (see Fig. 3.11). Assume that the angular flux is uniform over the surface and is given by $\Phi(\mu)$, where μ is the cosine of the angle measured from the normal. Then the variation of the flux at the detector position D, as a function of the size of the source aperture bounded by $\theta_0 (\mu_0 = \cos \theta_0)$, can be described by

$$\Phi(\mu_0) = 2\pi \int_0^a \cos\theta \; \Phi(\mu) \frac{y \, dy}{R^2} \tag{3.198}$$

$$= \int_{\text{surface}} \Phi(\mu) \, d\bar{\Omega}_s \tag{3.199}$$

$$= 2\pi \int_{\mu_0}^1 \Phi(\mu) \, d\mu \, , \tag{3.200}$$

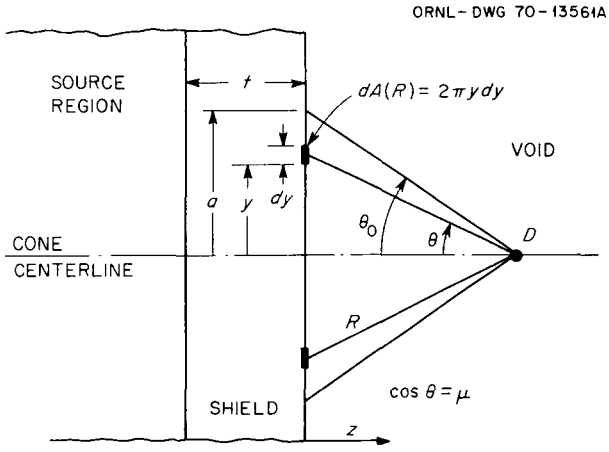

Fig. 3.11. Plane Geometry Source and Shield Bounded by Cone Defined by θ_0.

where

$\Phi(\mu_0)$ = total flux response at D due to a source aperture bounded by $\theta_0 = \cos^{-1} \mu_0$,

$\Phi(\mu)$ = angular flux (per unit solid angle) on the plane surface,

$d\bar{\Omega}_s$ = differential solid angle subtended by the differential surface $2\pi y\, dy$,

$$d\bar{\Omega}_s = \frac{2\pi y\, dy \cos\theta}{R^2}\,, \tag{3.201}$$

$$d\bar{\Omega}_s = 2\pi d\mu\,. \tag{3.202}$$

The function $\Phi(\mu_0)$ can also be interpreted as the variation of the total flux with distance from a disk source, since μ_0 depends on distance. With $\mu_0 = 0$ (i.e., infinite plane source) there is no variation with distance. For example, the angular flux might be represented by

$$\Phi(\mu) = \frac{n+1}{2\pi}\,\mu^n\,, \tag{3.203}$$

which is normalized such that

$$\int_{2\pi} \frac{(n+1)}{2\pi}\,\mu^n\, d\bar{\Omega}_s = 1\,. \tag{3.204}$$

Then, for the flux at D,

$$\Phi(\mu_0) = 1 - \mu_0^{n+1}\,. \tag{3.205}$$

If the volume source density is uniform and exponential attenuation with a cross section Σ is assumed for the semi-infinite (infinite transverse dimensions) volumetric source and shield regions (Fig. 3.11), the angular distribution on the shield surface implied by the kernel method can be shown to be proportional to exp $(-\Sigma t/\mu)$. For a reasonably thick shield region, this function will be highly peaked in the forward direction. For $\Sigma t = 2$, for example, the distribution is proportional to about μ^2 or μ^3, but most practical shields have $\Sigma t > 5$, which implies a highly peaked distribution. Because of this, the kernel-predicted flux along the centerline of the configuration will remain high and be conservative. That is, based on the kernel approach

$$\Phi(\mu_0) = 1 - \mu_0 E_2(\Sigma t/\mu_0)/E_2(\Sigma t)\,, \tag{3.206}$$

where

$$E_2(x) = x\int_x^\infty e^{-y}\, y^{-2}\, dy\,. \tag{3.207}$$

This result will always be greater than values from Eq. 3.205 for typical values of n and Σt, because the detector does not see as much of the off-centerline emission from the surface if the angular distribution is peaked in the forward direction.

A third type of breakdown of kernel methods has been demonstrated in some space reactor applications, such as in a study by ORNL to use a boiling potassium-cooled reactor. Such designs incorporate a relatively small reactor with a large radiator (Fig. 3.12, from ref. 122). The diameter of the "thin-shell" radiator would be about 25 ft and the diameter of the reactor shield about 6 or 7 ft. Obviously, the dose rate due to scattering off the radiator surface, which is "seen" by the crew or instrument compartment, would not be accounted for by a simple kernel method. Using the "buildup factor method" to compute the flux at the thin surface of the radiator and then computing a new source with the angular scattering cross section based on the original photon energy would underpredict the dose because of the preferential forward scattering of the higher energy photons. Using a kernel employing an estimate of the spectrum, such as the differential energy spectrum method,[123] would improve the accuracy.

The third type of breakdown is further illustrated by the case of an asymmetric 2π shield design such as shown in Fig. 3.13 (ref. 124). The asymmetry was intended to give a dose rate for a radial detector of at least 100 times the dose rate of an axial detector at a distance of 100 ft from the surfaces. A simple buildup factor calculation yielded a dose rate of about 1 mrad/hr of gamma rays at the axial detector (crew compartment), whereas a

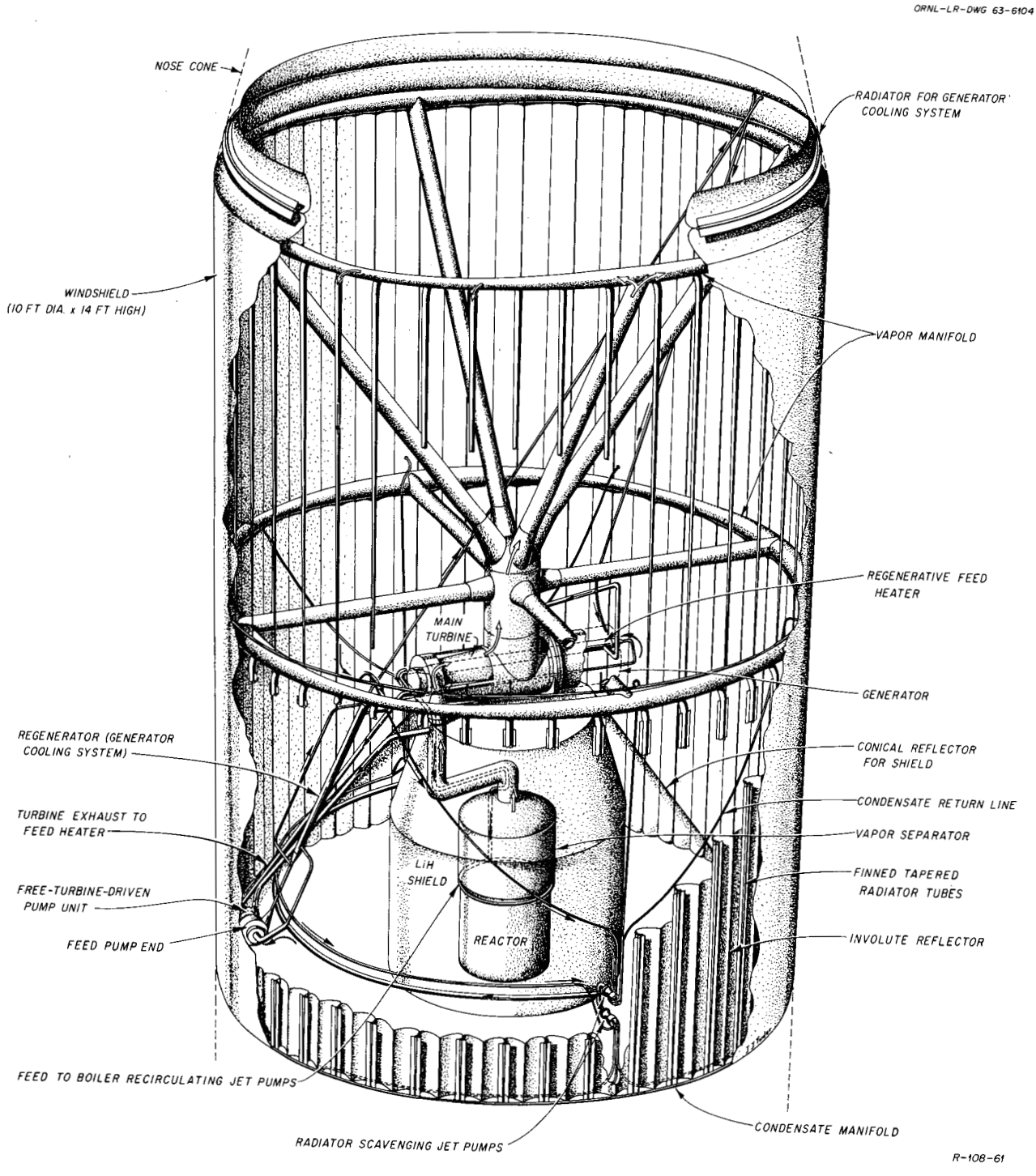

Fig. 3.12. SNAP Reactor and Radiator Geometry. (From ref. 122.)

discrete ordinates calculation[125] (DOT and SPACETRAN codes) gave a dose rate of 47 mrad/hr. The difference is explained by Table 3.11, which shows that some of the gamma rays that leaked through the relatively thin tungsten side shield were scattered in the crew direction by the lithium hydride side shield. In fact, 98% of the gamma-ray dose rate reaching the crew compartment was due either to these scattered gamma rays or to gamma rays produced by neutron captures in the lithium hydride side shield. The last line in the table shows that only 1% was due to captures. The third line shows that most of the gamma rays reaching the crew compartment do so by passing through the top surface of the side shield rather than scattering through the front shield. This is evident by the large reduction in the dose when the top surface of the side shield was not included in the top surface integral.

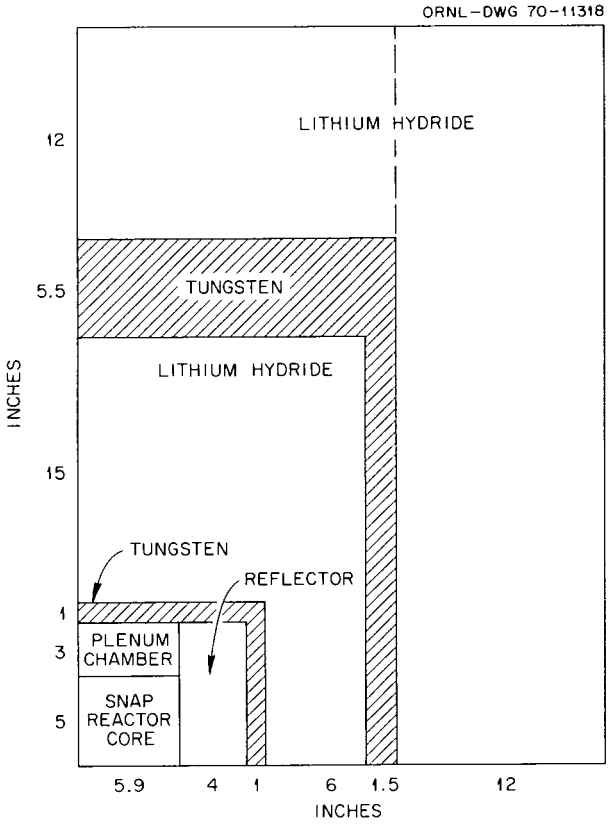

Fig. 3.13. SNAP Reactor with 2π Tungsten and Lithium Hydride Shield. (From ref. 124.)

Table 3.11. Analysis of Gamma-Ray Dose Rate at Crew Position[a,b]

Assumptions	Gamma-Ray Dose Rate (mrad/hr/MW)	Percentage
All regions considered	47.1	100
LiH side shield completely removed	1.04	2.2
Top surface of LiH side shield not included in surface integral	6.67	14.2
No captures allowed in outer LiH zone	46.5	99

[a]From ref. 124.
[b]See Fig. 3.13.

3.9. Combination Removal-Diffusion Methods

The removal cross section concept described in Section 3.8.2 provides a method for calculating the dose due to high-energy neutrons that penetrate a hydrogenous shield; however, the technique cannot be used to predict the dose due to neutrons that have been moderated or to calculate the thermal-neutron flux, which is used to obtain the capture gamma-ray source distribution within the shield.*

The energy and spatial distributions of the moderated neutrons throughout a shield have sometimes been calculated by using the elementary theories of neutron moderation and diffusion (see Section 3.6). But these methods of reactor physics are normally used to predict the average behavior of neutrons involved in reactor criticality problems and implicitly assume that all neutrons are nearly isotropic in their flight directions. In contrast, the neutrons of importance to the shielding problem are born with energies much greater than the average and develop a highly anisotropic angular distribution as they penetrate through the shield. Elementary core calculation methods cannot accurately describe the transport of these neutrons.

The inadequacy of both the removal concept and the elementary methods of reactor core physics to calculate the whole shielding problem has resulted in neutron transport being regarded as a two-step process: a step in which a high-energy neutron penetrates to some position within the shield where it suffers a collision that degrades its energy significantly; and another step in which the resulting moderated neutron enters a diffusion process. Characteristically, the distance traveled by the neutron during the diffusion process is very much less than that which it traveled as a fast neutron, and once it has entered this second phase, the methods of reactor physics could apply. It was such reasoning that prompted the first-flight correction to the age in Fermi age theory.[1] This correction was necessary because a neutron cannot enter a process described as continuous slowing down (as required by Fermi age theory) until it has had at least one collision.

*Calculations of capture gamma-ray doses are discussed in Section 3.10.

The development of high-speed computers and the resulting extensive use of multigroup diffusion theory for reactor criticality problems made the development of a technique that utilized diffusion theory even more attractive. In one of the first attempts to develop such a technique, Haffner[126] in 1958 used diffusion theory to calculate thermal-neutron fluxes within a reactor shield and then normalized the results at each space point according to the fast-neutron dose rate obtained with the Albert-Welton kernel (see Section 3.8.2). Anderson and Shure[127] used a similar technique when they applied a known pure water kernel to normalize diffusion (actually P_1 multigroup) results for a metal-water mixture. In general, they obtained good results for laminated iron-water shields. (Shure[2,128] later showed that a straightforward P_3 calculation without the use of a kernel also gave good results.) The main assumption in the Anderson-Shure technique is that the multigroup procedure correctly calculates the ratio between the fluxes in water and those in a metal-water mixture.

After several attempts had been made to develop a technique by correcting diffusion theory results, a different approach to the problem evolved: a correction was made *before* the diffusion theory calculation was performed. In the early calculations this was done by computing the singly scattered neutron flux from the uncollided flux and then using it as a source for the diffusion theory calculation. A difficulty inherent in this procedure, especially for hydrogenous media, is that the penetrating component does not consist of uncollided neutrons alone, but rather is composed largely of neutrons that have had one or more collisions but have suffered only small angular deflections. When these neutrons were accounted for, the first successful two-step model for neutron-penetration calculations became available. The combination of the fast-neutron removal concept and age-diffusion theory is commonly referred to as the "Spinney method," after its chief developer. The remainder of this section is devoted to a description of the original version of this removal-age-diffusion method and subsequent variations of it.

3.9.1. THE SPINNEY METHOD

The Spinney method as first described by Avery *et al.*[129] is characterized by the following basic physical assumptions:*

1. The penetrating component of the source neutrons consists of the high-energy neutrons that suffer only small energy loss through small-angle elastic collisions plus the uncollided neutrons.
2. Neutrons that suffer large energy loss through either wide-angle elastic or inelastic scattering are regarded as being removed from the fast beam. This process can be described by an energy-dependent "removal" cross section.
3. The removed neutrons are further degraded in energy in accordance with age theory and do not travel significantly from the point of removal.
4. Near the source, the removed neutrons have a spectral and spatial distribution closely described by the conventional age-diffusion theory.
5. Neutrons removed after they have penetrated deep into a homogeneous medium develop an equilibrium spectrum and are attenuated at the same rate that the penetrating component is attenuated.
6. The equilibrium spectrum of the degraded neutrons is disturbed near the boundaries between dissimilar media.

The neutron flux that corresponds to the penetrating component of the source neutrons is given by the kernel

$$\Phi^0(r,E) = \frac{S_0(E)\, e^{-\Sigma_R(E) r}}{4\pi r^2}, \qquad (3.207)$$

where

$\Phi^0(r,E)$ is called the "removal flux" and is differential with respect to the source energy E,

$S_0(E)$ = source strength of fission-spectrum neutrons per unit energy about the source energy E,

$\Sigma_R(E)$ = removal cross section evaluated at the source energy E (determined experimentally or approximated by the transport cross section),†

r = distance from the source.

The removed neutrons are regarded as a local source of degraded neutrons, the behavior of which can be adequately described by diffusion theory. The intensity of this source is given by

$$S(r) = \int \Phi^0(r,E)\, \Sigma_R(E)\, dE = \int \frac{S_0(E)\, \Sigma_R(E)\, e^{-\Sigma_R(E) r}}{4\pi r^2}\, dE. \qquad (3.208)$$

In the earliest formulation these neutrons (that is, the removed neutrons) are then introduced into the highest energy group of an appropriate set of one-dimensional multigroup diffusion equations in order to calculate the distribution of the low-energy neutron flux. The equations comprising the multigroup set are given by

$$\nabla^2 \Phi_1(r) - \kappa_1^2\, \Phi_1(r) - \frac{\Sigma_1^q}{D_1} \Phi_1(r) + \frac{S(r)}{D_1} = 0, \quad G = 1,$$

$$\nabla^2\, \Phi_G(r) - \kappa_G^2\, \Phi_G(r) - \frac{\Sigma_G^a}{D_G}\, \Phi_G(r) + \frac{D_{G-1}\, \kappa_{G-1}^2\, \Phi_{G-1}(r)}{D_G} = 0, \; G > 1, \qquad (3.209)$$

where

Φ_G = group flux for the Gth group,

Σ_G^a = group-averaged macroscopic absorption cross section,

D_G = group-averaged diffusion coefficient,

κ_G^{-1} = slowing-down length for the Gth group.

The slowing-down length is calculated according to age theory and for the Gth group is given by

$$\left(\frac{1}{\kappa_G}\right)^2 = \int_{E_{g+1}}^{E_g} \frac{dE}{3\, \xi(E)\, \Sigma_s(E)\, \Sigma_{tr}(E)\, E}, \qquad (3.210)$$

where

$\xi(E)$ = average change in lethargy per collision for neutrons of energy E,

$\Sigma_s(E)$ = macroscopic scattering cross section for neutrons of energy E,

$\Sigma_{tr}(E)$ = macroscopic transport cross section for neutrons of energy E.

In the original formulation of the Spinney method, five energy groups were taken for the multigroup diffusion calculation. The bottom group, which was a thermal group, had an upper energy of 2.81 kT (k = 8.61×10^{-5} eV/°K), and the highest group (G = 1) had an upper energy of 2 MeV. It was assumed that all removed source neutrons were placed directly into the highest group. Solution of the group diffusion equations, of course, required that boundary conditions be

*Items 4, 5, and 6 are intrinsically associated only with the earliest versions of the Spinney method. Most versions – certainly the most recent versions – are in no way constrained by these assumptions.

†See Section 3.8.

specified at the inner and outer surfaces of the shield. A zero reentrant condition was imposed at the outer boundary; this was stated in terms of the extrapolated boundary condition, which requires the group fluxes to vanish at a distance 2.13 D_G beyond the physical boundary. The boundary conditions at the inner surface of the shield were established by requiring that the fluxes be equal to those determined from reactor core calculations.

This original formulation was used with some success to predict the distribution of low-energy neutrons in concrete shields for existing graphite-moderated reactors, but it was not suited for general application. Some of its inadequacies were that (1) all the removed neutrons were placed in one group, which neglected any additional diffusion-type transport that could have been accomplished at energies greater than 2 MeV, (2) not enough groups were used to adequately represent the slowing-down process, and (3) the transfer of neutrons from one energy group to the next lower group did not describe the large energy losses experienced by neutrons that had suffered an inelastic scattering or a collision with hydrogen.

3.9.2. MODERN VARIATIONS OF THE SPINNEY METHOD

Many modifications to and variations of the Spinney method have been developed, the most recent of which are exemplified by the RASH E, MAC, NRN, SABINE, and ATTOW codes.

RASH E

In the RASH E* formulation[130,131] the modifications include an increase in the number of groups to 16 and a broader energy range (0–10 MeV). Also, the one-dimensional multigroup equations have been modified to include a direct source of removed neutrons into the nine highest energy groups. The equations so modified are as follows:

$$\nabla^2 \Phi_1(r) - \kappa_1^2 \Phi_1(r) - \frac{\Sigma_1^a}{D_1} \Phi_1(r) + \frac{\psi_1(r)}{D_1} = 0,$$

$$G = 1 ,$$

$$\nabla^2 \Phi_G(r) - \kappa_G^2 \Phi_G(r) - \frac{\Sigma_G^a}{D_G} \Phi_G(r) + \frac{D_{G-1} \kappa_{G-1}^2}{D_G} \Phi_{G-1}(r) + \frac{\psi_G(r)}{D_G} = 0,$$

$$G = 2, 3, \ldots 9 ,$$

$$\nabla^2 \Phi_G(r) - \kappa_G^2 \Phi_G(r) - \frac{\Sigma_G^a}{D_G} \Phi_G(r) + \frac{D_{G-1} \kappa_{G-1}^2}{D_G} \Phi_{G-1}(r) = 0 ,$$

$$G = 10, 11, \ldots 15 ,$$

$$\nabla^2 \Phi_T(r) - \frac{\Sigma_T^a}{D_T} \Phi_T(r) + \frac{D_{15} \kappa_{15}^2}{D_T} \Phi_{15}(r) = 0 ,$$

$$G = 16 , \quad (3.211)$$

where the subscript T corresponds to $G = 16$ designates the thermal-neutron energy group.

The source term for the Gth group resulting from removed neutrons is given by

$$\psi_g(r) = \sum_B S_B(r) ,$$

where $S_B(r)$ is determined in the following manner. The fission spectrum is divided into 18 energy bands of 1-MeV width. Neutrons removed from the Bth energy band are given by

$$S_B(r) = \int_{E_{b+1}}^{E_b} \frac{S_0(E) \Sigma_R(E) e^{-\Sigma_R(E) r}}{4\pi r^2} dE ,$$

$$B = 1, 2, \ldots 18 . \quad (3.212)$$

The neutrons from each of the removal bands in the energy range 0 to 8 MeV (B = 18, 17, 16, ... 11) are introduced into the energy group whose upper energy limit corresponds to the mid-energy of the band. Neutrons from all the bands above 8 MeV (B = 10, 9, 8, ... 1) have a mean energy of about 10 MeV and are all introduced into the highest energy group (group 1), which has an upper energy of 10 MeV. This transfer scheme, along with the removal-band and energy-group structures for RASH E, is presented in Table 3.12.

*RASH E is the latest member of the RASH family of codes utilizing the Spinney method. RASH E is included in a FORTRAN code package known as COMPRASH and can be obtained from the Radiation Shielding Information Center (RSIC) (see Appendix 3B).

Table 3.12. Removal-Band and Energy-Group Structures Used in RASH E[a]

Removal Bands			Diffusion Groups			Band-to-Group Transfer Scheme
Band No.	Energy Limits (MeV)		Group No.	Energy Limits (MeV)		
	Upper	Lower		Upper	Lower	
1	18	17	1	1.0×10^{1}	7.5×10^{0}	1 → 1
2	17	16	2	7.5×10^{0}	6.5×10^{0}	2 → 1
3	16	15	3	6.5×10^{0}	5.5×10^{0}	3 → 1
4	15	14	4	5.5×10^{0}	4.5×10^{0}	4 → 1
5	14	13	5	4.5×10^{0}	3.5×10^{0}	5 → 1
6	13	12	6	3.5×10^{0}	2.5×10^{0}	6 → 1
7	12	11	7	2.5×10^{0}	1.5×10^{0}	7 → 1
8	11	10	8	1.5×10^{0}	5.0×10^{-1}	8 → 1
9	10	9	9	5.0×10^{-1}	5.0×10^{-2}	9 → 1
10	9	8	10	5.0×10^{-2}	5.0×10^{-3}	10 → 1
11	8	7	11	5.0×10^{-3}	5.0×10^{-4}	11 → 2
12	7	6	12	5.0×10^{-4}	5.0×10^{-5}	12 → 3
13	6	5	13	5.0×10^{-5}	5.0×10^{-6}	13 → 4
14	5	4	14	5.0×10^{-6}	5.5×10^{-7}	14 → 5
15	4	3	15	5.5×10^{-7}	7.0×10^{-8}	15 → 6
16	3	2	16	Thermal		16 → 7
17	2	1				17 → 8
18	1	0				18 → 9

[a]From ref. 130.

MAC

In the MAC* formulation[132,133] the number of energy groups for the one-dimensional group-diffusion calculation is increased to 31 over an energy range from 0 to 10 MeV. Again the fission spectrum is divided into 18 removal bands of 1-MeV width. The flux from the removed neutrons (usually called "removal flux") corresponding to the Bth removal band is given by

$$\Phi_B^0(r) = \int_{E_{b+1}}^{E_b} \frac{S_0(E)\, e^{-\Sigma_R(E)r}}{4\pi r^2}\, dE . \qquad (3.213)$$

The removed neutrons are introduced into the five highest energy groups only. The transfer scheme, along with the removal-band and energy-group structures, is presented in Table 3.13.

The MAC formulation differs from the original Spinney method in two major respects: (1) the removal flux is added directly to the group-diffusion flux after the diffusion calculation has been performed, and the combined flux is then used to calculate source neutrons for the lower-energy diffusion groups, and (2) the general treatment of the downscatter transfer of neutrons allows for a more accurate representation of inelastic scattering and collisions with hydrogen.

The highest energy group ($G = 1$) is not actually treated as a diffusion group. The collision density,

$$\Sigma_{1G'}\left[\sum_{B=1}^{12} \Phi_B^0(r)\right],$$

*Available from RSIC in several versions (see Appendix 3B).

Table 3.13. Removal-Band and Energy-Group Structures Used in MAC[a]

Removal Bands			Diffusion Groups			Band-to-Group Transfer Scheme
Band No.	Energy Limits (MeV)		Group No.	Energy Limits (MeV)		
	Upper	Lower		Upper	Lower	
1	18	17	1	1.000×10	6.065×10^{0}	1 → 1
2	17	16	2	6.065×10^{0}	3.679×10^{0}	2 → 1
3	16	15	3	3.679×10^{0}	2.231×10^{0}	3 → 1
4	15	14	4	2.231×10^{0}	1.353×10^{0}	4 → 1
5	14	13	5	1.353×10^{0}	8.208×10^{-1}	5 → 1
6	13	12	6	8.208×10^{-1}	3.876×10^{-1}	6 → 1
7	12	11	7	3.876×10^{-1}	1.830×10^{-1}	7 → 1
8	11	10	8	1.830×10^{-1}	6.733×10^{-2}	8 → 1
9	10	9	9	6.733×10^{-2}	2.600×10^{-2}	9 → 1
10	9	8	10	2.600×10^{-2}	2.000×10^{-2}	10 → 1
11	8	7	11	2.000×10^{-2}	9.118×10^{-3}	11 → 1
12	7	6	12	9.118×10^{-3}	3.355×10^{-3}	12 → 1
13	6	5	13	3.355×10^{-3}	1.234×10^{-3}	13 → 2
14	5	4	14	1.234×10^{-3}	4.540×10^{-4}	14 → 2
15	4	3	15	4.540×10^{-4}	3.199×10^{-4}	15 → 2
16	3	2	16	3.199×10^{-4}	2.255×10^{-4}	16 → 3
17	2	1	17	2.255×10^{-4}	1.120×10^{-4}	17 → 4
18	1	0	18	1.120×10^{-4}	6.147×10^{-5}	18 → 5
			19	6.147×10^{-5}	3.374×10^{-5}	
			20	3.374×10^{-5}	1.515×10^{-5}	
			21	1.515×10^{-5}	1.016×10^{-5}	
			22	1.016×10^{-5}	4.565×10^{-6}	
			23	4.565×10^{-6}	1.375×10^{-6}	
			24	1.375×10^{-6}	9.214×10^{-7}	
			25	9.214×10^{-7}	6.716×10^{-7}	
			26	6.716×10^{-7}	4.140×10^{-7}	
			27	4.140×10^{-7}	2.775×10^{-7}	
			28	2.775×10^{-7}	1.860×10^{-7}	
			29	1.860×10^{-7}	1.247×10^{-7}	
			30	1.247×10^{-7}	7.595×10^{-8}	
			31	7.595×10^{-8}	0	

[a]From ref. 132.

which is based on the removal fluxes (corresponding to the energy bands 1 through 12), provides neutrons by downscattering from the first group into the G'th group, $G' = 2, 3, \ldots 31$. The kinds of possible interactions, as described by their respective group-to-group transfer cross section $\Sigma_{I,G'}$, will determine the extent of the downscatter. A diffusion calculation is then performed on the second group, with the neutrons removed from group 1 used as the source. Solution of the group-2 diffusion equation,

$$D_2 \nabla^2 \Phi_2(r) - \sum_{G'=3}^{31} \Sigma_{2G'} \Phi_2(r) - \Sigma_2^a \Phi_2(r) + \Sigma_{1,2} \left[\sum_{B=1}^{12} \Phi_B^0(r) \right] = 0 , \quad (3.214)$$

yields the group-diffusion flux $\Phi_2(r)$. The group-2 removal fluxes are then added to the diffusion flux in order to calculate the downscatter source of neutrons from group 2 into the lower-energy groups. The downscatter source into group G ($G = 3, 4, \ldots 31$) is given by

$$\Sigma_{2G} \left[\Phi_2(r) + \sum_{B=13}^{15} \Phi_B^0(r) \right] .$$

The calculation proceeds in a similar fashion from one group to the next lower group and so on. In general, for $G > 2$, the group-diffusion equations are given by

$$D_G \nabla^2 \Phi_G(r) - \sum_{G'=G+1}^{31} \Sigma_{GG'} \Phi_G(r) - \Sigma_G^a \Phi_G(r) + \sum_{G'=G-1}^{1} \Sigma_{G'G} \left[\Phi_{G'}(r) + \sum_{B(G')} \Phi_B^0(r) \right] = 0 , \quad G = 3, 4, \ldots , \quad (3.215)$$

and the downscatter source term from the Gth group into the G'th group is

$$\Sigma_{GG'} \left[\Phi_G(r) + \Phi_B^0(r) \right] .$$

It is noted that there are no band-to-group transfers for $G > 5$ and the downscatter source term becomes simply $\Sigma_{GG'} \Phi_G(r)$.

NRN

In the NRN* formulation [134,135] the energy structure for the removal bands and energy groups differs significantly from that used in the RASH and MAC formulations. The group structure for the group-diffusion calculation consists of 24 groups over an energy range 0 to 18 MeV, and the fission spectrum is divided into 30 bands of varying widths. The removal-band and energy-group structures are presented in Table 3.14.

The NRN method allows for the transfer of removed neutrons from each removal band to many diffusion groups. The source for the Gth diffusion group arising from all removal collisions is

$$\sum_B \Sigma_{BG}^0 \Phi_B^0(r) ,$$

where Φ_B^0 = removal flux in the Bth energy band, and Σ_{BG}^0 = energy-averaged removal cross section for the transfer of neutrons from the Bth removal band into the Gth energy group.

The calculation also allows transfer from each diffusion group to all lower-energy diffusion groups. The one-dimensional group-diffusion equation for the Gth group is given by

$$D_G \nabla^2 \Phi_G(r) - \sum_{G'=G+1}^{24} \Sigma_{GG'} \Phi_G(r) - \Sigma_G^a \Phi_G(r) + \sum_{G'=G-1}^{1} \Sigma_{G'G} \Phi_{G'}(r) + \sum_B \Sigma_{BG}^0 \Phi_B^0(r) = 0 , \quad (3.216)$$

where the various diffusion theory parameters have conventional definitions.

SABINE

The SABINE code,[136,137] developed and used in Europe later than RASH and NRN, employs 19 removal bands and 26 diffusion groups, the energy structures of which are shown in Table 3.15. The code is also one dimensional and can solve problems in slab, cylindrical, and spherical geometries. Particular attention has been paid to the coupling of the removal flux with the diffusion equations. The assumed model in SABINE makes use of the same transfer matrix for band-to-group and group-to-group transfers, that is,

$$\Sigma_{BG} \equiv \Sigma_{G'G} ,$$

where the removal band B and diffusion group G' correspond to the same energy and $G' \neq G$. There is also within-group transfers of removal neutrons to the diffusion group of the same energy range. This source is given by

$$\psi_{GG}(r) = \Sigma_{BB}^* \Phi_B^0(r) ,$$

where B and G are for the same energy range and

$$\Sigma_{BB}^* = \Sigma_R(B) - \Sigma_B^a - \sum_{G'=B+1}^{G_{max}} \Sigma_{BG'} ,$$

*Available from RSIC.

Table 3.14. Removal-Band and Energy-Group Structures Used in NRN[a]

Removal Bands			Diffusion Group		
Band No.	Energy Limits (MeV)		Group No.	Energy Limits (MeV)	
	Upper	Lower		Upper	Lower
1	1.8×10^{1}	1.43×10^{1}	1	1.8×10^{1}	1.35×10^{1}
2	1.43×10^{1}	1.136×10^{1}	2	1.35×10^{1}	1.0×10^{1}
3	1.136×10^{1}	9.021×10^{0}	3	1.0×10^{1}	7.8×10^{0}
4	9.021×10^{0}	7.166×10^{0}	4	7.8×10^{0}	5.9×10^{0}
5	7.166×10^{0}	5.692×10^{0}	5	5.9×10^{0}	4.4×10^{0}
6	5.692×10^{0}	4.521×10^{0}	6	4.4×10^{0}	3.4×10^{0}
7	4.521×10^{0}	3.591×10^{0}	7	3.4×10^{0}	2.6×10^{0}
8	3.591×10^{0}	2.853×10^{0}	8	2.6×10^{0}	2.0×10^{0}
9	2.853×10^{0}	2.267×10^{0}	9	2.0×10^{0}	1.5×10^{0}
10	2.267×10^{0}	1.800×10^{0}	10	1.5×10^{0}	1.2×10^{0}
11	1.800×10^{0}	1.430×10^{0}	11	1.2×10^{0}	9.0×10^{-1}
12	1.430×10^{0}	1.136×10^{0}	12	9.0×10^{-1}	7.0×10^{-1}
13	1.136×10^{0}	9.021×10^{-1}	13	7.0×10^{-1}	5.1×10^{-1}
14	9.021×10^{-1}	7.166×10^{-1}	14	5.1×10^{-1}	3.8×10^{-1}
15	7.166×10^{-1}	5.692×10^{-1}	15	3.8×10^{-1}	3.0×10^{-1}
16	5.692×10^{-1}	4.521×10^{-1}	16	3.0×10^{-1}	1.0×10^{-1}
17	4.521×10^{-1}	3.591×10^{-1}	17	1.0×10^{-1}	3.10×10^{-2}
18	3.591×10^{-1}	2.853×10^{-1}	18	3.10×10^{-2}	1.10×10^{-2}
19	2.853×10^{-1}	2.267×10^{-1}	19	1.10×10^{-2}	1.10×10^{-3}
20	2.267×10^{-1}	1.800×10^{-1}	20	1.10×10^{-3}	1.10×10^{-4}
21	1.800×10^{-1}	1.430×10^{-1}	21	1.10×10^{-4}	1.10×10^{-5}
22	1.430×10^{-1}	1.136×10^{-1}	22	1.10×10^{-5}	1.10×10^{-6}
23	1.136×10^{-1}	9.021×10^{-2}	23	1.10×10^{-6}	1.05×10^{-7}
24	9.021×10^{-2}	7.166×10^{-2}	24	Thermal	
25	7.166×10^{-2}	5.692×10^{-2}			
26	5.692×10^{-2}	4.521×10^{-2}			
27	4.521×10^{-2}	3.591×10^{-2}			
28	3.591×10^{-2}	2.853×10^{-2}			
29	2.853×10^{-2}	2.267×10^{-2}			
30	2.267×10^{-2}	1.80×10^{-2}			

[a]From ref. 134.

Table 3.15. Removal-Band and Energy-Group Structures Used in SABINE[a]

Removal Bands		Diffusion Groups		
Band No.	Upper Energy Limit	Group No.	Upper Energy Limit	Lethargy Width
		0	18 MeV	–
1	18 Mev	1	14.918	0.9
2	16.5	2	6.065	0.5
3	14.918	3	3.68	0.5
4	14	4	2.23	0.5
5	13	5	1.35	0.5
6	12	6	821 keV	0.5
7	11	7	498	0.5
8	10	8	302	0.5
9	9	9	183	0.75
10	8	10	86.5	1.00
11	7	11	31.8	1.00
12	6.065	12	11.7	1.00
13	5.2	13	4.31	1.00
14	4.4	14	1.58	1.00
15	3.68	15	583 eV	1.00
16	3.00	16	214	1.00
17	2.23	17	78.9	1.00
18	1.35	18	29.0	1.00
19	0.821	19	10.7	0.75
		20	5.04	0.5
		21	3.06	0.5
		22	1.85	0.5
		23	1.12	0.5
		24	0.682	0.5
		25	0.414	0.728
		26	0.200	--

[a]From ref. 136.

$\Sigma_R(B)$ being the removal cross section for the removal band B. Although the developers for the RASH code did not find that experimental energy-dependent cross sections improved results, the developers of SABINE used cross sections for water, carbon, aluminum, iron, lead, and terphenil measured at a 5.5-MeV accelerator.

Gamma-ray transport is accomplished by using seven energy groups and empirical region-dependent buildup factors based on transport calculations. Both primary sources (fission gamma rays) in the reactor core and secondary sources (capture and inelastic-scattering gamma rays) generated within the shield can be included.

ATTOW*

The ATTOW code[138] is a two-dimensional (finite cylinder or 2D rectangular) diffusion code which can accept removal sources prepared by a built-in subroutine. The removal-source subroutine calculates sources at points determined by the routine and fits two-dimensional polynomials, of order chosen by the user, to the results. These data are put on tape in a form which can be used by ATTOW. The spatial integration over the reactor core is performed by a Gaussian scheme using a stored table of zeros and weights.

Removal cross sections Σ_{BG} are input to the program, allowing the user control of the removal assumptions. The full group-to-group transfer matrix $\Sigma_{G'G}$ is also assumed for the diffusion treatment.

The ATTOW code has been used extensively in the United Kingdom for solving problems associated with fast-breeder reactors. It was found that the results were somewhat sensitive to the energy group structure chosen.[139] The 23-group structure (see Table 3.16) was judged best. This sensitivity is most pronounced when materials such as graphite are present and is attributed to the continuous slowing-down (age theory) assumption, although even a full-scatter matrix cannot preserve the energy-angle correlation in diffusion theory.[140] These difficulties should not be apparent in hydrogenous materials which generally have short diffusion lengths.

*Available from RSIC.

3.9.3. DIFFERENCES IN MODERN METHODS

A comparison of the preceding formulations shows that, with respect to the removal-band and energy-group schemes, RASH E and MAC are similar in concept and identical in many respects. The NRN, SABINE or ATTOW approach is more general and should provide the most accurate model if the required removal and transfer cross sections are known.

With regard to removal cross sections, RASH E and MAC use the cross sections suggested by the original Spinney formulation, which have the general form

$$\Sigma_R = \Sigma_t - f\,\Sigma_{el}\,, \qquad (3.217)$$

where

Σ_R = removal cross section,

Σ_t = total macroscopic cross section,

Σ_{el} = elastic scattering cross section,

f = fraction of elastic collisions that can be regarded as glancing.

Table 3.16. Energy Group Structure Used in ATTOW[a]

Group Number	Lower Energy Limit (MeV)[b]		
	49-Group Scheme	23-Group Scheme	16-Group Scheme
1	7.5	7.5	7.5
2	6.5	6.5	6.5
3	5.5	5.5	5.5
4	4.5	4.5	4.5
5	3.5	3.5	3.5
6	2.5	2.5	2.5
7	1.5	1.5	1.5
8	0.85	0.85	5(−1)[c]
9	0.5	0.5	5(−2)
10	0.35	0.15	5(−3)
11	0.225	5(−2)	5(−4)
12	0.15	1.5(−2)	5(−5)
13	0.1	5(−3)	5(−6)
14	7(−2)	1.5(−3)	5.5(−7)
15	5(−2)	5(−4)	7(−8)
16	3.5(−2)	1.5(−4)	Thermal
17	2.25(−2)	5(−5)	
18	1.5(−2)	1.5(−5)	
19	1(−2)	5(−6)	
20	7(−3)	1.5(−6)	
21	5(−3)	5.5(−7)	
22	3.5(−3)	7.0(−8)	
23	2(−3)	Thermal	
24	1.5(−3)		
25	1(−3)		
26	7(−4)		
27	5(−4)		
28	3.8(−4)		
29	2.25(−4)		
30	1.5(−4)		
31	1(−4)		
32	7(−5)		
33	5(−5)		
34	3.5(−5)		
35	2.25(−5)		
36	1.5(−5)		
37	1(−5)		
38	7(−6)		
39	5.5(−6)		
40	4.65(−6)		
41	3.5(−6)		
42	2.25(−6)		
43	1.60(−6)		
44	1.3(−6)		
45	1(−6)		
46	7(−7)		
47	5.5(−7)		
48	7(−8)		
49	Thermal		

[a]From ref. 138.
[b]Upper energy limit of Group 1 was 10 MeV in all cases.
[c]Read: 5×10^{-1}.

If f is taken to be the average cosine of scattering in the laboratory system, $\overline{\mu}_0$, the removal cross section becomes the transport cross section originally used by Spinney. In general, the parameter f cannot be determined intrinsically, and so a value must be assumed or determined empirically. This has been accomplished for a large variety of typical shield configurations, and the removal cross sections thus determined are used with a high degree of confidence.

NRN removal cross sections are obtained by experimentally determining the angles of scatter above which elastic collisions can be considered as removals. The removal cross section is given by

$$\Sigma_R = \Sigma_t - 2\pi \int_{\cos\theta_{rem}}^{1} \sigma(\theta)\, d(\cos\theta)\,, \quad (3.218)$$

where $\sigma(\theta)$ = differential elastic scattering cross section per unit solid angle about the scattering angle θ in the center-of-mass system, and θ_{rem} = scattering angle above which the collision is considered to be a removal. The value of θ_{rem} is determined by comparison of predicted neutron reaction rates with experimental values. A "best" value of $\cos\theta_{rem} = 0.45$ was obtained for hydrogen, and $\cos\theta_{rem} = 0.60$ was obtained for other nuclides. With these values of θ_{rem} a full set of removal cross sections can be derived.

The NRN removal cross sections do not appear to have any advantage over the Spinney-type cross sections since each scheme involves only a single adjustable parameter, θ_{rem} and f respectively.

The MAC scheme for transferring removed neutrons into energy groups differs significantly from that used by either RASH E or NRN. The procedure in MAC is to add the removal flux to the newly calculated group-diffusion flux in order to establish the group-to-group downscatter source. In contrast, RASH E and NRN introduce the removed neutrons into given groups as source neutrons to that group, a more natural procedure for the group-diffusion calculation. RASH E has a very restricted transfer scheme wherein the removed neutrons from a given removal band are introduced into a prescribed energy group and into no other. NRN provides for a much more general scheme, employing a removal matrix to describe the transfer of removed neutrons from a given removal band into any of the lower-energy groups.

Of the various methods considered here, the slowing-down model embodied in NRN, and especially in SABINE, gives the most accurate description of the

slowing-down process. It involves a general transfer matrix (from one group to any lower energy group) using detailed elastic and inelastic scattering cross sections for all nuclides. A similar scheme is employed by MAC; however, some inaccuracy is allowed in the description of the nonhydrogen elastic scattering.

RASH E uses a group-to-group transfer cross section based on the continuous slowing-down (age) model, which allows transfer to the next lower energy group only. This could lead to serious inaccuracies, particularly with respect to inelastic scatterings and collisions with hydrogen.

In conclusion, it can be stated that the Spinney method, used much more in Europe than in the U.S., seems to usually provide reliable results, but since it is an empirical method, it should be treated with some caution. That is, before being used extensively for design, results from rigorous calculational methods or experiments with similar configurations should be compared. Its simplicity and speed of computation could be a significant advantage over more sophisticated methods in design work.

3.10 Application of Kernel Technique to Secondary Gamma-Ray Dose Calculations

Often a large fraction of the radiation dose behind reactor and shelter shields is due to the gamma rays produced by neutron capture, and possibly to inelastic scattering, within the shield. If the spatial distribution of the neutron flux is known, the gamma-ray dose rate may be calculated for a large number of configurations by integrating the dose kernel over the source volume. Using the kernel technique as exemplified by Eq. 3.148 and slab geometry as shown in Fig. 3.14, the dose rate $\Gamma(t,a,b)$ on the shield surface due to a distributed monoenergetic isotropic gamma-ray source $S(x)$ bounded by planes at a and b is given by

$$\Gamma(t,a,b) = G(E) \int_a^b S(x)\, dx \int_0^\infty B_r(\mu R) \frac{e^{-\mu R}}{4\pi R^2} 2\pi\rho\, d\rho \quad , \tag{3.219}$$

where

x = one-dimensional spatial coordinate measured from the reference plane,

t = shield thickness,

ρ = radial distance to source point measured from the detector axis,

R = distance from the source point to the detector,

μ = total macroscopic cross section for gamma rays of source energy E,

$G(E)$ = uncollided flux-to-dose conversion factor, which for conversion to rads/hr is $5.767 \times 10^{-5} \dfrac{\mu_{at}(E)}{\rho_t} E$, where $\dfrac{\mu_{at}}{\rho_t}$ is the mass energy absorption coefficient for tissue,

$B_r(\mu R)$ = dose buildup factor for gamma rays of source energy E.

Since $R^2 = \rho^2 + z^2$,

$$\Gamma(t,a,b) = \frac{G(E)}{2} \int_a^b S(x)\, dx \int_{t-x}^\infty B_r(\mu R) \frac{e^{-\mu R}}{R} dR \ . \tag{3.220}$$

The gamma-ray source term can sometimes be represented quite well either by fitting with several terms or by piecewise fitting of the thermal-neutron flux distribution* (or of the fast flux distribution if inelastic scattering is being considered) with a function of the form

$$S(x) = S_a\, e^{-k(x-a)} \ , \ a \leqslant x \leqslant b \ , \tag{3.221}$$

where S_a is the gamma-ray source at a and k is the reciprocal of the effective neutron relaxation length. Usually S_a can be calculated by

$$S_a = y\, \Phi(a)\, \Sigma \ , \tag{3.222}$$

where

y = number of photons of energy E released per neutron capture (or per inelastic scattering),

$\Phi(a)$ = neutron flux (usually thermal flux for capture and fast flux for inelastic scattering),

Σ = macroscopic neutron cross section for thermal-neutron capture (or for inelastic scattering).

When exponential or polynomial forms of the buildup factor are used (see Section 3.8.1), together with the source description given by Eq. 3.221, then Eq. 3.220 can be integrated analyti-

*The production of secondary gamma rays by the capture of nonthermal neutrons is usually insignificant in shelter design.

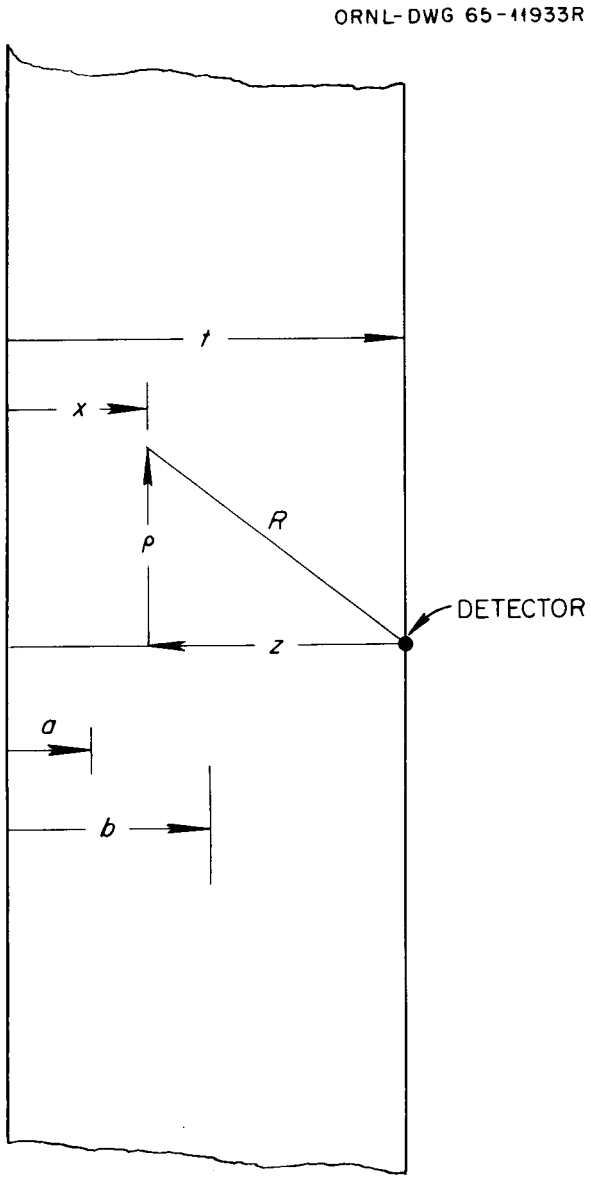

Fig. 3.14. Geometry for Integration over Exponential Source Distribution.

cally and very useful results obtained. In the paragraphs given below, examples of such integrations are given for two cases of interest: a slab shield of finite thickness t and a semi-infinite shield ($t = \infty$), the latter corresponding to a real problem in which the shield is very thick.

3.10.1. CALCULATION FOR SLAB SHIELD

Trubey[67] calculated the secondary gamma-ray dose rate for a slab shield by using the Berger form of the buildup factor,

$$B_r(E,\mu R) = 1 + C(E)\,\mu R\,e^{D\mu R}\,, \qquad (3.223)$$

in Eq 3.220. The equation then becomes

$$\Gamma(t,a,b) = \frac{G(E)}{2} S_a \int_a^b e^{-kx}\,dx \left[\int_{\mu[t-x]}^{\infty} \frac{e^{-\mu R}}{\mu R}\,d(\mu R) + \int_{\mu[t-x]}^{\infty} C(E)\,e^{\mu[D-1]R}\,d(\mu R)\right], \qquad (3.224)$$

where the uncollided dose rate $\Gamma_0(t,a,b)$ is represented by the first term, and the scattered dose rate $\Gamma_s(t,a,b)$ is given by the second term.

Letting $\mu[t-x] = y$ and integrating the first term of Eq. 3.224 by parts,* the dose rate from the uncollided gamma-ray dose rate is given by

$$\Gamma_0(t,a,b) = \frac{G(E)\,S_a\,e^{-\alpha\mu t}}{2\alpha\mu}\left[e^{\alpha y}E_1(y)\Big|_{\mu[t-b]}^{\mu[t-a]} + \int_{\mu[t-b]}^{\mu[t-a]} e^{\alpha y}\,\frac{e^{-y}}{y}\,dy\right]$$

$$= \frac{G(E)\,S_a\,e^{-\alpha\mu t}}{2\alpha\mu}\{e^{\alpha\mu(t-a)}E_1(\mu[t-a]) - E_1([1-\alpha]\mu[t-a]) + E_1([1-\alpha]\mu[t-b]) - e^{\alpha\mu[t-b]}E_1(\mu[t-b])\}\,, \qquad (3.225)$$

*The interpretation of $\mu[t-x]$ is $\mu \times [t-x]$ rather than μ with an argument $[t-x]$.

where $\alpha = k/\mu$ and E_1 is an exponential function of the first order and is defined by

$$E_1(x) = \int_x^\infty \frac{e^{-y}}{y} dy . \qquad (3.226)$$

Graphs of the exponential functions and other details of their properties are shown in Appendix 3H.

If $\alpha = 1$ or 0 (case of uniform source distribution) or if $b = t$, indeterminate forms result which may be resolved by L'Hôpital's rule, by series expansions, or by integrating Eq. 3.224 for $k = \mu$, $k = 0$, and $b = t$, respectively. These cases are as follows:

For $b < t$ and $\alpha = 0$

$$\Gamma_0(t,a,b) = \frac{G(E)\,S_a}{2\mu} \{\mu[b-a]\,E_1(\mu[t-b]) + \mu t\,E_1(\mu[t-a]) - \mu t\,E_1(\mu[t-b])\} . \qquad (3.227)$$

For $b < t$ and $\alpha = 1$

$$\Gamma_0(t,a,b) = \frac{G(E)\,S_a}{2\mu} \left\{e^{-\mu a} E_1(\mu[t-a]) - e^{-\mu b} E_1(\mu[t-b]) + e^{-\mu t} \ln\frac{t-a}{t-b}\right\} . \qquad (3.228)$$

For $b = t$ and $\alpha \neq 0$ or 1

$$\Gamma_0(t,a,t) = \frac{G(E)\,S_a}{2\mu\alpha} \left(e^{-\alpha\mu a} E_1(\mu[t-a]) - e^{-\alpha\mu t} \{E_1(\mu[1-\alpha][t-a]) + \ln|1-\alpha|\}\right) . \qquad (3.229)$$

For $b = t$ and $\alpha = 0$

$$\Gamma_0(t,a,t) = \frac{G(E)\,S_a}{2\mu} \{1 + \mu[t-a]\,E_1(\mu[t-a]) - e^{-\mu[t-a]}\} \qquad (3.230)$$

For $b = t$ and $\alpha = 1$

$$\Gamma_0(t,a,t) = \frac{G(E)\,S_a}{2\mu} \{e^{-\mu a} E_1(\mu[t-a]) - e^{-\mu t} \ln(\gamma\mu[t-a])\}, \qquad (3.231)$$

where $\ln \gamma = 0.577215665 \ldots$, Euler's constant.

For the special case of $b = t$ and $a = 0$, Eq. 3.229 can be represented by

$$\Gamma_0(t,0,t) = \frac{G(E)\,S_a}{\mu} \psi_0(\mu t, \alpha) , \qquad (3.232)$$

where

$$\psi_0(\mu t, \alpha) = \frac{1}{2\alpha} \left(E_1(\mu t) - e^{-\alpha\mu t} \{E_1([1-\alpha]\,\mu t) + \ln|1-\alpha|\}\right) . \qquad (3.233)$$

Equation 3.233 is shown plotted in Figs. 3J.1 through 3J.3 of Appendix 3J as a function of the number of mean free paths μt with α as a parameter.

[Note: Equations 3.227 through 3.233 can be used to calculate the *total* gamma-ray dose (uncollided + scattered) when the Taylor form of the buildup factor is used (see Section 3.8.1).]

Since $z = t - x$, the scattered dose rate behind a slab shield can be determined by expressing the second term of Eq. 3.224 (i.e., the Berger term) as

$$\Gamma_s(t,a,b) = \frac{G(E)\,C(E)\,S_a\,e^{-\alpha\mu t}}{2} \int_{t-b}^{t-a} dz \int_{\mu z}^{\infty} e^{\alpha\mu z}\, e^{-(1-D)\mu R}\, d(\mu R) . \qquad (3.234)$$

Integrating Eq. 3.234 gives

$$\Gamma_s(t,a,b) = \frac{G(E)\,C(E)\,S_a\,e^{-\alpha\mu t}}{2(1-D)(1-D-\alpha)\,\mu} \{e^{-(1-D-\alpha)\mu[t-b]} - e^{-(1-D-\alpha)\mu[t-a]}\} . \qquad (3.235)$$

Examination of Eq. 3.234 and Eq. 3.235 reveals that unless $D < 1$, negative doses are obtained. However, D is always significantly <1, as is shown in Fig. 3.5 in Section 3.8.

When $\alpha + D = 1$, Eq. 3.235 gives an indeterminate form which, when resolved, becomes

$$\Gamma_s(t,a,b) = \frac{G(E)\,C(E)\,S_a\,e^{-\alpha\mu t\,|\,b-a\,|}}{2(1-D)}. \quad (3.236)$$

For the special case when $b = t$ and $a = 0$, Eq. 3.236 can be expressed as

$$\Gamma_s(t,0,t) = \frac{G(E)\,C(E)\,S_a\,e^{D\mu t}}{\mu(1-D)}\,\psi_1(\mu t,\alpha'), \quad (3.237)$$

The dose rate from the uncollided flux is represented by the first term and is given by

$$\psi_0(\mu t) = \frac{1}{2\alpha}\left(E_1(\mu t) - e^{-\alpha\mu t}\left\{E_1([1-\alpha]\,\mu t) - \ln\left|\frac{1+\alpha}{1-\alpha}\right|\right\}\right), \quad (3.241)$$

and the sum of the next three terms represents the scattered contribution. The terms are

$$\psi_1(\mu t) = \frac{e^{-\alpha\mu t}}{2}\left[\frac{1-e^{-(1-\alpha)\mu t}}{1-\alpha} + \frac{1}{1+\alpha}\right], \quad (3.242)$$

$$\psi_2(\mu t) = \frac{4e^{-\alpha\mu t} - (1+\alpha)^2(2-\alpha)\,e^{-\mu t} - (1+\alpha)^2(1-\alpha)\,\mu t\,e^{-\mu t}}{4(1-\alpha)^2(1+\alpha)^2}, \quad (3.243)$$

where

$$\psi_1(\mu t,\alpha') = \frac{e^{-\alpha'\mu t}[1-e^{-\mu t[1-\alpha']}]}{2} \quad (3.238)$$

and $\alpha' = \alpha + D$. The function given by Eq. 3.238 is shown in Figs. 3J.4 through 3J.6 in Appendix 3J.

$$\psi_3(\mu t) = \frac{2}{3}\psi_2 + \left[\frac{1}{(1-\alpha)^3} + \frac{1}{(1+\alpha)^3}\right]\frac{e^{-\alpha\mu t}}{6} - \left[\frac{(\mu t)^2}{2(1-\alpha)} + \frac{\mu t}{(1-\alpha)^2} + \frac{1}{(1-\alpha)^3}\right]\frac{e^{-\mu t}}{6}. \quad (3.244)$$

When $\alpha = 0$, an indeterminate form occurs in Eq. 3.241, and when $\alpha = 1$, indeterminate forms occur in Eqs. 3.241 through 3.244. The following equations result when the indeterminate forms are evaluated:

For $\alpha = 0$

$$\psi_0(\mu t) = 1 + \frac{\mu t}{2}E_1(\mu t) - \frac{e^{-\mu t}}{2} = 1 - \frac{1}{2}E_2(\mu t). \quad (3.245)$$

For $\alpha = 1$

$$\psi_0(\mu t) = \frac{E_1(\mu t)}{2} + \frac{e^{-\mu t}}{2}\ln(2\gamma\mu t), \quad (3.246)$$

$$\psi_1(\mu t) = \left(\mu t + \frac{1}{2}\right)\frac{e^{-\mu t}}{2}, \quad (3.247)$$

3.10.2. CALCULATION FOR SEMI-INFINITE SHIELD

Solutions of Eq. 3.220 for a semi-infinite shield, that is, for $b = \infty$, give useful results that are generally applicable for the special case in which $a = 0$, particularly if one is interested in a gamma-ray heating rate within a shield. Using the polynomial form of the buildup factor,

$$B_r(\mu R) = \sum_{n=0}^{3} A_n(\mu R)^n, \quad (3.239)$$

Claiborne[141] determined solutions to Eq. 3.220 for this case, which were all in the form

$$\Gamma(\mu x) = \frac{G(E)\,S_a}{\mu}\sum_{n=0}^{3} n!\,A_n\,\psi_n. \quad (3.240)$$

$$\psi_2(\mu t) = \frac{\psi_1}{2} + \left[2(\mu t)^2 + 1\right]\frac{e^{-\mu t}}{16}, \quad (3.248)$$

$$\psi_3(\mu t) = \frac{2\psi_2}{3} + \left[\frac{(\mu t)^3}{3} + \frac{1}{4}\right]\frac{e^{-\mu t}}{12}. \quad (3.249)$$

The functions given by Eqs. 3.246 through 3.249 for the semi-infinite medium are plotted in Figs. 3J.7 through 3J.10 in Appendix 3J for various values of α. Figures 3J.7 and 3J.8 may be compared with Figs. 3J.1 and 3J.4, which are the corresponding functions evaluated for a slab shield.

These solutions contain the contribution from the gamma-ray sources between the detector position at t and infinity, since integration of Eq. 3.220 from $x = 0$ to $x = \infty$ produces two integrals: one giving the contribution from the interval $0 \leqq x \leqq t$ and the other giving the contribution from the interval $t \leqq x \leqq \infty$. In the usual shield, however, the contribution from the second interval at deep penetrations is small, and the gamma-ray dose rate outside a shield of thickness t will be only slightly less than that calculated for a distance t within a semi-infinite shield.

If Eq. 3.240 is used for gamma-ray heating calculations within a shield, the coefficients A_n must correspond to the polynomial fit of the energy absorption buildup factor, and the conversion factor for expressing the heating rate in W/g becomes

$$G(E) = 1.6 \times 10^{-13}\,\frac{\mu_a}{\rho}\,E, \quad (3.250)$$

where μ_a/ρ is the mass energy absorption coefficient of the material in which heat is generated.

Appendix 3A. Derivation of the Integrodifferential and Several Integral Forms of the Adjoint Boltzmann Transport Equation

Integrodifferential Adjoint Boltzmann Transport Equation. – The integrodifferential equation which is adjoint to the Boltzmann transport equation (Eq. 3.1) mathematically defines the adjoint flux and the characteristics of hypothetical particles called adjunctons. The use of the equation is discussed in Section 3.1, and its derivation is described as follows.

Consider an as yet unspecified function $\Phi^*(\bar{r},E,\bar{\Omega},t)$ which exists over the same phase space and satisfies the same kind of boundary conditions that are satisfied by the forward angular flux $\Phi(\bar{r},E,\bar{\Omega},t)$. Further, let an operator O* be defined such that the following integral relationship is satisfied:

$$\iiiint \Phi^*(\bar{r},E,\bar{\Omega},t)\, O\, \Phi(\bar{r},E,\bar{\Omega},t)\, d\bar{r}\, dE\, d\bar{\Omega}\, dt = \iiiint \Phi(\bar{r},E,\bar{\Omega},t)\, O^*\, \Phi^*(\bar{r},E,\bar{\Omega},t)\, d\bar{r}\, dE\, d\bar{\Omega}\, dt + (\text{boundary terms}) .$$

The O* operator will be referred to as the adjoint operator to the corresponding forward operator O.

Multiply each term of the Boltzmann transport equation, Eq. 3.1, by the function $\Phi^*(\bar{r},E,\bar{\Omega},t)$ and integrate the resultant equation (term by term) over all phase space:

$$\begin{aligned}
&\iiiint \Phi^*(\bar{r},E,\bar{\Omega},t)\, \frac{1}{v}\, \frac{\partial}{\partial t}\, \Phi(\bar{r},E,\bar{\Omega},t)\, d\bar{r}\, dE\, d\bar{\Omega}\, dt + \iiiint \Phi^*(\bar{r},E,\bar{\Omega},t)\, \nabla\cdot\bar{\Omega}\, \Phi(\bar{r},E,\bar{\Omega},t)\, d\bar{r}\, dE\, d\bar{\Omega}\, dt \\
&\qquad + \iiiint \Phi^*(\bar{r},E,\bar{\Omega},t)\, \Sigma_t(\bar{r},E)\, \Phi(\bar{r},E,\bar{\Omega},t)\, d\bar{r}\, dE\, d\bar{\Omega}\, dt \\
&\qquad = \iiiint \Phi^*(\bar{r},E,\bar{\Omega},t)\, S(\bar{r},E,\bar{\Omega},t)\, d\bar{r}\, dE\, d\bar{\Omega}\, dt \\
&\qquad + \iiiint \Phi^*(\bar{r},E,\bar{\Omega},t) \iint \Sigma_s(\bar{r},E' \to E,\bar{\Omega}' \to \Omega)\, \Phi(\bar{r},E',\bar{\Omega}',t)\, dE'\, d\bar{\Omega}'\, d\bar{r}\, dE\, d\bar{\Omega}\, dt . \qquad \text{(A1)}
\end{aligned}$$

It can be shown that the following adjoint relationships are true for the conditions associated with a particle transport problem:

$$\begin{aligned}
&\iiiint \Phi^*(\bar{r},E,\bar{\Omega},t)\, \frac{1}{v}\frac{\partial}{\partial t}\, \Phi(\bar{r},E,\bar{\Omega},t)\, d\bar{r}\, dE\, d\bar{\Omega}\, dt \\
&\qquad = -\iiiint \Phi(\bar{r},E,\bar{\Omega},t)\, \frac{1}{v}\, \frac{\partial}{\partial t}\, \Phi^*(\bar{r},E,\bar{\Omega},t)\, d\bar{r}\, dE\, d\bar{\Omega}\, dt \\
&\qquad + \left[\iiiint \frac{1}{v}\, \frac{\partial}{\partial t}\, \Phi(\bar{r},E,\bar{\Omega},t)\, \Phi^*(\bar{r},E,\bar{\Omega},t)\, d\bar{r}\, dE\, d\bar{\Omega}\, dt\right]_{\text{Boundary Term}} , \qquad \text{(A2)}
\end{aligned}$$

$$\iiiint \Phi^*(\bar{r},E,\bar{\Omega},t)\, \Sigma_t(\bar{r},E)\, \Phi(\bar{r},E,\bar{\Omega},t)\, d\bar{r}\, dE\, d\bar{\Omega}\, dt = \iiiint \Phi(\bar{r},E,\bar{\Omega},t)\, \Sigma_t(\bar{r},E)\, \Phi^*(\bar{r},E,\bar{\Omega},t)\, d\bar{r}\, dE\, d\bar{\Omega}\, dt , \qquad \text{(A3)}$$

$$\begin{aligned}
&\iiiint \Phi^*(\bar{r},E,\bar{\Omega},t)\, \nabla\cdot\bar{\Omega}\, \Phi(\bar{r},E,\bar{\Omega},t)\, d\bar{r}\, dE\, d\bar{\Omega}\, dt \\
&\qquad = -\iiiint \Phi(\bar{r},E,\bar{\Omega},t)\, \nabla\cdot\bar{\Omega}\Phi^*(\bar{r},E,\bar{\Omega},t)\, d\bar{r}\, dE\, d\bar{\Omega}\, dt \\
&\qquad + \left[\iiiint \Phi(\bar{r},E,\bar{\Omega},t)\, \Phi^*(\bar{r},E,\bar{\Omega},t)\bar{\Omega}\cdot d\bar{s}\, dE\, d\bar{\Omega}\, dt\right]_{\text{Boundary Term}} , \qquad \text{(A4)}
\end{aligned}$$

$$\iiiint \Phi^*(\bar{r},E,\bar{\Omega},t) \iint \Sigma_s(\bar{r},E' \to E,\bar{\Omega}' \to \bar{\Omega})\, \Phi(\bar{r},E',\bar{\Omega}',t)\, dE'\, d\bar{\Omega}'\, d\bar{r}\, dE\, d\bar{\Omega}\, dt$$

$$= \iiiint \Phi(\bar{r},E,\bar{\Omega},t) \iint \Sigma_s(\bar{r},E \to E',\bar{\Omega} \to \bar{\Omega}')\, \Phi^*(\bar{r},E',\bar{\Omega}',t)\, dE'\, d\bar{\Omega}'\, d\bar{r}\, dE\, d\bar{\Omega}\, dt . \quad \text{(A5)}$$

The boundary terms which occur in Eqs. A2 and A4 may vanish while conforming to the natural characteristics of the system under analysis. For example, the extent of the time domain can be defined such that initial and final values of Φ and/or Φ^* are zero (and the boundary term of Eq. A2 vanishes). Also the surface within which the spatial domain of phase space is contained can be so located that the combination $[\Phi\Phi^*]$ is zero everywhere on that surface (and the boundary term of Eq A4 vanishes).

For Monte Carlo analysis the elimination of the boundary terms presents no problem and in no way restricts the generality of the solution obtained. However when the adjoint problem is solved in a deterministic manner[142] (for example, by the discrete ordinates method) wherein boundary conditions must be formally satisfied, the boundary term of Eq. A4 will in general not vanish and some complications may result in specifying the adjoint source and subsequently in interpreting the adjoint flux so defined.

Using the adjoint relationships given by Eqs. A2-A5, Eq. A1 can be rewritten as

$$-\iiiint \Phi(\bar{r},E,\bar{\Omega},t)\, \frac{1}{v}\frac{\partial}{\partial t}\, \Phi^*(\bar{r},E,\bar{\Omega},t)\, d\bar{r}\, dE\, d\bar{\Omega}\, dt - \iiiint \Phi(\bar{r},E,\bar{\Omega},t)\, \nabla\cdot\bar{\Omega}\, \Phi^*(\bar{r},E,\bar{\Omega},t)\, d\bar{r}\, dE\, d\bar{\Omega}\, dt$$

$$+ \iiiint \Phi(\bar{r},E,\bar{\Omega},t)\, \Sigma_t(\bar{r},E)\, \Phi^*(\bar{r},E,\bar{\Omega},t)\, d\bar{r}\, dE\, d\bar{\Omega}\, dt = \iiiint \Phi(\bar{r},E,\bar{\Omega},t)\, S^*(\bar{r},E,\bar{\Omega},t)\, d\bar{r}\, dE\, d\bar{\Omega}\, dt$$

$$+ \iiiint \Phi(\bar{r},E,\bar{\Omega},t) \iint \Sigma_s(\bar{r},E \to E',\bar{\Omega} \to \bar{\Omega}')\, \Phi^*(\bar{r},E',\bar{\Omega}',t)\, dE'\, d\bar{\Omega}'\, d\bar{r}\, dE\, d\bar{\Omega}\, dt , \quad \text{(A6)}$$

where the adjoint source term $S^*(\bar{r},E,\bar{\Omega},t)$ is defined such that

$$\iiiint \Phi(\bar{r},E,\bar{\Omega},t)\, S^*(\bar{r},E,\bar{\Omega},t)\, d\bar{r}\, dE\, d\bar{\Omega}\, dt = \iiiint \Phi^*(\bar{r},E,\bar{\Omega},t)\, S(\bar{r},E,\bar{\Omega},t)\, d\bar{r}\, dE\, d\bar{\Omega}\, dt$$

$$- \left[\iiint \Phi(\bar{r},E,\bar{\Omega},t)\, \Phi^*(\bar{r},E,\bar{\Omega},t)\bar{\Omega}\cdot d\bar{s}\, dE\, d\bar{\Omega}\, dt \right]_{\text{Boundary Term}} \quad \text{(A7)}$$

Noting that the forward flux $\Phi(\bar{r},E,\bar{\Omega},t)$ can be factored from each term, Eq. A6 can be rearranged as follows:

$$\iiiint \Phi(\bar{r},E,\bar{\Omega},t) \left[-\frac{1}{v}\frac{\partial}{\partial t}\, \Phi^*(\bar{r},E,\bar{\Omega},t) - \nabla\cdot\bar{\Omega}\, \Phi^*(\bar{r},E,\bar{\Omega},t) + \Sigma_t\,(\bar{r},E)\, \Phi^*(\bar{r},E,\bar{\Omega},t) - S^*(\bar{r},E,\bar{\Omega},t) \right.$$

$$\left. - \iint \Sigma_s(\bar{r},E \to E',\bar{\Omega} \to \bar{\Omega}')\Phi^*(\bar{r},E',\bar{\Omega}',t)\, dE'\, d\bar{\Omega}' \right] d\bar{r}\, dE\, d\bar{\Omega}\, dt = 0 . \quad \text{(A8)}$$

It is required that the forward angular flux $\Phi(\bar{r},E,\bar{\Omega},t)$ correspond to nontrivial physical situations, that is, that $\Phi(\bar{r},E,\bar{\Omega},t) > 0$ over at least some portion of phase space. The observation is made that $\Phi^*(\bar{r},E,\bar{\Omega},t)$ is still essentially undefined and that many functions $\Phi^*(\bar{r},E,\bar{\Omega},t)$ probably satisfy Eq. A8. At this point, $\Phi^*(\bar{r},E,\bar{\Omega},t)$ is defined to be that function which satisfies the following equation:

$$\left[-\frac{1}{v}\frac{\partial}{\partial t}\, \Phi^*(\bar{r},E,\bar{\Omega},t) - \nabla\cdot\,\bar{\Omega}\Phi^*\,(\bar{r},E,\bar{\Omega},t) + \Sigma_t(\bar{r},E)\, \Phi^*(\bar{r},E,\bar{\Omega},t) - S^*(\bar{r},E,\bar{\Omega},t) \right.$$

$$\left. - \iint \Sigma_s(\bar{r},E \to E',\bar{\Omega} \to \bar{\Omega}')\, \Phi^*(\bar{r},E',\bar{\Omega}',t)\, dE'\, d\bar{\Omega}' \right] = 0 .$$

This condition also satisfies Eq. A8 exactly and provides the following $\Phi^*(\bar{r},E,\bar{\Omega},t)$-defining integrodifferential equation:

$$-\frac{1}{v}\frac{\partial}{\partial t}\, \Phi^*(\bar{r},E,\bar{\Omega},t) - \nabla\cdot\bar{\Omega}\, \Phi^*(\bar{r},E,\bar{\Omega},t) + \Sigma_t(\bar{r},E)\, \Phi^*(\bar{r},E,\bar{\Omega},t)$$

$$= S^*(\bar{r},E,\bar{\Omega},t) + \iint \Sigma_s(\bar{r},E \to E',\bar{\Omega} \to \bar{\Omega}')\, \Phi^*(\bar{r},E',\bar{\Omega}',t)\, dE'\, d\bar{\Omega}' , \quad \text{(A9)}$$

which is commonly called the adjoint integrodifferential Boltzmann equation.

The solution of Eq. A9 can be accomplished by the usual deterministic methods. However for certain applications, a Monte Carlo solution is the preferred method of analysis[143] and the integral forms of the adjoint transport equation are the formal basis for the random walk of the hypothetical particles called "adjunctons." The derivations of the "integral point-value equation," the "integral event-value equation," and the "integral emergent adjuncton density equation" are presented in this appendix along with comments describing the relationship of these integral equations to a Monte Carlo solution of the adjoint problem.

Integral Point-Value Equation. – Equation A9 is now transformed into an integral form. To accomplish this, the combination of the convection and storage terms are first expressed in terms of the spatial variable R which relates a fixed point in space $\bar{r}$ to an arbitrary point $\bar{r}' = \bar{r} + R\bar{\Omega}$, as shown in Fig. 3A.1. The total derivative of $\Phi^*(\bar{r},E,\bar{\Omega},t)$ with respect to R is given by

$$\frac{d}{dR}\,\Phi^*(\bar{r}',E,\bar{\Omega},t') = \frac{\partial x}{\partial R}\,\frac{\partial \Phi^*}{\partial x} + \frac{\partial y}{\partial R}\,\frac{\partial \Phi^*}{\partial y} + \frac{\partial z}{\partial R}\,\frac{\partial \Phi^*}{\partial z} + \frac{\partial t}{\partial R}\,\frac{\partial \Phi^*}{\partial t}\,,$$

which, according to Fig. 3A.1 and noting that the adjunction's speed v is equal to dR/dt, can be rewritten as

$$\frac{d}{dR}\,\Phi^*(\bar{r}',E,\bar{\Omega},t) = \Omega_x\,\frac{\partial \Phi^*}{\partial x} + \Omega_y\,\frac{\partial \Phi^*}{\partial y} + \Omega_z\,\frac{\partial \Phi^*}{\partial z} + \frac{1}{v}\,\frac{\partial \Phi^*}{\partial t} = \bar{\Omega}\cdot\nabla\Phi^*(\bar{r}',E,\bar{\Omega},t') + \frac{1}{v}\,\frac{\partial}{\partial t}\,\Phi^*(\bar{r}',E,\bar{\Omega},t')\,. \tag{A10}$$

Using the integrating factor

$$\exp\left[-\int_0^R \Sigma_t(\bar{r}+R'\bar{\Omega},E)\,dR'\right]$$

provides the following relationship:

$$\frac{d}{dR}\left\{\Phi^*(\bar{r}',E,\bar{\Omega},t')\,\exp\left[-\int_0^R \Sigma_t(\bar{r}+R'\bar{\Omega},E)\,dR'\right]\right\}$$

$$= \exp\left[-\int_0^R \Sigma_t(\bar{r}+R'\bar{\Omega},E)\,dR'\right]\left[\frac{d}{dR}\,\Phi^*(\bar{r}',E,\bar{\Omega},t') - \Sigma_t(\bar{r}',E)\,\Phi^*(\bar{r}',E,\bar{\Omega},t')\right]. \tag{A11}$$

Equation A11, together with Eq. A10, can be arranged to give

$$\left[-\frac{1}{v}\,\frac{\partial}{\partial t}\,\Phi^*(\bar{r}',E,\bar{\Omega},t') - \nabla\cdot\bar{\Omega}\,\Phi^*(\bar{r}',E,\bar{\Omega},t') + \Sigma_t(\bar{r}',E)\,\Phi^*(\bar{r}',E,\bar{\Omega},t')\right]$$

$$= \exp\left[+\int_0^R \Sigma_t(\bar{r}+R'\bar{\Omega},E)\,dR'\right]\frac{d}{dR}\left\{\Phi^*(\bar{r}',E,\bar{\Omega},t')\,\exp\left[-\int_0^R \Sigma_t(\bar{r}+R'\bar{\Omega},E)\,dR'\right]\right\}. \tag{A12}$$

It is noted that Eq. A12 is identically the lefthand side of Eq. A9, which can now be rewritten as

$$-\frac{d}{dR}\left\{\Phi^*(\bar{r}',E,\bar{\Omega},t')\,\exp\left[-\int_0^R \Sigma_t(\bar{r}+R'\bar{\Omega})\,dR'\right]\right\}$$

$$= \exp\left[-\int_0^R \Sigma_t\,(\bar{r}+R'\bar{\Omega},E)\,dR'\right]\left[S^*(\bar{r}',E,\bar{\Omega},t') + \iint\Sigma_s(\bar{r}',E\to E',\bar{\Omega}\to\bar{\Omega}')\,\Phi^*(\bar{r}',E',\bar{\Omega}',t')\,dE'\,d\bar{\Omega}'\right]. \tag{A13}$$

Multiplying Eq. A13 by dR, integrating from $R = 0$ to $R = \infty$, and assuming that

$$\Phi^*(\infty,E,\bar{\Omega},t_\infty)\,\exp\left[-\int_0^\infty \Sigma_t(\bar{r}+R'\bar{\Omega},E)\,dR'\right] \equiv 0\,,$$

yields the following expression for $\Phi^*(\bar{r},E,\bar{\Omega},t)$:

$$\Phi^*(r,E,\bar{\Omega},t) = \int_0^\infty dR\,\exp\left[-\int_0^\infty \Sigma_t(\bar{r}+R'\bar{\Omega},E)\,dR'\right]\left[S^*(\bar{r}+R\bar{\Omega},E,\bar{\Omega},t+R/v)\right.$$

$$\left.+\iint\Sigma_s(\bar{r}+R\bar{\Omega},E\to E',\bar{\Omega}\to\bar{\Omega}')\,\Phi^*(\bar{r}+R\bar{\Omega},E',\bar{\Omega}',t+R/v)\right]. \tag{A14}$$

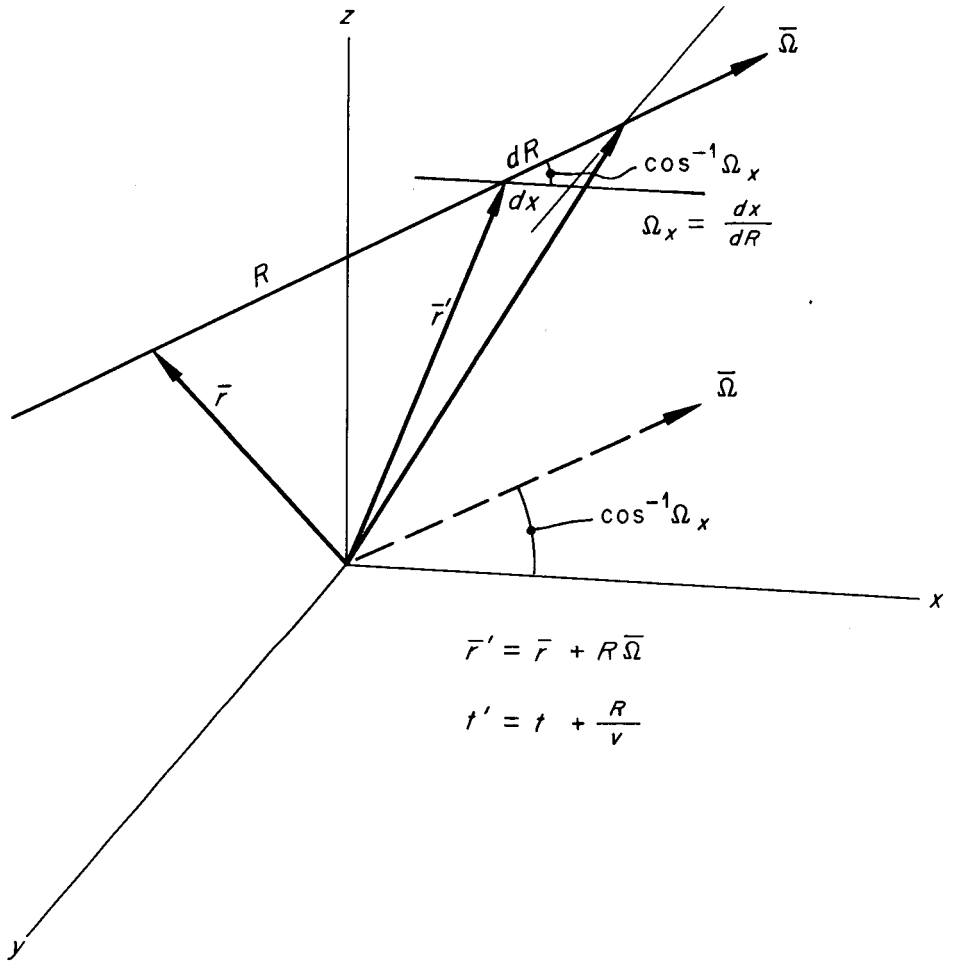

Fig. 3A.1. The Spatial Variable *R*.

By redefining the source term as

$$S_T^*(\bar{r},E,\bar{\Omega},t) \equiv \int_0^R dR \exp\left[-\int_0^R \Sigma_t(\bar{r}+R'\bar{\Omega},E)\,dR'\right] S^*(\bar{r}+R\bar{\Omega},E,\bar{\Omega},t+R/v)\,, \tag{A15}$$

Eq. A14 can be rewritten as

$$\Phi^*(\bar{r},E,\bar{\Omega},t) = S_T^*(\bar{r},E,\bar{\Omega},t)$$

$$+ \int dR\, \Sigma_t(\bar{r}',E) \exp\left[-\int_0^\infty \Sigma_t(\bar{r}+R'\bar{\Omega},E)\,dR'\right] \iint \frac{\Sigma_s(\bar{r}',E\to E',\bar{\Omega}\to\bar{\Omega}')}{\Sigma_t(\bar{r}'E)} \Phi^*(\bar{r}',E',\bar{\Omega}',t')\,dE'\,d\bar{\Omega}'\,. \tag{A16}$$

In terms of the transport integral operator* and collision integral* operator, Eq. A16 becomes

$$\Phi^*(\bar{r},E,\bar{\Omega},t) = S_T^*(\bar{r},E,\bar{\Omega},t) + T(\bar{r}\to\bar{r}',E,\bar{\Omega})\, C(\bar{r}',E\to E',\bar{\Omega}\to\bar{\Omega}')\, \Phi^*(\bar{r}',E',\bar{\Omega}',t')\,. \tag{A17}$$

*These integral operators are defined by Eqs. 3.112 and 3.113, Sec. 3.5.

A comparison of Eq. A17 with Eqs. 3.116, 3.117, and 3.118 reveals that the function $\Phi^*(\bar{r},E,\bar{\Omega},t)$ as defined by Eq. A17 is adjoint to the emergent particle density $\chi(\bar{r},E,\bar{\Omega},t)$ as defined by Eq. 3.117. Therefore, let $\Phi^*(\bar{r},E,\bar{\Omega},t)$ be denoted by $\chi^*(\bar{r},E,\bar{\Omega},t)$ and Eq. A17 becomes

$$\chi^*(\bar{r},E,\bar{\Omega},t) = S_T^*(\bar{r},E,\bar{\Omega},t) + T(\bar{r}\rightarrow\bar{r}',E,\bar{\Omega})\, C(\bar{r}',E\rightarrow E',\bar{\Omega}\rightarrow\bar{\Omega}')\, \chi^*(\bar{r}',E',\bar{\Omega}',t') \,. \tag{A18}$$

The nature of $\chi^*(\bar{r},E,\bar{\Omega},t)$ will depend on $S_T^*(\bar{r},E,\bar{\Omega},t)$ – how or on what basis should $S_T^*(\bar{r},E,\bar{\Omega},t)$ be specified? If $S^*(\bar{r},E,\bar{\Omega},t)$ is set equal to $P^{\Phi}(\bar{r},E,\bar{\Omega},t)$ (the response function of the effect of interest λ due to a unit angular flux), then

$$\iiiint \Phi(\bar{r},E,\bar{\Omega},t)\, S^*(\bar{r},E,\bar{\Omega},t)\, d\bar{r}\, dE\, d\bar{\Omega}\, dt = \iiiint \Phi(\bar{r},E,\bar{\Omega},t)\, P^{\Phi}(\bar{r},E,\bar{\Omega},t)\, d\bar{r}\, dE\, d\bar{\Omega}\, dt = \lambda \,. \tag{A19}$$

According to Eq. A7, assuming that the "boundary term" is zero, the effect of interest λ is also given by

$$\lambda = \iiiint \chi^*(\bar{r},E,\bar{\Omega},t)\, S(\bar{r},E,\bar{\Omega},t)\, d\bar{r}\, dE\, d\bar{\Omega}\, dt \,, \tag{A20}$$

so that $\chi^*(\bar{r},E,\bar{\Omega},t)$ can be interpreted as the value (to the effect of interest) of a particle leaving an event at $\bar{r}$ with phase space coordinates $(\bar{r},E,\bar{\Omega},t)$. Therefore, $\chi^*(\bar{r},E,\bar{\Omega},t)$ will be called the "point-value function," and the $\chi^*(\bar{r},E,\bar{\Omega},t)$-defining equation, Eq. A18, will be referred to as the "integral point-value equation."

As suggested by Eq. A19, the adjoint source $S^*(\bar{r},E,\bar{\Omega},t)$ is identified as

$$S^*(\bar{r},E,\bar{\Omega},t) = P^{\Phi}(\bar{r},E,\bar{\Omega},t) \,. \tag{A21}$$

Substitution of Eq. A21 into Eq. A15 yields

$$S_T^*(\bar{r},E,\bar{\Omega},t) = \int dR\, \exp\left[-\int_0^R \Sigma_t(\bar{r}+R'\bar{\Omega},E)\, dR'\right] P^{\Phi}(\bar{r}',\bar{\Omega},E,t') \,,$$

which can be rewritten as

$$S_T^*(\bar{r},E,\bar{\Omega},t) = \int dR\, \Sigma_t(\bar{r}',E)\, \exp\left[-\int_0^R \Sigma_t(\bar{r}+R'\bar{\Omega},E)\, dR'\right]\left[\frac{P^{\Phi}(\bar{r}',\bar{\Omega},E,t')}{\Sigma_t(\bar{r}',E)}\right]. \tag{A22}$$

The effect of interest λ as given by Eq. A19 can be rewritten as

$$\lambda = \iiiint \Sigma_t(\bar{r},E)\, \Phi(\bar{r},E,\bar{\Omega},t)\left[\frac{P^{\Phi}(r,E,\bar{\Omega},t)}{\Sigma_t(\bar{r},E)}\right] d\bar{r}\, dE\, d\bar{\Omega}\, dt = \iiiint \psi(\bar{r},E,\bar{\Omega},t)\, P^{\psi}(\bar{r},E,\bar{\Omega},t)\, d\bar{r}\, dE\, d\bar{\Omega}\, dt \,, \tag{A23}$$

where $\psi(\bar{r},E,\bar{\Omega},t)$ is the collision density and $P^{\psi}(\bar{r},E,\bar{\Omega},t)$ is the response function of the effect of interest λ due to a unit event at $(\bar{r},E,\bar{\Omega},t)$ in phase space and

$$P^{\psi}(\bar{r},E,\bar{\Omega},t) = \frac{P^{\Phi}(\bar{r},E,\bar{\Omega},t)}{\Sigma_t(\bar{r},E)} \,. \tag{A24}$$

Substituting Eq. A24 into Eq. A22 and introducing the transport integral operator yields

$$S_T^*(\bar{r},E,\bar{\Omega},t) = T(\bar{r}\rightarrow\bar{r}',E,\bar{\Omega})\, P^{\psi}(\bar{r}',E,\bar{\Omega},t') \,, \tag{A25}$$

and the integral point-value equation becomes

$$\chi^*(\bar{r},E,\bar{\Omega},t) = T(\bar{r}\rightarrow\bar{r}',E,\bar{\Omega})\, [P^{\psi}(\bar{r}',E,\bar{\Omega},t') + C(\bar{r}',E\rightarrow E',\bar{\Omega}\rightarrow\bar{\Omega}')\, \chi^*(\bar{r}',E',\bar{\Omega}',t')] \,. \tag{A26}$$

The effect of interest λ can also be expressed in terms of the emergent particle density; that is

$$\lambda = \iiiint \chi(\bar{r},E,\bar{\Omega},t)\, P^{\chi}(\bar{r},E,\bar{\Omega},t)\, d\bar{r}\, dE\, d\bar{\Omega}\, dt \,, \tag{A27}$$

where $\chi(\bar{r},E,\bar{\Omega},t)$ is the emergent particle density and $P^{\chi}(\bar{r},E,\bar{\Omega},t)$ is related to the other response functions by considering a particle which emerges from a collision at $\bar{r}$ with phase space coordinates $(\bar{r},E,\bar{\Omega},t)$. The particle will experience an event in dR about $\bar{r}' = \bar{r} + R\bar{\Omega}$ at time $t' = t + R/v$ with the probability

$$\Sigma_t(\bar{r}',E) \exp\left[-\int_0^R \Sigma_t(\bar{r} + R'\bar{\Omega},E)\, dR'\right] dR ,$$

and the contribution of this event is the response function $P^{\psi}(\bar{r}',E,\bar{\Omega},t')$. The sum of all such contributions to the effect of interest is given by

$$\int_0^{\infty} dR\, \Sigma_t(\bar{r}',E) \exp\left[-\int_0^R \Sigma_t(\bar{r} + R'\bar{\Omega},E)\, dR'\right] P^{\psi}(\bar{r}',E,\bar{\Omega},t') ,$$

and should be the same as the response function $P^{\chi}(\bar{r},E,\bar{\Omega},t)$ which is based on emergent particle density. This leads to the relationships,

$$P^{\chi}(\bar{r},E,\bar{\Omega},t) = \int_0^{\infty} dR\, \Sigma_t(\bar{r}',E) \exp\left[-\int_0^R \Sigma_t(\bar{r} + R'\bar{\Omega},E)\, dR'\right] P^{\psi}(\bar{r}',E,\bar{\Omega},t') = T(\bar{r} \to \bar{r}',E,\bar{\Omega})\, P^{\psi}(\bar{r}',E,\bar{\Omega},t') , \tag{A28}$$

and since $P^{\Phi}(\bar{r},E,\bar{\Omega},t) = \Sigma_t(\bar{r},E)\, P^{\psi}(\bar{r},E,\bar{\Omega},t)$,

$$P^{\chi}(\bar{r},E,\bar{\Omega},t) = \int_0^{\infty} dR \exp\left[-\int_0^R \Sigma_t(\bar{r} + R'\bar{\Omega},E)\, dR'\right] P^{\Phi}(\bar{r}',E,\bar{\Omega},t') . \tag{A29}$$

Another form of the integral point-value equation is obtained by substituting Eq. A28 into A26, yielding

$$\chi^*(\bar{r},E,\bar{\Omega},t) = P^{\chi}(\bar{r},E,\bar{\Omega},t) + T(\bar{r} \to r',E,\bar{\Omega})\, C(\bar{r}',E \to E',\bar{\Omega} \to \bar{\Omega}')\, \chi^*(\bar{r}',E',\bar{\Omega}',t') . \tag{A30}$$

Integral Event-Value Equation. – A value function based on the collision density can be related to the point-value function by considering a particle leaving a collision at $\bar{r}$ with phase space coordinates $(\bar{r},E,\bar{\Omega},t)$. The value of this particle to the effect of interest is the point-value function $\chi^*(\bar{r},E,\bar{\Omega},t)$. This particle will experience an event in dR about $\bar{r}' = \bar{r} + R\bar{\Omega}$, with the probability

$$\Sigma_t(\bar{r}',E) \exp\left[-\int_0^R \Sigma_t(\bar{r} + R'\bar{\Omega},E)\, dR'\right] dR$$

and the value of this event (to the effect of interest λ) will be referred to as the event-value and be denoted by $W(\bar{r}',E,\bar{\Omega},t')$. That is, the event-value function $W(r',E,\Omega,t')$ is defined as the value (to the effect of interest) of having an event at $\bar{r}'$ with an incoming particle which has phase space coordinates $(\bar{r}',E,\bar{\Omega},t')$. The sum of all such contributions to the effect of interest is given by

$$\int_0^{\infty} dR\, \Sigma_t(\bar{r}',E) \exp\left[-\int_0^R \Sigma_t(\bar{r} + R'\bar{\Omega},E)\, dR'\right] W(\bar{r}',E,\bar{\Omega},t') ,$$

and, if the event-value function is properly defined, should equal the point-value function; that is,

$$\chi^*(\bar{r},E,\bar{\Omega},t) = \int_0^{\infty} dR\, \Sigma_t(\bar{r}',E) \exp\left[-\int_0^R \Sigma_t(\bar{r} + R'\bar{\Omega},E)\, dR'\right] W(\bar{r}',E,\bar{\Omega},t') , \tag{A31}$$

and, introducing the transport integral operator, Eq. A31 can be rewritten as

$$\chi^*(\bar{r},E,\bar{\Omega},t) = T(\bar{r} \to \bar{r}',E,\bar{\Omega})\, W(\bar{r}',E,\bar{\Omega},t') . \tag{A32}$$

A comparison of Eq. A32 with Eq. A26 would show that $W(\bar{r},E,\bar{\Omega},t)$ can be identified as

$$W(\bar{r},E,\bar{\Omega},t) = P^{\psi}(\bar{r},E,\bar{\Omega},t) + C(\bar{r},E \to E',\bar{\Omega} \to \bar{\Omega}')\, \chi^*(\bar{r},E',\bar{\Omega}',t) \tag{A33}$$

and substitution of Eq. A32 into Eq. A33 yields the defining equation for the event-value function:

$$W(\bar{r},E,\bar{\Omega},t) = P^{\psi}(\bar{r},E,\bar{\Omega},t) + C(\bar{r},E \to E',\bar{\Omega} \to \bar{\Omega}')\, T(\bar{r} \to \bar{r}',E',\bar{\Omega}')\, W(\bar{r}',E',\bar{\Omega}',t') . \tag{A34}$$

Equation A34 will be referred to as the "integral event-value equation." A comparison of Eq. A34 with Eq. 3.116 would show that the event-value function $W(\bar{r},E,\bar{\Omega},t)$ is adjoint to the collision density $\psi(\bar{r},E,\bar{\Omega},t)$. Therefore the effect of interest is also given by

$$\lambda = \iiiint T(\bar{r}' \rightarrow \bar{r},E,\bar{\Omega})\, S(\bar{r}',E,\bar{\Omega},t')\, W(\bar{r},E,\bar{\Omega},t) d\bar{r}\, dE\, d\bar{\Omega}\, dt\,. \tag{A35}$$

The term $T(\bar{r}' \rightarrow \bar{r},E,\bar{\Omega})\, S(\bar{r}',E,\bar{\Omega},t')$ can be identified as the "first collision source" and denoted by

$$S_c\,(\bar{r},E,\bar{\Omega},t) \equiv T(\bar{r}' \rightarrow r,E,\bar{\Omega})\, S(\bar{r}',E,\bar{\Omega},t')\,, \tag{A36}$$

and Eq. A35 can be rewritten as

$$\lambda = \iiiint S_c\,(\bar{r},E,\bar{\Omega},t)\, W(\bar{r},E,\bar{\Omega},t)\, d\bar{r}\, dE\, d\bar{\Omega}\, dt\,. \tag{A37}$$

Integral Emergent Adjuncton Density Equation. – The solution of either the point-value equation, Eq. A30, or the event-value equation, Eq. A34, could be accomplished by Monte Carlo procedures; however, the random walk would not be the same as that implied by the integral emergent particle density equation, Eq. 3.117. It would be desirable to use the same random walk logic (and therefore the same Monte Carlo computer program) for both forward and adjoint calculations.

Consider the following altered form of Eq. A30,

$$\chi^*(\bar{r},E,\bar{\Omega},t) = P^{\chi}(\bar{r},E,\bar{\Omega},t) + \int_0^{\infty} dR\, \Sigma_t(\bar{r},E) \exp\left[-\int_0^R \Sigma_t(\bar{r}+R'\bar{\Omega},E) dR'\right] \left[\frac{\Sigma_t(\bar{r}',E)}{\Sigma_t(\bar{r},E)}\right]$$

$$\cdot \iint \frac{\Sigma_s(\bar{r}',E \rightarrow E',\bar{\Omega} \rightarrow \bar{\Omega}')}{\iint \Sigma_s(\bar{r}',E \rightarrow E',\bar{\Omega} \rightarrow \bar{\Omega}') dE\, d\bar{\Omega}} \left[\frac{\iint \Sigma_S(\bar{r}',E \rightarrow E',\bar{\Omega} \rightarrow \bar{\Omega}')\, dE\, d\bar{\Omega}}{\Sigma_t(\bar{r}',E)}\right] \chi^*(\bar{r}',E',\bar{\Omega}',t')\, dE'\, d\bar{\Omega}'\,. \tag{A38}$$

The additional weight factor $[\Sigma_t(\bar{r}',E)/\Sigma_t(\bar{r},E)]$ arises since Eq. A30 and its altered form, Eq. A38, are actually flux-like equations, even though $\chi^*(\bar{r},E,\bar{\Omega},t)$ is adjoint to the emergent particle density $\chi^*(\bar{r},E,\bar{\Omega},t)$.

In a fashion analogous to the forward problem, the following new quantities are defined:

$$H(\bar{r},E,\bar{\Omega},t) \equiv \Sigma_t(\bar{r},E)\, \chi^*(\bar{r},E,\bar{\Omega},t) \tag{A39}$$

and

$$H(\bar{r},E,\bar{\Omega},t) \equiv T(\bar{r}' \rightarrow \bar{r}\,,E,\bar{\Omega})\, G(\bar{r}',E,\bar{\Omega},t')\,. \tag{A40}$$

Since $\chi^*(\bar{r},E,\bar{\Omega},t)$ is a flux-like variable, the new variable $H(\bar{r},E,\bar{\Omega},t)$ can be regarded as a collision density and $G(\bar{r},E,\bar{\Omega},t)$ as an emergent adjuncton density. The defining equation for $G(r,E,\Omega,t)$ should be the proper basis for an adjoint random walk.

The defining equation for the adjoint event density formation $H(\bar{r},E,\bar{\Omega},t)$ is obtained by considering the altered form of Eq. A26,

$$\chi^*(\bar{r},E,\bar{\Omega},t) = \int_0^{\infty} dR\, \Sigma_t(\bar{r}',E) \exp\left[-\int_0^R \Sigma_t(\bar{r}+R'\bar{\Omega},E)\, dR'\right] \left[P^{\psi}(\bar{r}',E,\bar{\Omega},t')\right.$$

$$\left. + C(\bar{r}',E \rightarrow E',\bar{\Omega} \rightarrow \bar{\Omega}')\, \chi^*(\bar{r}',E',\bar{\Omega}',t')\right]\,, \tag{A41}$$

multiplying it by $\Sigma_t(\bar{r},E)$, and rearranging it as follows:

$$\Sigma_t(\bar{r},E)\,\chi^*(\bar{r},E,\bar{\Omega},t) = \int_0^\infty dR\;\Sigma_t(\bar{r},E)\exp\left[-\int_0^R \Sigma_t(\bar{r}+R'\bar{\Omega},E)\,dR'\right]$$

$$\cdot\left[\Sigma_t(\bar{r}',E)\,P^{\psi}(\bar{r}',E,\bar{\Omega},t') + \hat{C}(\bar{r}',E\to E',\bar{\Omega}\to\bar{\Omega}')\,\Sigma_t(\bar{r}',E')\,\chi^*(\bar{r}',E',\bar{\Omega}',t')\right], \qquad \text{(A42)}$$

where

$$\hat{C}(\bar{r}',E\to E',\bar{\Omega}\to\bar{\Omega}') \equiv \frac{\Sigma_t(\bar{r}',E)}{\Sigma_t(\bar{r}',E')}C(\bar{r}',E\to E',\bar{\Omega}\to\bar{\Omega}')\,. \qquad \text{(A43)}$$

Noting that

$$H(\bar{r},E,\bar{\Omega},t) = \Sigma_t(\bar{r},E)\,\chi^*(\bar{r},E,\bar{\Omega},t)\,,$$

$$\int_0^\infty dR\;\Sigma_t(\bar{r},E)\exp\left[-\int_0^R \Sigma_t(\bar{r}+R'\bar{\Omega})\,dR'\right] = T(\bar{r}'\to r,E,\bar{\Omega})\,,$$

and

$$\Sigma_t(\bar{r},E)\,P^{\psi}(\bar{r},E,\bar{\Omega},t) = P^{\Phi}(\bar{r},E,\bar{\Omega},t)\,,$$

Eq. A42 becomes

$$H(\bar{r},E,\bar{\Omega},t) = T(\bar{r}'\to\bar{r},E,\bar{\Omega})\left[P^{\Phi}(\bar{r}',E,\bar{\Omega},t') + \hat{C}(\bar{r}',E\to E',\bar{\Omega}\to\bar{\Omega}')\,H(\bar{r}',E',\bar{\Omega}',t')\right]. \qquad \text{(A44)}$$

A comparison of Eq. A44 with Eq. A40 reveals that

$$G(\bar{r},E,\bar{\Omega},t) = P^{\Phi}(\bar{r},E,\bar{\Omega},t) + \hat{C}(\bar{r},E\to E',\,\bar{\Omega}\to\bar{\Omega}')\,H(\bar{r},E',\bar{\Omega}',t)\,, \qquad \text{(A45)}$$

and the subsequent substitution of Eq. A40 into Eq. A45 yields the following defining equation for the adjoint emergent particle density:

$$G(\bar{r},E,\bar{\Omega},t) = P^{\Phi}(\bar{r},E,\bar{\Omega},t) + \hat{C}(\bar{r},E\to E',\bar{\Omega}\to\bar{\Omega}')\,T(\bar{r}'\to\bar{r},E',\bar{\Omega}')\,G(\bar{r}',E',\bar{\Omega}',t)\,. \qquad \text{(A46)}$$

Equation A46 is almost identical with Eq. 3.117, which defines the forward emergent particle density and also serves as the formal basis for the forward random walk. In order to facilitate a Monte Carlo solution, Eq. A46 can be interpreted in terms of the transport of pseudo-particles called "adjunctons" in the $(P'\to P)$ direction of transport. This presents two immediate problems: (1) the transport of the adjunctons from $\bar{r}' = \bar{r} + R\bar{\Omega}$ to $\bar{r}$ would be in a direction opposite to the direction vector $\bar{\Omega}$; therefore, the direction vector for the adjuncton should be $\hat{\Omega} \equiv -\bar{\Omega}$, and $\bar{r}' = \bar{r} - R\hat{\Omega}$; and (2) the collision kernel should be interpreted as describing the $(P'\to P)$ change in phase space experienced by the adjuncton during its random walk; therefore, let

$$C(\bar{r},E'\to E,\hat{\Omega}'\to\hat{\Omega}) \equiv \hat{C}(\bar{r},E\to E',\bar{\Omega}\to\bar{\Omega}') = \iint\frac{\Sigma_s(\bar{r},E\to E',\bar{\Omega}\to\bar{\Omega}')}{\Sigma_t(\bar{r},E')}\,dE'\,d\bar{\Omega}'\,. \qquad \text{(A47)}$$

Equation A47 may be rewritten in terms of a normalized collision kernel and a weight factor:

$$C(\bar{r},E'\to E,\hat{\Omega}'\to\hat{\Omega}) = \iint\frac{\Sigma_s(\bar{r},E\to E',\bar{\Omega}\to\bar{\Omega}')}{\iint\Sigma_s(\bar{r},E\to E',\bar{\Omega}\to\bar{\Omega}')\,dE\,d\bar{\Omega}}\left[\frac{\iint\Sigma_s(\bar{r},E\to E',\bar{\Omega}\to\bar{\Omega}')\,dE\,d\bar{\Omega}}{\Sigma_t(\bar{r},E')}\right]dE'\,d\bar{\Omega}'\,. \qquad \text{(A48)}$$

The selection of the new energy (E) and direction ($\hat{\Omega} = -\bar{\Omega}$) is made from the normalized collision kernel and the weight of the adjuncton is modified by the weight factor

$$\left[\frac{\iint \Sigma_s(\bar{r},E \to E',\bar{\Omega} \to \bar{\Omega}')\, dE\, d\bar{\Omega}}{\Sigma_t(\bar{r},E')}\right],$$

which is no longer a simple nonabsorption probability and may assume values in excess of unity. Therefore, there is no "analog" scattering for adjunctons and the adjuncton's weight may increase at some collisions.

Equation A46 can be written as

$$G(\bar{r},E,\hat{\Omega},t) = P^{\Phi}(\bar{r},E,\hat{\Omega},t) + C(\bar{r},E' \to E,\hat{\Omega}' \to \hat{\Omega})\, T(\bar{r}' \to \bar{r},E',\hat{\Omega}')\, G(\bar{r}',E',\hat{\Omega}',t')\,, \tag{A49}$$

which now corresponds to the transport of adjunctons and provides the desired basis for the adjoint random walk. Equation A49 can also be referred to as the "integral emergent adjuncton density equation." Note that the source of adjunctons is provided by $P^{\Phi}(\bar{r},E,\hat{\Omega},t)$, which is related to $P^{\Phi}(\bar{r},E,\bar{\Omega},t)$ as follows:

$$P^{\Phi}(\bar{r},E,\hat{\Omega},t) = P^{\Phi}(\bar{r},E,-\bar{\Omega},t)\,, \tag{A50}$$

which must be taken into consideration if the response function $P^{\Phi}(\bar{r},E,\bar{\Omega},t)$ has angular dependence; however, many physical situations permit an isotropic assumption.

A Monte Carlo solution of Eq. A49, the integral emergent adjuncton density equation, will generate data from which the adjuncton flux $\chi^*(\bar{r},E,\hat{\Omega},t)$ and other quantities of interest can be determined. The general use of $\chi^*(\bar{r},E,\hat{\Omega},t)$ must take into account the reversal of direction between adjunctons and real particles, i.e., $\hat{\Omega} = -\bar{\Omega}$. For example, consider the various ways of calculating the answer of interest:

$$\lambda = \int\!\!\int\!\!\int\!\!\int P^{\Phi}(\bar{r},E,\bar{\Omega},t)\, \Phi(\bar{r},E,\bar{\Omega},t)\, d\bar{r}\, dE\, d\bar{\Omega}\, dt = \int\!\!\int\!\!\int\!\!\int \frac{P^{\Phi}(\bar{r},E,\bar{\Omega},t)}{\Sigma_t(\bar{r},E)} T(\bar{r}' \to \bar{r},E,\bar{\Omega})\, \chi(\bar{r}',E,\bar{\Omega},t')\, d\bar{r}\, dE\, d\bar{\Omega}\, dt, \tag{A51}$$

$$\lambda = \int\!\!\int\!\!\int\!\!\int S(\bar{r},E,\bar{\Omega},t)\, \chi^*(\bar{r},E,\bar{\Omega},t)\, d\bar{r}\, dE\, d\bar{\Omega}\, dt = \int\!\!\int\!\!\int\!\!\int S(\bar{r},E,\bar{\Omega},t)\, \chi^*(\bar{r},E,-\hat{\Omega},t)\, d\bar{r}\, dE\, d\bar{\Omega}\, dt\,, \tag{A52}$$

$$\lambda = \int\!\!\int\!\!\int\!\!\int S_c(\bar{r},E,\bar{\Omega},t)\, W(\bar{r},E,\bar{\Omega},t)\, d\bar{r}\, dE\, d\bar{\Omega}\, dt = \int\!\!\int\!\!\int\!\!\int S_c(\bar{r},E,\bar{\Omega},t)\, W(\bar{r},E,-\hat{\Omega},t)\, d\bar{r}\, dE\, d\bar{\Omega}\, dt\,, \tag{A53}$$

$$\lambda = \int\!\!\int\!\!\int\!\!\int \frac{S(\bar{r},E,\bar{\Omega},t)}{\Sigma_t(\bar{r},E)} H(\bar{r},E,\bar{\Omega},t)\, d\bar{r}\, dE\, d\bar{\Omega}\, dt = \int\!\!\int\!\!\int\!\!\int \frac{S(\bar{r},E,\bar{\Omega},t)}{\Sigma_t(\bar{r},E)} H(\bar{r},E,-\hat{\Omega},t)\, d\bar{r}\, dE\, d\bar{\Omega}\, dt\,, \tag{A54}$$

$$\lambda = \int\!\!\int\!\!\int\!\!\int \frac{S(\bar{r},E,\bar{\Omega},t)}{\Sigma_t(\bar{r},E)} T(\bar{r}' \to \bar{r},E,\bar{\Omega})\, G(\bar{r}',E,\bar{\Omega},t')\, d\bar{r}\, dE\, d\bar{\Omega}\, dt$$

$$= \int\!\!\int\!\!\int\!\!\int \frac{S(\bar{r},E,\bar{\Omega},t)}{\Sigma_t(\bar{r},E)} T(\bar{r}' \to \bar{r},E,-\hat{\Omega})\, G(\bar{r}',E,-\hat{\Omega},t')\, d\bar{r}\, dE\, d\bar{\Omega}\, dt\,. \tag{A55}$$

Further, if outward boundary crossings would be scored in the forward problem, the corresponding source adjunctons would be introduced in the inward direction. Likewise, adjunctons would be scored for entering a volume from which the source particles in the forward problem would be emitted. It should be noted that many sources and response functions are isotropic and the problem of direction reversal need not be considered.

Appendix 3B. Computer Code Abstracts

Computer codes which utilize the methods described in this chapter are abstracted below. These abstracts with more details also appear in ORNL-RSIC-13,[144] a publication of the Radiation Shielding Information Center which is continually updated to include new codes as they become available. It is emphasized that the abstracts given here do not represent all the codes available from RSIC, nor the many shielding codes not in the RSIC collection for reasons such as obsolescence, nonavailability due to proprietary interests, or insufficient testing or documentation.

All codes and auxiliary routines received by RSIC are checked out for operability; that is, sample problems are run by the RSIC staff. If the code is operable, it is packaged and assigned a CCC number, and a code abstract is written and distributed. The codes, as packaged, run on certain computers. Operating them on these computers should provide a minimum of difficulty. Translating to different machines may or may not prove difficult, depending on various factors.

Inquiries or requests for a code package should be mailed to

CODES COORDINATOR
Radiation Shielding Information Center
Oak Ridge National Laboratory
P. O. Box X
Oak Ridge, Tennessee 37830

or telephoned to

Area Code 615; 483-8611, Ext. 3-6944, or to
FTS 615-483-6944.

A reel of magnetic tape should accompany each request for a code.

Members of the RSIC staff are always available for consultation in connection with the shielding code packages, either in regard to operation of the code or to its applicability for a particular shielding problem. Cross-section data libraries on magnetic tape for use in the various codes are also available. These are constantly being revised and extended. Also, RSIC maintains a file indicating whether a code package has been made available in additional machine languages, made operable on other machines, etc.

3B.1. DISCRETE ORDINATES PROGRAMS

DTF-IV (CCC-42*), DTF-69 (CCC-130). – The Los Alamos Scientific Laboratory program DTF-IV[8,145,146] solves the multigroup, one-dimensional Boltzmann transport equation for plane, cylindrical, or spherical geometries. Anisotropic scattering is represented by Legendre polynomial expansion of the differential scattering cross section. Energy dependence is treated by the multigroup approximation and angular dependence by a general discrete ordinates approximation. Iteration processes for within-group scattering and upscattering are accelerated by system-wide renormalization procedures.

General anisotropic scattering capability is provided in each of the three geometries, upscattering convergence acceleration is used, an optional group- and pointwise convergence test is available, and a neutron-conserving negative flux correction routine is used.

An auxiliary routine, GAMLEG, provides cross sections for photon transport problems in a form suitable for input to DTF-IV.

DTF-IV is written in FORTRAN IV language and is operable on IBM-7090/30, IBM-3600, B-5500 and CDC-6000 computers.

A special version of DTF-IV, called DTF-69,[147] was developed by Sandia Laboratories to treat X-ray transport. A special version of GAMLEG prepares the necessary cross sections which include effects not normally treated in gamma-ray shielding.

ANISN (CCC-82). – ANISN,[9] a code developed jointly by the Oak Ridge Computing Technology Center and Oak Ridge National Laboratory, solves the one-dimensional Boltzmann transport equation in slab, spherical, or cylindrical geometry. The source may be a fixed source, a fission source, or a subcritical combination of the two. A criticality search may be performed on any one of several parameters. Cross sections may be weighted using the space- and energy-dependent flux generated in solving the transport equation. In this way, fine-group libraries can be reduced or "collapsed" to a

*Refers to RSIC code package number.

few-group structure for economical production calculations.

The solution technique is an advanced discrete ordinates method which represents a generalization of the method originated by Wick[4] and greatly developed and extended to curvilinear geometry by Carlson[6] at Los Alamos Scientific Laboratory.

ANISN has been used for many shielding problems, including deep-penetration problems in which angle-dependent spectra are calculated in detail. The principal feature that makes ANISN suitable for such problems is the use of an advanced programming technique with optional data-storage configurations, which allows efficient execution of small, intermediate, and extremely large problems. ANISN also includes an efficient technique for handling general anisotropic scattering, pointwise convergence criteria, and alternate step-function difference equations that effectively prevent oscillating flux distributions that sometimes occur in discrete ordinates solutions.

ANISN can be used in the adjoint mode to produce importance functions for Monte Carlo calculations or to produce dose transmission functions for differential sources.

ANISN is written in FORTRAN IV language for use on IBM-7090 and -7094 computers and in FORTRAN IV (H) language for use on the IBM-360, CDC-6600, CDC-1604 and B-5500 computers.

BIGGI 3P or 4T (CCC-66). – The BIGGI 3P program,[148,149] developed by EURATOM, Ispra (Varese), Italy, solves the Boltzmann transport equation in plane multilayer geometry. It computes gamma-ray angular fluxes, spectra, buildup factors, and albedos. The sources must be monoenergetic and located on one outer boundary; their angular distribution can be isotropic or collimated.

BIGGI 3P integrates the Boltzmann equation numerically. The basis is the pair of coupled integral equations, discussed for the case of neutrons by Weinberg and Wigner.[1] Discrete ordinate meshes are defined in each of the three concerned dimensions (angle, space, and gamma-ray wavelength), and the integrals figuring in the transport equation are approximated by sums. The program solves the integral equations without iteration, since they are of the Volterra type (as long as only energetic downscattering is assumed). The gamma-ray cross sections (in Thompson units per electron) of each slab must be given in the input. The contribution of the low-energy tail below the cutoff energy to the four buildup factors (energy flux, particle flux, dose rate, and energy absorption rate) and to the two albedos (energy and particle current) is estimated. An exponential transformation allows rather great spatial integration steps, up to 2 or 3 mean free paths.

BIGGI 3P is written in FORTRAN language for use on the IBM-7090 computer.

BIGGI 4T, available for the IBM-360 computers, is an extension of BIGGI 3P which allows spherical geometry, arbitrary source location, multiple source energies, additional layers, and other improvements.

DOT-I, II, II-W (CCC-89). – The DOT two-dimensional code, developed jointly by the Oak Ridge Computing Technology Center and Oak Ridge National Laboratory, was first available in 1966.[11] DOT-II[12] and DOT-II-W,[150] the latter a modification by Westinghouse Astronuclear Laboratory, became available in 1969.

DOT is a general-purpose program which solves the linear, energy-dependent, Boltzmann transport equation for two-dimensional r-z, x-y, and r-θ geometries. The basic form of the solution is the flux, averaged in the spatial interval surrounding r_i, z_j, integrated over the energy group g, and averaged in the solid angle segment surrounding a direction Ω.

The gradient or convection term in the Boltzmann equation is approximated by the discrete ordinates finite difference technique (Carlson's S_n method). The inscatter integral is approximated by expanding the differential cross section in a Legendre series which allows the integral to be computed by quadrature. DOT will solve forward or adjoint, homogeneous or inhomogeneous problems. An inhomogeneous problem may have a volume-distributed source or a specified angular flux at the right or top boundaries; fissions may be included for a subcritical system. For the homogeneous or eigenvalue problem the following can be determined: (1) the static multiplication factor k, (2) time absorption, "Rossi α," (3) fissile material concentration for a specified k, (4) zone thickness for a specified k.

The primary differences between previous two-dimensional codes and DOT are the following: (1) general anisotropic scattering is allowed; (2) boundary sources may be treated by specifying the angular flux at the right or top boundaries; (3) angular fluxes may be printed or written on binary tape; (4) if specified, a pointwise inner iteration flux convergence criterion is used instead of the integral test; (5) the integral inner iteration convergence criterion specifies that the average absolute pointwise flux error be less than a specified quantity epsilon; (6) input data are processed by the FIDO routine used in DTF-II and ANISN; and (7) if the linear difference equations produce a negative flux, the flux is recalculated using the step function difference equations to inhibit oscillation due to extrapolation (optional).

The major improvements of the DOT-II-W code over the DOT code are the inclusion of acceleration techniques on the group flux solution, improved convergence logic, asymmetric quadrature capability, and improved tape operations.

DOT-I is operational on the IBM-7090 computer, DOT-II on the IBM-360/75/91 computers, and DOT-II-W on the CDC-6600 computer.

XSDRN (CCC-123). – XSDRN, developed jointly by the Oak Ridge Computing Technology Center and Oak Ridge National Laboratory, uses the Nordheim integral treatment, narrow resonance, or an infinite-mass approximation to process resonance data on a master neutron cross section library and thus obtain microscopic fine-group cross sections for a large number of nuclides. The code[151] then uses the cross sections in an independent calculation to solve for fluxes, eigenvalues, critical dimensions, etc., in a discrete ordinates, diffusion, or infinite-medium theory calculation. The fine-group fluxes thus obtained can then be used to collapse the fine-group cross-section data to a more tenable few-group structure for use in several independent computer codes.

The two principal calculations performed by XSDRN (resonance calculation and ANISN flux calculation) both employ numerical finite-difference techniques. For the resonance calculation, this involves a Simpson integration to solve for the collision density in the resonance range. The flux calculations employ a multigroup energy structure, an arbitrary spatial structure and a mechanical angular quadrature, all of which must be used in the various integration and differencing schemes in the code. The flexible dimensioning scheme employed allows optimal use of core storage. A unique method of storing cross sections is employed which eliminates impossible and/or zero transfer cross sections.

The master cross-section library tape for XSDRN is produced by XLACS.[152] Cross-section tapes can be generated for ANISN, DOT, CITATION, ROD, or the EXTERMINATOR-II codes.

XSDRN is available in FORTRAN IV for the IBM-360 computer. The library of data is available on tape from RSIC.

ASOP (CCC-126). – ASOP[153-155] is a shield optimization program based on the one-dimensional discrete ordinates transport code ANISN (see above). It has been used to design optimum shields for SNAP uranium-zirconium hydride thermoelectric reactors and uranium oxide thermionic reactors. For weight optimization, ASOP generates coefficients of linear equations describing the logarithm of the dose and dose-weight derivatives as functions of position from data obtained in an automated sequence of ANISN calculations. With the dose constrained to a design value and all dose-weight derivatives required to be equal, the linear equations may be solved for a new set of shield dimensions. Since changes in the shield dimensions may cause the linear functions to change, the entire procedure is repeated until convergence is obtained.

The detailed calculation of the radiation transport through shield configurations for every step in the procedure distinguish ASOP from other shield optimization programs which rely on multiple component sources and attenuation coefficients to describe the transport.

ASOP is written in FORTRAN for the IBM-360 computers.

TWOTRAN (CCC-129). – The discrete ordinates TWOTRAN program,[156-158] originated at Gulf General Atomic and expanded at Los Alamos, solves two-dimensional particle transport problems in x-y, r-z, and r-θ geometries.* Both forward and adjoint, homogeneous (k_{eff} or parametric eigenvalue searches) or inhomogeneous time-independent problems are solved subject to vacuum, reflective, white, periodic, or input specification of boundary flux conditions. Both anisotropic inhomogeneous problems and general anisotropic scattering problems are treated, and arbitrary numbers of groups of up or down scattering are allowed.

Energy dependence is treated by the multigroup approximation and the angular dependence by a discrete ordinates approximation. Space dependence is approximated by the diamond difference scheme with a set-to-zero negative flux control. Anisotropic scattering and anisotropic inhomogeneous sources are represented by finite spherical harmonics expansions. Within-group iterations, upscattering iterations, k_{eff} iterations, and eigenvalue search iterations are accelerated by a coarse-mesh particle rebalancing algorithm.

The variable dimensioning capability of Fortran-IV is used so that any combination of problem parameters leading to a blank common vector length less than LENXCA can be used. For a 65 K machine LENXCA can be greater than 35,000, depending on local system requirements. With a few exceptions, only within-group problem data are stored in fast memory and data for all other groups are stored in auxiliary bulk memory such as extended core storage.

*As of this writing, June, 1970, only the x-y version is available from RSIC, but the general version is expected to be available in the near future.

TWOTRAN is programmed in Fortran-IV with a small amount of mixed integer-floating arithmetic, generalized subscripting, encode statements, and minor use of 10 H Hollerith formats. It is operable on the CDC-6600 and IBM-360 computers.

3B.2. MONTE CARLO PROGRAMS

O5R (CCC-17). – Oak Ridge National Laboratory's code system O5R[35] was designed to calculate, by Monte Carlo methods, any quantity related to neutron transport in reactor or shielding problems. Arbitrary three-dimensional geometries bounded by quadric surfaces may be treated, and the sources may have arbitrary spatial, energy, and angular distributions specified by a subroutine written by the user. Anisotropic scattering can be included for both elastic and inelastic processes. Fissionable as well as nonfissionable media can be treated. Several variance reduction techniques are available.

For maximum flexibility, a calculation generally consists of two main operations. The primary routine, called the O5R Generator, is used to generate neutron case histories and produce collision tapes on which are written any, or all, of 34 distinct parameters describing each collision. These tapes are subsequently processed by analysis routines, usually written by the user, to produce Monte Carlo estimates of any desired quantity. Analysis routine STATEST[159] is included in the prototype of the O5R system for shielding problems (a "prototype" code is one which is a completely assembled version, including sample input and output). STATEST provides for statistical estimation of the flux in energy bins for an array of space points.

A batch system of generating case histories is employed to obtain a very detailed table of cross sections in fast memory. The cross sections in memory at one time encompass only a small energy range. All collisions of a batch for which these cross sections are needed are generated before another group of cross sections are read from tape. Cross-section data are prepared for use in O5R by XSECT, a code which performs a variety of manipulations: preparing, updating, and editing a master tape and performing cross-section arithmetic.

Source data are generated by subroutine SOURCE, usually written by the code package user for his specific problem.

A very general geometry subroutine permits the treatment of complicated geometries. As many as 16 media are permitted and boundaries may be either planes or quadric surfaces, arbitrarily oriented and intersecting in arbitrary fashion.

The O5R program is available in FORTRAN language for the IBM-7090, IBM-360, CDC-1604, CDC-6600, and UNIVAC-1108 computers. A revision and extension of O5R is available as O6R (see below).

O6R (CCC-128). – Oak Ridge National Laboratory's code system O6R,[36] the name of which derives from O5R Revised, was developed primarily to take advantage of the larger machine fast memories now available and to read the standard ENDF/B cross-section format; however, it also incorporates other improvements, including time dependence and albedo "scattering."

The O5R concept of an energy supergroup-subgroup structure is retained in O6R, but the greater storage capacity may allow all the cross sections to be stored simultaneously, depending on the number of supergroups used and the energy range of a supergroup variable. At this writing, O6R does not utilize ENDF/B resonance parameters.

As O5R does, O6R may output "collision tapes" containing neutron history parameters for selected events to be analyzed later; however, provisions for analyzing during the calculation any event which can be recorded on a collision tape have been added. The methods of analysis are as described in the manual on ACTIFK,[160] all options of the FORTRAN-IV ACTIFK being available to the user.

O6R also provides for the generation of secondary gamma rays during the neutron transport problem. At each scattering, if gamma-ray generation has been specified, the code calls subroutine GAMMA, which prepares and writes a magnetic tape of the parameters of the gamma rays generated by the user-provided subroutine GAMGEN.

Versions of O6R are available for the CDC-1604 and IBM-360/75/91 computers. For use on the IBM-360 computer, the general-geometry and special-geometry packages must be compiled in double precision. This requires that variables used from or passed to the geometry package in COMMON or as a formal parameter be of type REAL*8. Subroutines NORML and GOMFLP have been added to the geometry packages to handle albedo reflections.

MORSE (CCC-127). – The MORSE code, developed by Oak Ridge National Laboratory, is a multipurpose neutron and gamma-ray transport Monte Carlo code.[37] It uses multigroup cross sections, which allow the solution of neutron, gamma-ray, or coupled neutron and gamma-ray problems in either the forward or adjoint mode. Time dependence for both shielding and criticality problems is provided. General three-dimensional geometry, as well as specialized one-dimensional geometry descriptions, may be used with an albedo option available at any material surface.

Standard multigroup cross sections such as those used in discrete ordinates codes may be used as input; either ANISN or DTF-IV cross-section formats are acceptable. Anisotropic scattering is treated for each group-to-group transfer by utilizing a generalized Gaussian quadrature technique. The modular form of the code with built-in analysis capability for all types of estimators makes it possible to solve a complete neutron-gamma-ray problem as one job, and without the use of tapes.

CDC-1604, CDC-6600, and IBM-360/75/91 versions of MORSE are available.

TRG-SGD (CCC-25). – The Monte Carlo code TRG-SGD,[161] written by the Technical Research Group for the Air Force Weapons Laboratory (Kirtland), calculates the time and space distribution of secondary gamma-ray doses and dose rates from a nuclear weapon detonation in the atmosphere or in the ground near the surface of the earth. The neutron source is given as leakage from the exploded device. The effects of the blast and fireball on the transport of the neutrons and gamma rays are taken into account.

The neutron reactions considered are elastic scattering, inelastic scattering, radiative capture, and non-radiative capture. The (n,2n) reaction is treated as inelastic scattering by cross-section modification. The prompt neutrons are degraded 14-MeV neutrons from a fusion reaction, fission neutrons, and neutrons which are assumed to have a "bomb thermal Maxwell-Boltzmann spectrum." The delayed neutrons are from a fission source with a time-dependent volume distribution. The only gamma-ray reactions considered are Compton scattering and absorption, the latter being the total of pair production and photoelectric effects.

The Monte Carlo method is used to generate the neutron distribution, the secondary gamma ray source distribution, and the secondary gamma-ray dose distribution. The effects of the air-ground interface, an inhomogeneous atmosphere, and time-dependent hydrodynamics are taken into account. The type and yield of weapon and the detonation altitude determine the initial conditions. The geometric system is taken to be axially symmetric. In addition to statistical estimation of the gamma-ray source and dose distributions, various importance-sampling techniques are used. These include Russian roulette for low-contribution particles and generalized quota sampling. In addition, all random variables are picked from a truncated exponential distribution. This procedure is controlled by input parameters.

TRG-SGD is written in FORTRAN language and is operable on the CDC-1604 computer.

DIPSEA (CCC-35). – The Monte Carlo code DIPSEA[162] was developed by Technical Operations Research to determine the radiation dose resulting from a point isotropic gamma-ray source in an atmosphere of air whose density varies exponentially. The source may be monoenergetic or polyenergetic. A cylindrical geometry is used to describe the atmospheric region surrounding the point source. The assumed cylinder, divided into a layered series of square toroids of uniform cross section, extends from a lower altitude of 11 km to an upper altitude of 100 km and has a variable radius that normally has a maximum limit imposed by statistical fluctuations inherent in Monte Carlo calculations. The code assumes that the photon is lost after passing these boundaries.

The atmosphere is assumed to be divided into two zones, each zone having its own exponential expression for the density. The range of each zone is set equal to the altitude interval in which the gradient of the molecular-scale temperature is nearly constant.

Energies in the program are expressed in units of Compton wavelength. All interactions in the media are considered to be either Compton scattering or pair production; pholoelectric absorption is accounted for by reducing the weight at each collision.

The components calculated are the scattered, direct, and total doses in the center of each toroidal cross section, in units of both keV/g and ion pairs/cm^3. The scattered dose is computed by the Monte Carlo method and the unscattered dose is computed analytically.

DIPSEA is written in FORTRAN and FAP languages and can be used on IBM-704, -709, -7090, and -7094 computers.

OGRE (CCC-46). – The OGRE code system[163,164] was designed by Oak Ridge National Laboratory to calculate by Monte Carlo methods any quantity related to gamma-ray transport. The system is represented by two typical codes: OGRE-P1 and OGRE-G. The OGRE-P1 code is a simple prototype which calculates the dose rate on one side of a slab due to a plane source on the other side. OGRE-G, a prototype of a code utilizing a general-geometry routine, calculates the dose rate at arbitrary points and provides for a very general source description by allowing the user to prepare his own source tape.

Case histories of gamma rays in the prescribed geometry are generated and then analyzed to produce averages of any desired quantity, which in the case of the prototypes is the gamma-ray dose rate. The system is designed to achieve generality by ease of modification. No importance sampling is built into the prototypes.

A very general geometry subroutine permits the treatment of complicated geometries. This is essentially the same routine used in the O5R neutron-transport system (see above). Boundaries may be either planes or quadric surfaces, arbitrarily oriented and intersecting each other in arbitrary fashion.

Cross-section data are prepared by an auxiliary master cross-section code (MASTAPE), which may be used to originate, update, or edit the master cross-section tape. The master cross-section tape is utilized in the OGRE codes to produce detailed tables of the macroscopic cross sections required for the Monte Carlo calculations.

OGRE is available in FORTRAN II and IV languages for use on the IBM-7090 computer, in FORTRAN IV for IBM-360/50 and -360/75 computers, and in FORTRAN 63 and CODAP for the CDC-1604 and CDC-3600 computers.

Cross-section routines are now available to read ENDF/B format.

ADONIS (CCC-13A,B), UNC-SAM and UNC-SAM-2 (CCC-81), UNC-SAM-3 (CCC-133). – The United Nuclear Corporation stochastic approximation method, developed originally as ADONIS[165] and later as UNC-SAM,[166] calculates the solution to the Boltzmann transport equation in three-dimensional geometry by Monte Carlo methods. ADONIS tracks either neutrons or gamma rays through shields composed of rectangular parallelepipeds of different compositions. Particle splitting is used to improve the efficiency of the calculation by assigning importance weights to each of the regions. The program computes fluxes and their standard deviations in each of up to 80 regions. By use of response functions the dose and strength of secondary gamma rays from any neutron-induced reaction can be computed throughout the configuration. UNC-SAM will calculate fluxes, flux-dependent functionals such as doses, and their standard deviations in geometry comprised of rectangular parallelepipeds, which in turn, may contain spheres, cylinders, parallelepipeds, or wedges. Importance sampling is used to increase efficiency. In evaluating neutron fluxes in small-volume detectors, a scoring by analytical estimation, referred to as "flux at a point," is used.

A modified version of UNC-SAM, identified as UNC-SAM-2,[167] treats time-dependent neutron and photon transport through matter.

ADONIS versions are available in FORTRAN-FAP language for the IBM-7090 and -7094 computers (CCC-13A) and in FORTRAN-CODAP language for the CDC-1604 computer (CCC-13B).

UNC-SAM and UNC-SAM-2 are written in FORTRAN 63 language and are operable on the CDC-1604 computer.

UNC-SAM-3 is a modified program[168] for the CDC-1604 and CDC-6600 computers which accepts a revised cross-section format.[169] The cross sections are prepared by ENDT from ENDF/B tapes.

SAM-C (CCC-114). – The code SAM-C,[170,171] was developed by Mathematical Applications Group, Inc., White Plains, New York; U.S. Army Ballistic Research Laboratory, Aberdeen Proving Ground, Maryland; and U.S. Army Nuclear Defense Laboratory, Edgewood Arsenal, Maryland. It calculates the time-dependent transport of neutrons or gamma rays through complex three-dimensional geometrical configurations. The code calculates the total flux in each region in a specified group of energy and time bins, and it can also compute fluxes at specified points within the geometry.

SAM-C is based on the UNC-SAM-2 Monte Carlo program, the primary difference being in the techniques employed to describe the geometry. SAM-C uses combinatorial geometry and is therefore capable of representing more complex assemblies. To use this geometry capability necessitated a number of modifications in the logic and storage requirements of UNC-SAM-2. In addition, a ray-tracing volume calculation routine was added, since for many of the shapes produced by the combinatorial geometry it is impractical to determine the volume analytically. All the nuclear interaction routines of UNC-SAM-2 are unchanged.

Combinatorial geometry is a new and significant advance in the state-of-the-art of representing, in a computer, a complex three-dimensional structure. In effect, one represents a structure such as an armored tank in terms of sums, differences, and intersections of relatively simple bodies such as spheres, cylinders, etc. The input for such a description consists of the geometric location of the simple bodies and their dimensions, followed by a region definition table consisting of a series of equations defining each particular region of the structure in terms of the basic bodies. For example, if the total structure is a tank, then one region would be the gun barrel, which might be represented as the material located between two concentric cylinders.

Versions of SAM-C are available for the IBM-360, CDC-1604 and CDC-6600 computers.

AMC (CCC-90). – The Oak Ridge National Laboratory program AMC (for Albedo Monte Carlo) calculates the transmission of neutrons and their concomitant capture gamma rays through large concrete-walled rectangular ducts of varying complexity to establish design criteria for entryway shielding against initial weapons radiation.[172] AMC can be used to calculate the fluxes and dose rates inside the ducts due to neutrons of all energies incident upon the duct mouth, and

an option in the code allows a simultaneous calculation of the secondary gamma-ray dose rates arising from wall capture. The code treats duct transmission by employing the albedo concept in conjunction with a Monte Carlo treatment of history generation.

In its present form the code can calculate the fast-neutron dose rates, epicadmium differential energy fluxes, thermal fluxes, and wall-capture secondary gamma-ray dose rates arising from an arbitrary incident neutron source for the following concrete-walled rectangular structures: (1) a completely enclosed room, (2) an open straight duct or a straight duct closed at one end, (3) an open or closed two-legged duct with one right-angle bend, (4) an open or closed three-legged duct with two right-angle bends, (5) a three-legged duct which has two right-angle bends, is open or closed at the mouth and opens into a room at the end of the third leg, and (6) the geometries given by 3–5 with the first leg sloping downward, the mouth and the remaining legs being horizontal. AMC operates on the IBM-360/75 computer.

FASTER (CCC-98). – The Monte Carlo program FASTER[173–175] is the result of a cooperative effort by Westinghouse Astronuclear Laboratory, Pittsburgh, Pennsylvania; NASA George C. Marshall Space Flight Center, Huntsville, Alabama; ART Research Corporation, Los Angeles, California; Aerojet General Corporation, Sacramento, California; and the Boeing Company, Huntsville, Alabama.

FASTER calculates energy-dependent neutron or photon fluxes at points, on surfaces, and in regions of complex geometries. The general quadric surface equation describes the geometry. Equations for planes, cones, elliptical cylinders and ellipsoids can also be used as input description of the surfaces. The source is described in rectangular, cylindrical, or spherical coordinates. The spatial, angular, and energy source description is assumed to be separable.

FASTER treats the entire spectrum of particle energies simultaneously, which eliminates much of the usual repetitive geometric computations resulting in significant computer time savings. Sampling all possible scattering energies for each collision and extensive importance sampling reduces the variance. For neutron transport, using group cross sections results in additional time savings.

Distinctive features of the Monte Carlo method as employed in the FASTER program include: (1) application of random sampling to the spatial and angular integrations only, (2) consistent use of energy-averaged sampling functions, (3) approximation of importance functions by point kernel techniques, (4) analytic treatment of the energy variable over its entire range, and (5) zero variance energy integration of the scattered source equations.

Versions of FASTER are available for the IBM-7090/94, the IBM-360/75, and the UNIVAC-1108 computers.

AIRTRANS (CCC-110). – The function of the AIRTRANS system,[176,177] developed by United Nuclear Corporation, Elmsford, New York, and Lockheed Missile and Space Company, Sunnyvale, California, is to calculate by Monte Carlo methods the radiation field produced by neutron and/or gamma-ray sources which are located in the atmosphere. The radiation field is expressed as the time- and energy-dependent flux at a maximum of 50 point detectors in the atmosphere. The system calculates uncollided fluxes analytically and collided fluxes by the "once more collided flux-at-a-point" technique.

Energy-dependent response functions can be applied to the fluxes to obtain desired flux functionals, such as doses, at the detector point. AIRTRANS also can be employed to generate sources of secondary gamma radiation.

Neutron interactions treated in the calculational scheme include elastic (isotropic and anisotropic) scattering, inelastic (discrete level and continuum) scattering, and absorption. Charged-particle (n,p) reactions are treated as absorptions. A built-in kernel option can be employed to take neutrons from 150 keV to thermal energy, thus eliminating the need for particle tracking in this energy range. Another option used in conjunction with the neutron transport problem creates an "interaction tape" which describes all the collision events that can lead to the production of secondary gamma rays. This interaction tape subsequently can be used to generate a source of secondary gamma rays.

The gamma-ray interactions considered include Compton scattering, pair production, and the photoelectric effect; the latter two processes are treated as absorption events.

Incorporated in the system is an option to use a simple importance sampling technique (splitting) for detectors that are many mean free paths from the source. In essence, particles which fly far from the source are split into fragments, the degree of fragmentation being proportional to the penetration distance from the source. Each fragment is tracked separately, thus increasing the percentage of computer time spent following particles at the deep penetration. Each fragment is assigned a "weight" which is inversely proportional to the degree of fragmentation suffered by the original source particle. All estimates of flux

contributions by such a fragment are then multiplied by its assigned weight.

The code is available for the CDC-1604 and UNIVAC-1108 computers.

GADJET (CCC-115). – The GADJET code,[178,179] was developed by Radioptics, Inc., Plainview, New York; U.S. Naval Radiological Defense Laboratory, San Francisco, California; and the Office of Civil Defense, Washington, D.C. It is designed to calculate the effectiveness of structures (of arbitrary complexity) in shielding against gamma rays from fallout fields (finite or infinite) and to calculate the relative importance of each fallout region in contributing to the exposure rate in the structure. Complex realistic structures can be assumed, with windows, sills, black surfaces, etc., being allowed.

The code solves by Monte Carlo the adjoint transport equation for the so-called "importance" function. A knowledge of the importance function, coupled with the source distribution, solves the problem of determining the response of an arbitrary gamma-ray detector located in a structure that is exposed to fallout gamma-ray sources.

GADJET handles the transport of photon energy through matter having a three-dimensional geometry composed of rectangular parallelepipeds, which, in turn, may contain spheres, cylinders, parallelepipeds, or wedges. The geometry routines are based on those used in the UNC-SAM-1 code with only minor modifications.[166]

A CDC-6600 version of GADJET is available.

ANTE (CCC-131). – The ANTE code,[180] developed by Mathematical Applications Group, Inc. (MAGI), is designed to treat the time-dependent neutron transport equation in a three-dimensional geometry by the adjoint Monte Carlo technique, which is especially effective for point detectors and distributed sources. An important feature of ANTE is the powerful geometric capabilities of the combinatorial geometry system. Additional code improvements implemented in the ANTE 2 version include a treatment of the fission process, the (n,3n) and (n,n'3α) reactions, detector regions distributed in space, and increased geometrical scoring capabilities. The cross-section routines read ENDF/B data and provide adjoint cross sections for the Monte Carlo routines.

ANTE is written in FORTRAN IV for the CDC-6600 computer.

ETRAN (CCC-107). – The ETRAN code,[181,182] developed by the Center for Radiation Research, National Bureau of Standards, Washington, D. C., computes by Monte Carlo methods the transport of electrons and photons through plane-parallel semi-infinite slabs. The incident radiation can consist of a beam of either electrons or photons with specified spectral and directional distribution. Options are available by which all orders of the electron-photon cascade can be included in the calculation. Thus electrons are allowed to give rise to secondary knock-on electrons, continuous bremsstrahlung, and characteristic X rays, and photons are allowed to produce photoelectrons, Compton electrons, and electron-positron pairs. Annihilation quanta, fluorescence radiation, and Auger electrons are also taken into account. Also, the Monte Carlo histories of all generations of secondary radiations can be followed.

The information produced by ETRAN includes the following items: (1) the reflection and transmission of electrons or photons differential in energy and direction; (2) the production of continuous bremsstrahlung and characteristic X rays by electrons and the emergence of such radiations from the target (differential in photon energy and direction); (3) the spectrum of the amounts of energy left behind in a thick target by an incident electron beam; (4) the deposition of energy and charge by an electron beam as a function of the depth in the target; and (5) the flux of electrons, differential in energy, as a function of the depth in the target.

The photon component of the electron-photon cascade is calculated by conventional random sampling that imitates the physical processes of Compton scattering, photoelectric absorption, and pair production. In the calculation of the electron component, no attempt is made to follow successive individual interactions with atoms and atomic electrons because these are too numerous. Instead, a Monte Carlo model is used in which attention is focused on the effect of groups of successive collisions.

The electron tracks to be sampled are divided into a large number of short segments, and the energy loss and angular deflection in each segment are sampled from pertinent theoretical multiple scattering distributions. At the end of each short step, the direction of motion of the electron is changed by a multiple scattering angular deflection that is sampled from the Goudsmit-Saunderson distribution. This distribution is assumed to be the same for all short steps lying within a given step. The energy loss in a step, resulting from the cumulative effect of many inelastic collisions, is sampled from a distribution that is a convolution of a Landau distribution with a Gaussian. An option is also provided for using the continuous-slowing-down approximation in which energy-loss fluctuations are disregarded and the

energy loss by collisions is simply computed with the use of the stopping-power formula.

The production of knock-on electrons is sampled in each short step with the use of a probability distribution derived from the Moller cross section for collisions between free electrons (binding effects are disregarded). Histories of these particles are then followed by procedures identical with those used for the primary electrons.

The production of continuous bremsstrahlung photons is sampled in each short step with the use of a probability distribution derived from the bremsstrahlung cross section (Bethe-Heitler theory with modifications taking into account the correct high-frequency limit, empirical corrections, etc.). The probability is usually quite small that more than one bremsstrahlung photon will be produced in a single short step. Allowance is made for such a contingency by sampling the frequency of bremsstrahlung production events from a Poisson distribution. The energy of the secondary bremsstrahlung photons is subtracted from the energy of the electrons producing them. Thus photon emission contributes to the energy-loss straggling of the electrons. The photons are started out at a random position in the short step in a direction relative to that of the primary electron specified by the sampled intrinsic bremsstrahlung emission angle. For problems in which the production of thick-target bremsstrahlung is of prime interest, there is an option to increase the rate of occurrence of bremsstrahlung events artifically by a specified factor.

The production of secondary characteristic X rays in each short step is sampled with the use of the K-ionization cross sections of Arthurs and Moiseiwitsch and Kolbenstvedt.

The program is arranged so as to treat simultaneously many slab targets with different thicknesses.

Boundary crossings (transmission and reflection) usually occur in the middle of a short step. The energy with which the electron crosses the border is determined by subtracting from the energy at the beginning of the step an energy loss sampled from the Landau-Blunck-Leisegang distribution for the fraction of the step taken to the boundary. The direction at the time of crossing is determined by changing the direction of motion at the beginning of the short step involved, using a deflection sampled from an exponential approximation to the Goudsmit-Saunderson distribution for the fraction of the short step to the boundary.

The target is subdivided into many thin sublayers of equal thickness, and the energy deposited in each sublayer is recorded for each sampled track. The energy allowed to be deposited is that dissipated by electrons in inelastic collisions resulting in the production of slow secondary electrons with energies below the chosen cutoff value. The energy given to fast secondary electrons with energies above the cutoff is not immediately scored, because the histories of these electrons are followed further so that the energy may eventually be deposited in a sublayer different from the one in which the electrons were produced. Bremsstrahlung losses are similarly not scored immediately. Photons are allowed first to penetrate further through the medium so that the energy of the electrons set in motion by them may eventually be deposited in a different sublayer.

The treatment of charge deposition is quite similar to that of energy deposition, involving the scoring of charge deposited in sublayers. A track is assumed to "end" when the residual range of the electron is so small compared to the size of the sublayers that escape to a different sublayer is no longer possible. When secondary electrons are produced, either as the result of a knock-on collision, a Compton scattering or a photoelectric absorption, a unit charge is withdrawn from the sublayer in which the electron is born. The charge is then allowed to be carried to a different sublayer. Electron-positron pairs are excluded from this scheme because on the average their production does not lead to a net transfer of charge.

A Monte Carlo estimate of the flux is obtained by dividing the target into many sublayers and scoring the tracklength of electrons with specified energies in each of the sublayers. The average tracklength per incident electron divided by the thickness of the sublayer provides an estimate of the average flux in the sublayer.

The flux calculation includes primary as well as secondary electrons with energies down to some cutoff value which is chosen so that the electron is effectively trapped in the sublayer in which it finds itself because its residual range is smaller than the distance to the nearest sublayer boundaries.

IBM-360/75/91 and UNIVAC-7108 versions of ETRAN are available.

BETA (CCC-117). – BETA,[183] developed by A.R.T. Research Corporation, Los Angeles, California, and Air Force Weapons Laboratory, Albuquerque, New Mexico, is a Monte Carlo program for bremsstrahlung and electron transport analysis in generalized three-dimensional geometry. Relatively high-energy electrons and bremsstrahlung are treated explicitly over the energy range 0.1 to 15 MeV. Arbitrary sources are handled as functions of energy, time, space, and angle. Point, surface, and volume detectors are considered.

The effects of electric fields due to charge buildup are treated.

Results from BETA include energy deposition, time dependence of energy deposition, and charge trapping.

BETA uses random sampling techniques to perform the integrations of the order-of-scattering equations to give the unscattered and scattered components of the flux. Electron transport considers electron-nucleus, electron-electron, and electron-bremsstrahlung scattering. Wide angle scatterings are considered explicitly while narrow angle scatterings are grouped and the net effect lumped together. Klein-Nishina scattering is considered for photon transport. BETA will recognize simple surfaces such as planes, cones, elliptic cylinders and ellipsoids in specifying the geometry. Multiple-energy and angular-dependent sources in rectangular, cylindrical, and spherical geometry may be considered with the geometry of each source being superimposed over the various geometric regions. Flux estimation at points, on surfaces, and in volumes is accomplished by summing contributions from all order-of-scatter components. Legendre moments of the angular flux are used to construct azimuthally averaged differential angular fluxes. The time dependence is obtained by computing temporal moments and then analytically regenerating temporal dependence from these moments.

BETA is written for the IBM-7090/94 computers.

3B.3. PROGRAMS BASED ON KERNEL INTEGRATION

QAD (CCC-48). – The QAD point-kernel code system[184] was developed by Los Alamos Scientific Laboratory for calculating fast-neutron and gamma-ray penetration in various shield configurations. In the gamma-ray calculation the point kernel method involves representing the gamma-ray source by a number of point isotropic sources and computing the line-of-sight distance from each source point to the detector point. From the distance through the shielding regions and the characteristics of the shielding materials, the geometric attenuation and material attenuation are calculated. The energy transferred along the line of sight is then calculated on the basis of this attenuation and the appropriate buildup factor to account for the scattered radiation. With a distributed source the point kernel including the buildup factor is integrated over the source volume for each source energy considered.

The neutron-penetration calculation is made using a kernel obtained from the moments-method solution to the Boltzmann equation which has been fit by an exponential expression. In this method the neutron spectrum penetrating a shield is determined on the basis of equivalent length of a reference material between the source point and the receiver point. The equivalent length is calculated by weighting the penetration distance for each material in accordance with the material removal cross section. Provisions are also made for computing an alternate neutron dose rate based on the Albert-Welton kernel.

The input data consist of a description of the source distribution and intensity by a number of point isotropic sources, a mathematical representation of the physical geometry with quadratic surfaces, and the tabulation of attenuation coefficients, buildup factors, and conversion factors.

There are several versions of QAD:

1. QAD-IV, the general-purpose basic QAD prototype, which estimates the uncollided gamma-ray flux, dose rate, and energy deposition at specified detector points, and also the fast-neutron dose,
2. QAD-P5, which incorporates a technique for interpolating the results of neutron calculations, has additional source description routines, and has an increased number of output options,
3. QAD-HD (ref. 185), which evaluates the heat deposition and temperature rise of the propellant and the dose to a crew during nuclear rocket reactor operation,
4. QAD-P5A, another version of QAD-P5, which includes a built-in library of gamma-ray attenuation coefficients, buildup factor coefficients, neutron removal cross sections, and neutron moments-method spectra coefficients,
5. QAD-INT, which calculates gamma-ray heating rates within a source region or in a semi-infinite region surrounding the source zone, as well as unscattered and total fluxes and dose rates,
6. QAD-V, which permits heating calculations with a two-dimensional integration scheme,
7. QAD-B, which is an expanded version of QAD-P5 with a simplified input format and a more detailed output format and which includes a data library of many of the required input parameters.

All codes in the QAD system are available in FORTRAN IV language for use on IBM-7090 and -7094 computers. QAD-P5 is in addition available in FORTRAN II for use on IBM-7090 and -7094 computers, and in FORTRAN IV for the IBM-360 and UNIVAC-1108 computers.

SDC (CCC-60). – The SDC code,[186] developed by Oak Ridge National Laboratory, is designed to calculate the gamma-ray shielding requirements for chemical processing, fabrication, or fuel handling facilities. It will handle 13 source geometries (point, line, disk, plane, slab, cylinder with shield at side, cylinder with shield at end, sphere, ring, rod cluster, skew line, annular cylinder with shield at side, and annular cylinder with shield at end) either unshielded or shielded by slab shields. Materials of construction for shield, cladding, or source volume may be selected from a list of 17. As many as 12 gamma-ray energy groups, covering an energy range of 0.10 to 10 MeV, with corresponding source strengths, may be used to describe the gamma-ray spectrum.

Integration of the basic exponential attenuation point kernel over the various geometries provides the uncollided gamma-ray flux in SDC. Speed is achieved by utilizing many of the integrations found in Rockwell.[52] Biological dose rate was obtained by multiplying this uncollided flux by the product of a flux-weighted buildup factor and a dose-conversion factor. Two major options in the code permit calculation of (1) required shield thickness when a dose-rate level is specified, or (2) dose rate when the shield thickness is given. Calculation of dose rates from unshielded sources as well as surface intensities for cylinders and spheres is also included.

Results from PHOEBE, an auxiliary routine,[187] are given in terms of photon-emission rates for each group, gamma-ray energy emission rates for each group, total gamma-ray emission rate, total gamma-ray energy emission rate, beta particle emission, total average beta-ray energy emission rate, and total energy release rate.

The code is available on the CDC-1604, IBM-7090/94 and -360 computers.

ISOSHLD (CCC-79). – ISOSHLD, a code[188-190] developed by Battelle Memorial Institute, Pacific Northwest Laboratories, calculates the decay gamma-ray and bremsstrahlung dose at the exterior of a shielded radiation source. The source may be one of a number of common geometric shapes. If the radiation source originates as one or a group of fission products produced under known irradiation conditions, then the strength of the source is also calculated. The code calculates shield region mass attenuation coefficients, buildup factors, and other basic data necessary to solve the specific problem.

ISOSHLD performs kernel integration for common geometric shapes. The "standard" point attenuation kernel (buildup factor times the exponential attenuation divided by the geometry factor) is numerically integrated over the source volume for 25 source energy groups. Buildup is considered to be characteristic of the last shield region (or a different specified region) but dependent on the total number of mean free paths from source to dose point, and is obtained by interpolation based on the effective atomic number in a table of point isotopic buildup factor data. Mixed mass attenuation coefficients are obtained from a library of basic data using code input material density specifications. The source strength may be specified (1) as the emissions from a selection of fission products irradiated under specific conditions, (2) as the curies of particular fission and/or activation products, or (3) as a number of photons per second of energy E specified by input. An exponential source distribution may be specified for those source geometries which are applicable. If the source originates in a combination of fission products and their daughters, these are calculated by a fission-product inventory procedure which runs through transmutation (decay chain) calculations for each fission product and daughter. A modification (ISOSHLD II)[191] adds the capability for calculating shielded dose rates from bremsstrahlung sources. This addition consists of routines for calculating the bremsstrahlung source spectra from the beta decay properties of the isotope(s) of interest. Bremsstrahlung photons per group for 25 energy groups (9 groups below 0.1 MeV have been added) are obtained by interpolation from tables of resolved spectra. This spectral mesh, for internal and external bremsstrahlung, is tabulated as a function of the following parameters: beta-emitting and stopping nuclides with atomic numbers of 10, 30, 50, 70, and 90; ratios of photon energy to beta endpoint energy for 25 intervals from 0.00375 to 1.0; beta endpoint energies at the intervals 0.1, 0.2, 0.5, 1, 2, and 4 MeV. Buildup factors for photon energies less than 0.1 MeV are interpolated in a table which contains data for 5 values of initial photon energy in the range 0.01 to 0.2 MeV, seven values of shield thickness in the range 1 to 20 mfp, and 6 atomic numbers in the range 13 to 92.

A second modification (ISOSHLD III) was made to include an updated photon probability library.[192,193]

The entire shielding problem is solved for most types of isotope shielding applications without reference to shielding handbooks for basic data. Versions of ISOSHLD are available for IBM-7090/94 and -360 computers and for the UNIVAC-1108 computer.

PLUME (CCC-99). – PLUME,[194] developed by Oak Ridge National Laboratory, makes estimates of certain internal and external radiation doses delivered to receptors exposed to a cloud of radioactive effluent for various periods of time and at various locations relative

to the point of emission (the stack at the site of a reactor accident). The internal dose considered is the thyroid dose due to the inhalation of iodine. The external doses are upper limits to the whole body doses to be expected from iodine and noble gases floating downward from the reactor site.

It is assumed that volatile fission products are released into a reactor containment volume via a reactor accident, that the fission products are mixed instantaneously with the building air, and that the homogeneous mixture is emitted to the atmosphere at a constant rate through a stack. The concentration of radioisotopes downwind is expressed in terms of the product of the "stack factor," which contains information on atmospheric dispersion, and a "source term" containing information on the rate of emission, decay, and dilution within the building. The atmospheric dispersion is estimated by the Gaussian plume formula corrected for ground reflection and the presence of a thermal inversion layer. Meteorological data are built into the program which allows the plume description for various stability conditions and wind velocities. The source terms available in the code allow for treatment of iodine isotopes (neglecting iodine daughters), treatment of noble gases with solid daughters removed by filtering, and treatment of noble gas daughters of iodine parents removed by filtering.

The internal dose is taken as that due to inhalation of iodine parents only and involves the evaluation of an expression which is the time integral of the concentration multiplied by appropriate factors. The external dose requires an integration of the time-integrated concentrations over the plume volume, with appropriate gamma-ray buildup factors being used. The program uses a Gauss-Hermite quadrature scheme on the y-integration and a Gauss-Legendre quadrature scheme on the x- and y-integrations.

PLUME is operational on the IBM-360/75 computers.

SPACETRAN (CCC-120). – SPACETRAN,[106] developed by Oak Ridge National Laboratory, is designed to calculate the energy-dependent total flux, or some proportional quantity such as kerma, due to the radiation leakage from the surface of a right-circular cylinder at detector positions located arbitrary distances from the surface. In two published versions, SPACETRAN I and SPACETRAN II, the assumption is made that the radiation emerging from the finite cylinder has no spatial dependence. In an unpublished version, SPACETRAN II, spatial dependence is allowed. The source input is the leakage current calculated by DOT.

SPACETRAN-I uses the surface angular fluxes calculated by the discrete ordinates S_n code, CCC-82/ANISN, as input. SPACETRAN-II assumes that the surface angular flux for all energies can be represented as a function $\cos^n\phi$, where ϕ is the angle between the surface outward normal and the radiation direction, and n is an integer specified by the user.

For both versions the energy group structure and the number and location of detectors are arbitrary. The flux (or a flux-dependent functional) for a given energy group at some detection point is computed by summing the contributions from each surface area element over the entire surface. The surface area elements are defined by input data.

SPACETRAN-I handles contributions either from a cylinder "end" or "side," so the total contribution must be obtained by adding the results of separate end and side runs. ANISN angular fluxes are specified for discrete directions. In general, the pathway between the detector and the contributing area will not exactly coincide with one of these discrete directions. In this case, the ANISN angular flux for the "closest" discrete direction is used to approximate the contribution to the detector.

SPACETRAN-II handles contributions from both the side and end of a cylinder in a single run. Since the assumed angular distribution is specified by a continuous function, it is not necessary to perform the angle selection described above.

For each detector specified, both versions compute the flux and a response proportional to the flux in each energy group and also compute the sum of these quantities over all energy groups.

The code is operational on the IBM-360 computer.

KAP-V (CCC-94). – The KAP-V code,[195–197] developed by Westinghouse Astronuclear Laboratory, Pittsburgh, Pennsylvania, and NASA George C. Marshall Space Flight Center, Huntsville, Alabama, is part of a system of codes for shield design called "Synthesis of Calculational Methods for the Design and Analysis of Radiation Shields for Nuclear Rocket Systems." The codes in this system are packaged by RSIC as CCC-94 through CCC-98. The programs in CCC-94, CCC-95, and CCC-96 are termed by the originators as the "early" design method.

The KAP-V code calculates neutron and/or gamma radiation levels at detector points located within or outside a complex radiation source geometry describable by a combination of quadratic surfaces. A variety of options are available for describing cylindrical, spherical, disc, line, or point sources or source distributions in complex geometries. The output can be flux, dose, or heating rate.

The attenuation function, or kernel, for gamma rays employs exponential attenuation with a buildup factor. Three optional fast-neutron attenuation functions are included: (1) a modified Albert-Welton function for calculating fast-neutron dose rate using removal cross sections, (2) a bivariant polynomial expression for computing neutron spectra using infinite-medium-moments data, and (3) a monovariant polynomial expression for computing neutron spectra using infinite-medium moments data.

The KAP-V is operational on the IBM-7090/94 computers.

3B.4. PROGRAMS BASED ON SPINNEY REMOVAL-DIFFUSION METHOD

MAC and MAC-RAD (CCC-22). – The MAC code,[132,198] originally developed by Hanford Atomic Products Operation and placed with RSIC by Pacific Northwest Laboratory, Battelle-Northwest, calculates the neutron energy spectrum and dose rate and the gamma-ray dose rate as a function of distance through large reactor shields of concrete or hydrogenous material in slab geometry. The results are given as multigroup neutron fluxes for as many as 35 energy groups and as neutron dose rates, approximate neutron spectra, total gamma-ray dose rates (with a breakdown of the contribution from each region in the shield), and approximate gamma-ray spectra.

The code is based on the Spinney method, which uses a high-energy kernel as the source of neutrons in a multigroup diffusion procedure. This kernel is proportional to the energy-dependent removal flux, which is calculated similarly to the uncollided flux except for the use of a removal cross section equal in magnitude to the usual transport cross section. The removal flux, divided into 18 groups, is calculated for neutrons above 0.5 MeV.

The diffusion equation is reduced to a system of three first-order differential equations which are numerically integrated. In the MAC code the boundary conditions are the diffusion flux at the core-shield interface and a zero incoming flux at the outside edge of the shield. In the MAC-RAD code,[133,199] originated by Allgemeine Elektricitats-Gasellschaft, Kernenergie-anlagen at Frankfurt, Germany, the removal flux is added to the diffusion flux at the core-shield interface to obtain the input boundary value. In the first group the entire flux is removal flux. Secondary gamma-ray sources are discontinuous at boundaries.

In both codes the gamma-ray dose rate is calculated for seven source energy groups by using buildup factor kernels.

MAC and MAC-RAD are available in FORTRAN II language for use on the IBM-7090 computer. MAC-RAD is also operational on the IBM-360 and CDC-3600 computers.

NRN (CCC-54). – NRN,[134,135,200,201] a system of codes developed by Aktiebolaget Atomenergi, Stockholm, Sweden, is built around the Spinney method of combining high-energy exponential attenuation with low-energy diffusion. The high-energy exponentially attenuating flux is broken into several energy groups, each of which requires removal cross sections.

Given a distribution of fissions (e.g., power distribution) in certain allowed geometric regions, NRN solves for neutron flux densities, absorption rates (from which secondary gamma-ray source rates may be determined), dose rates, and energy deposit rates (by energy groups) in primary knock-on atoms. Two of its auxiliary routines, REBOX and REMC, can be adapted to compute gamma-ray dose rates from gamma-ray sources in the central region (core).

The routine NECO computes all the required macroscopic quantities, including removal cross sections, from the microscopic quantities and the material compositions. The calculation of removal cross sections is a unique feature of NRN.

The exponential attenuation of the fast group fluxes (removal fluxes) is carried out by the REBOX routine if the source region is a parallelepiped or a large cylinder, and by the REMC routine if the source region is a sphere or a small cylinder. The integration over the source volume is carried out by a mesh-sum procedure in REBOX and by a Monte Carlo procedure in REMC.

NEDI, a diffusion routine, uses as sources the removal fluxes in the shield region computed by REBOX or REMC. Since the geometry of NEDI is limited to multiregion infinite slabs, infinite cylinders, and spheres, there is a geometric inconsistency, except for the sphere, with REBOX and REMC. This is to be interpreted as an approximation, not an error. NEDI further provides for transverse bucklings in the slab and cylindrical cases in order to estimate the effect of truncating the infinite systems. NEDI solves the diffusion equation by preserving the form $\nabla \cdot D \nabla \Phi$, which would allow the cross sections within a region to be continuously varied, although no such provision for use of a spatially dependent D has actually been included.

The specification of reasonable external boundary conditions in the shield region is relatively simple, but the specification of reasonable internal boundary conditions is very difficult. If a significant part of the final answer depends heavily upon the diffusion current or flux (rather than on the removal current or flux) at the

interior shield boundary, this program should be used only with great circumspection.

NRN is available in FORTRAN IV and MAP languages for use on IBM-7090 and -7044 and the CDC-3600 computers.

COMPRASH (CCC-72). – COMPRASH[131,202] is the latest one-dimensional code made available in a series of programs developed by the Shielding Groups of the Atomic Energy Research Establishment at Harwell for calculating fast-neutron spectra, thermal-neutron flux densities, and secondary gamma-ray dose rates for reactor shields in slab geometry. It uses the two-step Spinney removal-diffusion method of calculating neutron transport. The basic assumption is that the penetrating component from a point source can be calculated by a kernel given by

$$\Phi_0(E,R) = \frac{S f(E)\, e^{-\Sigma_r(E)R}}{4\pi R^2} \quad ,$$

where

$\Phi_0(E,R)$ = removal flux density,

$f(E)$ = fission neutron spectrum,

S = source normalization,

$\Sigma_r(E)$ = energy-dependent removal cross section,

R = distance from source.

The removal source function

$$S(R,E) = \Sigma_r(E)\, \Phi_0(E,R)$$

is then made the source term in a conventional multigroup age-diffusion calculation to calculate the diffusing neutron spectra, including a thermal-neutron group.

The value of the removal cross section is taken to be the usual transport cross section, an assumption that is justified by the remarkable success of the model in predicting the thermal-neutron flux densities measured in bulk concrete shields.

The secondary gamma-ray transport is calculated with the use of an analytic form of the buildup factor.

COMPRASH is written in FORTRAN II and FAP languages for use on the IBM-7090 computer and is operational on the CDC-3600 computer.

SABINE (CCC-121). – SABINE,[136,203] developed by the EURATOM Joint Nuclear Research Center, Ispra, Italy, determines the energy-dependent neutron flux and gamma-ray flux-dependent quantities as functions of distance through a reactor shield. The neutron source is a fission source arbitrarily distributed inside the core. The gamma-ray source may include fission and fission-product gamma rays in the core, and neutron-capture gamma rays in the core and shield. One-dimensional slab, spherical, and cylindrical source and shield regions may be treated in various combinations.

The removal-diffusion method has been applied to calculate neutron fluxes. The gamma-ray dose is the product of the uncollided dose times a region-dependent buildup factor, which is interpolated from a table of values.

Other quantities calculated include neutron response, gamma-ray dose and energy deposition. Particular attention has been paid to the coupling of the removal bands to the diffusion groups.

The code is operational on the IBM-360 computer.

KDLIBE (CCC-124). – KDLIBE,[204,205] developed by the General Electric Company, Nuclear Systems Programs, Cincinnati, Ohio, is a shield-design system composed of nine separate codes and a data library. The nine codes are:

1. QADRD – a modified QAD kernel code designed to compute uncollided or removal fluxes in three dimensions for up to 30 energy groups at specified receiver points in a source-shield assembly. The removal fluxes are stored on tape, disks, or cards for later use.
2. RAMP – a data processor to combine the multigroup removal neutron flux from QADRD with multigroup scattering cross sections to produce source terms for input to the GEORGE multigroup diffusion code.
3. GEORGE – a one-dimensional neutron diffusion code which can run in either of two modes: (1) normal mode (space-independent buckling) with continuous slowing down and (2) transverse buckling mode. The code has a 20-group structure which includes one thermal-neutron group.
4. GAMMIX – a gamma-ray production cross-section processor which produces group macroscopic composition cross sections for REORG.
5. REORG – a data processor to combine diffusion fluxes from GEORGE, removal fluxes from QADRD, and gamma-ray production cross sections from GAMMIX to produce gamma-ray sources for QADRR.
6. QADRR – a modified QAD kernel code for general use or for calculating gamma-ray transport from sources produced by REORG. Modified Albert-

Welton fast-neutron kernels, buildup factors (including the Kalos formula), and other data are used.

7. SURF – an uncollided and single-scattering code for analysis of thin structures.
8. ZIP-III – a one-dimensional cylindrical neutron diffusion code with a matched savings algorithm limited to three diffusion groups for fast survey or parametric calculations.
9. UPDONC – a data processor which prepares, duplicates, updates, adds, deletes, punches, graphs, and lists data on the nuclear data tape used by GEORGE and ZIP-III.

The removal cross sections are similar to those of NRN.

The original version of the KDLIBE system was for the GE-635 computer.

ATTOW (CCC-132). ATTOW,[206] developed by the United Kingdom Atomic Energy Authority, Risley, is a shielding code programmed in FORTRAN IV for the IBM-7090 computer. It solves the multigroup diffusion equations in two dimensions (r-z or x-y geometry) for nonmultiplying media. Any number of groups is allowed but neutron transfer is allowed only from higher groups to lower groups. There may be up to 100 X 100 mesh points over a rectangle within which materials may be mapped out as required. Any distribution of neutron sources can be specified, derived if desired from the built-in removal program. Output includes flux prints, neutron currents and detector activations.

ATTOW was designed specifically as a two-dimensional shielding program with special facilities for source problems. As compared with previous codes, big economies in computing time were to be expected if all effects of a particular group on higher-energy groups were ignored: thus fluxes could be calculated in sequence, from top group downwards, without the need of an outer iteration round the groups. In addition, the total number of groups acceptable would be limited by running time rather than machine capacity. The only limitation this was expected to introduce in practice was that, if a core region were included, fission neutrons would have to be introduced in the form of a source distribution previously evaluated with some other program.

The program expresses the diffusion equation in finite-difference form and solves it by iteration using accelerated successive line over-relaxation. It has been found that convergence is usually satisfactory over a range of about 12 decades. Problems with a greater range of attenuation often reach a solution, but sometimes fail to converge.

Removal cross sections are input to the removal program, which allows the user control of the removal assumptions. The full energy transfer matrix is also assumed for the diffusion treatment.

The original version of ATTOW is for the IBM-7090 computer.

Appendix 3C. Derivation of Time-Dependent Discrete Ordinates Equations

The derivation of the discrete ordinates equations in Section 3.3 is extended here to include time dependence. The formal starting point is the general time-dependent integrodifferential form of the Boltzmann transport equation, Eq. 3.1, rather than the steady-state form, Eq. 3.2. This equation includes an additional term, the storage term, and considers the full seven-dimensional phase space $(\bar{r},E,\bar{\Omega},t)$. The conservative one-dimensional form of Eq. 3.1 can be written as

$$\frac{1}{v}\frac{\partial}{\partial t}\Phi(r,E,\mu,t)+\frac{\mu}{r^2}\frac{\partial}{\partial r}\left[r^2\Phi(r,E,\mu,t)\right]+\frac{1}{r}\frac{\partial}{\partial \mu}\left[(1-\mu^2)\,\Phi(r,E,\mu,t)\right]$$

$$+\Sigma_t(r,E)\,\Phi(r,E,\mu,t)=S(r,E,\mu,t)+\int_0^{\infty}\int_{-1}^{+1}\Sigma_s(r,E'\rightarrow E,\mu_0)\,\Phi(r,E',\mu',t)\,dE'\,d\mu'. \qquad \text{(C1)}$$

The differential phase space cell is given by $4\pi r^2\,dr\,dE\,d\mu\,dt$ and the finite-difference cell becomes $V_I\,\Delta E_G\,\Delta\mu_D\,\Delta t_Q$.* Following the same formal procedures used in Section 3.1, the following integral operator is applied to each term of Eq. C1:

$$\text{Integral Operator}=\int_{r\epsilon V_I}\int_{E\epsilon\Delta E_G}\int_{\mu\epsilon\Delta\mu_D}\int_{t\epsilon\Delta t_Q}4\pi r^2\,dr\,dE\,d\mu\,dt\,. \qquad \text{(C2)}$$

The first application is to the storage term:

$$\int_{r\epsilon V_I}\int_{E\epsilon\Delta E_G}\int_{\mu\epsilon\Delta\mu_D}\int_{t\epsilon\Delta t_Q}\left[\frac{1}{v}\frac{\partial}{\partial t}\Phi(r,E,\mu,t)\right]4\pi r^2\,dr\,dE\,d\mu\,dt\,,$$

which can be rewritten as

$$4\pi\int_{r\epsilon V_I}\int_{\mu\epsilon\Delta\mu_D}\int_{t\epsilon\Delta t_Q}\frac{\partial}{\partial t}\left[\int_{E\epsilon\Delta E_G}\frac{1}{v}\Phi(r,E,\mu,t)\,dE\right]r^2\,dr\,d\mu\,dt\,. \qquad \text{(C3)}$$

The particle speed averaged over the Gth group is defined as

$$\frac{1}{v_G}\equiv\frac{\int_{E\epsilon\Delta E_G}\frac{1}{v}\Phi(r,E,\mu,t)\,dE}{\Phi_G(r,\mu,t)}, \qquad \text{(C4)}$$

*Following the convention established in Sec. 3.3, the subscript Q will refer to the Qth time interval and subscripts $q+1$ and q will denote the endpoint values of the Qth interval; i.e., $\Delta t_Q = t_{q+1} - t_q$.

where

$$\Phi_G(r,\mu,t) = \int_{E\epsilon\Delta E_G} \Phi(r,E,\mu,t)\, dE\,,$$

and Eq. C3 becomes

$$\frac{4\pi}{\nu_G} \int_{r\epsilon V_I} \int_{\mu\epsilon\Delta\mu_D} \int_{t\epsilon\Delta t_Q} \frac{\partial}{\partial t} \Phi_G(r,\mu,t)\, r^2\, dr\, d\mu\, dt\,. \tag{C5}$$

Using the mean value theorem (see Section 3.3, Eq. 3.24) for the evaluation of the r and μ integrals, Eq. C5 becomes

$$\frac{V_I\, \Delta\mu_D}{\nu_G} \int_{t\epsilon\Delta t_Q} \frac{\partial}{\partial t} \Phi_{I,G,D}(t)\, dt\,. \tag{C6}$$

The remaining integration over the time variable is accomplished in the following manner:

$$\begin{aligned} \frac{V_I\, \Delta\mu_D}{\nu_G} \int_{t\epsilon\Delta t_Q} \frac{\partial}{\partial t} \Phi_{I,G,D}(t)\, dt &= \frac{V_I\, \Delta\mu_D}{\nu_G} \int_{t\epsilon\Delta t_Q} d\Phi_{I,G,D}(t) \\ &= \frac{V_I\, \Delta\mu_D}{\nu_G} \left[\Phi_{I,G,D,q+1} - \Phi_{I,G,D,q}\right]\,, \end{aligned} \tag{C7}$$

where

$$\Phi_{I,G,D,q+1} \equiv \Phi_{I,G,D}(t_{q+1}) \text{ and } \Phi_{I,G,D,q} \equiv \Phi_{I,G,D}(t_q)\,.$$

The effect of applying the integral operator to all the other terms in Eq. C1 is the same and thus will be illustrated by considering only the source term:

$$\int_{r\epsilon V_I} \int_{E\epsilon\Delta E_G} \int_{\mu\epsilon\Delta\mu_D} \int_{t\epsilon\Delta t_Q} S(r,E,\mu,t)\, 4\pi r^2\, dr\, dE\, d\mu\, dt\,. \tag{C8}$$

Evaluation of the energy integral yields

$$4\pi \int_{r\epsilon V_I} \int_{\mu\epsilon\Delta\mu_D} \int_{t\epsilon\Delta t_Q} S_G(r,\mu,t)\, r^2\, dr\, d\mu\, dt\,,$$

where

$$S_G(r,\mu,t) \equiv \int_{E\epsilon\Delta E_G} S(r,E,\mu,t)\, dE\,.$$

The remaining integrations are performed using the mean value theorem with the result:

$$V_I\, \Delta\mu_D\, \Delta t_Q\, S_{I,G,D,Q}\,, \tag{C9}$$

where

$$S_{I,G,D,Q} \equiv S_G(\bar{r}_I, \bar{\mu}_D, \bar{t}_Q) .$$

Therefore the convective, removal, and inscattering terms are modified by adding the centered subscript (Q) to all discrete ordinate fluxes and the time increment Δt_Q occurs as a common factor. For example, the modified removal term becomes

$$V_I \, \Delta\mu_D \, \Delta t_Q \, \Sigma^t_{IG} \, \Phi_{I,G,D,Q} . \tag{C10}$$

Finally, the discrete ordinates equation, Eq. 3.59, is modified by including the discrete ordinates storage term, Eq. C7, divided by ($\Delta\mu_D \, \Delta t_Q$) and by adding the centered subscript (Q) to all other discrete ordinates fluxes and to the source term:

$$\frac{V_I}{v_G \, \Delta t_Q}(\Phi_{I,G,D,q+1} - \Phi_{I,G,D,q}) + \bar{\mu}_D(A_{i+1} \, \Phi_{i+1,G,D,Q} - A_i \, \Phi_{i,G,D,Q})$$

$$+ \frac{1}{\Delta\mu_D}(B_{I,d+1} \, \Phi_{I,G,d+1,Q} - B_{I,d} \, \Phi_{I,G,d,Q}) + V_I \, \Sigma^t_{I,G} \, \Phi_{I,G,D,Q}$$

$$= V_I \, S_{I,G,D,Q} + \frac{V_I}{2} \sum_{n=0}^{N} P_n(\bar{\mu}_D) \sum_{G'=1}^{NQG} \Sigma^{n,I(\mathrm{mod})}_{G' \to G} \sum_{D'=1}^{NQA} \Phi_{I,G',D',Q} \, P_n(\bar{\mu}_{D'}) \, \Delta\mu_{D'} . \tag{C11}$$

Noting that the fixed source and inscattering terms effectively involve only centered subscripts, the single source term $S'_{I,G,D,Q}$ is introduced in their place, and Eq. C11 can be rewritten as

$$\frac{V_I}{v_G \, \Delta t_Q}(\Phi_{I,G,D,q+1} - \Phi_{I,G,D,q}) + \bar{\mu}_D(A_{i+1} \, \Phi_{i+1,G,D,Q} - A_i \, \Phi_{i,G,D,Q})$$

$$+ \frac{1}{\Delta\mu_D}(B_{I,d+1} \, \Phi_{I,G,d+1,Q} - B_{I,d} \, \Phi_{I,G,d,Q})$$

$$+ V_I \, \Sigma^t_{I,G} \, \Phi_{I,G,D,Q} = V_I \, S'_{I,G,D,Q} . \tag{C12}$$

The time-dependent discrete ordinates equation, Eq. C12, contains both centered and endpoint (space, direction, time) subscripts. Therefore (for the reasons presented in Sec. 3.3) three additional equations which relate the centered and endpoint fluxes are required. For reasons of stability and generality, the weighted diamond difference equations are used:[158]

$$\Phi_{I,G,D,Q} = A \, \Phi_{i+1,G,D,Q} + (1 - A) \, \Phi_{i,G,D,Q} , \quad \mu > 0 , \tag{C13a}$$

or

$$\Phi_{I,G,D,Q} = (1 - A) \, \Phi_{i+1,G,D,Q} + A \, \Phi_{i,G,D,Q} , \quad \mu < 0 , \tag{C13b}$$

$$\Phi_{I,G,D,Q} = B \, \Phi_{I,G,d+1,Q} + (1 - B) \, \Phi_{I,G,d,Q} , \tag{C14}$$

$$\Phi_{I,G,D,Q} = C \, \Phi_{I,G,D,q+1} + (1 - C) \, \Phi_{I,G,D,q} , \tag{C15}$$

where A, B, and C will assume values such that positivity is assured and accuracy is enhanced. This deviates significantly from the steady-state procedure wherein $A = B = \frac{1}{2}$ (ordinary diamond difference) were used almost exclusively except for correction of negative fluxes when $A = B = 1$ (step diamond difference).

Optimum values for A, B, and C are not obvious; however acceptable approximations are suggested by the following procedures. Equations C14 and C15 are substituted into Eq. C12, the resultant equation being an explicit expression for $\Phi_{i+1,G,D,Q}$:

$$\Phi_{i+1,G,D,Q} = \frac{S'_{I,G,D,Q}\, V_I + C_1\, \Phi_{I,G,D,q} + C_3\, \Phi_{I,G,d,Q} + [\bar{\mu}_D\, A_i - (1-A)\, D_2]\, \Phi_{i,G,D,Q}}{A\, D_0} . \tag{C16}$$

Similarly, Eqs. C13*a* and C15 are substituted into Eq. C12 to obtain an explicit expression for $\Phi_{I,G,d+1,Q}$:

$$\Phi_{I,G,d+1,Q} = \frac{S'_{I,G,D,Q}\, V_I + C_1\, \Phi_{I,G,D,q} + C_2\, \Phi_{i,G,D,Q} + [B_{I,d}/\Delta\mu_D - (1-B)\, D_3]\, \Phi_{I,G,d,Q}}{B\, D_0} . \tag{C17}$$

Also, Eqs. C13*a* and C14 are substituted into Eq. C12, yielding an explicit expression for $\Phi_{I,G,D,q+1}$:

$$\Phi_{I,G,D,q+1} = \frac{S'_{I,G,D,Q}\, V_I + C_2\, \Phi_{i,G,D,Q} + C_3\, \Phi_{I,G,d,Q} + [V_I/v_G \Delta t_Q - (1-C)\, D_1]\, \Phi_{I,G,D,q}}{C\, D_0} , \tag{C18}$$

where

$$C_1 = V_I/v_G\, \Delta T_Q\, C ,$$
$$C_2 = \bar{\mu}_D\, [A_i + A_{i-1}\, (1/A - 1)] ,$$
$$C_3 = B_{I,d}/\Delta\mu_D + B_{I,d+1}\, (1/A - 1)/\Delta\mu_D ,$$
$$D_0 = \Sigma^t_{I,G}\, V_I + C_1 + \bar{\mu}_D\, A_{i+1}/A + B_{I,d+1}/\Delta\mu_D\, B ,$$
$$D_1 = D_0 - C_1 ,$$
$$D_2 = D_0 - \bar{\mu}_D\, A_{i+1}/A ,$$
$$D_3 = D_0 - B_{I,d+1}/\Delta\mu_D B .$$

If the previously calculated fluxes and the source term (which includes fixed and inscatter sources) are positive, then all but the bracketed terms in the numerators of Eqs. C16, C17, and C18 are always positive. Therefore to ensure positivity of the bracketed terms and thereby to ensure that the newly calculated fluxes are always positive, the following inequalities must be true:

$$(1-A) < \bar{\mu}_D\, A_i/(\Sigma^t_{I,G}\, V_I + V_I/v_G\, \Delta t_Q\, C + B_{I,d+1}/\Delta\mu_D\, B) , \tag{C19}$$

$$(1-B) < B_{I,d}/\Delta\mu_D\, (\Sigma^t_{I,G}\, V_I + V_I/v_G\, \Delta t_Q\, C + \bar{\mu}_D\, A_{i+1}/A) , \tag{C20}$$

$$(1-C) < V_I/v_G\, \Delta t_Q\, (\Sigma^t_{I,G}\, V_I + \bar{\mu}_D\, A_{i+1}/A + B_{I,d+1}/\Delta\mu_D\, B) . \tag{C21}$$

Experience with time-dependent discrete ordinates calculations is limited; however two sets of approximate expressions* for A, B, and C have been used with some success. The first set is due to Lathrop[158] and is given as follows:

$$(1-A) = \bar{\mu}_D\, A_i/(\Sigma^t_{I,G}\, V_I + 2V_I/v_G\, \Delta t_Q + 2B_{I,d+1}/\Delta\mu_D) , \tag{C22}$$

*These expressions can also be interpreted as defining the relationships that must exist between the V_I, $\Delta\mu_D$, and Δt_Q for given values of A, B, and C.

$$(1-B) = B_{I,d}/\Delta\mu_D(\Sigma^t_{I,G}\ V_I + 2V_I/v_G\ \Delta t_Q + 2\bar{\mu}_D\ A_{i+1})\ , \tag{C23}$$

$$(1-C) = V_I/v_G\ \Delta t_Q(\Sigma^t_{I,G}\ V_I + 2\bar{\mu}_D\ A_{i+1} + 2B_{I,d+1}/\Delta\mu_D)\ . \tag{C24}$$

Lathrop satisfied the inequalities defined by Eqs. C19–C21 by setting $A = B = C = \frac{1}{2}$ everywhere except within the factors $(1-A)$, $(1-B)$, and $(1-C)$. Based on considerations of accuracy, it is desirable for the constants A, B, and C to be as close to 0.5 as possible (ordinary diamond difference). However using Eqs. C22–C24 usually leads to values for A, B, and C which are equal to or very nearly 1.0. If the positivity of the entire numerator is considered in defining the inequalities, the constants A, B, and C so calculated may result in the numerators of Eqs. C16–C18 being positive but very (vanishingly) small. This condition results in an unstable phenomenon similar to diamond difference breakdown (described in Sec. 3.3).

To avoid the aforementioned instability and to calculate values for the constants closer to 0.5, inequality conditions intermediate to those already considered are required. Engle[207] suggests that the combination of the source term and the bracketed term which occur in the numerators of Eqs. C16–C18 be always positive. This leads to the second and preferred set of equations:

$$(1-A) = (\bar{\mu}_D\ A_i + S'_{I,G,D,Q}\ V_I/\Phi_{i,G,D,q})/(\Sigma^t_{I,G}\ V_I + 2V_i/v_G\ \Delta t_Q + 2B_{I,d+1}/\Delta\mu_D)\ , \tag{C25}$$

$$(1-B) = (B_{I,d}/\Delta\mu_D + S'_{I,G,D,Q}\ V_I/\Phi_{I,G,d,Q})/(\Sigma^t_{I,G}\ V_I + 2V_I/v_G\ \Delta t_Q + 2\bar{\mu}_D\ A_{i+1})\ , \tag{C26}$$

$$(1-C) = (V_I/v_G\Delta t_Q + S'_{I,G,D,Q}\ V_I/\Phi_{I,G,D,q})/(\Sigma^t_{I,G}\ V_I + 2\bar{\mu}_D\ A_{i+1} + 2B_{I,d+1}/\Delta\mu_D)\ . \tag{C27}$$

An explicit expression for the centered flux $\Phi_{I,G,D,Q}$ in terms of the endpoint fluxes $\Phi_{i,G,D,Q}$, $\Phi_{I,G,d,Q}$, and $\Phi_{I,G,D,q}$ is obtained by substituting the diamond difference equations, Eq. C13*a* ($\mu > 0$) or Eq. C13*b* ($\mu < 0$),* Eq. C14 and Eq. C15 into Eq. C12, yielding

$$\Phi_{I,G,D,Q} = \frac{S'_{I,G,D,Q}\ V_I + (V_I/v_G\ \Delta t_Q\ C)\ \Phi_{I,G,D,q} + \bar{\mu}_D\left[A_i + \left(\frac{1}{A} - 1\right) A_{i+1}\right]\ \Phi_{i,G,D,Q} + \frac{1}{\Delta\mu_D}\left[B_{i,d} + \left(\frac{1}{B} - 1\right) B_{I,d+1}\right]\Phi_{I,G,d,Q}}{\Sigma^t_{I,G}\ V_I + V_I/v_G\ \Delta t_Q\ C + \bar{\mu}_D\ A_{i+1}/A + B_{I,d+1}/\Delta\mu_D\ B}\ . \tag{C28}$$

Equation C28 in addition to the diamond difference equations, Eqs. C13*a* ($\mu > 0$), C14, and C15, is required for the numerical solution of a typical time-dependent problem. Given the endpoint fluxes $\Phi_{i,G,D,Q}$, $\Phi_{I,G,d,Q}$, and $\Phi_{I,G,D,q}$, Eq. C28 is solved for the centered flux $\Phi_{I,G,D,Q}$, and the extrapolated fluxes $\Phi_{i+1,G,D,Q}$, $\Phi_{I,G,d+1,Q}$, and $\Phi_{I,G,D,q+1}$ are calculated by Eq. C13*a* ($\mu > 0$) or C13*b* ($\mu < 0$), C14, and C15 respectively. The constants A, B, and C are determined from Eqs. C22–C24 or Eqs. C25–C27.

The time-dependent problem is "initial valued" with respect to the time variable, and the calculation begins at zero or some initial time and proceeds sequentially through all the time increments in a single sweep. For a given energy group and time increment, the spatial and angle sweeps are converged before the newly calculated centered group fluxes are extrapolated to the next point in time and the energy sweep continued to the next lower energy group – and so on. It is noted that essentially a complete space-energy-angle problem (similar to the steady-state analysis described in Sec. 3.3) is solved for each time interval. However the time absorption effect significantly reduces the number of inner iterations required in a single time step. Also for many problems the projection of fluxes from the previous time step provides a good flux guess for the next time step and reduces the total running time to almost that for a steady-state problem.

---

*Equation C28 is derived for the ($\mu > 0$) i to $i+1$ spatial mesh sweep. For $\mu < 0$, Eq. C28 is modified by interchanging the i and $i+1$ subscripts and replacing $\bar{\mu}_D$ by $|\bar{\mu}_D|$.

Appendix 3D. Coefficients for Various Formulas Representing Gamma-Ray Buildup Factors

This appendix consists of tabulations of coefficients for various formulas representing gamma-ray buildup factors (see Section 3.8.1) for the most common gamma-ray shielding materials. Tables 3D.1 and 3D.2 give coefficients for the Taylor and polynomial forms as determined by Buscaglione and Manzini,[64] and Tables 3D.3 and 3D.4 give coefficients for the linear, quadratic, and Berger forms as determined by Trubey.[67] In all cases, the coefficients for the elements are based on the buildup factors calculated by Goldstein and Wilkins,[14] and those for the four different concretes are based on the buildup factors reported by Walker and Grotenhuis,[51] which in turn are based on the Goldstein-Wilkins data. (An effective atomic number for the concrete mixture is determined, and its buildup factor is then that of the equivalent element.)

Table 3D.5, which has been added in this revised version of the chapter, gives Berger formula coefficients for three of the concretes plus four other materials (air, sand, wood, and LiH). These coefficients, determined by Trubey,[215] differ from those in Tables 3D.3 and 3D.4 in that they are based on fits to buildup factors calculated specifically for these materials.[54-57]

Table 3D.1. Coefficients for the Taylor Form of the Dose Buildup Factor[a]

Material	E (MeV)	A	$-\alpha_1$	α_2	Maximum Deviation (%)[b]
Water	0.5	100.845	0.12687	−0.10925	−27.4, $\mu x = 10$
	1	19.601	0.09037	−0.02522	−10.8, $\mu x = 10$
	2	12.612	0.05320	0.01932	4.2, $\mu x = 1$
	3	11.110	0.03550	0.03206	1.7, $\mu x = 1$
	4	11.163	0.02543	0.03025	0.8, $\mu x = 20$
	6	8.385	0.01820	0.04164	−0.5, $\mu x = 2$
	8	4.635	0.02633	0.07097	0.6, $\mu x = 7$
	10	3.545	0.02991	0.08717	−0.7, $\mu x = 1$
Aluminum	0.5	38.911	0.10015	−0.06312	−12.2, $\mu x = 10$
	1	28.782	0.06820	−0.02973	−8.6, $\mu x = 10$
	2	16.981	0.04588	0.00271	−5.2, $\mu x = 10$
	3	10.583	0.04066	0.02514	−2.5, $\mu x = 10$
	4	7.526	0.03973	0.03860	1.8, $\mu x = 20$
	6	5.713	0.03934	0.04347	1.6, $\mu x = 20$
	8	4.716	0.03837	0.04431	−1.3, $\mu x = 15$
	10	3.999	0.03900	0.04130	1.2, $\mu x = 20$
Barytes concrete[c]	0.5	33.026	0.06129	−0.02883	7.5, $\mu x = 2$
	1	23.014	0.06255	−0.02217	8.9, $\mu x = 20$
	2	9.350	0.05700	0.03850	9.0, $\mu x = 2$
	3	6.269	0.06064	0.04440	4.8, $\mu x = 20$
	4	4.730	0.06500	0.05883	4.8, $\mu x = 2$
	6	3.240	0.08000	0.06407	5.0, $\mu x = 2$
	8	2.167	0.09514	0.07857	1.3, $\mu x = 20$
	10	1.433	0.11201	0.13021	3.2, $\mu x = 20$
Ferrophosphorous concrete[c]	0.5	61.341	0.07292	−0.05265	11.0, $\mu x = 2$
	1	46.087	0.05202	−0.02845	10.3, $\mu x = 2$
	2	14.790	0.04720	0.00867	3.0, $\mu x = 2$
	3	10.399	0.04290	0.02211	2.6, $\mu x = 20$
	4	6.240	0.05280	0.03765	1.7, $\mu x = 2$
	6	4.425	0.05880	0.04262	−1.0, $\mu x = 2$
	8	3.000	0.06750	0.05730	0.8, $\mu x = 4$
	10	2.279	0.07575	0.06438	0.4, $\mu x = 6$
Ordinary concrete[c]	0.5[d]	38.225	0.14824	−0.10579	−7.5, $\mu x = 4$
	1	25.507	0.07230	−0.01843	11.1, $\mu x = 2$
	2	18.089	0.04250	0.00849	4.9, $\mu x = 2$
	3	13.640	0.03200	0.02022	4.3, $\mu x = 2$
	4	11.460	0.02600	0.02450	−5.1, $\mu x = 2$
	6	10.781	0.01520	0.02925	−2.7, $\mu x = 2$
	8	8.972	0.01300	0.02979	−3.7, $\mu x = 2$
	10	4.015	0.02880	0.06844	−2.2, $\mu x = 2$
Magnetite concrete[c]	0.5	75.471	0.07479	−0.05534	15.9, $\mu x = 2$
	1	49.916	0.05195	−0.02796	11.5, $\mu x = 2$
	2	14.260	0.04692	0.01531	4.0, $\mu x = 2$
	3	8.160	0.04700	0.04590	5.0, $\mu x = 2$
	4	5.580	0.05200	0.05728	2.7, $\mu x = 2$
	6	3.437	0.06000	0.11520	4.3, $\mu x = 4$
	8	2.480	0.06645	0.14002	4.0, $\mu x = 20$
	10	1.743	0.08082	0.27209	5.3, $\mu x = 20$

Table 3D.1 (continued)

Material	E (MeV)	A	$-\alpha_1$	α_2	Maximum Deviation (%)[b]
Iron	0.5	31.379	0.06842	−0.03742	−6.5, $\mu x = 10$
	1	24.957	0.06086	−0.02463	−6.4, $\mu x = 10$
	2	17.622	0.04627	−0.00526	4.0, $\mu x = 2$
	3	13.218	0.04431	−0.00087	−3.0, $\mu x = 10$
	4	9.624	0.04698	0.00175	−2.7, $\mu x = 10$
	6	5.867	0.06150	−0.00186	2.1, $\mu x = 20$
	8	3.243	0.07500	0.02123	3.8, $\mu x = 4$
	10	1.747	0.09900	0.06627	3.7, $\mu x = 2$
Lead	0.5[d]	1.677	0.03084	0.30941	−0.8, $\mu x = 10$
	1	2.984	0.03503	0.13486	−1.0, $\mu x = 1$
	2	5.421	0.03482	0.04379	−0.6, $\mu x = 1$
	3	5.580	0.05422	0.00611	1.3, $\mu x = 4$
	4	3.897	0.08468	−0.02383	1.4, $\mu x = 20$
	6	0.926	0.17860	−0.04635	1.3, $\mu x = 20$
	8	0.368	0.23691	−0.05684	1.8, $\mu x = 15$
	10	0.311	0.24024	−0.02783	−0.5, $\mu x = 1$
Tin	0.5[d]	11.440	0.01800	0.03187	−1.6, $\mu x = 1$
	1	11.426	0.04266	0.01606	−2.6, $\mu x = 10$
	2	8.783	0.05349	0.01505	−2.8, $\mu x = 10$
	3	5.400	0.07440	0.02080	4.3, $\mu x = 20$
	4	3.496	0.09517	0.02598	−3.9, $\mu x = 10$
	6	2.005	0.13733	−0.01501	−2.8, $\mu x = 10$
	8	1.101	0.17288	−0.01787	−3.4, $\mu x = 15$
	10	0.708	0.19200	0.01552	2.6, $\mu x = 15$
Tungsten	0.5[d]	2.655	0.01740	0.11340	−4.9, $\mu x = 2$
	1[d]	3.234	0.04754	0.13058	−0.9, $\mu x = 10$
	2[d]	3.504	0.06053	0.08862	2.1, $\mu x = 10$
	3	4.722	0.06468	0.01404	−2.4, $\mu x = 10$
	4	5.520	0.08857	−0.04570	1.3, $\mu x = 20$
	6	1.273	0.17257	−0.12178	−2.9, $\mu x = 15$
	8	0.664	0.20710	0.04692	1.4, $\mu x = 10$
	10	0.509	0.21743	0.05025	−3.6, $\mu x = 15$
Uranium	0.5[d]	1.444	0.02459	0.35167	−0.9, $\mu x = 10$
	1[d]	2.081	0.03862	0.22639	−0.7, $\mu x = 10$
	2[d]	3.287	0.03997	0.08635	−0.5, $\mu x = 1$
	3	4.883	0.04950	0.00981	−0.9, $\mu x = 15$
	4	2.800	0.08240	0.00370	1.4, $\mu x = 4$
	6	0.975	0.15886	0.21101	−2.2, $\mu x = 15$
	8	0.602	0.19189	0.02774	−2.1, $\mu x = 15$
	10	0.399	0.21314	0.02083	−2.9, $\mu x = 15$

[a] From ref. 64.

[b] The values of μx given in this column are the values for which the corresponding errors are valid.

[c] Based on buildup factors for an "effective" atomic number (see text).

[d] For some materials the values of the buildup factor for given energies are known only in the interval of $1 \leq \mu x \leq 15$. In these cases, the parameters are valid up to $\mu x = 15$.

Table 3D.2. Coefficients for the Polynomial Form of the Dose Buildup Factor[a,b]

Material	E (MeV)	β_0	β_1	β_2	β_3	Maximum Deviation (%)[c]	Average Deviation (%)
Ordinary concrete	1	5.1902(−1)[d]	1.6152(0)	5.4702(−2)	1.8803(−3)	−3.6, $\mu x = 4$	1.8
	2	7.7342(−1)	9.1835(−1)	2.7260(−2)	−3.9911(−4)	1.2, $\mu x = 2$	0.4
	3	1.0530(0)	6.3743(−1)	1.6185(−2)	−3.8875(−4)	−3.9, $\mu x = 2$	1.2
	4	1.1506(0)	4.9800(−1)	1.0547(−2)	−2.9613(−4)	−1.9, $\mu x = 8$	0.8
	5	1.1806(0)	4.1634(−1)	7.2376(−3)	−2.2268(−4)	2.8, $\mu x = 2$	1.3
	6	1.1846(0)	3.6314(−1)	5.0942(−3)	−1.6888(−4)	2.1, $\mu x = 8$	0.9
	7	1.1784(0)	3.2590(−1)	3.6051(−1)	−1.2895(−4)	−1.3, $\mu x = 4$	0.4
Magnetite concrete	1	5.2780(−1)	1.1562(0)	9.7936(−2)	−1.4084(−3)	1.8, $\mu x = 20$	0.8
	2	9.3721(−1)	8.0638(−1)	3.1686(−2)	−4.9503(−4)	1.5, $\mu x = 8$	0.6
	3	9.5856(−1)	6.5113(−1)	1.3680(−2)	−2.0725(−4)	−1.6, $\mu x = 4$	0.6
	4	9.7216(−1)	5.3998(−1)	7.8749(−3)	−1.0316(−4)	−2.3, $\mu x = 10$	1.7
	5	9.8690(−1)	4.5747(−1)	5.8668(−3)	−6.0375(−5)	1.8, $\mu x = 10$	1.0
	6	1.0010(0)	3.9452(−1)	5.2611(−3)	−4.1859(−5)	3.0, $\mu x = 10$	2.3
	7	1.0237(0)	3.4521(−1)	5.2272(−3)	−3.4147(−5)	2.6, $\mu x = 8$	1.4
Ferrophosphorus concrete	1	5.2446(−1)	1.1570(0)	6.6197(−2)	−2.6909(−4)	1.4, $\mu x = 10$	0.7
	2	9.0796(−1)	8.0470(−1)	2.4051(−2)	−1.3747(−4)	1.4, $\mu x = 20$	0.5
	3	9.7879(−1)	6.3258(−1)	1.3122(−2)	−2.8460(−5)	−3.6, $\mu x = 20$	1.1
	4	9.9224(−1)	5.2504(−1)	8.2727(−3)	8.2210(−5)	−2.0, $\mu x = 12$	1.5
	5	9.9175(−1)	4.5156(−1)	5.5458(−3)	1.7478(−4)	2.6, $\mu x = 20$	1.0
	6	9.8751(−1)	3.9831(−1)	3.7988(−3)	2.4954(−4)	3.3, $\mu x = 20$	2.4
	7	9.8244(−1)	3.5799(−1)	2.5837(−3)	3.1005(−4)	2.4, $\mu x = 6$	1.6
Barytes concrete	1	1.4863(0)	4.2184(−1)	1.3686(−1)	−2.7616(−3)	2.1, $\mu x = 4$	1.0
	2	1.0139(0)	6.7003(−1)	3.5826(−2)	−5.2672(−4)	2.2, $\mu x = 8$	1.1
	3	9.3467(−1)	5.9469(−1)	2.0106(−2)	−2.9295(−4)	−5.4, $\mu x = 6$	2.6
	4	9.1379(−1)	5.1277(−1)	1.3442(−2)	−5.0691(−5)	−3.8, $\mu x = 14$	2.2
	5	9.0721(−1)	4.4778(−1)	9.2573(−3)	1.8044(−4)	2.4, $\mu x = 8$	1.5
	6	9.0525(−1)	3.9750(−1)	6.2307(−3)	3.8250(−4)	5.3, $\mu x = 8$	3.8
	7	9.0500(−1)	3.5806(−1)	3.8974(−3)	5.5449(−4)	4.0, $\mu x = 8$	2.9

[a] From ref. 64.

[b] Based on buildup factors for an "effective" atomic number (see text).

[c] The values of μx given in this column are the values for which the corresponding errors are valid.

[d] Read: 5.1902×10^{-1}, etc.

Table 3D.3. Coefficients for Linear, Quadratic, and Berger Forms of Dose Buildup Factors Fitted over the Range 0 to 7 Mean Free Paths from Point Isotropic Sources[a]

Material	E (MeV)	Linear		Quadratic			Berger		
		A_1	Maximum Error (%)[b]	A_2	b	Maximum Error (%)	C	D	Maximum Error (%)
Water	0.255	8.6524	F3.1	−0.2525	1.4984	30	1.7506	0.2609	10
	0.5	4.6800	F2.3	0.6684	0.6750	8	1.3245	0.2078	5
	1	1.9953	40	1.0053	0.1666	2	1.0622	0.1052	3
	2	1.0301	10	0.8242	0.0346	2	0.8093	0.0408	1
	3	0.7397	3	0.6962	0.0073	1	0.6876	0.0125	1
	4	0.5884	1	0.5801	0.0014	1	0.5800	0.0024	1
	6	0.4321	3	0.4616	−0.0050	1	0.4655	−0.0126	1
	8	0.3406	4	0.3782	−0.0063	1	0.3860	−0.0214	1
	10	0.2877	4	0.3251	−0.0063	1	0.3342	−0.0257	1
Aluminum	0.5	2.6461	F1.5	1.0688	0.2654	2	1.2435	0.1250	3
	1	1.6089	30	0.9316	0.1140	2	0.9589	0.0864	3
	2	0.9686	13	0.7437	0.0378	2	0.7267	0.0486	2
	3	0.7197	5	0.6355	0.0142	1	0.6294	0.0227	1
	4	0.5663	3	0.5284	0.0064	1	0.5253	0.0127	1
	6	0.4334	2	0.4142	0.0032	1	0.4177	0.0061	1
	8	0.3476	1	0.3346	0.0022	1	0.3371	0.0050	1
	10	0.2847	2	0.2715	0.0022	1	0.2752	0.0055	1
Iron	0.5	1.4283	25	0.8642	0.0949	1	0.9081	0.0752	2
	1	1.2373	20	0.8026	0.0731	1	0.8214	0.0684	2
	2	0.8556	12	0.6526	0.0342	5	0.7020	0.0319	3
	3	0.6691	9	0.5338	0.0228	1	0.5323	0.0384	1
	4	0.5403	7	0.4366	0.0175	1	0.4366	0.0358	1
	6	0.4297	8	0.3237	0.0178	1	0.3271	0.0457	1
	8	0.3391	8	0.2473	0.0154	1	0.2563	0.0464	1
	10	0.2681	8	0.1785	0.0151	1	0.1876	0.0592	1
Tin	0.5	0.5153	3	0.5479	−0.0055	2	0.5608	−0.0146	1
	1	0.7199	6	0.6153	0.0176	1	0.6219	0.0244	1
	2	0.6731	8	0.5455	0.0215	1	0.5498	0.0338	1
	3	0.5837	11	0.4284	0.0261	1	0.4379	0.0479	1
	4	0.5146	12	0.3420	0.0290	1	0.3583	0.0601	1
	6	0.4153	17	0.2082	0.0348	2	0.2369	0.0925	1
	8	0.3317	17	0.1371	0.0327	2	0.1692	0.1103	1
	10	0.2550	16	0.0945	0.0270	2	0.1232	0.1190	1
Tungsten	0.5	0.1903	8	0.2692	−0.0133	2	0.2938	−0.0751	2
	1	0.3817	5	0.4269	−0.0076	2	0.4425	−0.0255	1
	2	0.4376	2	0.4164	0.0036	1	0.4172	0.0080	1
	3	0.4171	5	0.3515	0.0110	1	0.3501	0.0295	1
	4	0.4054	12	0.2540	0.0255	1	0.2710	0.0666	1
	6	0.3363	17	0.1435	0.0324	2	0.1771	0.1049	1
	8	0.2624	16	0.0957	0.0281	2	0.1245	0.1223	1
	10	0.2073	14	0.0748	0.0223	2	0.0974	0.1238	1

Table 3D.3 (continued)

Material	E (MeV)	Linear		Quadratic			Berger		
		A_1	Maximum Error (%)[b]	A_2	b	Maximum Error (%)	C	D	Maximum Error (%)
Lead	0.5	0.1549	8	0.2273	−0.0122	3	0.2526	−0.0848	2
	1	0.2990	6	0.3613	−0.0105	2	0.3779	−0.0403	1
	2	0.3796	1	0.3787	0.0001	1	0.3862	0.0032	1
	3	0.3810	5	0.3164	0.0109	1	0.3267	0.0253	1
	4	0.3523	10	0.2389	0.0191	1	0.2530	0.0547	1
	5.1	0.3219	13	0.1747	0.0248	1	0.1936	0.0839	1
	6	0.3034	15	0.1346	0.0284	2	0.1622	0.1027	1
	8	0.2419	15	0.0894	0.0257	3	0.1220	0.1112	2
	10	0.1933	13	0.0642	0.0217	3	0.0939	0.1167	2
Uranium	0.5	0.1054	7	0.1637	−0.0098	2	0.1825	−0.0951	2
	1	0.2264	7	0.2990	−0.0122	2	0.3204	−0.0599	2
	2	0.3023	3	0.3250	−0.0038	1	0.3321	−0.0162	1
	3	0.3169	4	0.2760	0.0069	1	0.2814	0.0196	1
	4	0.3010	7	0.2199	0.0136	1	0.2283	0.0458	1
	6	0.2571	12	0.1314	0.0212	1	0.1476	0.0916	1
	8	0.2081	12	0.0885	0.0201	1	0.1081	0.1076	1
	10	0.1621	11	0.0638	0.0165	1	0.0798	0.1163	1
Ordinary concrete[c]	0.5	3.7443	30	1.3563	0.4018	7	1.4489	0.1586	10
	1	1.9057	40	1.0980	0.1359	7	1.0448	0.1014	7
	2	1.0226	12	0.8238	0.0335	2	0.8062	0.0403	2
	3	0.7303	7	0.6189	0.0187	1	0.6267	0.0254	1
	4	0.5736	5	0.6106	−0.0062	3	0.6451	−0.0207	3
	6	0.4329	6	0.4667	−0.0057	4	0.5086	−0.0286	3
	8	0.3376	6	0.3794	−0.0070	3	0.4085	−0.0334	2
	10	0.2923	5	0.3344	−0.0071	3	0.3584	−0.0356	2
Ferrophosphorous concrete[c]	0.5	1.9407	F1.5	0.9330	0.1696	8	0.9059	0.1283	8
	1	1.4657	30	0.8542	0.1029	3	0.8467	0.0921	5
	2	0.9264	10	0.7481	0.0300	2	0.7327	0.0397	2
	3	0.6996	4	0.6198	0.0134	1	0.6331	0.0164	1
	4	0.5611	6	0.4980	0.0106	2	0.4879	0.0237	2
	6	0.4399	2	0.4119	0.0047	2	0.4346	0.0011	2
	8	0.3493	2	0.3243	0.0042	2	0.3390	0.0043	2
	10	0.2827	3	0.2574	0.0043	1	0.2563	0.0165	1
Magnetite concrete[c]	0.5	2.3150	F1.5	0.9510	0.2295	3	1.1049	0.1221	4
	1	1.6021	33	0.8847	0.1207	3	0.9006	0.0965	4
	2	0.9757	10	0.7636	0.0357	2	0.7770	0.0380	1
	3	0.7110	5	0.6163	0.0159	2	0.6321	0.0194	1
	4	0.5634	4	0.5177	0.0077	1	0.5241	0.0119	2
	6	0.4410	2	0.4200	0.0035	2	0.4401	−0.0004	2
	8	0.3391	2	0.3127	0.0044	1	0.3225	0.0080	1
	10	0.2840	2	0.2670	0.0029	1	0.2682	0.0096	1

Table 3D.3 (continued)

Material	E (MeV)	Linear A_1	Linear Maximum Error (%)[b]	Quadratic A_2	Quadratic b	Quadratic Maximum Error (%)	Berger C	Berger D	Berger Maximum Error (%)
Barytes concrete[c]	0.5	1.4414	23	0.8769	0.0950	2	0.9313	0.0724	1
	1	1.2066	21	0.7599	0.0752	1	0.7764	0.0737	2
	2	0.8740	10	0.6886	0.0312	1	0.7006	0.0368	1
	3	0.6556	6	0.5345	0.0204	3	0.5508	0.0289	2
	4	0.5634	9	0.4682	0.0160	3	0.4413	0.0418	3
	6	0.4571	10	0.3344	0.0207	1	0.3342	0.0525	2
	8	0.3519	5	0.2836	0.0115	1	0.2901	0.0321	1
	10	0.2684	7	0.1894	0.0133	1	0.1990	0.0495	1

[a]From ref. 67.
[b]F3.1 means "factor of 3.1," etc.
[c]Based on buildup factors for an "effective" atomic number (see text).

Table 3D.4. Coefficients for Linear, Quadratic, and Berger Forms of Dose Buildup Factors Fitted over the Range 0 to 20 Mean Free Paths from Point Isotropic Sources[a]

Material	E (MeV)	Linear A_1	Linear Maximum Error (%)[b]	Quadratic A_2	Quadratic b	Quadratic Maximum Error (%)[b]	Berger C	Berger D	Berger Maximum Error (%)
Water	0.255	36.1015	F12	−12.9947	3.0515	F∞	2.5048	0.1623	30
	0.5	13.0926	F5.6	−0.9744	0.8743	F3	1.8035	0.1224	25
	1	3.4788	F2	1.1152	0.1469	6	1.2282	0.0649	11
	2	1.2549	25	0.9173	0.0210	6	0.8594	0.0240	5
	3	0.7863	6	0.7218	0.0040	2	0.7004	0.0074	2
	4	0.5951	1	0.5907	0.0003	1	0.5826	0.0014	1
	6	0.4030	5	0.4471	−0.0027	2	0.4853	−0.0082	1
	8	0.3085	7	0.3561	−0.0038	2	0.3741	−0.0124	2
	10	0.2584	7	0.3002	−0.0026	3	0.3206	−0.0139	2
Aluminum	0.5	5.7374	F3	0.6696	0.3150	20	1.4412	0.0850	12
	1	2.5385	F1.9	1.1185	0.0883	10	1.0831	0.0535	9
	2	1.1928	30	0.8751	0.0197	8	0.7869	0.0266	6
	3	0.8061	12	0.6812	0.0078	3	0.6504	0.0137	3
	4	0.6075	6	0.5503	0.0036	2	0.5343	0.0082	2
	6	0.4626	6	0.4252	0.0023	2	0.4182	0.0063	1
	8	0.3697	5	0.3395	0.0019	1	0.3366	0.0058	1
	10	0.3087	5	0.2750	0.0021	1	0.2738	0.0074	1
Iron	0.5	2.3773	F1.9	0.9019	0.0917	3	0.9814	0.0548	7
	1	1.8643	F1.6	0.9212	0.0586	7	0.8932	0.0460	7
	2	1.1194	33	0.7423	0.0234	6	0.7173	0.0277	4
	3	0.8446	25	0.5840	0.0162	4	0.5571	0.0261	4
	4	0.6942	25	0.4605	0.0145	2	0.4518	0.0268	3
	6	0.6134	34	0.3201	0.0182	1	0.3381	0.0368	3
	8	0.5245	40	0.2207	0.0189	3	0.2603	0.0428	2
	10	0.4759	50	0.1143	0.0225	6	0.1902	0.0553	1

Table 3D.4 (continued)

Material	E (MeV)	Linear A_1	Linear Maximum Error (%)[b]	Quadratic A_2	Quadratic b	Quadratic Maximum Error (%)[b]	Berger C	Berger D	Berger Maximum Error (%)
Tin	0.5	0.5090	4	0.5150	−0.0005	3	0.5457	−0.0063	3
	1	0.8495	18	0.6666	0.0114	3	0.6378	0.0180	3
	2	0.8521	25	0.5826	0.0168	3	0.5678	0.0254	3
	3	0.8509	40	0.4254	0.0264	1	0.4533	0.0388	3
	4	0.8643	F1.58	0.2845	0.0360	5	0.3700	0.0518	3
	6	1.0786	F2.2	−0.1374	0.0756	40	0.2401	0.0891	2
	8	1.1907	F2.8	−0.4693	0.1032	F3	0.1669	0.1145	1
	10	1.1075	F3.0	−0.6523	0.1094	F12	0.1190	0.1278	5
Tungsten	0.5	0.1550	13	0.2206	−0.0054	5	0.2692	−0.0477	5
	1	0.3382	9	0.4149	−0.0048	2	0.4279	−0.0150	2
	2	0.4671	8	0.4072	0.0037	3	0.4163	0.0070	4
	3	0.5919	30	0.3255	0.0165	2	0.3484	0.0324	2
	4	0.8102	F1.8	0.0995	0.0442	15	0.2727	0.0653	1
	6	1.2616	F3	−0.5462	0.1124	F4	0.1704	0.1160	2
	8	1.3753	F3.5	−0.9399	0.1439	F∞	0.1161	0.1405	6
	10	1.2730	F3.8	−0.9502	0.1382	F∞	0.0882	0.1510	7
Lead	0.5	0.1043	15	0.1791	−0.0047	5	0.2243	−0.0500	5
	1	0.2549	11	0.3133	−0.0036	5	0.3530	−0.0211	4
	2	0.3947	3	0.3695	0.0015	2	0.3791	0.0021	1
	3	0.5123	30	0.2990	0.0133	2	0.3244	0.0279	1
	4	0.6378	F1.6	0.1449	0.0306	10	0.2526	0.0557	1
	5.1	0.8560	F2.1	−0.1480	0.0624	40	0.1904	0.0883	2
	6	1.1247	F2.8	−0.5070	0.1014	F4	0.1554	0.1143	4
	8	1.4165	F4	−1.1408	0.1589	F∞	0.1075	0.1440	12
	10	1.2370	F4	−1.0279	0.1408	F∞	0.0824	0.1513	12
Uranium	0.5	0.0812	11	0.1262	−0.0037	5	0.1635	−0.0606	5
	1	0.1914	11	0.2556	−0.0053	5	0.2991	−0.0385	5
	2	0.2838	5	0.3185	−0.0022	2	0.3240	−0.0084	2
	3	0.4081	20	0.2614	0.0091	2	0.2781	0.0234	1
	4	0.4991	43	0.1621	0.0210	6	0.2273	0.0475	1
	6	0.8088	F2.3	−0.2492	0.0658	F2	0.1426	0.1011	2
	8	0.9323	F2.9	−0.5357	0.0912	F5	0.1004	0.1274	5
	10	0.9203	F3.3	−0.6560	0.0980	F∞	0.0721	0.1442	7
Ordinary concrete[c]	0.5	5.0124	F2.3	0.8341	0.5016	10	1.5177	0.1413	12
	1	2.9917	F2	1.1821	0.1125	10	1.2208	0.0562	11
	2	1.2334	25	0.9344	0.0186	7	0.8579	0.0231	5
	3	0.7857	12	0.7141	0.0044	6	0.6589	0.0115	5
	4	0.5942	4	0.5662	0.0017	5	0.6056	−0.0018	4
	6	0.4145	5	0.4440	−0.0018	5	0.4769	−0.0093	4
	8	0.3200	4	0.3445	−0.0015	5	0.3789	−0.0113	4
	10	0.2737	5	0.3015	−0.0017	5	0.3318	−0.0128	4

Table 3D.4 (continued)

Material	E (MeV)	Linear A_1	Linear Maximum Error (%)[b]	Quadratic A_2	Quadratic b	Quadratic Maximum Error (%)[b]	Berger C	Berger D	Berger Maximum Error (%)
Ferrophosphorous concrete[c]	0.5	3.4067	F2.2	1.1051	0.1431	15	1.1098	0.0704	15
	1	2.1096	F1.7	1.1170	0.0617	15	0.9892	0.0481	10
	2	1.1583	30	0.7992	0.0223	4	0.7703	0.0256	3
	3	0.8138	16	0.6488	0.0103	2	0.6373	0.0152	2
	4	0.6702	16	0.4923	0.0111	2	0.4966	0.0186	2
	6	0.5469	18	0.3622	0.0115	5	0.4118	0.0167	3
	8	0.4477	19	0.2692	0.0111	5	0.3207	0.0196	4
	10	0.3972	25	0.1971	0.0124	5	0.2456	0.0287	3
Magnetite concrete[c]	0.5	4.2793	F2.5	1.4544	0.1756	23	1.3246	0.0736	18
	1	2.3058	F1.7	1.2562	0.0652	20	1.0651	0.0492	12
	2	1.1752	25	0.8756	0.0186	5	0.8208	0.0227	5
	3	0.8098	15	0.6616	0.0092	3	0.6445	0.0143	2
	4	0.6263	10	0.5280	0.0061	2	0.5265	0.0108	1
	6	0.4781	7	0.4257	0.0033	2	0.4312	0.0062	2
	8	0.3805	9	0.3195	0.0038	2	0.3204	0.0106	2
	10	0.3399	12	0.2428	0.0060	3	0.2623	0.0156	2
Barytes concrete[c]	0.5	2.2489	F1.8	1.1064	0.0710	11	1.0183	0.0496	10
	1	1.8761	F1.7	1.0022	0.0543	14	0.8555	0.0495	12
	2	1.1122	30	0.7591	0.0219	4	0.7291	0.0265	4
	3	0.8068	24	0.6047	0.0126	6	0.5673	0.0222	4
	4	0.6873	21	0.4913	0.0122	4	0.4689	0.0242	4
	6	0.6277	30	0.3420	0.0178	2	0.3542	0.0355	4
	8	0.5574	40	0.1882	0.0229	10	0.2806	0.0409	3
	10	0.4943	50	0.0936	0.0249	10	0.1949	0.0555	2

[a]From ref. 67.

[b]F12 means "factor of 12," etc.

[c]Based on buildup factors for an "effective" atomic number (see text).

Table 3D.5. Coefficients for Berger Form of Dose Buildup Factors Fitted Over the Range 0 to 20 Mean Free Paths from Point Isotropic Sources[a,b]

Material	E (MeV)	C	D	Maximum Error (%)
Ordinary concrete[c]	0.5	1.3029	0.08610	18
	1.0	1.0914	0.54566	15
	2.0	0.8126	0.01980	9
	3.0	0.6731	0.00942	4
	4.0	0.5953	0.00299	2
	6.0	0.4915	−0.00159	3
	8.0	0.4164	−0.00172	6
	10.0	0.3585	−0.00005	9
Ordinary concrete[c]	0.5	1.3110	0.08073	12
	1.0	1.0221	0.05160	9
	2.0	0.7744	0.02456	5
	3.0	0.6525	0.01258	3
	4.0	0.5672	0.00753	2
	6.0	0.4718	0.00198	1
	8.0	0.4203	0.00096	1
	10.0	0.3716	0.00127	1
Magnetite concrete	0.5	1.0971	0.06458	8
	1.0	0.9281	0.04768	8
	2.0	0.7318	0.02620	5
	3.0	0.6154	0.01836	4
	4.0	0.5308	0.01513	3
	6.0	0.4345	0.01118	2
	8.0	0.3752	0.01199	2
	10.0	0.3245	0.01624	2
Barytes concrete	0.5	0.7002	0.01624	1
	1.0	0.7237	0.03007	4
	2.0	0.6270	0.02373	4
	3.0	0.5367	0.02158	4
	4.0	0.4645	0.02122	3
	6.0	0.3727	0.02233	3
	8.0	0.3172	0.02588	2
	10.0	0.2667	0.02878	2
Air	0.5	1.6001	0.10094	18
	1.0	1.1571	0.05749	11
	2.0	0.8363	0.02430	5
	3.0	0.6974	0.01617	3
	4.0	0.6081	0.00324	1
	6.0	0.5146	−0.00316	1
	8.0	0.4635	−0.00362	1
	10.0	0.4235	−0.00350	1
Sand	0.5	1.4474	0.08932	14
	1.0	1.0876	0.05482	10
	2.0	0.8077	0.02503	5
	3.0	0.6758	0.01239	3
	4.0	0.5875	0.00651	2
	6.0	0.4886	0.00091	1
	8.0	0.4334	0.00009	1
	10.0	0.3883	−0.00224	1

Table 3D.5 (continued)

Material	E (MeV)	C	D	Maximum Error (%)
Wood	0.5	1.6187	0.10280	19
	1.0	1.1676	0.05802	11
	2.0	0.8457	0.02392	5
	3.0	0.7051	0.00913	3
	4.0	0.6149	0.00253	1
	6.0	0.5176	−0.00342	1
	8.0	0.4727	−0.00438	1
	10.0	0.4328	−0.00390	1
LiH	0.5	2.0198	0.13997	34
	1.0	1.2652	0.07091	16
	2.0	0.8391	0.02272	6
	3.0	0.6607	0.00546	2
	4.0	0.5778	−0.00157	1
	6.0	0.4671	−0.01017	2
	8.0	0.4047	−0.01213	3
	10.0	0.3676	−0.01135	3

[a]From ref. 215.

[b]Based on fits to buildup factors calculated specifically for the material (see text).

[c]The first set of coefficients for ordinary concrete is based on buildup factors reported by Chilton (ref. 57) for ranges up to 50 mean free paths. The second set of coefficients for ordinary concrete is based on buildup factors reported by Clark and Trubey (ref. 54) for ranges up to 20 mean free paths.

Appendix 3E. Geometric Transformations for Kernels

Results from calculations and experiments for one geometry may be transformed to kernels for other geometries. The purpose is usually to compare results or apply basic data, such as for a point source, to particular design situations. Blizard developed many of these transformations, and while they were more frequently employed in the pre-computer era of shielding, they are still useful in many situations. The basic assumption is that the medium is isotropic, homogeneous, and infinite, so that the kernels are dependent only on the distance to the source. These conditions are never fully met, but in many practical cases the transformation results are valid to a good approximation. The kernels are unspecified; they may be dose rate, flux density, or similar quantities. A few of the most important transformations are given here, with more complete expositions available in articles by Blizard.[92,93,208]

Point to Infinite Plane. – The dose from an infinite plane, $D(z,\infty)$, is obtained by integrating the point-source kernel, $K(R)$, over the entire plane. That is,

$$D(z,\infty) = \int_0^\infty S\,K(R)\,2\pi\,\rho\,d\rho$$

$$= 2\pi S \int_z^\infty K(R)\,R\,dR\,, \qquad \text{(E1)}$$

where

S = source strength (particles per unit time per unit area),

z = distance to plane source,

$2\pi\,\rho\,d\rho$ = differential area on the plane, all points of which are at the same distance R from the detector point,

$R = \sqrt{\rho^2 + z^2}$.

Point to Disk. – The point-to-disk transformation is similar to the point-to-infinite-plane transformation but with an upper limit of integration which corresponds to the radius of the disk. The disk kernel is

$$D(z,a) = 2\pi S \int_z^{\sqrt{z^2+a^2}} K(r)\,R\,dR\,, \qquad \text{(E2)}$$

where a is the radius of the disk.

Infinite Plane to Disk. – The disk kernel as given by Eq. E2 can be rewritten as

$$D(z,a) = 2\pi S \int_z^\infty K(R)\,R\,dR - 2\pi S \int_{\sqrt{z^2+a^2}}^\infty K(R)\,R\,dR\,.$$

The two terms are infinite plane kernels as defined by Eq. E1 and the expression for the disk kernel can be rewritten as an infinite-plane-to-disk transformation:

$$D(z,a) = D(z,\infty) - D(\sqrt{z^2+a^2},\infty)\,. \qquad \text{(E3)}$$

Disk-to-Infinite Plane (Hurwitz Transformation). – It was observed by Hurwitz and recorded by Blizard that data for a disk source, such as that from the ORNL Lid Tank Shielding Facility, could be transformed to data for an infinite plane source by a summation process:

$$D(z,\infty) = 2\pi S \left[\int_z^{\sqrt{z^2+a^2}} K(R)\,dR + \int_{\sqrt{z^2+a^2}}^{\sqrt{z^2+2a^2}} K(R)\,dR + \int_{\sqrt{z^2+2a^2}}^{\sqrt{z^2+3a^2}} K(R)\,dR + \ldots \right]$$

$$= \sum_{\nu=0}^{\infty} D(z',a)\,, \qquad \text{(E4)}$$

where $D(z',a)$ is the dose due to a disk of radius a at a distance $z' = \sqrt{z^2 + \nu a^2}$. Thus the dose for an infinite plane could be obtained simply by adding the measured results at points z'. For materials such as water, the series converges in only a few terms, so a relatively

small range of distances where data can be obtained is generally adequate. Nevertheless, it is more satisfactory to estimate the remainder of the series. Blizard[92] has done this by assuming that terms up to ν' can be obtained and that the data can be extrapolated as an exponential function proportional to $e^{-\mu z'}$:

$$D(z,\infty) \cong \sum_{\nu=0}^{\nu'-1} D(z',a) + (\alpha + \tfrac{1}{2})\, D(\sqrt{z^2 + \nu' a^2}, a)\,, \quad \text{(E5)}$$

where

$$\alpha = \frac{2}{(\mu a^2)^2}\,(\mu\sqrt{z^2 + \nu' a^2} + 1)\,.$$

Disk to Point. – In a manner similar to the transformation from a disk to an infinite plane, the data for a disk source may be transformed to that for a point source, but derivatives must be evaluated. That is,

$$K(z) \cong \sum_{\nu=0}^{\nu'-1} B(\sqrt{z^2 + \nu a^2}) + \left(\frac{2\sqrt{z^2 + \nu' a^2}}{\mu a^2} + \frac{1}{2}\right) B(\sqrt{z^2 + \nu' a^2})\,, \quad \text{(E6)}$$

where

$$B(z) = -\frac{1}{2\pi S z}\,\frac{\partial}{\partial z} D(z,a)\,.$$

Infinite Plane to Spherical Surface. – The dose for a spherical surface source of radius r is obtained by integrating the point kernel over the entire surface of the sphere. The spherical surface source kernel is given by

$$D_{ss}(r_0,r) = 2\pi S \int_{\theta=0}^{\pi} K(R)\, r^2 \sin\theta\, d\theta = 2\pi S \frac{r}{r_0} \int_{r_0 - r}^{r_0 + r} K(R)\, R\, dR\,, \quad \text{(E7)}$$

where r_0 is the distance from the detector to the center of the sphere. This result can be interpreted as the difference between the doses due to infinite planes located at the two points where the sphere intersects the axis containing the detector point and the center of the sphere. The infinite plane to spherical source transformation is given by

$$D_{ss}(r_0,r) = \frac{r}{r_0}\,[D(r_0 - r,\infty) - D(r_0 + r,\infty)]\,. \quad \text{(E8)}$$

This formulation presumes that the material within the sphere has the same attenuating properties as the shielding material.

Spherical Volume Source. – Consider a spherical volume source of radius r whose intensity $s(r')$ depends only on the distance from the center of the sphere r'. An equivalent surface source for a spherical shell of thickness dr' about r' is given by $s(r')\,dr'$. The detector response to this shell source would be the spherical surface source kernel $D_{ss}(r_0,r')/S$ multiplied by the source $s(r')\,dr'$, and the detector response from all such differential shell sources within the spherical volume is

$$D_{sv}(r_0,r) = \int_0^r s(r')\,\frac{D_{ss}(r_0,r')}{S}\,dr'\,, \quad \text{(E9)}$$

where $D_{ss}(r_0,r')$ is given by Eqs. E7 and E8. Equation E9, which is a transformation from a spherical surface to a spherical volume, can be rewritten as a transformation from an infinite plane to a spherical volume by substituting Eq. E8 into Eq. E9, which gives

$$D_{sv}(r_0,r) = \int_0^r s(r')\,\frac{r'}{r_0} \times \left[\frac{D(r_0 - r',\infty)}{S} - \frac{D(r_0 + r',\infty)}{S}\right] dr'\,. \quad \text{(E10)}$$

But in most cases,

$$D(r_0 - r,\infty) \gg D(r_0 + r,\infty)\,,$$

in which case

$$D_{sv}(r_0) \cong \int_0^r s(r')\,\frac{r'}{r_0}\,\frac{D(r_0 - r',\infty)}{S}\,dr'\,. \quad \text{(E11)}$$

The restriction that the material within the sphere have the same attenuating properties as the shielding material also applies to these results.

Appendix 3F. Neutron Kernels from Monte Carlo Transport Calculations

This appendix presents kernels (also called attenuation or transmission factors) obtained from Monte Carlo calculations of the penetration of neutrons through concrete and several other materials. Figures 3F.1 through 3F.10 show the data of Clark *et al.*[96] for monoenergetic beams of neutrons normally incident on ordinary concrete, both on a slab and on a semi-infinite medium. The density of the concrete was taken to be 2.43 g/cm^3, and its composition, other than its water content, was assumed to be that given for ordinary concrete 01 in ref. 97. The results are given as tissue kerma* as a function of concrete thickness.

Figures 3F.11 through 3F.15 present plots of neutron dose transmission factors calculated by Allen and Futterer[100] for monoenergetic neutrons incident at various angles on polyethylene. When the thickness is adjusted according to the key included at the top of each figure, these curves apply also to water, to concrete, and to Nevada Test Site soil, both dry and water-saturated. The doses calculated by Allen and Futterer are multicollision doses.*

The use of curves of this type is explained in Section 3.8.4.

*See the discussions of kerma, first-collision dose, and multicollision dose in Chapter 2 of this Handbook.

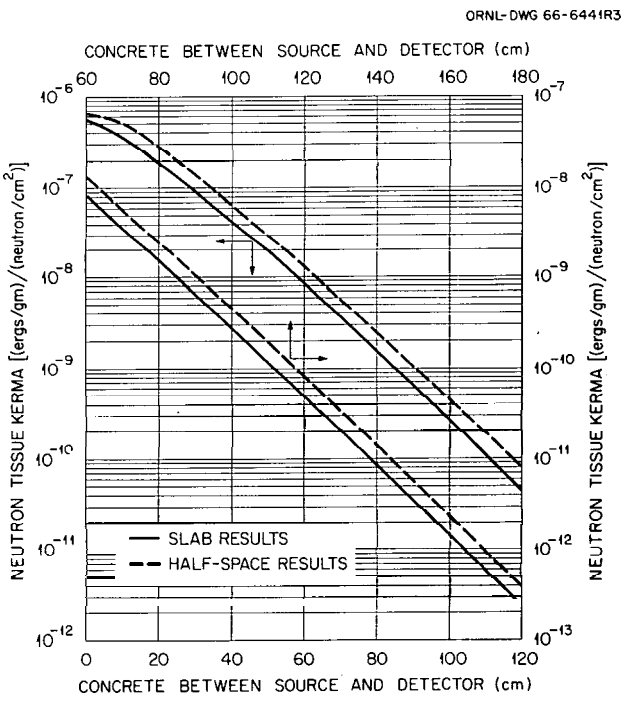

Fig. 3F.1. Dose in Ordinary Concrete Due to Normally Incident 14-MeV Neutrons. (From ref. 96.)

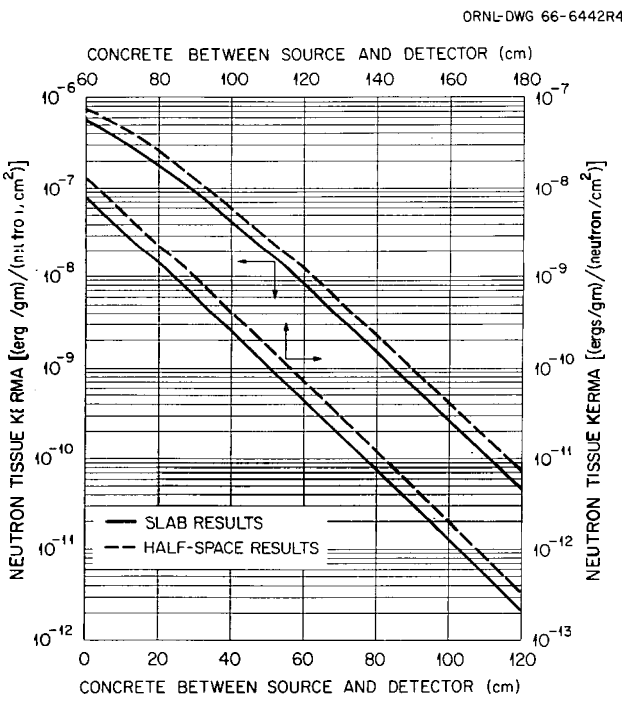

Fig. 3F.2. Dose in Ordinary Concrete Due to Normally Incident 12-MeV Neutrons. (From ref. 96.)

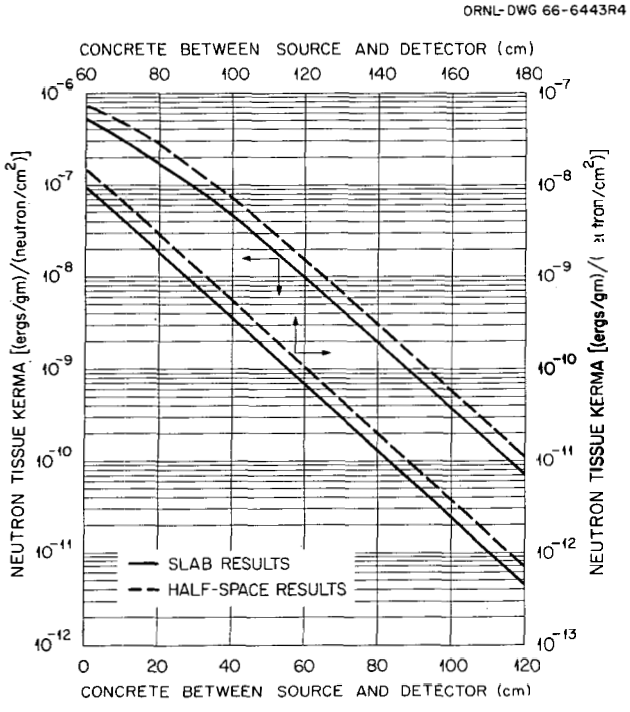

Fig. 3F.3. Dose in Ordinary Concrete Due to Normally Incident 10-MeV Neutrons. (From ref. 96.)

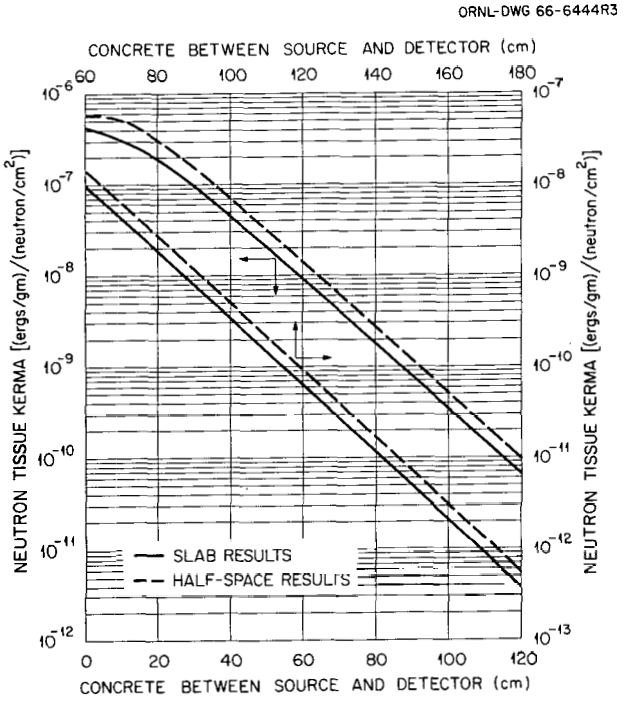

Fig. 3F.4. Dose in Ordinary Concrete Due to Normally Incident 8-MeV Neutrons. (From ref. 96.)

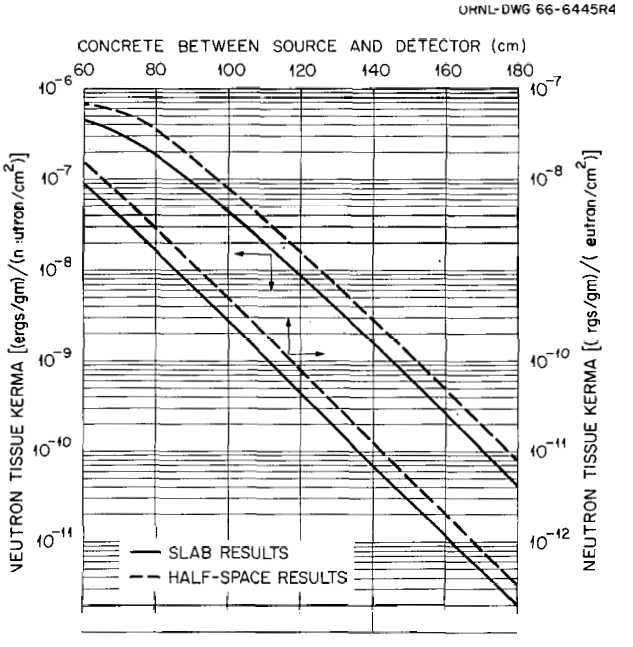

Fig. 3F.5. Dose in Ordinary Concrete Due to Normally Incident 6-MeV Neutrons. (From ref. 96.)

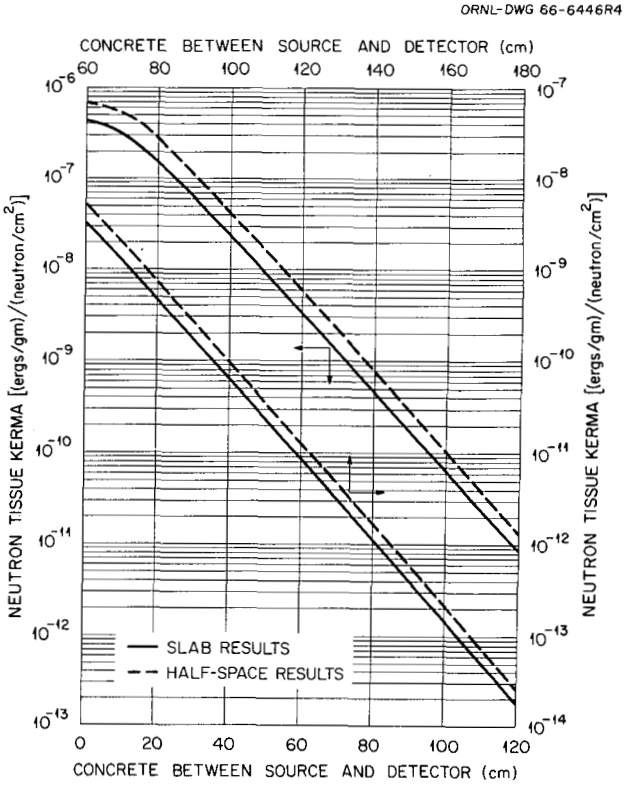

Fig. 3F.6. Dose in Ordinary Concrete Due to Normally Incident 4-MeV Neutrons. (From ref. 96.)

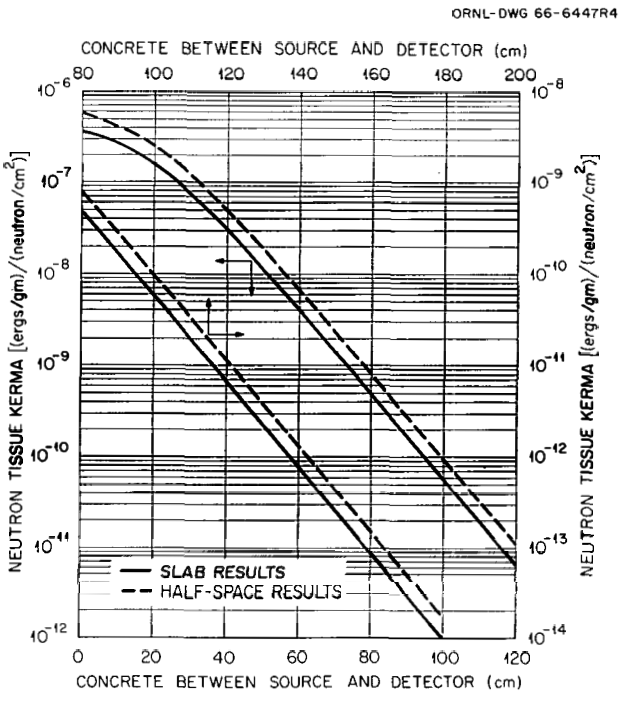

Fig. 3F.7. Dose in Ordinary Concrete Due to Normally Incident 3-MeV Neutrons. (From ref. 96.)

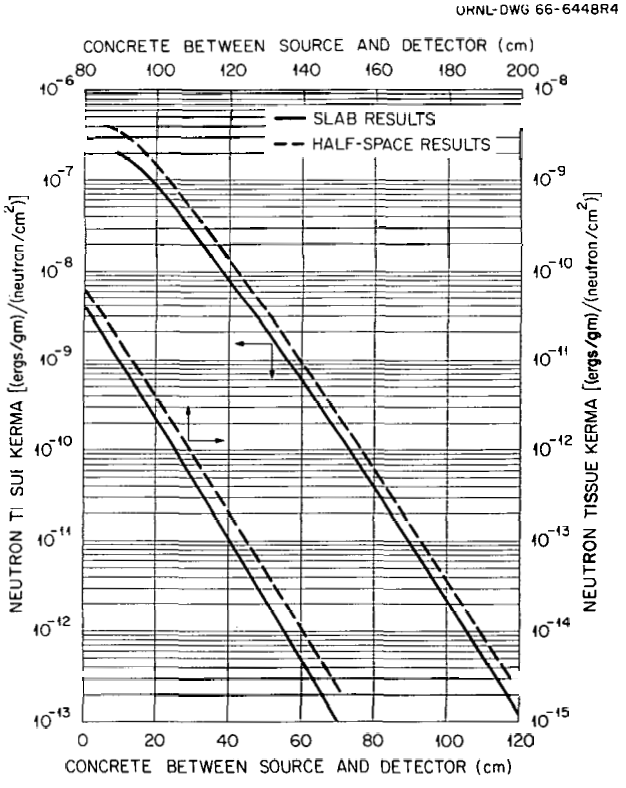

Fig. 3F.8. Dose in Ordinary Concrete Due to Normally Incident 2-MeV Neutrons. (From ref. 96.)

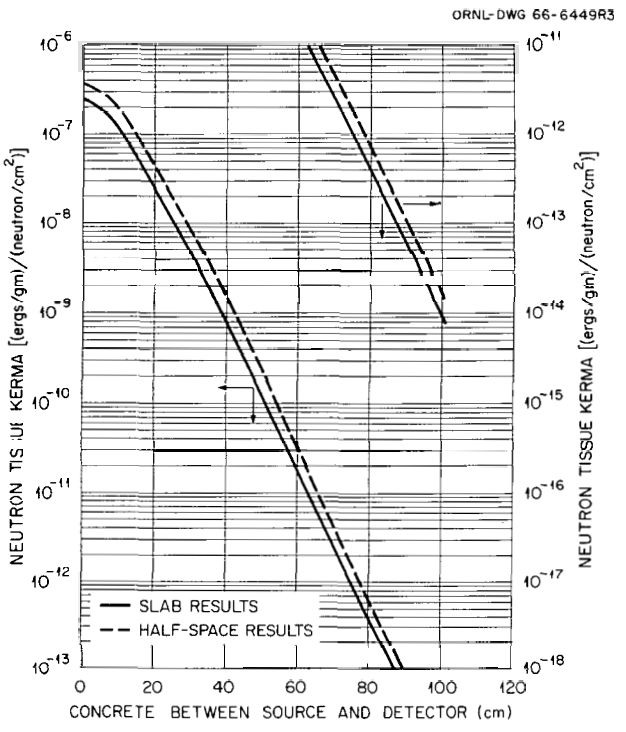

Fig. 3F.9. Dose in Ordinary Concrete Due to Normally Incident 1.3-MeV Neutrons. (From ref. 96.)

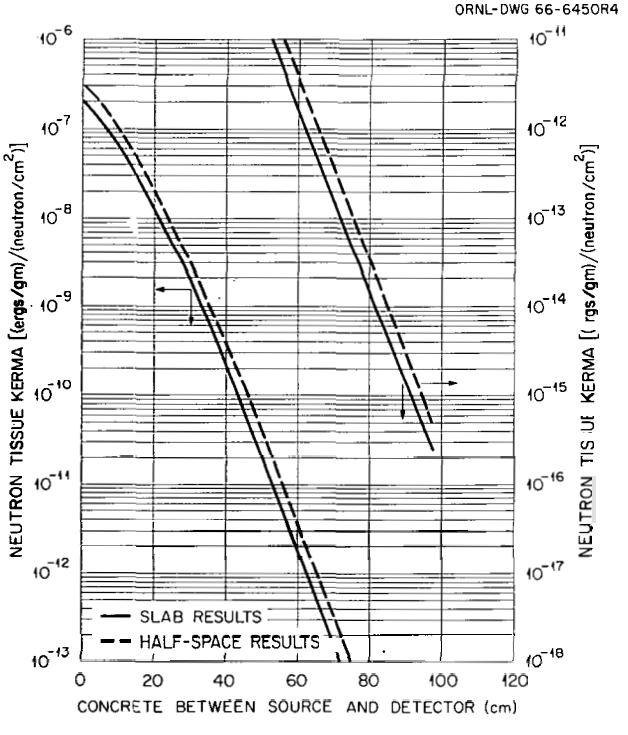

Fig. 3F.10. Dose in Ordinary Concrete Due to Normally Incident 0.7-MeV Neutrons. (From ref. 96.)

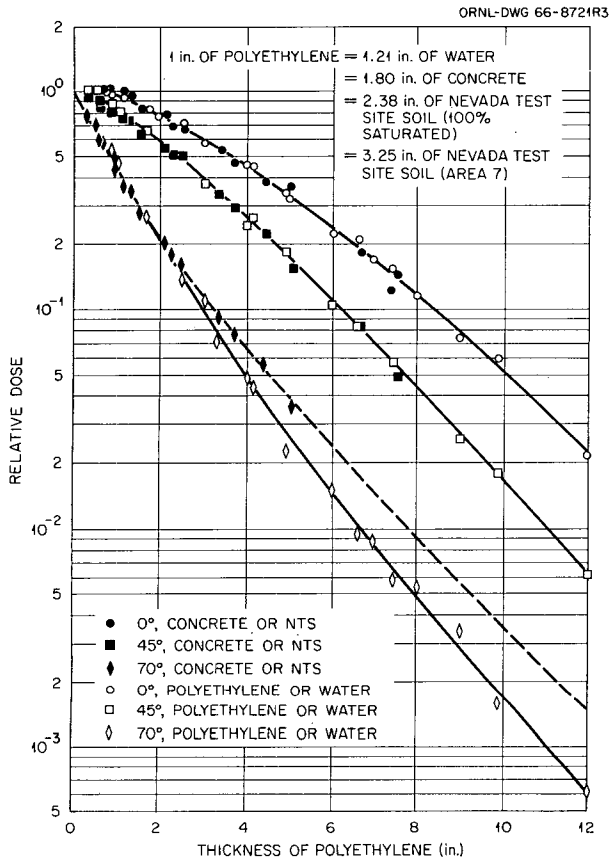

Fig. 3F.11. Penetration of 5-MeV Neutrons Incident on Various Materials at Various Angles. (From ref. 100.)

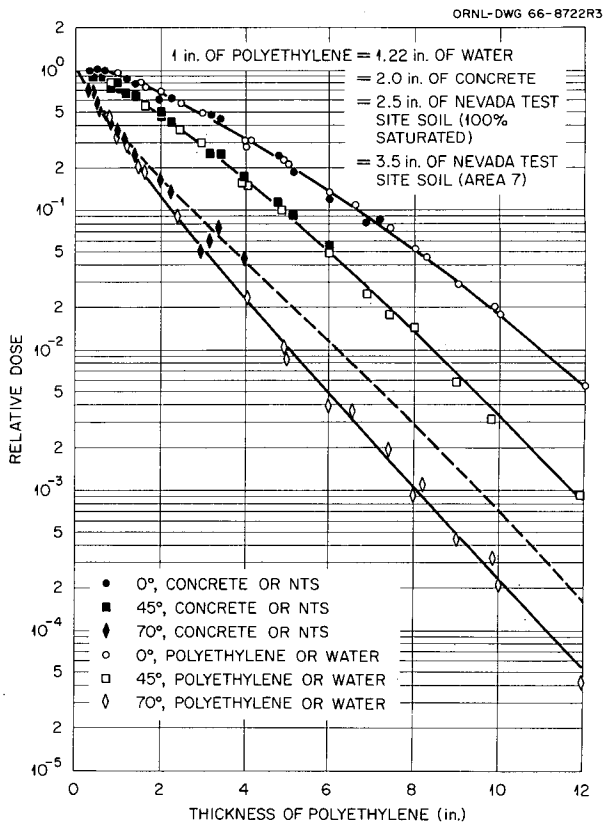

Fig. 3F.12. Penetration of 3-MeV Neutrons Incident on Various Materials at Various Angles. (From ref. 100.)

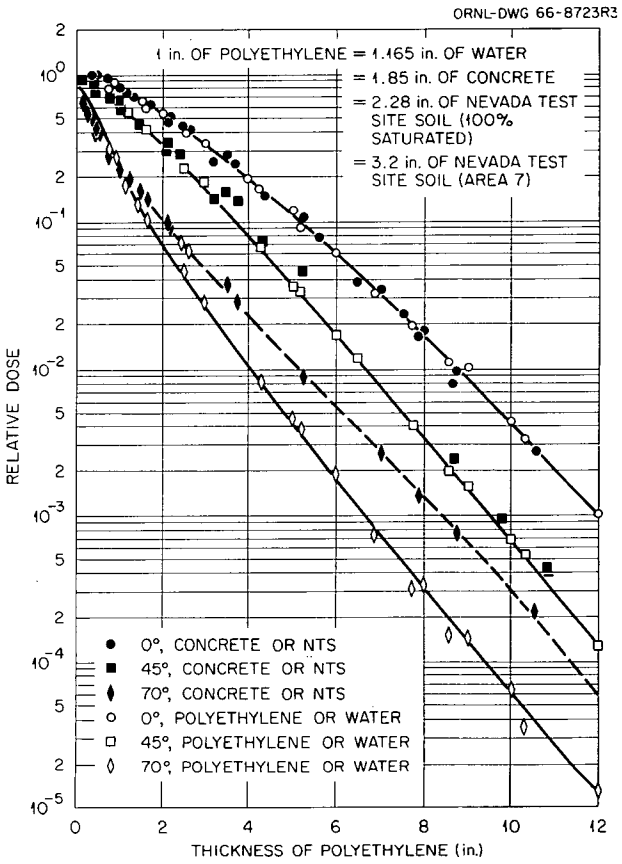

Fig. 3F.13. Penetration of 2-MeV Neutrons Incident on Various Materials at Various Angles. (From ref. 100.)

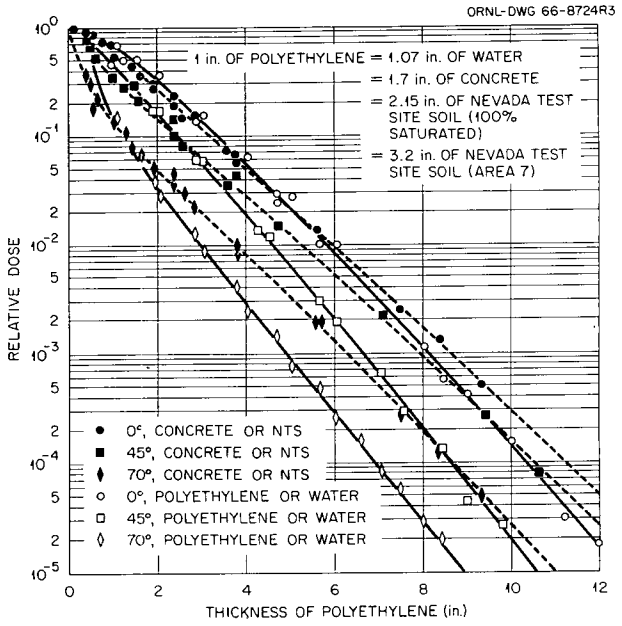

Fig. 3F.14. Penetration of 1-MeV Neutrons Incident on Various Materials at Various Angles. (From ref. 100.)

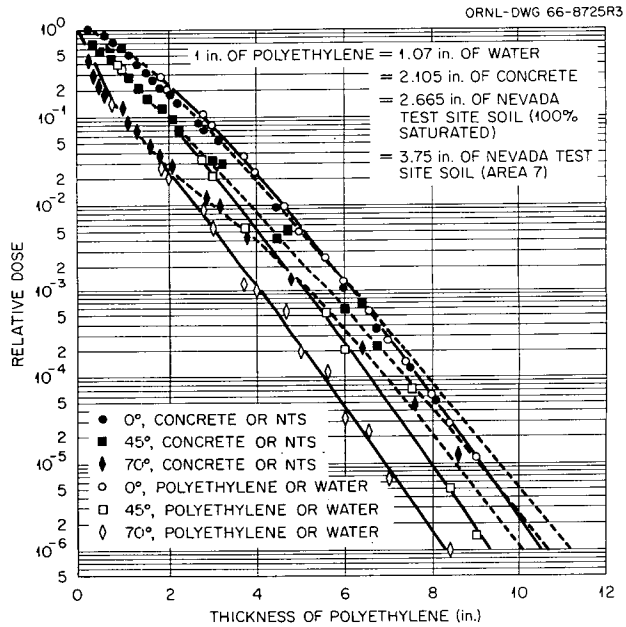

Fig. 3F.15. Penetration of 0.5-MeV Neutrons Incident on Various Materials at Various Angles. (From ref. 100.)

Appendix 3G. Neutron Kernels from Discrete Ordinates Transport Calculations

This appendix presents kernels (also called attenuation or transmission factors) obtained from discrete ordinates calculations of the penetration of neutrons through concrete. These kernels were computed by Roussin and Schmidt[99] with the ANISN code for several source energies and slab thicknesses and for both a normally incident source and a plane isotropic source. The results are given in terms of tissue dose equivalent.* Figures 3G.1 and 3G.2 give the neutron tissue dose equivalent as a function of neutron energy for several concrete slab thicknesses for normally incident and isotropically incident sources respectively. Figures 3G.3 and 3G.4 give the same data as a function of slab thickness for specific source energy bands, also for normally incident and isotropically incident sources respectively. Figure 3G.5 shows the relative importance of the neutron dose and the secondary gamma-ray dose produced by neutrons as a function of energy for various slab thicknesses. These ratios, which are for a normally incident source, can be applied to the data given in Figs. 3G.1 and 3G.2 to calculate corresponding secondary gamma-ray and/or total doses. Comparisons of the total dose (secondary gamma-ray dose plus neutron dose) for two source energies are shown in Fig. 3G.6.

The use of curves of this type is explained in Section 3.8.4.

*See the discussion of dose equivalents in Chapter 2 of this Handbook.

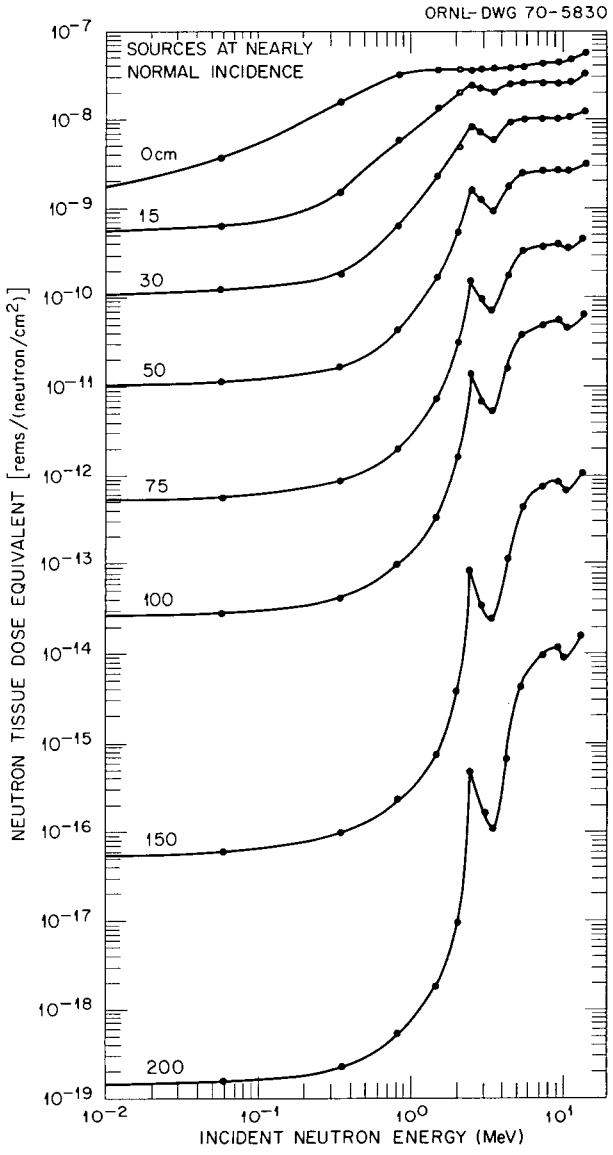

Fig. 3G.1. Neutron Tissue Dose Equivalent as a Function of Incident Neutron Energy for Various Concrete Slab Thicknesses (Normally Incident Source). (From ref. 99.)

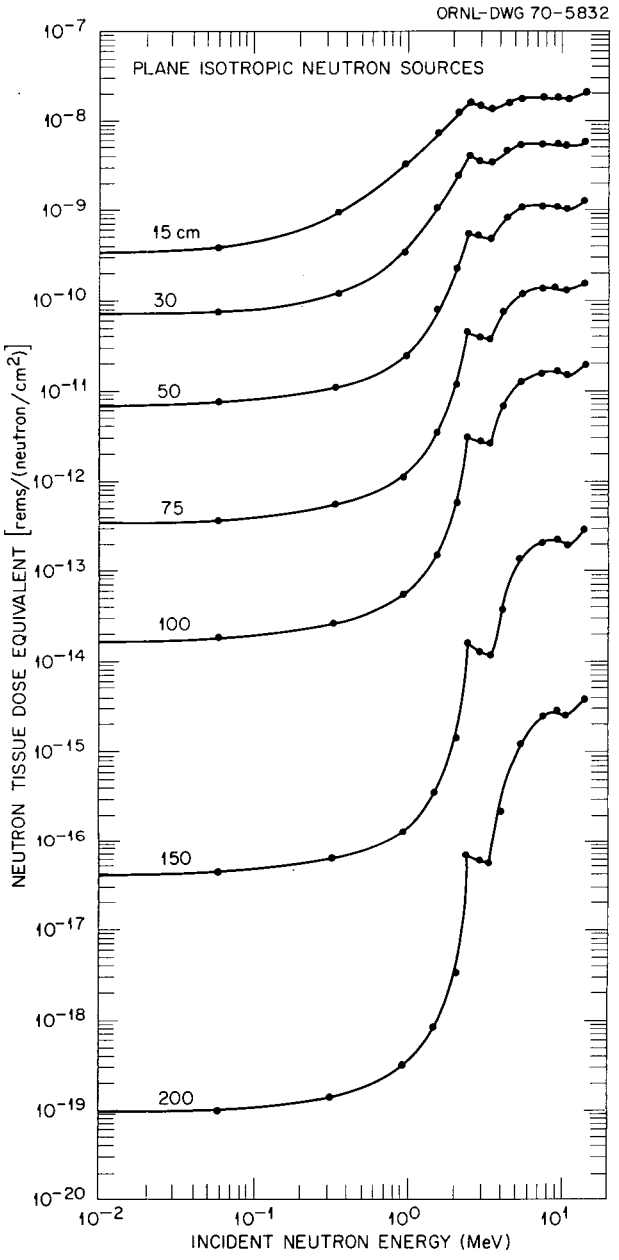

Fig. 3G.2. Neutron Tissue Dose Equivalent as a Function of Incident Neutron Energy for Various Concrete Slab Thicknesses (Plane Isotropic Source). (From ref. 99.)

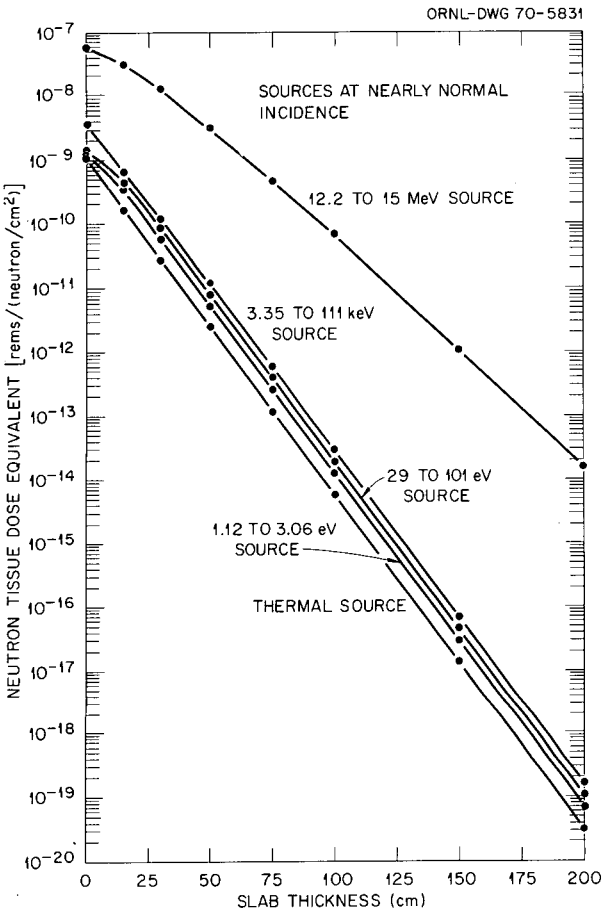

Fig. 3G.3. Neutron Tissue Dose Equivalent as a Function of Concrete Slab Thickness for Normally Incident Neutrons of Various Energies. (From ref. 99.)

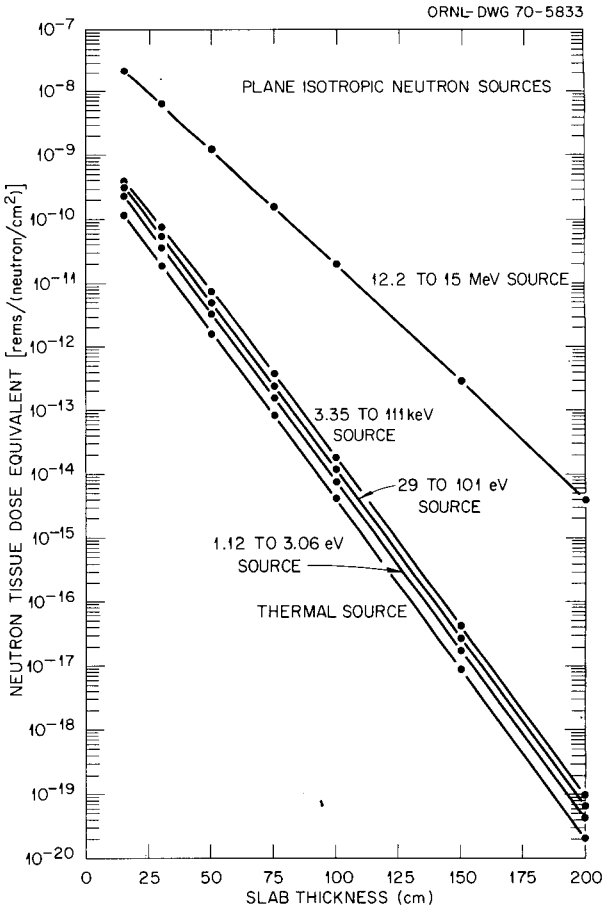

Fig. 3G.4. Neutron Tissue Dose Equivalent as a Function of Concrete Slab Thickness for Plane Isotropic Neutron Sources of Various Energies. (From ref. 99.)

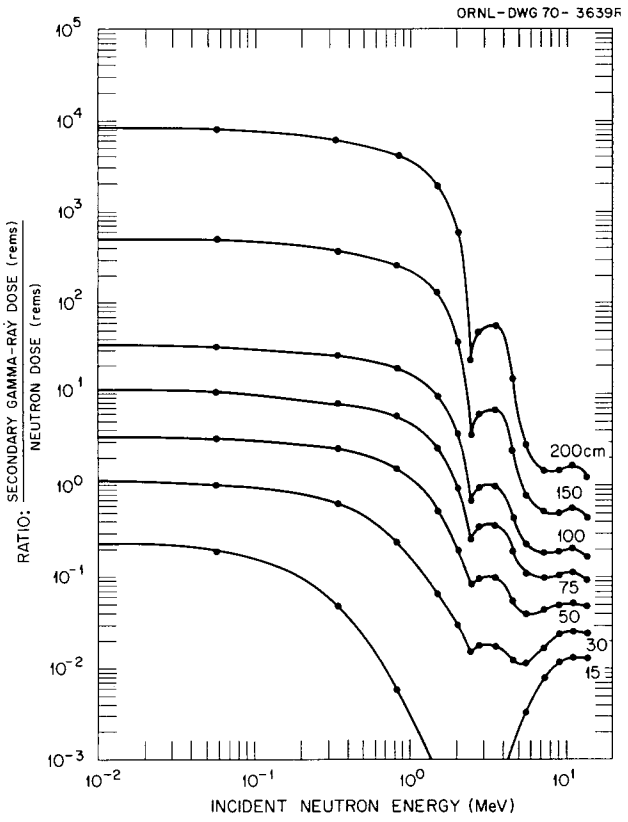

Fig. 3G.5. Ratio of Secondary Gamma-Ray Tissue Dose to Neutron Tissue Dose as a Function of Incident Neutron Energy for Various Concrete Slab Thicknesses (Normally Incident Source). (From ref. 99.)

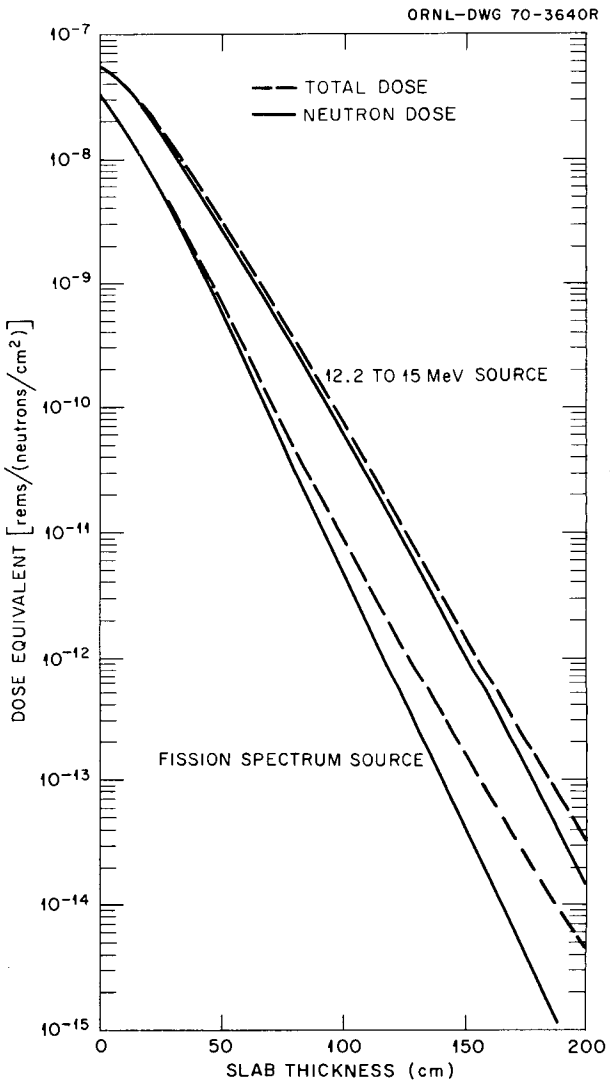

Fig. 3G.6. Neutron and Total Dose Equivalents as a Function of Concrete Slab Thickness for 12.2- to 15-MeV and Fission Neutron Sources at Nearly Normal Incidence. Total dose = neutron dose + secondary gamma-ray dose. (From ref. 99.)

Appendix 3H. Graphs and Formulas of Exponential and Exponential Integral Functions

Several exponential functions that are extremely useful in shielding calculations are presented in this appendix. They include the exponential function e^{-x} and the exponential integral functions $E_n(x)$, which are expressed in integral form by

$$E_n(x) = x^{n-1} \int_x^\infty e^{-y} \frac{dy}{y^n}, \qquad \text{(H1)}$$

$$E_n(x) = \int_1^\infty e^{-xy} \frac{dy}{y^n}, \qquad \text{(H2)}$$

$$E_n(x) = \int_0^1 y^{n-2} e^{-x/y}\, dy, \qquad \text{(H3)}$$

and in series form by

$$E_n(x) = \sum_{\substack{m=0 \\ m \neq n-1}}^{\infty} \frac{(-x)^m}{(n-1-m)\, m!} + (-1)^n \frac{x^{n-1}}{(n-1)!} (\ln \gamma x - A_n), \qquad \text{(H4)}$$

where

$\ln \gamma = 0.577216 \ldots$,

$A_1 = 0$,

$A_n = \sum_{m=1}^{n-1} \frac{1}{m}$,

and $n = 0, 1, 2, 3, \ldots$. The recursion relation for the exponential integrals is

$$E_n(x) = \frac{1}{n-1} [e^{-x} - x E_{n-1}(x)] \quad \text{(ref. 209)}. \qquad \text{(H5)}$$

In particular, the first-order exponential integral is given by

$$E_1(x) = \int_x^\infty \frac{e^{-y}}{y}\, dy \qquad \text{(H6)}$$

and the series representation by

$$E_1(x) = -\ln \gamma x - \sum_{n=0}^{\infty} \frac{(-1)^n x^n}{n! n}. \qquad \text{(H7)}$$

In some publications the $E_1(x)$ function is denoted by $-Ei(-x)$; that is, $E_1(x) = -Ei(-x)$. In using tables of the exponential function, caution should always be exercised so as not to confuse $-Ei(-x)$ with $-Ei(x)$, which is defined below.

For negative arguments, the $E_1(x)$ function is frequently denoted by the symbol $Ei(x)$, which is defined by

$$Ei(x) \equiv \int_{-\infty}^x \frac{e^y}{y}\, dy \qquad \text{(H8)}$$

and related to $E_1(-x)$ by

$$-Ei(x) = E_1(-x) = \int_{-x}^\infty e^y \frac{dy}{y}. \qquad \text{(H9)}$$

Graphs of e^{-x} and $E_n(x)$ for $n = 1$, 2, and 3 are presented in Figs. 3C.1 through 3C.6 (from ref. 210). The function $Ei(x)$ is plotted in Figs. 3H.7 through 3H.10 (from ref. 211).

Some approximations that are frequently useful are

$$\frac{e^{-x}}{x+n} < E_n(x) \leq \frac{e^{-x}}{x+n-1}, \quad n \geq 1, \qquad \text{(H10)}$$

$$E_n(x) = \frac{e^{-x}}{x}\{1 - (n/x) + [n(n+1)/x^2] - [n(n+1)(n+2)/x^3] + \ldots\}\,,$$

$$x \gg 1\,, \qquad n = 0\,, \qquad \text{(H11)}$$

$$E_n(x) \cong \{(1 + x + n)/[x + (x + n)^2]\}\, e^{-x}\,,$$

$$x > 1 \quad \text{(ref. 212)}\,, \qquad \text{(H12)}$$

$$Ei(x) \cong e^x\left[\left(\frac{1}{x}\right) + \left(\frac{1}{x^2}\right) + \left(\frac{2!}{x^3}\right) + \left(\frac{3!}{x^4}\right) + \ldots\right]\,,$$

$$x > 10\,. \qquad \text{(H13)}$$

Further information concerning the exponential integrals can be found in ref. 213.

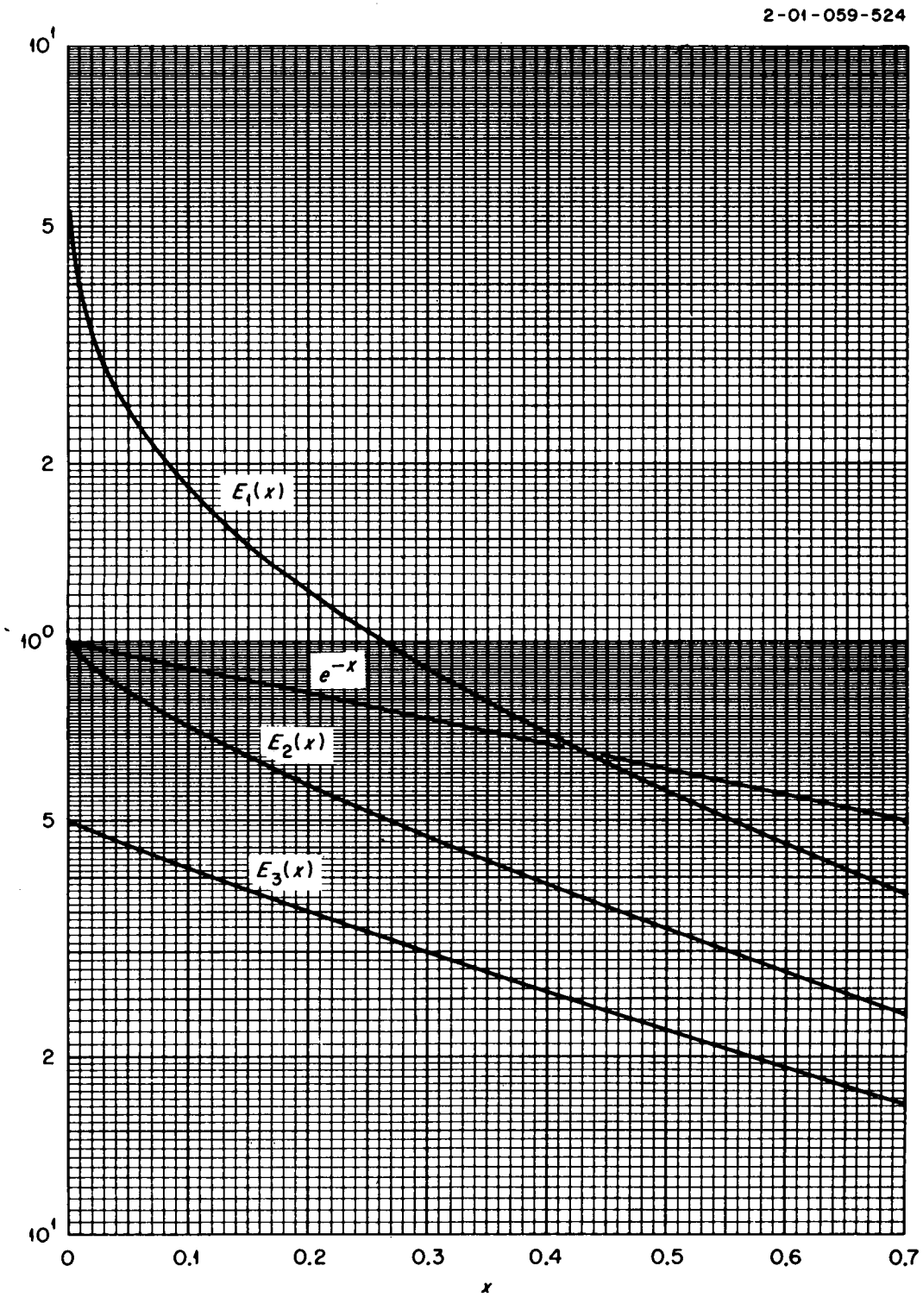

Fig. 3H.1. The Functions e^{-x}, $E_1(x)$, and $E_3(x)$ for $x = 0$ and 0.7. (Plotted from data tabulated in ref. 210.)

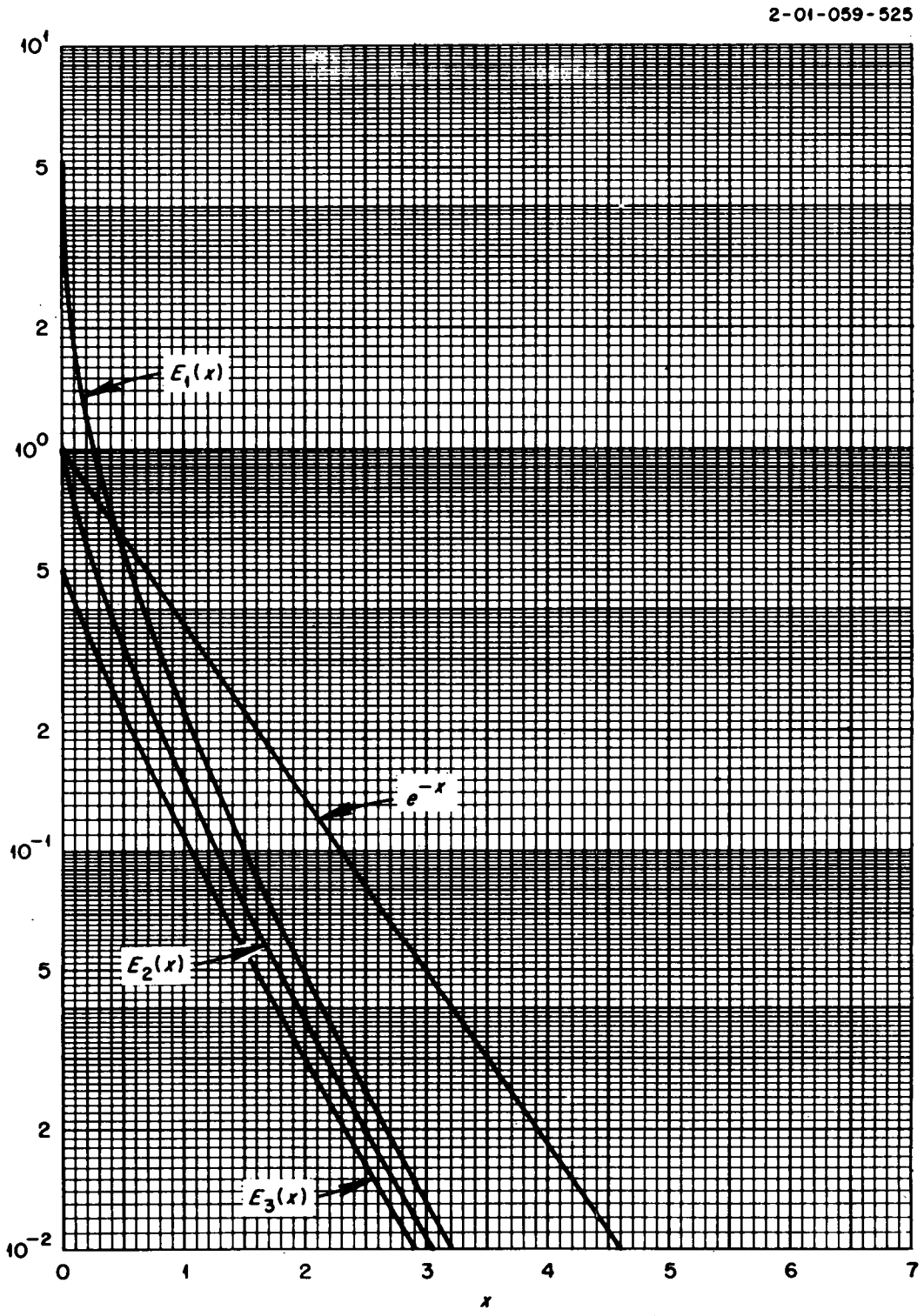

Fig. 3H.2. The Functions e^{-x}, $E_1(x)$, $E_2(x)$, and $E_3(x)$ for $x = 0$ to 3. (Plotted from data tabulated in ref. 210.)

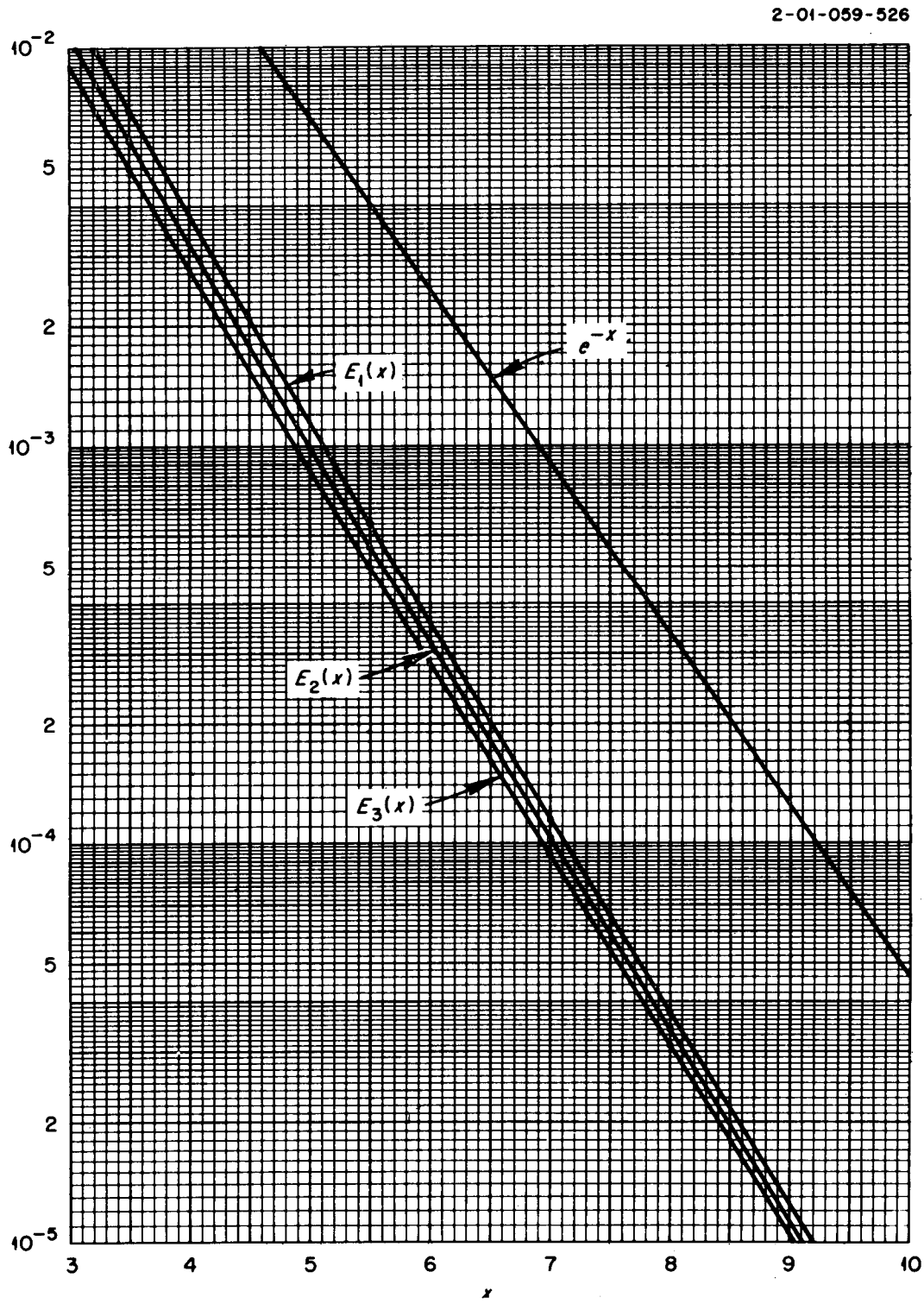

Fig. 3H.3. The Functions e^{-x}, $E_1(x)$, $E_2(x)$, and $E_3(x)$ for $x = 3$ to 9. (Plotted from data tabulated in ref. 210.)

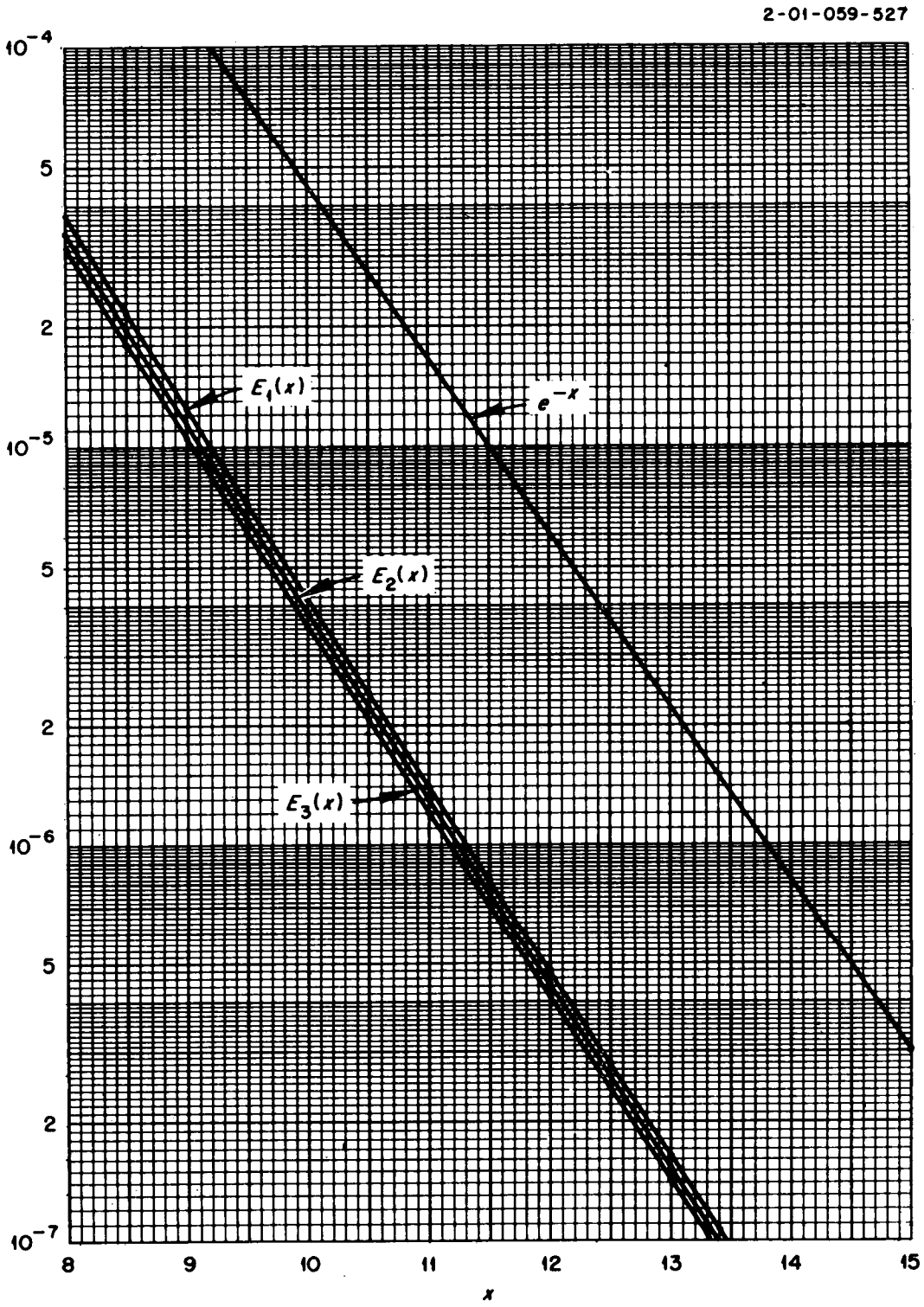

Fig. 3H.4. The Functions e^{-x}, $E_1(x)$, $E_2(x)$, and $E_3(x)$ for x = 8 to 15. (Plotted from data tabulated in ref. 210.)

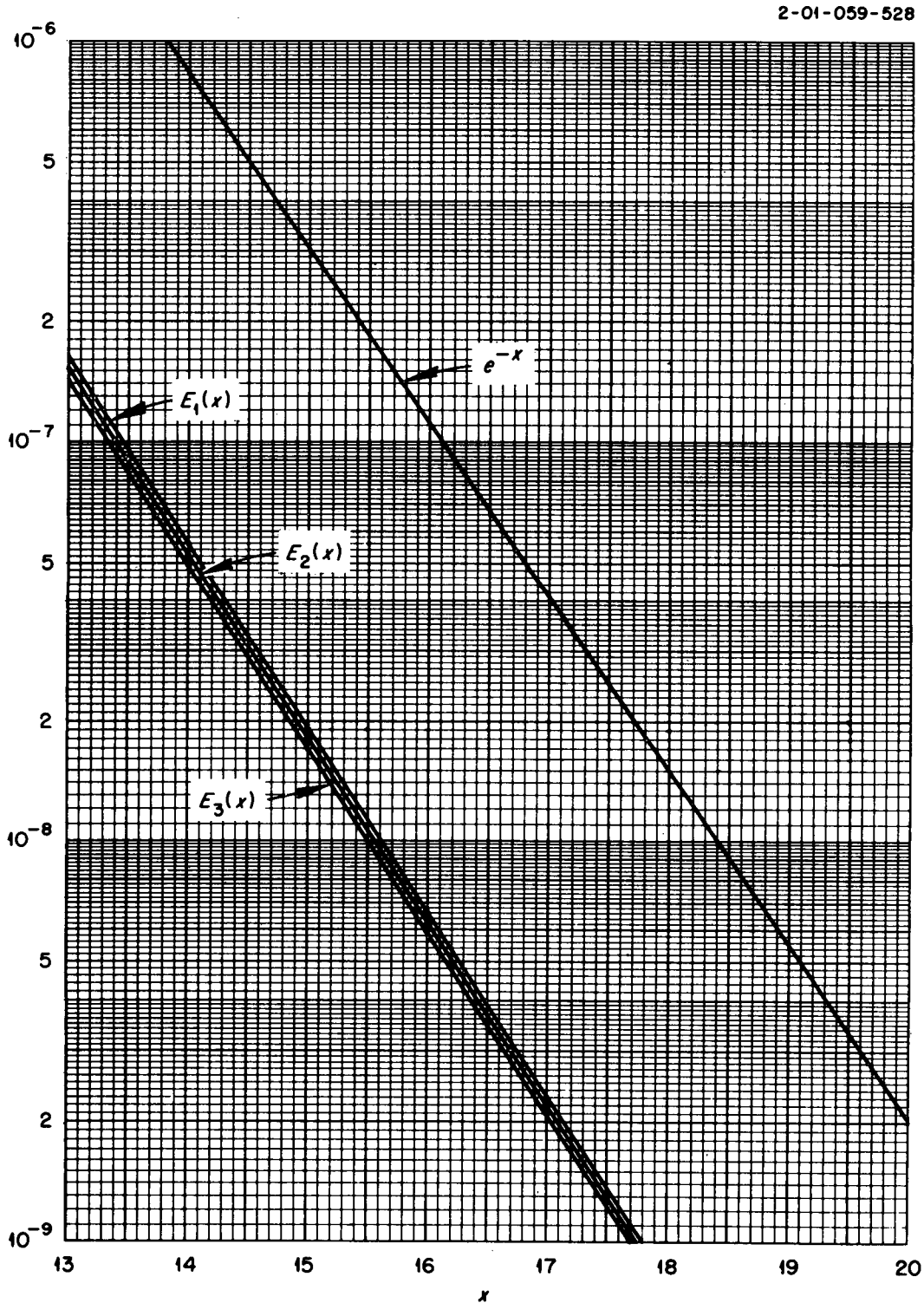

Fig. 3H.5. The Functions e^{-x}, $E_1(x)$, $E_2(x)$, and $E_3(x)$ for x = 13 to 20. (Plotted from data tabulated in ref. 210.)

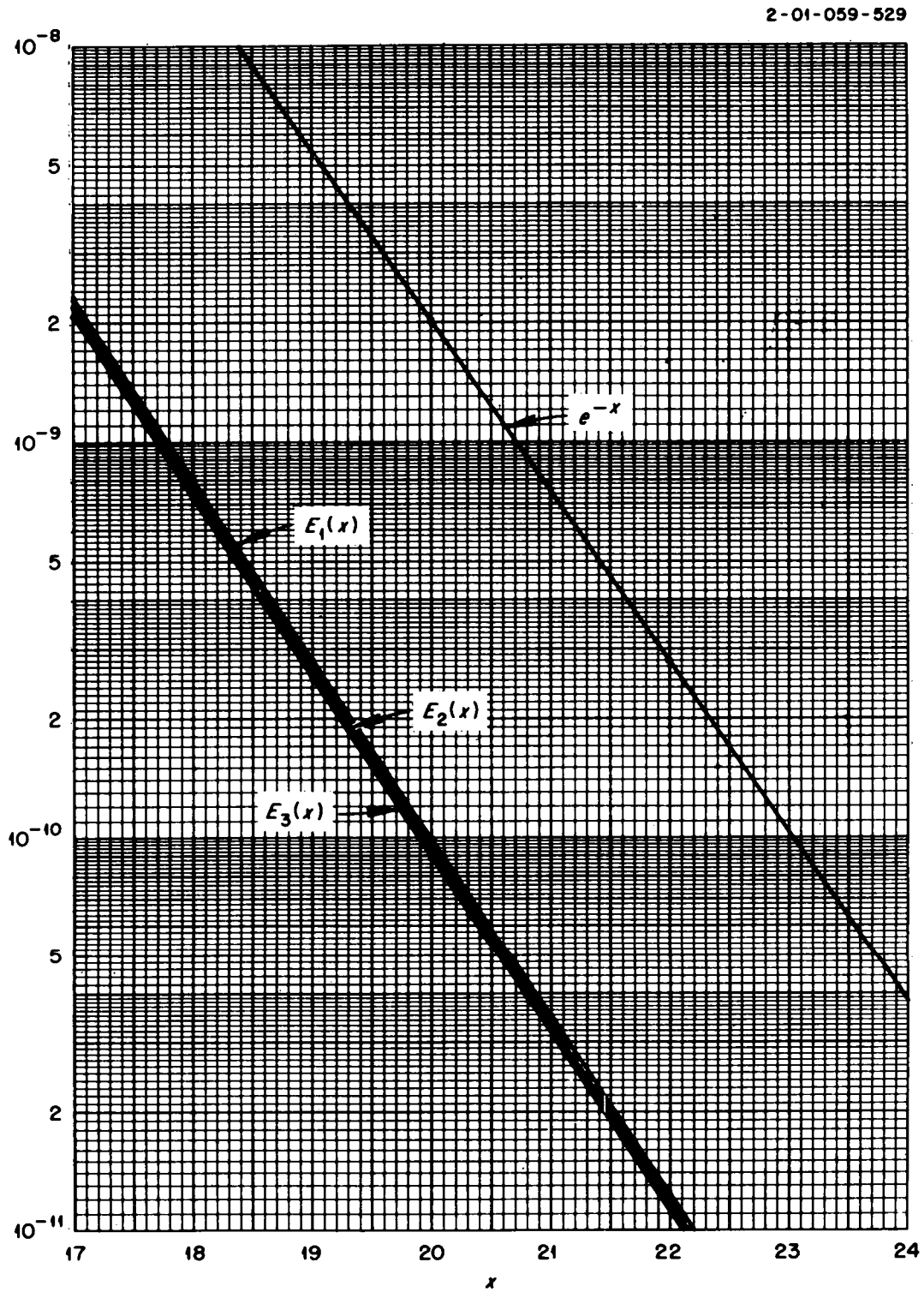

Fig. 3H.6. The Functions e^{-x}, $E_1(x)$, $E_2(x)$, and $E_3(x)$ for x = 17 to 24. (Plotted from data tabulated in ref. 210.)

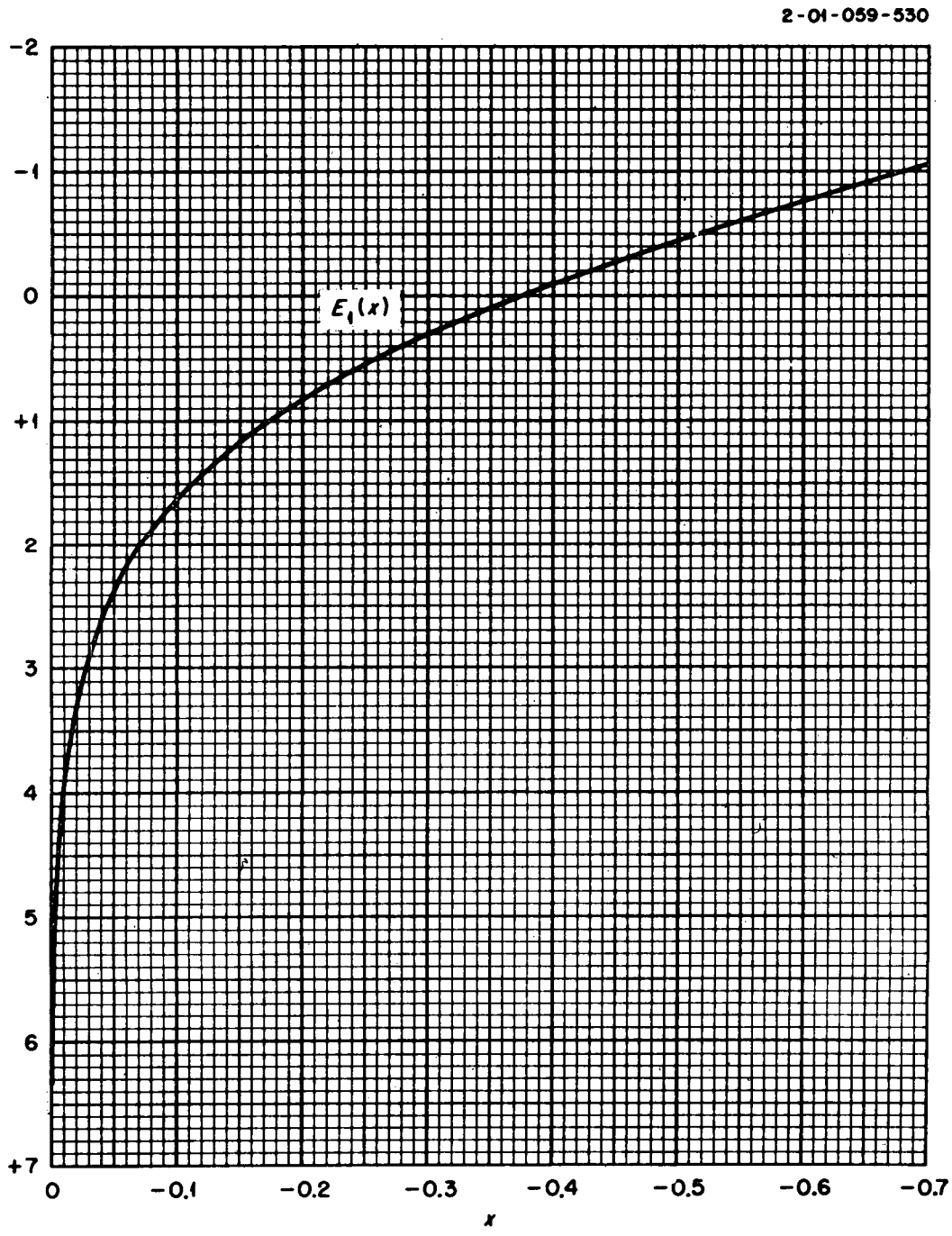

Fig. 3H.7. The Function $E_1(x)$ for Negative Arguments. (Plotted from data tabulated in ref. 211.)

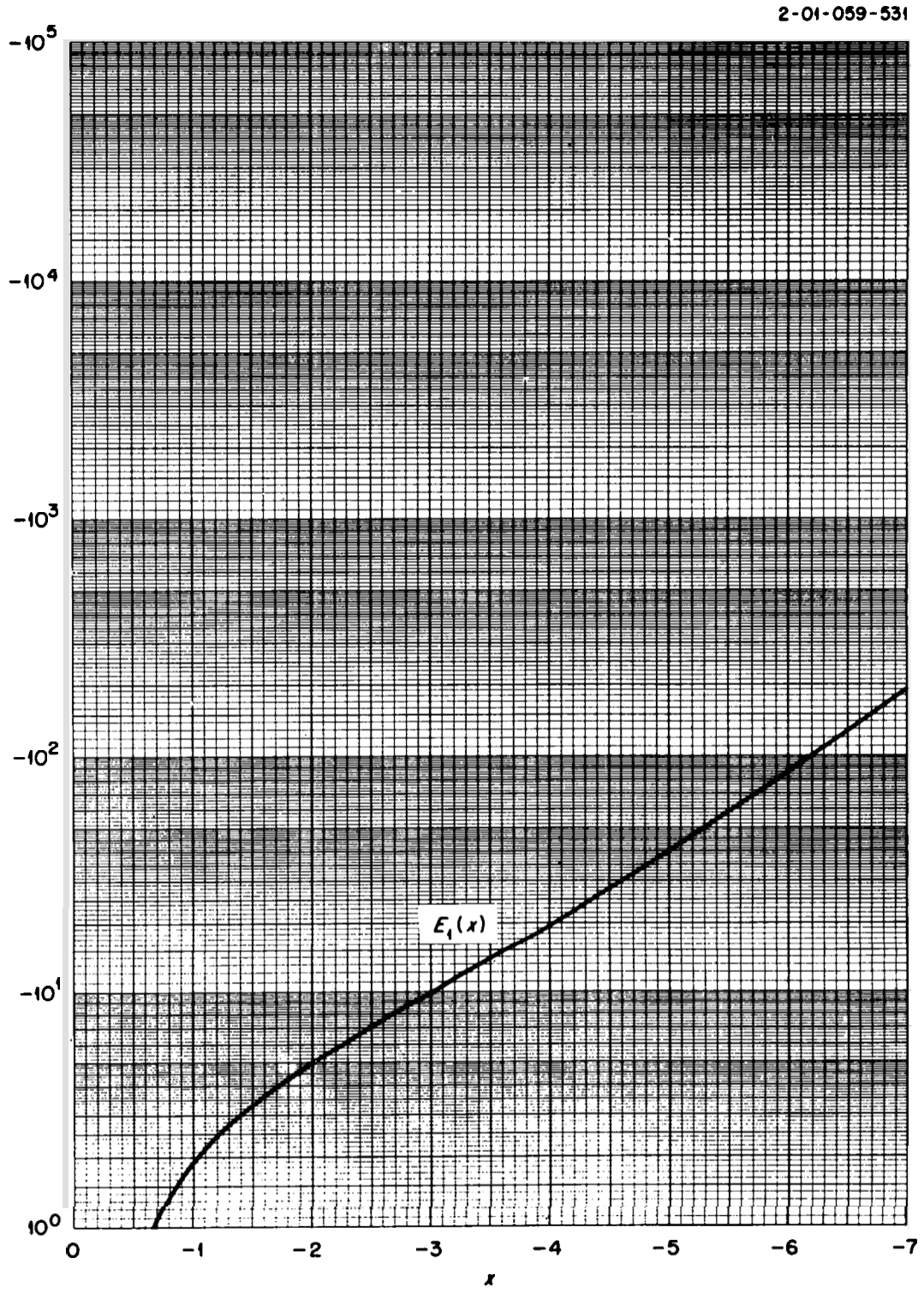

Fig. 3H.8. The Function $E_1(x)$ for Negative Arguments. (Plotted from data tabulated in ref. 211.)

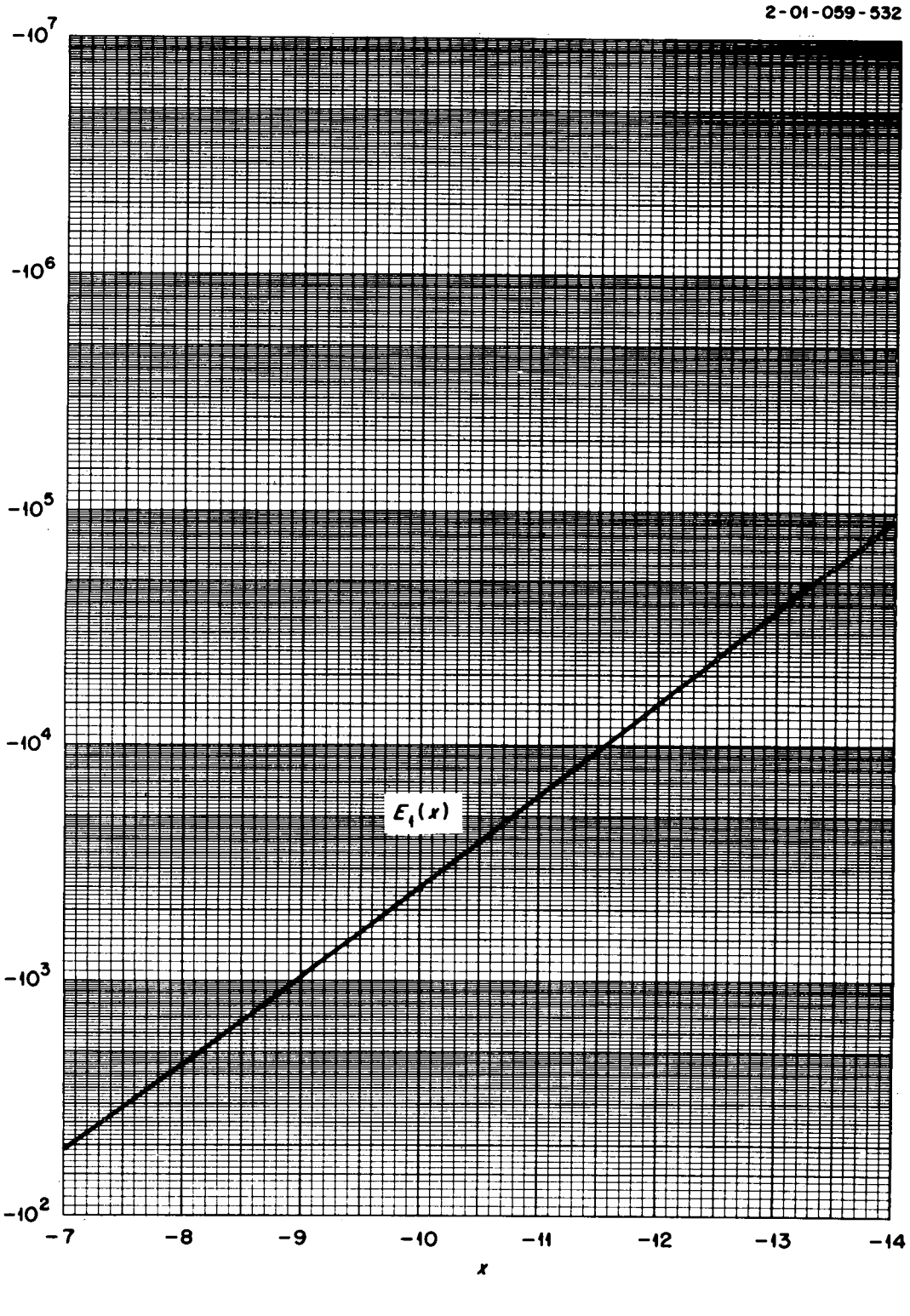

Fig. 3H.9. The Function $E_1(x)$ for Negative Arguments. (Plotted from data tabulated in ref. 211.)

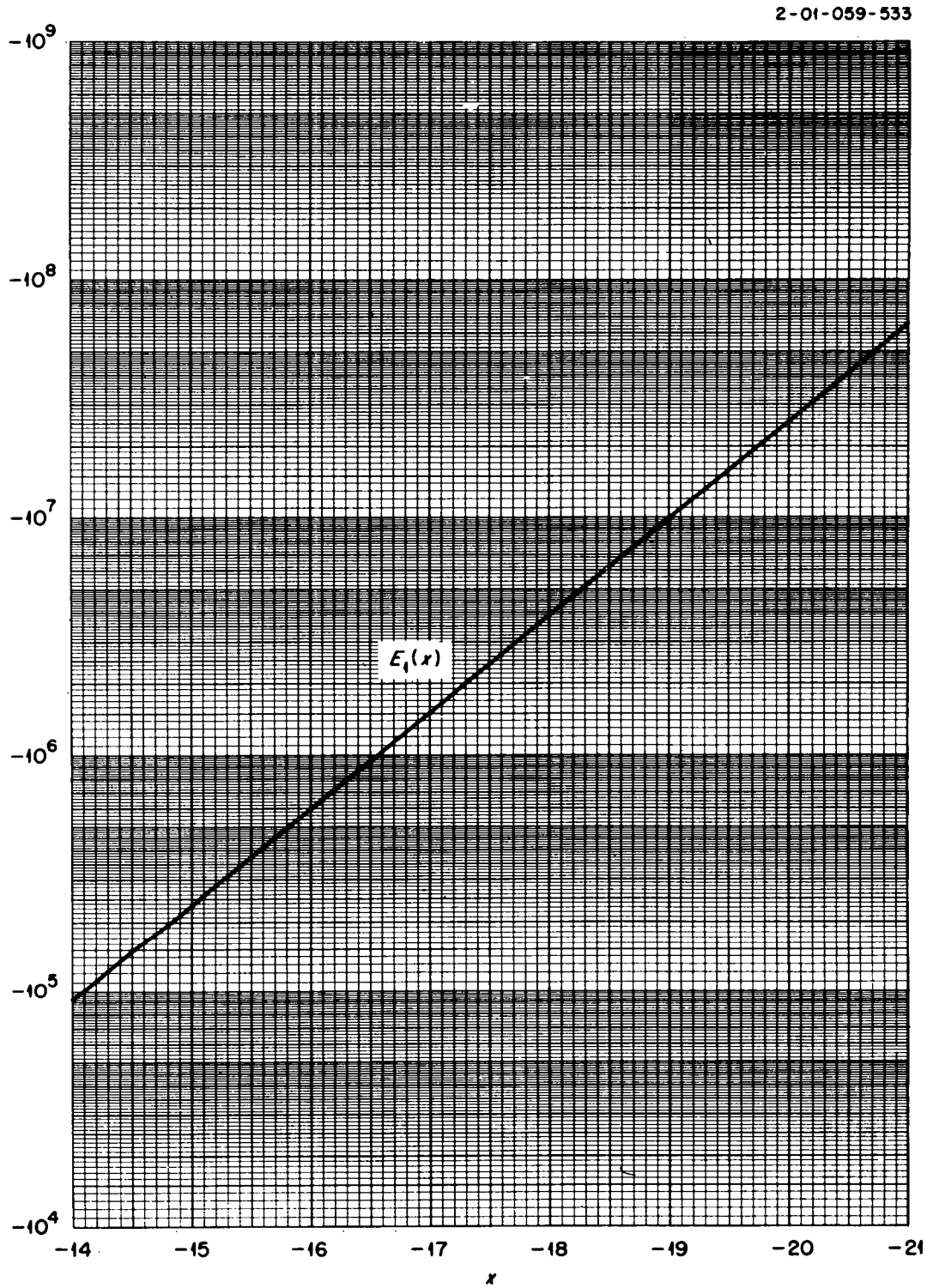

Fig. 3H.10. The Function $E_1(x)$ for Negative Arguments. (Plotted from data tabulated in ref. 211.)

Appendix 3I. Tables of Attenuation Functions for Finite Slab Geometry

This appendix consists of tabulations of attenuation functions for slab shields and disk or rectangular sources obtained by integrating over a point kernel of the form given for gamma rays in Section 3.8.1. The geometry for the disk-source configuration is shown in Figs. 3.7 and 3.8, and that for the rectangular-source configuration is shown in Fig. 3.9. Data are presented for sources with both isotropic and cosine angular distributions, the isotropic-source data being taken from the work of Hubbell *et al.*[114] and the cosine-source data from the work of Trubey.[115]

The variables for the disk source (see Tables 3I.1 and 3I.2) are

$\Gamma(\mu t, r_0/z, \rho/r_0)$ = dose rate,

$G(E)$ = flux-to-dose-rate conversion factor,

S = source strength (particles cm^{-2} sec^{-1}), 4π solid angle,

μt = optical shield thickness (mfp),

r_0/z = ratio of source radius to the source-detector distance,

ρ/r_0 = distance off axis (units of source radius),

$y = \mu t \sec\theta$.

For the case of an isotropic source the unscattered flux attenuation for the dose rate on the disk axis is given by

$$\frac{4\pi\,\Gamma(\mu t, r_0/z, 0)}{SG(E)} = \int_{\mu t}^{\mu t\sqrt{1+(r_0/z)^2}} e^{-y}\frac{2\pi\,dy}{y} = 2\pi\{E_1(\mu t) - E_1(\mu t\sqrt{1+[r_0/z]^2})\}, \quad \text{(I1)}$$

and for the case of a cosine current source (isotropic flux) it is given by

$$\frac{2\,\Gamma(\mu t, r_0/z, 0)}{\Phi_0\,G(E)} = \{E_2(\mu t) - (1+[r_0/z]^2)^{-1/2}\,E_2(\mu t\sqrt{1+[r_0/z]^2})\}, \quad \text{(I2)}$$

where

Φ_0 = isotropic flux at the source plane.

The variables for the rectangular source (see Tables 3I.3 and 3I.4) are

$\Gamma(\mu t, a, b)$ = dose rate on perpendicular to corner,

H, W = height and width of rectangle (cm),

a, b = dimensions of rectangle in units of detector distance, plus S, $G(E)$, and μt as defined above.

For the case of an isotropic source, the unscattered flux attenuation function for the dose rate at a corner position is given by

$$\frac{4\pi\,\Gamma(\mu t, a, b)}{SG(E)} = \int_0^b\int_0^a e^{-\mu r}\frac{dx\,dy}{r^2} \approx \frac{\pi}{2}[E_1(\mu t) - E_1(\mu t\sqrt{1+a^2})], \quad \text{for } a \cong b > 1, \quad \text{(I3)}$$

and for the cosine current source (isotropic flux) it is given by

$$\frac{2\Gamma(\mu t, a, b)}{\Phi_0\,G(E)} = \frac{1}{2\pi}\int_0^b\int_0^a e^{-\mu r}\frac{3}{r}\frac{dx\,dy}{r^2} \approx \frac{1}{4}[E_2(\mu t) - (1/\sqrt{1+a^2})\,E_2(\mu t\sqrt{1+a^2})], \quad \text{for } a \cong b > 1, \quad \text{(I4)}$$

where $r^2 = x^2 + y^2 + z^2$.

Table 31.1. Unscattered Flux from a Disk Source with an Isotropic Angular Distribution[a]

r_0/z	μt	$4\pi\Gamma/S\ G(E)$									
		$\rho/r_0 = 0$	$\rho/r_0 = 0.2$	$\rho/r_0 = 0.5$	$\rho/r_0 = 0.8$	$\rho/r_0 = 1.0$	$\rho/r_0 = 1.2$	$\rho/r_0 = 1.5$	$\rho/r_0 = 2.0$	$\rho/r_0 = 5.0$	$\rho/r_0 = 10.0$
10.0	0	1.45(1)[b]	1.44(1)	1.36(1)	1.15(1)	7.39(0)	3.60(0)	1.83(0)	9.00(−1)	1.28(−1)	3.16(−2)
	0.01	1.39(1)	1.38(1)	1.31(1)	1.10(1)	7.03(0)	3.33(0)	1.62(0)	7.53(−1)	7.84(−2)	1.17(−2)
	0.02	1.34(1)	1.33(1)	1.26(1)	1.06(1)	6.71(0)	3.08(0)	1.44(0)	6.31(−1)	4.81(−2)	4.31(−3)
	0.05	1.20(1)	1.19(1)	1.13(1)	9.54(0)	5.86(0)	2.47(0)	1.02(0)	3.76(−1)	1.13(−2)	
	0.1	1.01(1)	1.00(1)	9.57(0)	8.11(0)	4.81(0)	1.76(0)	5.99(−1)	1.66(−1)		
	0.2	7.38(0)	7.34(0)	7.10(0)	6.12(0)	3.45(0)	9.94(−1)	2.09(−1)	4.56(−2)	1.36(−3)	1.34(−4)
	0.5	3.50(0)	3.50(0)	3.46(0)	3.17(0)	1.66(0)	2.51(−1)	2.74(−2)	3.45(−3)	2.17(−5)	1.72(−5)
	1.0	1.38(0)	1.38(0)	1.38(0)	1.32(0)	6.63(−1)	4.25(−2)	1.03(−3)	2.49(−4)		
	2.0	3.08(−1)	3.08(−1)	3.08(−1)	3.05(−1)	1.49(−1)	2.11(−3)				
	5.0	7.22(−3)	7.22(−3)	7.21(−3)	7.21(−3)	3.54(−3)					
	10.0	2.61(−5)	2.61(−5)	2.61(−5)	2.61(−5)	1.29(−5)					
5.0	0	1.02(1)	1.01(1)	9.42(0)	7.65(0)	5.37(0)	3.25(0)	1.77(0)	8.90(−1)	1.28(−1)	3.16(−2)
	0.01	9.98(0)	9.87(0)	9.19(0)	7.44(0)	5.20(0)	3.11(0)	1.67(0)	8.13(−1)	1.00(−1)	1.92(−2)
	0.02	9.74(0)	9.62(0)	8.96(0)	7.25(0)	5.04(0)	2.98(0)	1.57(0)	7.43(−1)	7.83(−2)	1.17(−2)
	0.05	9.04(0)	8.94(0)	8.32(0)	6.71(0)	4.60(0)	2.63(0)	1.31(0)	5.70(−1)	3.76(−2)	2.63(−3)
	0.1	8.01(0)	7.92(0)	7.38(0)	5.93(0)	3.97(0)	2.15(0)	9.78(−1)	3.70(−1)	1.12(−2)	1.01(−3)
	0.2	6.35(0)	6.28(0)	5.88(0)	4.71(0)	3.17(0)	1.49(0)	5.66(−1)	1.62(−1)	3.48(−3)	3.16(−4)
	0.5	3.37(0)	3.35(0)	3.19(0)	2.60(0)	1.55(0)	5.79(−1)	1.37(−1)	2.19(−2)	1.62(−4)	4.90(−6)
	1.0	1.37(0)	1.37(0)	1.34(0)	1.14(0)	6.35(−1)	1.67(−1)	1.73(−2)	1.02(−3)		
	2.0	3.08(−1)	3.08(−1)	3.06(−1)	2.80(−1)	1.42(−1)	2.06(−2)	5.93(−4)			
	5.0	7.22(−3)	7.22(−3)	7.21(−3)	7.08(−3)	3.48(−3)	1.04(−4)	7.67(−7)			
	10.0	2.61(−5)	2.61(−5)	2.61(−5)	2.61(−5)	1.27(−5)	2.71(−8)				
2.0	0	5.06(0)	4.98(0)	4.53(0)	3.69(0)	2.96(0)	2.26(0)	1.49(0)	8.26(−1)	1.27(−1)	3.15(−2)
	0.01	4.98(0)	4.90(0)	4.46(0)	3.62(0)	2.90(0)	2.21(0)	1.45(0)	7.95(−1)	1.15(−1)	2.58(−2)
	0.02	4.90(0)	4.82(0)	4.39(0)	3.56(0)	2.84(0)	2.16(0)	1.41(0)	7.66(−1)	1.04(−1)	2.11(−2)
	0.05	4.68(0)	4.61(0)	4.19(0)	3.38(0)	2.69(0)	2.02(0)	1.30(0)	6.84(−1)	7.74(−2)	1.16(−2)
	0.1	4.34(0)	4.27(0)	3.87(0)	3.11(0)	2.45(0)	1.81(0)	1.13(0)	5.68(−1)	4.74(−2)	4.30(−3)
	0.2	3.73(0)	3.66(0)	3.32(0)	2.63(0)	2.03(0)	1.47(0)	8.69(−1)	3.94(−1)	1.79(−2)	
	0.5	2.38(0)	2.34(0)	2.11(0)	1.63(0)	1.21(0)	8.07(−1)	4.09(−1)	1.38(−1)	1.72(−3)	6.69(−5)
	1.0	1.16(0)	1.14(0)	1.03(0)	7.78(−1)	5.43(−1)	3.26(−1)	1.30(−1)	2.73(−2)	1.87(−5)	
	2.0	2.93(−1)	2.90(−1)	2.69(−1)	2.03(−1)	1.32(−1)	6.64(−2)	1.73(−2)	1.62(−3)		
	5.0	7.21(−3)	7.20(−3)	7.04(−3)	5.76(−3)	3.29(−3)	1.09(−3)	9.00(−5)	6.03(−7)		
	10.0	2.61(−5)	2.61(−5)	2.61(−5)	2.31(−5)	1.22(−5)	2.29(−6)	2.52(−8)			
1.0	0	2.18(0)	2.15(0)	1.99(0)	1.72(0)	1.51(0)	1.30(0)	1.01(0)	6.66(−1)	1.23(−1)	3.13(−2)
	0.01	2.15(0)	2.12(0)	1.96(0)	1.70(0)	1.49(0)	1.26(0)	9.95(−1)	6.52(−1)	1.17(−1)	2.83(−2)
	0.02	2.13(0)	2.10(0)	1.94(0)	1.68(0)	1.47(0)	1.20(0)	9.78(−1)	6.38(−1)	1.11(−1)	2.56(−2)
	0.05	2.05(0)	2.02(0)	1.87(0)	1.61(0)	1.41(0)	1.20(0)	9.29(−1)	5.99(−1)	9.57(−2)	1.90(−2)
	0.1	1.93(0)	1.90(0)	1.76(0)	1.51(0)	1.31(0)	1.12(0)	8.53(−1)	5.39(−1)	7.45(−2)	1.15(−2)
	0.2	1.71(0)	1.69(0)	1.55(0)	1.32(0)	1.14(0)	9.62(−1)	7.20(−1)	4.37(−1)	4.52(−2)	4.24(−3)
	0.5	1.20(0)	1.18(0)	1.07(0)	8.96(−1)	7.56(−1)	6.18(−1)	4.37(−1)	2.35(−1)	1.02(−2)	3.96(−4)
	1.0	6.64(−1)	6.51(−1)	5.85(−1)	4.73(−1)	3.87(−1)	3.02(−1)	1.95(−1)	8.65(−2)	1.06(−3)	2.27(−6)
	2.0	2.05(−1)	2.01(−1)	1.77(−1)	1.37(−1)	1.06(−1)	7.67(−2)	4.22(−2)	1.29(−2)	6.65(−6)	
	5.0	6.54(−3)	6.42(−3)	5.70(−3)	4.21(−3)	2.95(−3)	1.79(−3)	6.51(−4)	7.40(−5)		
	10.0	2.58(−5)	2.56(−5)	2.41(−5)	1.78(−5)	1.14(−5)	5.57(−6)	1.13(−6)	2.66(−8)		
0.5	0	7.01(−1)	6.96(−1)	6.71(−1)	6.27(−1)	5.91(−1)	5.52(−1)	4.90(−1)	3.92(−1)	1.10(−1)	3.03(−2)
	0.01	6.94(−1)	6.89(−1)	6.63(−1)	6.20(−1)	5.85(−1)	5.45(−1)	4.84(−1)	3.86(−1)	1.07(−1)	2.88(−2)
	0.02	6.86(−1)	6.81(−1)	6.56(−1)	6.14(−1)	5.78(−1)	5.39(−1)	4.78(−1)	3.81(−1)	1.04(−1)	2.74(−2)
	0.05	6.65(−1)	6.60(−1)	6.35(−1)	5.93(−1)	5.58(−1)	5.20(−1)	4.60(−1)	3.65(−1)	9.60(−2)	2.35(−2)
	0.1	6.31(−1)	6.26(−1)	6.02(−1)	5.61(−1)	5.27(−1)	4.90(−1)	4.32(−1)	3.40(−1)	8.40(−2)	1.83(−2)
	0.2	5.67(−1)	5.63(−1)	5.40(−1)	5.02(−1)	4.70(−1)	4.35(−1)	3.81(−1)	2.96(−1)	6.44(−2)	1.10(−2)
	0.5	4.13(−1)	4.09(−1)	3.91(−1)	3.60(−1)	3.34(−1)	3.05(−1)	2.62(−1)	1.95(−1)	2.91(−2)	2.41(−3)
	1.0	2.44(−1)	2.41(−1)	2.28(−1)	2.06(−1)	1.89(−1)	1.70(−1)	1.41(−1)	9.74(−2)	7.83(−3)	2.35(−4)
	2.0	8.47(−2)	8.36(−2)	7.79(−2)	6.85(−2)	6.09(−2)	5.29(−2)	4.12(−2)	2.50(−2)	6.16(−4)	
	5.0	3.59(−3)	3.52(−3)	3.17(−3)	2.60(−3)	2.16(−3)	1.72(−3)	1.14(−3)	4.77(−4)	2.28(−7)	
	10.0	1.89(−5)	1.84(−5)	1.61(−5)	1.24(−5)	9.55(−6)	6.86(−6)	3.45(−6)	9.02(−7)		

Table 3I.1. (continued)

r_0/z	μt	$4\pi\Gamma/S\ G(E)$									
		$\rho/r_0 = 0$	$\rho/r_0 = 0.2$	$\rho/r_0 = 0.5$	$\rho/r_0 = 0.8$	$\rho/r_0 = 1.0$	$\rho/r_0 = 1.2$	$\rho/r_0 = 1.5$	$\rho/r_0 = 2.0$	$\rho/r_0 = 5.0$	$\rho/r_0 = 10.0$
0.2	0	1.23(−1)	1.23(−1)	1.22(−1)	1.20(−1)	1.19(−1)	1.17(−1)	1.14(−1)	1.07(−1)	6.28(−2)	2.52(−2)
	0.01	1.22(−1)	1.22(−1)	1.21(−1)	1.19(−1)	1.18(−1)	1.16(−1)	1.12(−1)	1.06(−1)	6.27(−2)	2.51(−2)
	0.02	1.21(−1)	1.21(−1)	1.20(−1)	1.18(−1)	1.16(−1)	1.14(−1)	1.11(−1)	1.05(−1)	6.11(−2)	2.41(−2)
	0.05	1.17(−1)	1.17(−1)	1.16(−1)	1.14(−1)	1.13(−1)	1.11(−1)	1.08(−1)	1.01(−1)	5.85(−2)	2.25(−2)
	0.1	1.11(−1)	1.11(−1)	1.10(−1)	1.09(−1)	1.07(−1)	1.05(−1)	1.02(−1)	9.60(−2)	5.46(−2)	2.02(−2)
	0.2	1.01(−1)	1.01(−1)	9.96(−2)	9.81(−2)	9.66(−2)	9.50(−2)	9.20(−2)	8.62(−2)	4.74(−2)	1.61(−2)
	0.5	7.44(−2)	7.43(−2)	7.35(−2)	7.22(−2)	7.10(−2)	6.96(−2)	6.71(−2)	6.23(−2)	3.10(−2)	8.26(−3)
	1.0	4.49(−2)	4.48(−2)	4.43(−2)	4.33(−2)	4.25(−2)	4.14(−2)	3.97(−2)	3.62(−2)	1.53(−2)	2.71(−3)
	2.0	1.64(−2)	1.63(−2)	1.60(−2)	1.56(−2)	1.52(−2)	1.47(−2)	1.39(−2)	1.23(−2)	3.76(−3)	2.94(−4)
	5.0	7.91(−4)	7.87(−4)	7.66(−4)	7.29(−4)	6.97(−4)	6.60(−4)	5.97(−4)	4.83(−4)	5.71(−5)	3.77(−7)
	10.0	5.09(−6)	5.05(−6)	4.83(−6)	4.45(−6)	4.13(−6)	3.78(−6)	3.20(−6)	2.27(−6)	5.99(−8)	
0.1	0	3.13(−2)	3.12(−2)	3.12(−2)	3.11(−2)	3.10(−2)	3.08(−2)	3.06(−2)	3.01(−2)	2.51(−2)	1.57(−2)
	0.01	3.09(−2)	3.09(−2)	3.09(−2)	3.08(−2)	3.06(−2)	3.05(−2)	3.03(−2)	2.98(−2)	2.48(−2)	1.55(−2)
	0.02	3.06(−2)	3.06(−2)	3.06(−2)	3.04(−2)	3.03(−2)	3.02(−2)	3.00(−2)	2.95(−2)	2.45(−2)	1.53(−2)
	0.05	2.97(−2)	2.97(−2)	2.97(−2)	2.95(−2)	2.94(−2)	2.93(−2)	2.91(−2)	2.86(−2)	2.37(−2)	1.46(−2)
	0.1	2.83(−2)	2.83(−2)	2.82(−2)	2.81(−2)	2.80(−2)	2.79(−2)	2.76(−2)	2.72(−2)	2.24(−2)	1.36(−2)
	0.2	2.56(−2)	2.56(−2)	2.55(−2)	2.54(−2)	2.53(−2)	2.52(−2)	2.50(−2)	2.45(−2)	2.00(−2)	1.18(−2)
	0.5	1.89(−2)	1.89(−2)	1.89(−2)	1.88(−2)	1.87(−2)	1.86(−2)	1.84(−2)	1.80(−2)	1.43(−2)	7.75(−3)
	1.0	1.15(−2)	1.15(−2)	1.14(−2)	1.14(−2)	1.13(−2)	1.12(−2)	1.11(−2)	1.08(−2)	8.20(−3)	3.82(−3)
	2.0	4.21(−3)	4.21(−3)	4.19(−3)	4.16(−3)	4.13(−3)	4.09(−3)	4.03(−3)	3.90(−3)	2.68(−3)	9.31(−4)
	5.0	2.08(−4)	2.08(−4)	2.06(−4)	2.04(−4)	2.04(−4)	2.01(−4)	1.93(−4)	1.82(−4)	9.37(−5)	1.36(−5)
	10.0	1.39(−6)	1.38(−6)	1.37(−6)	1.34(−6)	1.31(−6)	1.28(−6)	1.22(−6)	1.10(−6)	3.53(−7)	1.26(−8)

[a] From ref. 114

[b] Read: 1.45×10^{1}, etc.

Table 31.2. Unscattered Flux from a Disk Source with a Cosine Angular Distribution (Isotropic Flux)

r_0/z	μt	$2\Gamma/\Phi_0 G(E)$									
		$\rho/r_0 = 0$	$\rho/r_0 = 0.2$	$\rho/r_0 = 0.5$	$\rho/r_0 = 0.8$	$\rho/r_0 = 1.0$	$\rho/r_0 = 1.2$	$\rho/r_0 = 1.5$	$\rho/r_0 = 2.0$	$\rho/r_0 = 5.0$	$\rho/r_0 = 10.0$
10.0	0	9.01(−1)[a]	8.97(−1)	8.77(−1)	7.88(−1)	4.30(−1)	9.65(−2)	2.79(−2)	8.56(−3)	4.18(−4)	5.06(−5)
	0.01	8.78(−1)	8.75(−1)	8.55(−1)	7.70(−1)	4.19(−1)	9.10(−2)	2.51(−2)	7.25(−3)	2.57(−4)	1.87(−5)
	0.02	8.56(−1)	8.53(−1)	8.35(−1)	7.53(−1)	4.08(−1)	8.60(−2)	2.27(−2)	6.15(−3)	1.59(−4)	6.96(−6)
	0.03	8.35(−1)	8.33(−1)	8.15(−1)	7.36(−1)	3.97(−1)	8.13(−2)	2.05(−2)	5.23(−3)	9.80(−5)	2.59(−6)
	0.1	7.08(−1)	7.06(−1)	6.95(−1)	6.35(−1)	3.36(−1)	5.65(−2)	1.06(−2)	1.77(−3)	3.59(−6)	2.75(−9)
	0.2	5.70(−1)	5.70(−1)	5.64(−1)	5.23(−1)	2.71(−1)	3.57(−2)	4.55(−3)	4.24(−4)	3.73(−8)	1.84(−13)
	0.5	3.26(−1)	3.26(−1)	3.26(−1)	3.12(−1)	1.57(−1)	1.12(−2)	5.01(−4)	9.12(−6)	8.01(−14)	1.13(−25)
	1.0	1.48(−1)	1.48(−1)	1.48(−1)	1.46(−1)	7.19(−2)	2.16(−3)	1.98(−5)	2.73(−8)	6.52(−23)	*b*
	2.0	3.75(−2)	3.75(−2)	3.75(−2)	3.74(−2)	1.83(−2)	1.19(−4)	5.43(−8)	4.86(−13)	*b*	*b*
	5.0	9.96(−4)	9.96(−4)	9.96(−4)	9.96(−4)	4.91(−4)	5.05(−8)	3.72(−15)	*b*	*b*	*b*
	10.0	3.83(−6)	3.81(−6)	3.83(−6)	3.82(−6)	1.89(−6)	2.85(−13)	*b*	*b*	*b*	*b*
5.0	0	8.04(−1)	7.98(−1)	7.61(−1)	6.30(−1)	3.83(−1)	1.54(−1)	5.25(−2)	1.68(−2)	8.35(−4)	1.01(−4)
	0.01	7.88(−1)	7.82(−1)	7.46(−1)	6.18(−1)	3.74(−1)	1.49(−1)	4.98(−2)	1.54(−2)	6.55(−4)	6.15(−5)
	0.02	7.72(−1)	7.67(−1)	7.32(−1)	6.06(−1)	3.66(−1)	1.44(−1)	4.72(−2)	1.42(−2)	5.13(−4)	3.75(−5)
	0.03	7.57(−1)	7.52(−1)	7.18(−1)	5.95(−1)	3.58(−1)	1.40(−1)	4.48(−2)	1.31(−2)	4.03(−4)	2.28(−5)
	0.1	6.60(−1)	6.56(−1)	6.28(−1)	5.23(−1)	3.09(−1)	1.12(−1)	3.14(−2)	7.41(−3)	7.51(−5)	7.24(−7)
	0.2	5.46(−1)	5.43(−1)	5.23(−1)	4.39(−1)	2.54(−1)	8.37(−2)	1.94(−2)	3.42(−3)	7.13(−6)	5.49(−9)
	0.5	3.23(−1)	3.22(−1)	3.15(−1)	2.71(−1)	1.50(−1)	3.84(−2)	5.34(−3)	4.07(−4)	7.94(−9)	3.19(−15)
	1.0	1.48(−1)	1.48(−1)	1.47(−1)	1.31(−1)	6.95(−2)	1.25(−2)	8.10(−4)	1.66(−5)	1.57(−13)	2.24(−25)
	2.0	3.75(−2)	3.75(−2)	3.75(−2)	3.52(−2)	1.79(−2)	1.77(−3)	2.77(−5)	4.61(−8)	1.25(−22)	*b*
	5.0	9.96(−4)	9.96(−4)	9.96(−4)	9.84(−4)	4.82(−4)	1.01(−5)	2.90(−9)	3.20(−15)	*b*	*b*
	10.0	3.83(−6)	3.83(−6)	3.83(−6)	3.83(−6)	1.87(−6)	3.73(−9)	1.64(−15)	*b*	*b*	*b*
2.0	0	5.53(−1)	5.44(−1)	4.94(−1)	3.84(−1)	2.81(−1)	1.86(−1)	9.50(−2)	3.70(−2)	2.06(−3)	2.52(−4)
	0.01	5.45(−1)	5.36(−1)	4.87(−1)	3.78(−1)	2.77(−1)	1.82(−1)	9.27(−2)	3.57(−2)	1.87(−3)	2.06(−4)
	0.02	5.37(−1)	5.28(−1)	4.79(−1)	3.72(−1)	2.72(−1)	1.79(−1)	9.04(−2)	3.47(−2)	1.69(−3)	1.69(−4)
	0.03	5.29(−1)	5.21(−1)	4.73(−1)	3.67(−1)	2.68(−1)	1.75(−1)	8.82(−2)	3.33(−2)	1.54(−3)	1.39(−4)
	0.1	4.78(−1)	4.71(−1)	4.27(−1)	3.30(−1)	2.39(−1)	1.53(−1)	7.43(−2)	2.60(−2)	7.77(−4)	3.46(−5)
	0.2	4.14(−1)	4.08(−1)	3.70(−1)	2.84(−1)	2.03(−1)	1.27(−1)	5.85(−2)	1.85(−2)	2.96(−4)	4.80(−6)
	0.5	2.71(−1)	2.67(−1)	2.43(−1)	1.85(−1)	1.28(−1)	7.48(−2)	2.94(−2)	6.85(−3)	1.72(−5)	1.35(−8)
	1.0	1.36(−1)	1.34(−1)	1.23(−1)	9.37(−2)	5.20(−2)	3.29(−2)	1.02(−2)	1.46(−3)	1.74(−7)	8.95(−13)
	2.0	3.67(−2)	3.64(−2)	3.43(−2)	2.64(−2)	1.65(−2)	7.38(−3)	1.49(−3)	8.58(−5)	2.54(−11)	5.82(−21)
	5.0	9.96(−4)	9.95(−4)	9.79(−4)	8.07(−4)	4.57(−4)	1.37(−4)	8.77(−6)	3.79(−8)	2.39(−22)	*b*
	10.0	3.83(−6)	3.83(−6)	3.82(−6)	3.42(−6)	1.80(−6)	3.07(−7)	3.29(−9)	2.17(−13)	*b*	*b*
1.0	0	2.93(−1)	2.88(−1)	2.61(−1)	2.15(−1)	1.79(−1)	1.43(−1)	9.85(−2)	5.18(−2)	3.93(−3)	4.98(−4)
	0.01	2.89(−1)	2.84(−1)	2.57(−1)	2.12(−1)	1.76(−1)	1.41(−1)	9.69(−2)	5.08(−2)	3.74(−3)	4.51(−4)
	0.02	2.86(−1)	2.81(−1)	2.54(−1)	2.09(−1)	1.74(−1)	1.39(−1)	9.54(−2)	4.98(−2)	3.56(−3)	4.08(−4)
	0.03	2.83(−1)	2.77(−1)	2.51(−1)	2.07(−1)	1.72(−1)	1.37(−1)	9.38(−2)	4.88(−2)	3.38(−3)	3.69(−4)
	0.1	2.60(−1)	2.55(−1)	2.31(−1)	1.89(−1)	1.56(−1)	1.24(−1)	8.37(−2)	4.23(−2)	2.39(−3)	1.84(−4)
	0.2	2.31(−1)	2.27(−1)	2.04(−1)	1.66(−1)	1.37(−1)	1.08(−1)	7.12(−2)	3.46(−2)	1.46(−3)	6.79(−5)
	0.5	1.62(−1)	1.59(−1)	1.43(−1)	1.14(−1)	9.20(−2)	7.05(−2)	4.42(−2)	1.91(−2)	3.35(−4)	3.48(−6)
	1.0	9.03(−2)	8.84(−2)	7.86(−2)	6.16(−2)	4.83(−2)	3.55(−2)	2.04(−2)	7.27(−3)	3.01(−5)	2.57(−8)
	2.0	2.82(−2)	2.76(−2)	2.44(−2)	1.85(−2)	1.39(−2)	9.51(−3)	4.68(−3)	1.16(−3)	2.78(−7)	1.63(−12)
	5.0	9.29(−4)	9.13(−4)	8.17(−4)	6.02(−4)	4.14(−4)	2.41(−4)	7.93(−5)	7.24(−6)	4.16(−13)	8.52(−25)
	10.0	3.80(−6)	3.77(−6)	3.54(−6)	2.65(−6)	1.68(−6)	7.93(−7)	1.45(−7)	2.78(−9)	1.84(−22)	*b*
0.5	0	1.06(−1)	1.04(−1)	9.91(−2)	9.01(−2)	8.27(−2)	7.47(−2)	6.28(−2)	4.50(−2)	6.60(−3)	9.52(−4)
	0.01	1.04(−1)	1.03(−1)	9.81(−2)	8.91(−2)	8.17(−2)	7.39(−2)	6.20(−2)	4.44(−2)	6.43(−3)	9.05(−4)
	0.02	1.03(−1)	1.02(−1)	9.70(−2)	8.81(−2)	8.08(−2)	7.30(−2)	6.12(−2)	4.38(−2)	6.26(−3)	8.51(−4)
	0.03	1.02(−1)	1.01(−1)	9.60(−2)	8.71(−2)	7.99(−2)	7.22(−2)	6.05(−2)	4.32(−2)	6.09(−3)	8.18(−4)
	0.1	9.50(−2)	9.40(−2)	8.90(−2)	8.06(−2)	7.38(−2)	6.65(−2)	5.54(−2)	3.92(−2)	5.07(−3)	5.74(−4)
	0.2	8.55(−2)	8.45(−2)	7.99(−2)	7.22(−2)	6.59(−2)	5.91(−2)	4.90(−2)	3.41(−2)	3.89(−3)	3.46(−4)
	0.5	6.22(−2)	6.15(−2)	5.79(−2)	5.18(−2)	4.69(−2)	4.16(−2)	3.38(−2)	2.26(−2)	1.77(−3)	7.61(−5)
	1.0	3.67(−2)	3.62(−2)	3.38(−2)	2.98(−2)	2.66(−2)	2.32(−2)	1.83(−2)	1.14(−2)	4.80(−4)	6.16(−6)
	2.0	1.28(−2)	1.26(−2)	1.16(−2)	9.96(−3)	8.66(−3)	7.33(−3)	5.43(−3)	2.97(−3)	3.67(−5)	4.22(−8)
	5.0	5.43(−4)	5.32(−4)	4.75(−4)	3.84(−4)	3.14(−4)	2.45(−4)	1.55(−4)	5.95(−5)	2.07(−8)	1.78(−14)
	10.0	2.87(−6)	2.80(−6)	2.45(−6)	1.86(−6)	1.42(−6)	1.01(−6)	5.16(−7)	1.17(−7)	1.28(−13)	7.29(−25)
0.2	0	1.94(−2)	1.94(−2)	1.91(−2)	1.87(−2)	1.84(−2)	1.79(−2)	1.72(−2)	1.57(−2)	7.10(−3)	1.80(−3)
	0.01	1.92(−2)	1.92(−2)	1.90(−2)	1.85(−2)	1.82(−2)	1.78(−2)	1.70(−2)	1.56(−2)	7.00(−3)	1.76(−3)
	0.02	1.90(−2)	1.90(−2)	1.88(−2)	1.84(−2)	1.80(−2)	1.76(−2)	1.68(−2)	1.54(−2)	6.90(−3)	1.72(−3)
	0.03	1.88(−2)	1.88(−2)	1.86(−2)	1.82(−2)	1.78(−2)	1.74(−2)	1.67(−2)	1.52(−2)	6.80(−3)	1.68(−3)
	0.1	1.75(−2)	1.75(−2)	1.73(−2)	1.69(−2)	1.66(−2)	1.62(−2)	1.55(−2)	1.41(−2)	6.16(−3)	1.44(−3)

Table 31.2. (continued)

r_0/z	μt	$2\Gamma/\Phi_0 G(E)$									
		$\rho/r_0 = 0$	$\rho/r_0 = 0.2$	$\rho/r_0 = 0.5$	$\rho/r_0 = 0.8$	$\rho/r_0 = 1.0$	$\rho/r_0 = 1.2$	$\rho/r_0 = 1.5$	$\rho/r_0 = 2.0$	$\rho/r_0 = 5.0$	$\rho/r_0 = 10.0$
	0.2	1.59(−2)	1.58(−2)	1.56(−2)	1.53(−2)	1.50(−2)	1.46(−2)	1.39(−2)	1.27(−2)	5.35(−3)	1.15(−3)
	0.5	1.17(−2)	1.17(−2)	1.15(−3)	1.12(−2)	1.10(−2)	1.07(−2)	1.02(−2)	9.16(−3)	3.51(−3)	5.91(−4)
	1.0	7.07(−3)	7.05(−3)	6.94(−3)	6.75(−3)	6.57(−3)	6.37(−3)	6.02(−3)	5.34(−3)	1.74(−3)	1.95(−4)
	2.0	2.58(−3)	2.57(−3)	2.52(−3)	2.43(−3)	2.35(−3)	2.26(−3)	2.11(−3)	1.81(−3)	4.28(−4)	2.12(−5)
	5.0	1.25(−4)	1.24(−4)	1.20(−4)	1.14(−4)	1.08(−4)	1.02(−4)	9.08(−5)	7.16(−5)	6.57(−6)	2.88(−8)
	10.0	8.00(−7)	7.93(−7)	7.57(−7)	6.94(−7)	6.41(−7)	5.82(−7)	4.88(−7)	3.36(−7)	6.77(−9)	5.46(−13)
0.1	0	4.96(−3)	4.96(−3)	4.94(−3)	4.92(−3)	4.89(−3)	4.86(−3)	4.80(−3)	4.68(−3)	3.57(−3)	1.77(−3)
	0.01	4.91(−3)	4.91(−3)	4.89(−3)	4.87(−3)	4.84(−3)	4.81(−3)	4.75(−3)	4.64(−3)	3.53(−3)	1.74(−3)
	0.02	4.86(−3)	4.86(−3)	4.85(−3)	4.82(−3)	4.79(−3)	4.76(−3)	4.71(−3)	4.59(−3)	3.49(−3)	1.72(−3)
	0.03	4.82(−3)	4.81(−3)	4.80(−3)	4.77(−3)	4.74(−3)	4.71(−3)	4.66(−3)	4.54(−3)	3.45(−3)	1.70(−3)
	0.1	4.49(−3)	4.49(−3)	4.47(−3)	4.45(−3)	4.42(−3)	4.39(−3)	4.34(−3)	4.23(−3)	3.19(−3)	1.54(−3)
	0.2	4.06(−3)	4.06(−3)	4.04(−3)	4.02(−3)	4.00(−3)	3.97(−3)	3.92(−3)	3.82(−3)	2.85(−3)	1.33(−3)
	0.5	3.01(−3)	3.00(−3)	2.99(−3)	2.97(−3)	2.95(−3)	2.93(−3)	2.89(−3)	2.81(−3)	2.04(−3)	8.73(−4)
	1.0	1.82(−3)	1.82(−3)	1.81(−3)	1.80(−3)	1.79(−3)	1.77(−3)	1.74(−3)	1.69(−3)	1.17(−3)	4.31(−4)
	2.0	6.68(−4)	6.68(−4)	6.64(−4)	6.58(−4)	6.52(−4)	6.45(−4)	6.33(−4)	6.07(−4)	3.81(−4)	1.05(−4)
	5.0	3.30(−5)	3.30(−5)	3.27(−5)	3.22(−5)	3.18(−5)	3.12(−5)	3.03(−5)	2.83(−5)	1.34(−5)	1.54(−6)
	10.0	2.20(−7)	2.19(−7)	2.16(−7)	2.11(−7)	2.06(−7)	2.01(−7)	0.91(−7)	1.72(−7)	5.06(−8)	1.37(−9)

[a] Read: 9.01×10^{-1}, etc.
[b] Effectively zero.

Table 31.3. Unscattered Flux at a Corner Position from a Rectangular Plane Source with an Isotropic Angular Distribution[a]

μt	$4\pi\Gamma/S\ G(E)$					
	$b = 0.1$, $a = 0.1$	$b = 0.2$, $a = 0.1$	$b = 0.2$, $a = 0.2$	$b = 0.5$, $a = 0.1$	$b = 0.5$, $a = 0.2$	$b = 0.5$, $a = 0.5$
0	9.93(−3)[b]	1.97(−2)	3.90(−2)	4.62(−2)	9.16(−2)	2.16(−1)
0.01	9.83(−3)	1.95(−2)	3.86(−2)	4.57(−2)	9.07(−2)	2.14(−1)
0.02	9.74(−3)	1.93(−2)	3.82(−2)	4.53(−2)	8.97(−2)	2.11(−1)
0.05	9.44(−3)	1.87(−2)	3.70(−2)	4.39(−2)	8.69(−2)	2.05(−1)
0.1	8.99(−3)	1.78(−2)	3.52(−2)	4.17(−2)	8.25(−2)	1.94(−1)
0.2	8.13(−3)	1.61(−2)	3.18(−2)	3.75(−2)	7.43(−2)	1.74(−1)
0.5	6.02(−3)	1.19(−2)	2.35(−2)	2.75(−2)	5.44(−2)	1.26(−1)
1.0	3.64(−3)	7.18(−3)	1.42(−2)	1.64(−2)	3.23(−2)	7.38(−2)
2.0	1.34(−3)	2.62(−3)	5.14(−3)	5.79(−3)	1.14(−2)	2.53(−2)
5.0	6.60(−5)	1.28(−4)	2.47(−4)	2.60(−4)	5.04(−4)	1.04(−3)
10.0	4.37(−7)	8.26(−7)	1.54(−6)	1.50(−6)	2.83(−6)	5.15(−6)
μt	$b = 1.0$, $a = 0.1$	$b = 1.0$, $a = 0.2$	$b = 1.0$, $a = 0.5$	$b = 1.0$, $a = 1.0$	$b = 2.0$, $a = 0.1$	$b = 2.0$, $a = 0.2$
0	7.83(−2)	1.55(−1)	3.69(−1)	6.40(−1)	1.10(−1)	2.19(−1)
0.01	7.75(−2)	1.54(−1)	3.65(−1)	6.32(−1)	1.09(−1)	2.17(−1)
0.02	7.66(−2)	1.52(−1)	3.60(−1)	6.24(−1)	1.08(−1)	2.14(−1)
0.05	7.40(−2)	1.47(−1)	3.48(−1)	6.01(−1)	1.04(−1)	2.06(−1)
0.1	7.00(−2)	1.39(−1)	3.29(−1)	5.65(−1)	9.70(−2)	1.93(−1)
0.2	6.26(−2)	1.24(−1)	2.93(−1)	4.99(−1)	8.53(−2)	1.69(−1)
0.5	4.47(−2)	8.85(−2)	2.07(−1)	3.45(−1)	5.82(−2)	1.15(−1)
1.0	2.56(−2)	5.06(−2)	1.17(−1)	1.87(−1)	3.14(−2)	6.20(−2)
2.0	8.49(−3)	1.67(−2)	3.74(−2)	5.61(−2)	9.57(−3)	1.88(−2)
5.0	3.85(−4)	7.55(−4)	1.77(−3)	7.99(−3)	3.37(−4)	6.54(−4)
10.0	1.67(−6)	3.16(−6)	5.77(−6)	6.49(−6)	1.67(−6)	3.16(−6)

Table 31.3. (continued)

	$4\pi\Gamma/S\ G(E)$					
μt	$b = 2.0$ $a = 0.5$	$b = 2.0$ $a = 1.0$	$b = 2.0$ $a = 2.0$	$b = 5.0$ $a = 0.1$	$b = 5.0$ $a = 0.2$	$b = 5.0$ $a = 0.5$
0	5.25(−1)	9.31(−1)	1.41(0)	1.37(−1)	2.73(−1)	6.57(−1)
0.01	5.18(−1)	9.18(−1)	1.38(0)	1.35(−1)	2.68(−1)	6.46(−1)
0.02	5.11(−1)	9.05(−1)	1.36(0)	1.33(−1)	2.64(−1)	6.35(−1)
0.05	4.91(−1)	8.67(−1)	1.30(0)	1.26(−1)	2.51(−1)	6.03(−1)
0.1	4.60(−1)	8.07(−1)	1.20(0)	1.16(−1)	2.31(−1)	5.55(−1)
0.2	4.03(−1)	7.01(−1)	1.02(0)	9.93(−2)	1.97(−1)	4.72(−1)
0.5	2.72(−1)	4.62(−1)	6.38(−1)	6.38(−2)	1.27(−1)	3.00(−1)
1.0	1.44(−1)	2.35(−1)	3.02(−1)	3.27(−2)	6.46(−2)	1.50(−1)
2.0	4.24(−2)	6.43(−2)	7.46(−2)	9.69(−3)	1.90(−2)	4.28(−2)
5.0	1.32(−3)	1.75(−3)	1.80(−3)	3.37(−4)	6.54(−4)	1.35(−3)
10.0	5.79(−6)	6.51(−6)	6.52(−6)	1.67(−6)	3.16(−6)	5.79(−6)
μt	$b = 5.0$ $a = 1.0$	$b = 5.0$ $a = 2.0$	$b = 5.0$ $a = 5.0$	$b = 10.0$ $a = 0.1$	$b = 10.0$ $a = 0.2$	$b = 10.0$ $a = 0.5$
0	1.19(0)	1.88(0)	2.73(0)	1.47(−1)	2.92(−1)	7.06(−1)
0.01	1.17(0)	1.84(0)	2.65(0)	1.44(−1)	2.86(−1)	6.92(−1)
0.02	1.15(0)	1.80(0)	2.58(0)	1.41(−1)	2.81(−1)	6.77(−1)
0.05	1.08(0)	1.69(0)	2.39(0)	1.33(−1)	2.65(−1)	6.38(−1)
0.1	9.92(−1)	1.53(0)	2.10(0)	1.21(−1)	2.41(−1)	5.79(−1)
0.2	8.35(−1)	1.26(0)	1.64(0)	1.02(−1)	2.02(−1)	4.84(−1)
0.5	5.14(−1)	7.27(−1)	8.53(−1)	6.42(−2)	1.27(−1)	3.01(−1)
1.0	2.47(−1)	3.20(−1)	3.44(−1)	3.27(−2)	6.47(−2)	1.50(−1)
2.0	6.51(−2)	7.57(−2)	7.69(−2)	9.69(−3)	1.90(−2)	4.28(−2)
5.0	1.75(−3)	1.80(−3)	1.80(−3)	3.37(−4)	6.54(−4)	1.35(−3)
10.0	6.51(−6)	6.53(−6)	6.54(−6)	1.67(−6)	3.16(−6)	5.79(−6)
μt	$b = 10.0$ $a = 1.0$	$b = 10.0$ $a = 2.0$	$b = 10.0$ $a = 5.0$	$b = 10.0$ $a = 10.0$	$b = 20.0$ $a = 0.1$	$b = 20.0$ $a = 0.2$
0	1.28(0)	2.07(0)	3.15(0)	3.80(0)	1.52(−1)	3.02(−1)
0.01	1.26(0)	2.02(0)	3.04(0)	3.64(0)	1.48(−1)	2.95(−1)
0.02	1.23(0)	1.97(0)	2.94(0)	3.49(0)	1.45(−1)	2.88(−1)
0.05	1.15(0)	1.83(0)	2.67(0)	3.10(0)	1.36(−1)	2.70(−1)
0.1	1.04(0)	1.63(0)	2.30(0)	2.58(0)	1.22(−1)	2.43(−1)
0.2	8.60(−1)	1.31(0)	1.74(0)	1.86(0)	1.02(−1)	2.03(−1)
0.5	5.18(−1)	7.34(−1)	8.65(−1)	8.78(−1)	6.39(−2)	1.27(−1)
1.0	2.47(−1)	3.21(−1)	3.44(−1)	3.45(−1)	3.27(−2)	6.47(−2)
2.0	6.51(−2)	7.56(−2)	7.69(−2)	7.68(−2)	9.69(−3)	1.90(−2)
5.0	1.75(−3)	1.80(−3)	1.80(−3)	1.80(−3)	3.37(−4)	6.54(−4)
10.0	6.51(−6)	6.53(−6)	6.53(−6)	6.53(−6)	1.67(−6)	3.16(−6)

Table 3I.3. (continued)

μt	$4\pi\Gamma/S\ G(E)$					
	$b = 20.0$ $a = 0.5$	$b = 20.0$ $a = 1.0$	$b = 20.0$ $a = 2.0$	$b = 20.0$ $a = 5.0$	$b = 20.0$ $a = 10.0$	$b = 20.0$ $a = 20.0$
0	7.31(−1)	1.33(0)	2.17(0)	3.38(0)	4.22(0)	4.88(0)
0.01	7.13(−1)	1.30(0)	2.10(0)	3.25(0)	4.01(0)	4.56(0)
0.02	6.96(−1)	1.27(0)	2.04(0)	3.12(0)	3.81(0)	4.28(0)
0.05	6.50(−1)	1.18(0)	1.88(0)	2.79(0)	3.30(0)	3.59(0)
0.1	5.86(−1)	1.05(0)	1.65(0)	2.36(0)	2.68(0)	2.81(0)
0.2	4.86(−1)	8.63(−1)	1.31(0)	1.75(0)	1.89(0)	1.92(0)
0.5	3.01(−1)	5.18(−1)	7.34(0)	8.63(−1)	8.79(−1)	8.82(−1)
1.0	1.50(−1)	2.47(−1)	3.21(0)	3.44(−1)	3.45(−1)	3.45(−1)
2.0	4.28(−2)	6.51(−2)	7.56(−2)	7.69(−2)	7.68(−2)	7.68(−2)
5.0	1.35(−3)	1.75(−3)	1.80(−3)	1.80(−3)	1.80(−3)	1.80(−3)
10.0	5.79(−6)	6.51(−6)	6.53(−6)	6.53(−6)	6.53(−6)	6.53(−6)

[a]From ref. 114.

[b]Read: 9.93×10^{-3}, etc.

Table 3I.4. Unscattered Flux at a Corner Position from a Rectangular Plane Source with a Cosine Angular Distribution (Isotropic Flux)

μt	$2\Gamma/\Phi_0 G(E)$					
	$b = 0.1$ $a = 0.1$	$b = 0.2$ $a = 0.1$	$b = 0.2$ $a = 0.2$	$b = 0.5$ $a = 0.1$	$b = 0.5$ $a = 0.2$	$b = 0.5$ $a = 0.5$
0	1.58(−3)[a]	3.11(−3)	6.12(−3)	7.09(−3)	1.40(−2)	3.21(−2)
0.01	1.56(−3)	3.08(−3)	6.06(−3)	7.01(−3)	1.38(−2)	3.17(−2)
0.02	1.55(−3)	3.04(−3)	6.00(−3)	6.94(−3)	1.37(−2)	3.14(−2)
0.05	1.53(−3)	3.01(−3)	5.94(−3)	6.87(−3)	1.36(−2)	3.10(−2)
0.1	1.43(−3)	2.81(−3)	5.53(−3)	6.39(−3)	1.26(−2)	2.88(−2)
0.2	1.29(−3)	2.54(−3)	5.00(−3)	5.76(−3)	1.14(−2)	2.59(−2)
0.5	9.54(−4)	1.88(−3)	3.69(−3)	4.22(−3)	8.30(−3)	1.88(−2)
1.0	5.78(−4)	1.13(−3)	2.22(−3)	2.51(−3)	4.93(−3)	1.10(−2)
2.0	2.12(−4)	4.14(−4)	8.08(−4)	8.90(−4)	1.74(−3)	3.77(−3)
5.0	1.04(−5)	2.01(−5)	3.87(−5)	4.00(−5)	7.70(−5)	1.54(−4)
10.0	6.92(−8)	1.30(−7)	2.45(−7)	2.31(−7)	4.36(−7)	7.79(−7)
μt	$b = 1.0$ $a = 0.1$	$b = 1.0$ $a = 0.2$	$b = 1.0$ $a = 0.5$	$b = 1.0$ $a = 1.0$	$b = 2.0$ $a = 0.1$	$b = 2.0$ $a = 0.2$
0	1.12(−2)	2.21(−2)	5.12(−2)	8.33(−2)	1.42(−2)	2.81(−2)
0.01	1.11(−2)	2.19(−2)	5.06(−2)	8.23(−2)	1.40(−2)	2.77(−2)
0.02	1.08(−2)	2.17(−2)	5.01(−2)	8.13(−2)	1.38(−2)	2.74(−2)
0.05	1.08(−2)	2.14(−2)	4.95(−2)	8.03(−2)	1.37(−2)	2.70(−2)
0.1	1.00(−2)	1.98(−2)	4.57(−2)	7.38(−2)	1.25(−2)	2.48(−2)
0.2	8.98(−3)	1.77(−2)	4.07(−2)	6.53(−2)	1.11(−2)	2.19(−2)
0.5	6.44(−3)	1.27(−2)	2.89(−2)	4.54(−2)	7.71(−3)	1.52(−2)
1.0	3.71(−3)	7.29(−3)	1.64(−2)	2.49(−2)	4.26(−3)	8.38(−3)
2.0	1.24(−3)	2.43(−3)	5.30(−3)	7.57(−3)	1.35(−3)	2.64(−3)
5.0	4.91(−5)	9.47(−5)	1.91(−4)	2.38(−4)	5.00(−5)	9.65(−5)
10.0	2.54(−7)	4.79(−7)	8.61(−7)	9.54(−7)	2.55(−7)	4.80(−7)

Table 3I.4. (continued)

	$2\Gamma/\Phi_0 G(E)$					
μt	$b = 2.0$ $a = 0.5$	$b = 2.0$ $a = 1.0$	$b = 2.0$ $a = 2.0$	$b = 5.0$ $a = 0.1$	$b = 5.0$ $a = 0.2$	$b = 5.0$ $a = 0.5$
0	6.55(−2)	1.09(−1)	1.48(−1)	1.56(−2)	3.08(−2)	7.23(−2)
0.01	6.47(−2)	1.08(−1)	1.45(−1)	1.53(−2)	3.04(−2)	7.12(−2)
0.02	6.39(−2)	1.06(−1)	1.43(−1)	1.51(−2)	3.00(−2)	7.02(−2)
0.05	6.30(−2)	1.05(−1)	1.41(−1)	1.49(−2)	2.95(−2)	6.92(−2)
0.1	5.77(−2)	9.52(−2)	1.27(−1)	1.35(−2)	2.68(−2)	6.26(−2)
0.2	5.08(−2)	8.32(−2)	1.09(−1)	1.18(−2)	2.34(−2)	5.45(−2)
0.5	3.49(−2)	5.58(−2)	7.05(−2)	8.02(−3)	1.58(−2)	3.64(−2)
1.0	1.89(−2)	2.92(−2)	3.49(−2)	4.33(−3)	8.53(−3)	1.93(−2)
2.0	5.78(−3)	8.34(−3)	9.26(−3)	1.35(−3)	2.65(−3)	5.81(−3)
5.0	1.95(−4)	2.44(−4)	2.49(−4)	5.00(−5)	9.65(−5)	1.95(−4)
10.0	8.63(−7)	9.56(−7)	9.58(−7)	2.55(−7)	4.80(−7)	8.63(−7)
μt	$b = 5.0$ $a = 1.0$	$b = 5.0$ $a = 2.0$	$b = 5.0$ $a = 5.0$	$b = 10.0$ $a = 0.1$	$b = 10.0$ $a = 0.2$	$b = 10.0$ $a = 0.5$
0	1.22(−1)	1.70(−1)	2.06(−1)	1.58(−2)	3.13(−2)	7.34(−2)
0.01	1.20(−1)	1.67(−1)	2.01(−1)	1.56(−2)	3.08(−2)	7.23(−2)
0.02	1.18(−1)	1.64(−1)	1.97(−1)	1.58(−2)	3.04(−2)	7.12(−2)
0.05	1.16(−1)	1.62(−1)	1.93(−1)	1.51(−2)	2.99(−2)	7.01(−2)
0.1	1.05(−1)	1.43(−1)	1.68(−1)	1.37(−2)	2.70(−2)	6.32(−2)
0.2	9.02(−2)	1.21(−1)	1.38(−1)	1.19(−2)	2.35(−2)	5.48(−2)
0.5	5.87(−2)	7.51(−2)	8.10(−2)	8.02(−3)	1.58(−2)	3.65(−2)
1.0	2.99(−2)	3.59(−2)	3.71(−2)	4.33(−3)	8.53(−3)	1.93(−2)
2.0	8.38(−3)	9.32(−3)	9.38(−3)	1.35(−3)	2.65(−3)	5.81(−3)
5.0	2.44(−4)	2.49(−4)	2.49(−4)	5.00(−5)	9.65(−5)	1.95(−4)
10.0	9.56(−7)	9.58(−7)	9.58(−7)	2.55(−7)	4.80(−7)	8.63(−7)
μt	$b = 10.0$ $a = 1.0$	$b = 10.0$ $a = 2.0$	$b = 10.0$ $a = 5.0$	$b = 10.0$ $a = 10.0$	$b = 20.0$ $a = 0.1$	$b = 20.0$ $a = 0.2$
0	1.24(−1)	1.75(−1)	2.15(−1)	2.28(−1)	1.58(−2)	3.14(−2)
0.01	1.22(−1)	1.71(−1)	2.10(−1)	2.22(−1)	1.56(−2)	3.09(−2)
0.02	1.20(−1)	1.68(−1)	2.05(−1)	2.16(−1)	1.54(−2)	3.04(−2)
0.05	1.18(−1)	1.65(−1)	2.01(−1)	2.11(−1)	1.51(−2)	3.00(−2)
0.1	1.06(−1)	1.46(−1)	1.72(−1)	1.78(−1)	1.37(−2)	2.71(−2)
0.2	9.08(−2)	1.22(−1)	1.40(−1)	1.43(−1)	1.19(−2)	2.35(−2)
0.5	5.88(−2)	7.53(−2)	8.13(−2)	8.17(−2)	8.02(−3)	1.58(−2)
1.0	2.99(−2)	3.59(−2)	3.71(−2)	3.71(−2)	4.33(−3)	8.53(−3)
2.0	8.38(−3)	9.32(−3)	9.38(−3)	9.38(−3)	1.35(−3)	2.65(−3)
5.0	2.44(−4)	2.49(−4)	2.49(−4)	2.49(−4)	5.00(−5)	9.65(−5)
10.0	9.56(−7)	9.58(−7)	9.58(−7)	9.58(−7)	2.55(−7)	4.81(−7)

Table 3I.4. *(continued)*

	$2\Gamma/\Phi_0 G(E)$					
μt	$b = 20.0$ $a = 0.5$	$b = 20.0$ $a = 1.0$	$b = 20.0$ $a = 2.0$	$b = 20.0$ $a = 5.0$	$b = 20.0$ $a = 10.0$	$b = 20.0$ $a = 20.0$
0	7.37(−2)	1.25(−1)	1.76(−1)	2.18(−1)	2.32(−1)	2.39(−1)
0.01	7.26(−2)	1.23(−1)	1.72(−1)	2.12(−1)	2.26(−1)	2.31(−1)
0.02	7.14(−2)	1.21(−1)	1.69(−1)	2.07(−1)	2.20(−1)	2.24(−1)
0.05	7.03(−2)	1.19(−1)	1.66(−1)	2.02(−1)	2.14(−1)	2.18(−1)
0.1	6.33(−2)	1.06(−1)	1.46(−1)	1.73(−1)	1.79(−1)	1.80(−1)
0.2	5.48(−2)	9.08(−2)	1.22(−1)	1.40(−1)	1.43(−1)	1.44(−1)
0.5	3.65(−2)	5.88(−2)	7.53(−2)	8.13(−2)	8.17(−2)	8.17(−2)
1.0	1.93(−2)	2.99(−2)	3.59(−2)	3.71(−2)	3.71(−2)	3.71(−2)
2.0	5.81(−3)	8.38(−3)	9.32(−3)	9.38(−3)	9.38(−3)	9.38(−3)
5.0	1.95(−4)	2.44(−4)	2.49(−4)	2.49(−4)	2.49(−4)	2.49(−4)
10.0	8.63(−7)	9.56(−7)	9.58(−7)	9.58(−7)	9.58(−7)	9.58(−7)

[a]Read: 1.58×10^{-3}, etc.

Appendix 3J. Graphs of the Ψ Function

Useful functions in calculating the shield penetration of secondary gamma-ray fluxes are the ψ functions defined in Section 3.10. The ψ_0 function is used to calculate the uncollided flux, and the ψ_n function ($n > 0$) is used for the collided flux. Values of these functions have been obtained by Trubey[67] and Schmidt[214] for the case of a slab shield and by Claiborne[141] for the case of a semi-infinite shield. The functions are plotted in Figs. 3J.1 through 3J.10.

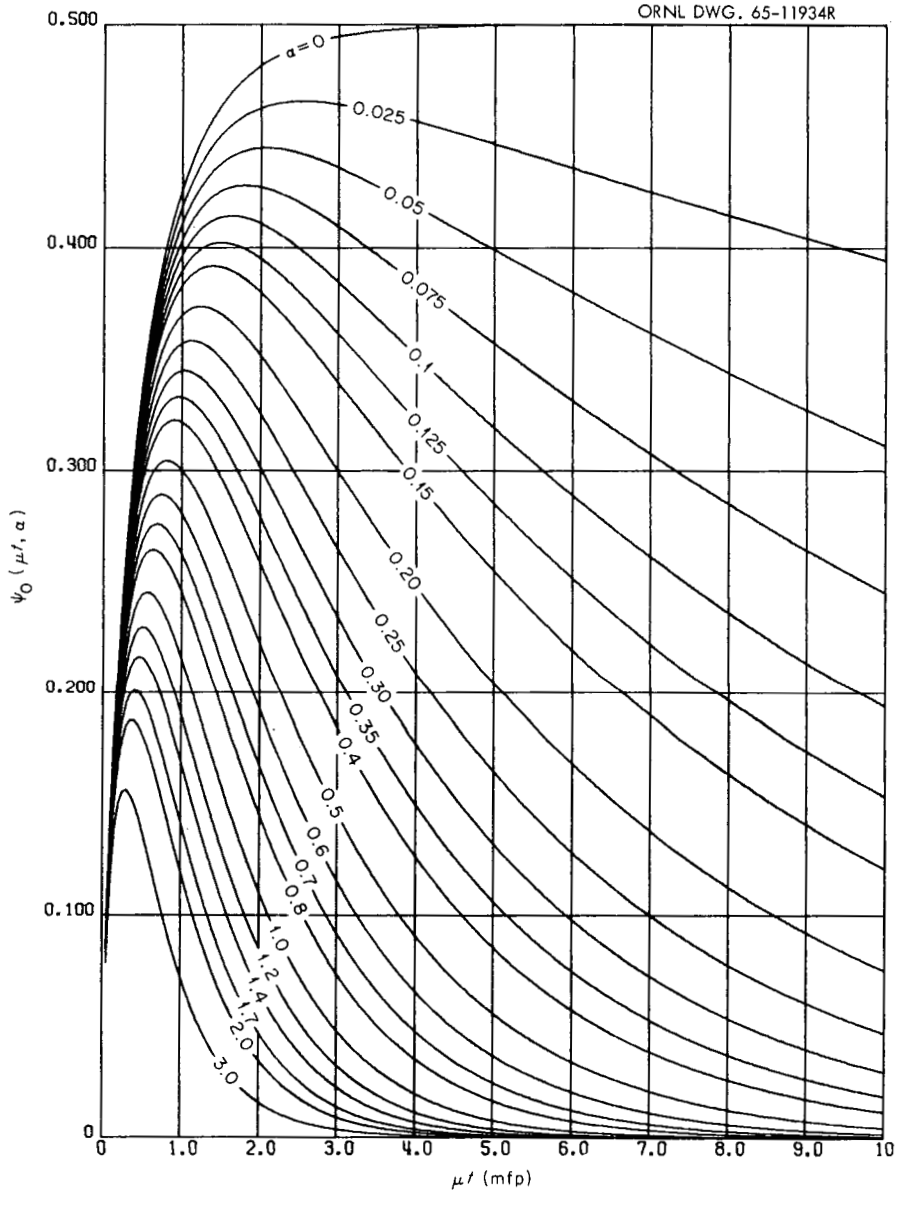

Fig. 3J.1. The Function $\Psi_0(\mu t, \alpha)$ for a Slab Shield (Linear Plot, $\alpha = 0$ to 3.0). (From ref. 67.)

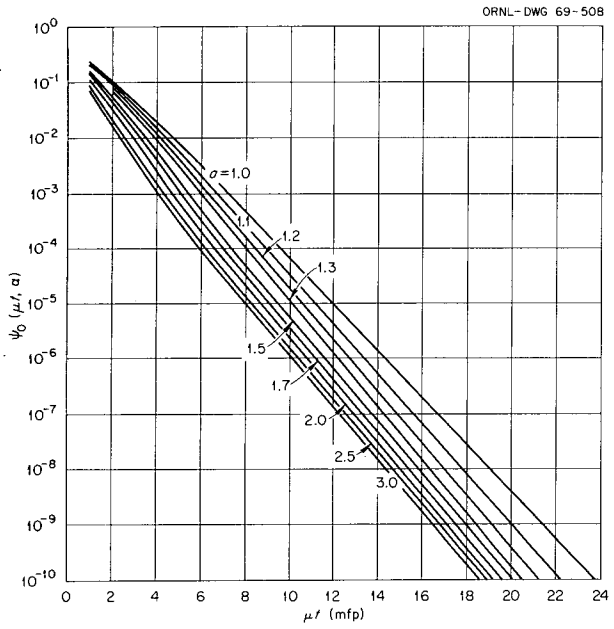

Fig. 3J.2. The Function $\Psi_0(\mu t,\alpha)$ for a Slab Shield (Semilog Plot, α = 1.0 to 3.0.) (From ref. 214.)

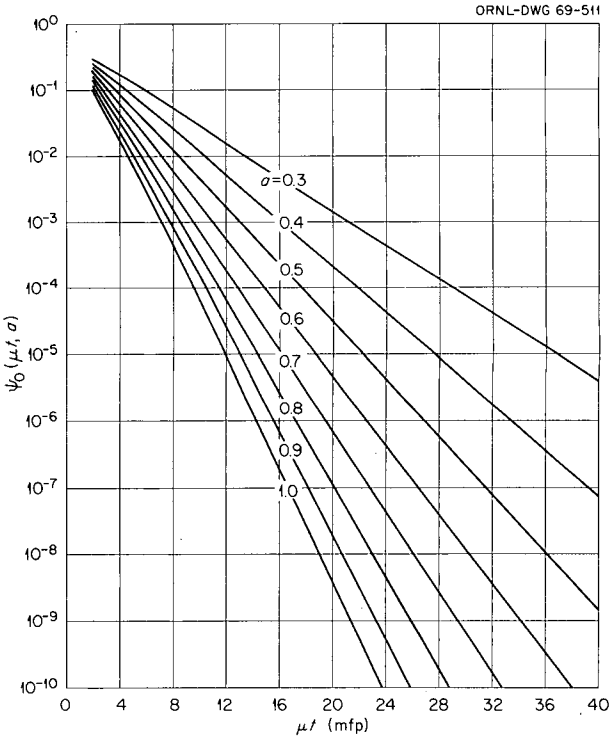

Fig. 3J.3. The Function $\Psi_0(\mu t,\alpha)$ for a Slab Shield (Semilog Plot, α = 0.3 to 1.0). (From ref. 214.)

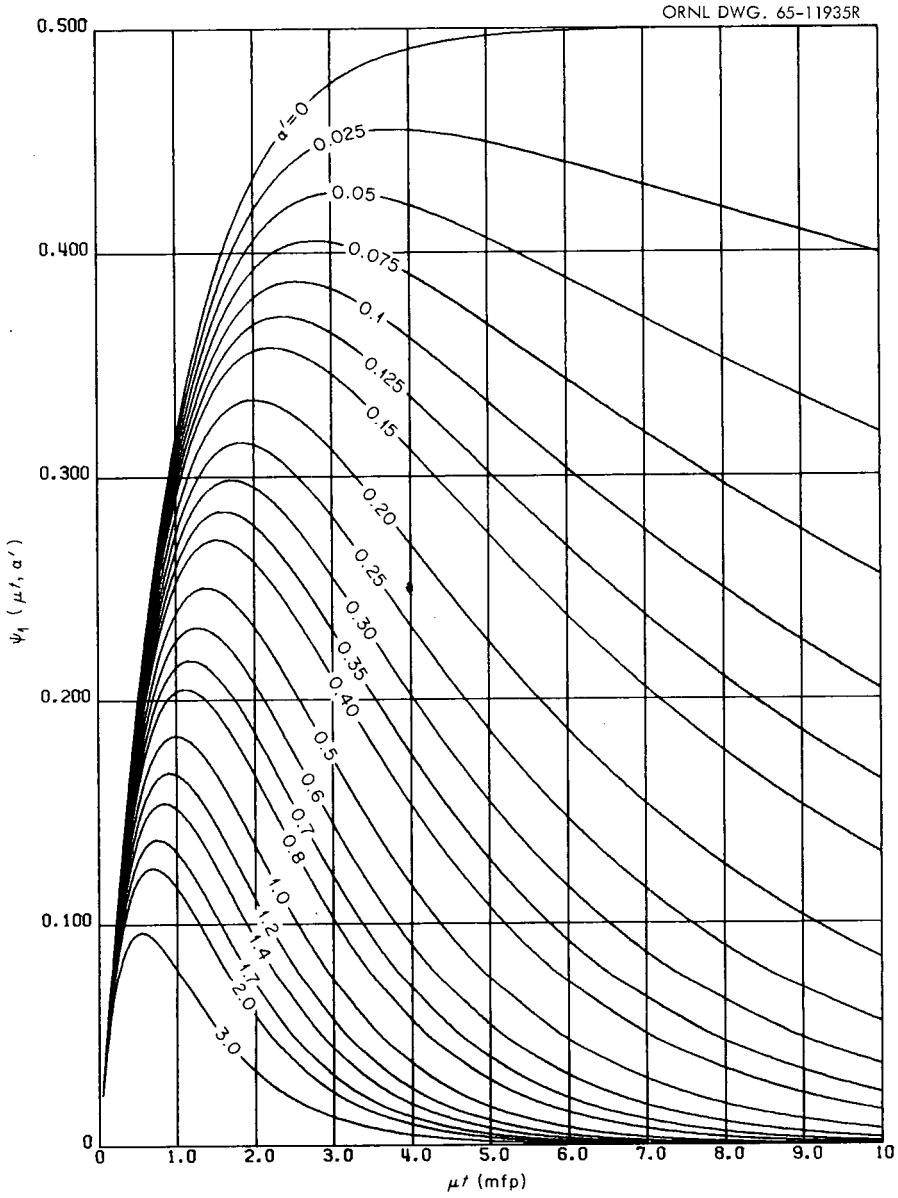

Fig. 3J.4. The Function $\Psi_1(\mu t,\alpha')$ for a Slab Shield (Linear Plot, $\alpha' = 0$ to 3.0). (From ref. 67.)

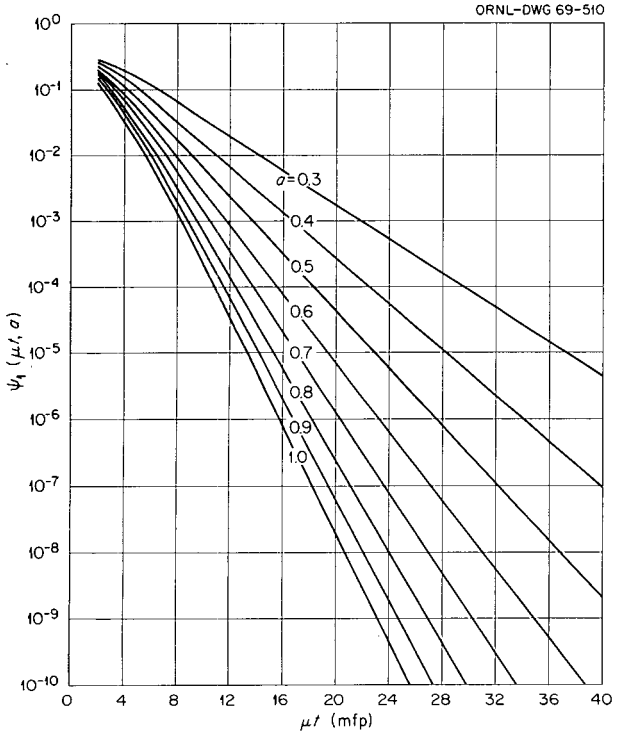

Fig. 3J.5. The Function $\Psi_1(\mu t,\alpha)$ for a Slab Shield (Semilog Plot, α = 0.3 to 1.0). (From ref. 214.)

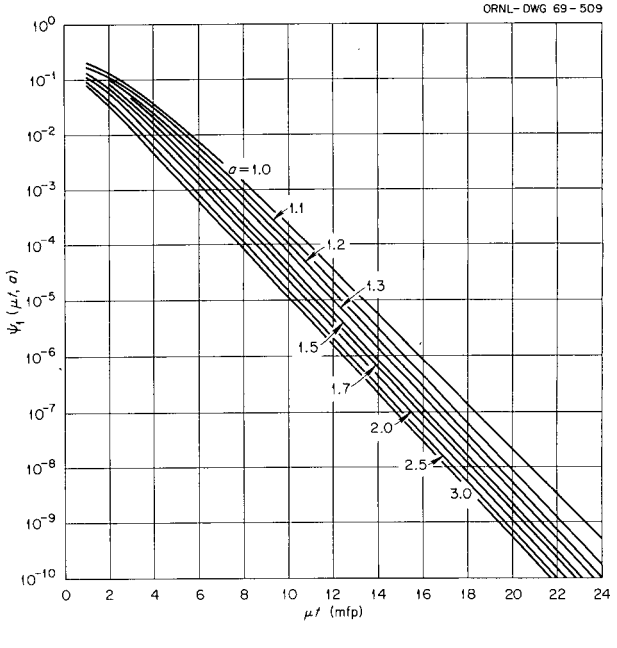

Fig. 3J.6. The Function $\Psi_1(\mu t,\alpha)$ for a Slab Shield (Semilog Plot, α = 1.0 to 3.0). (From ref. 214.)

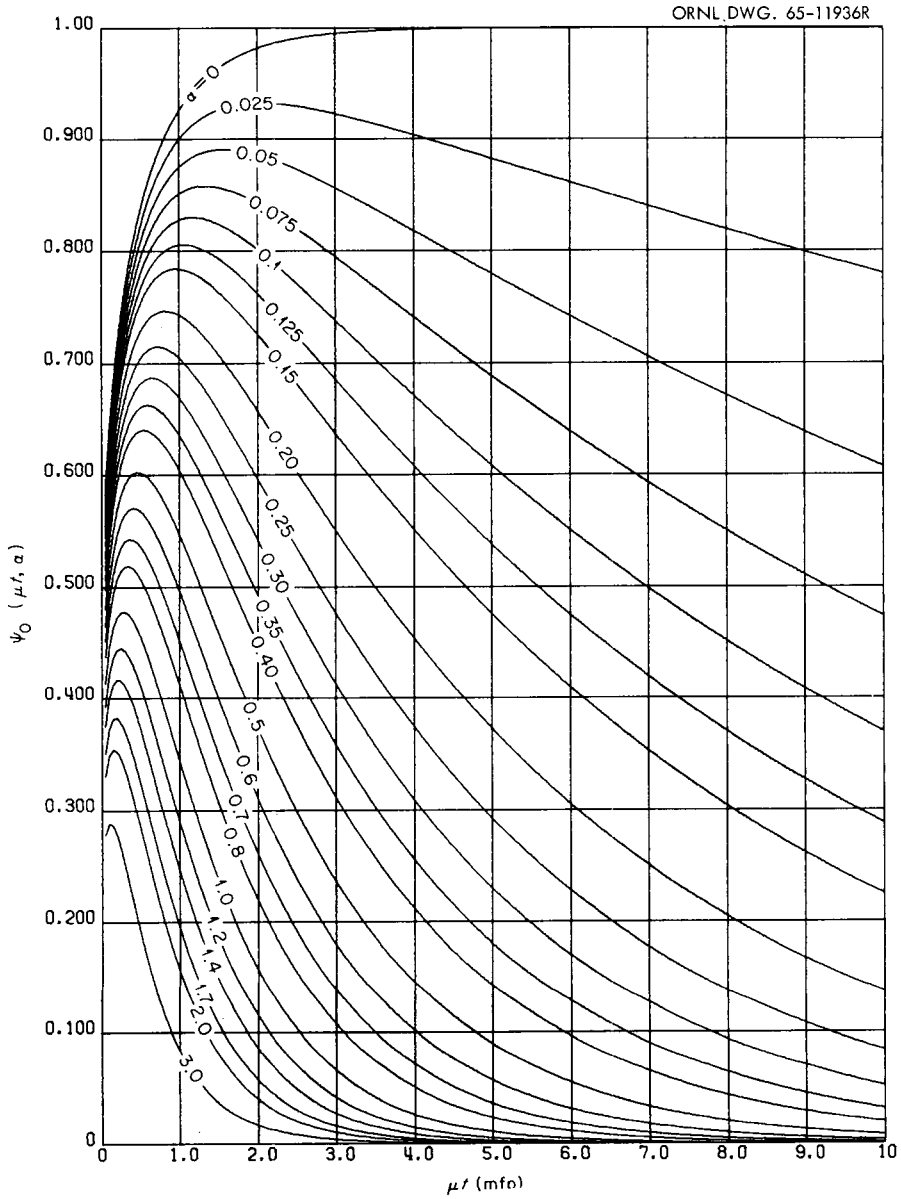

Fig. 3J.7. The Function $\Psi_0(\mu t,\alpha)$ for a Semi-Infinite Shield. (From ref. 141.)

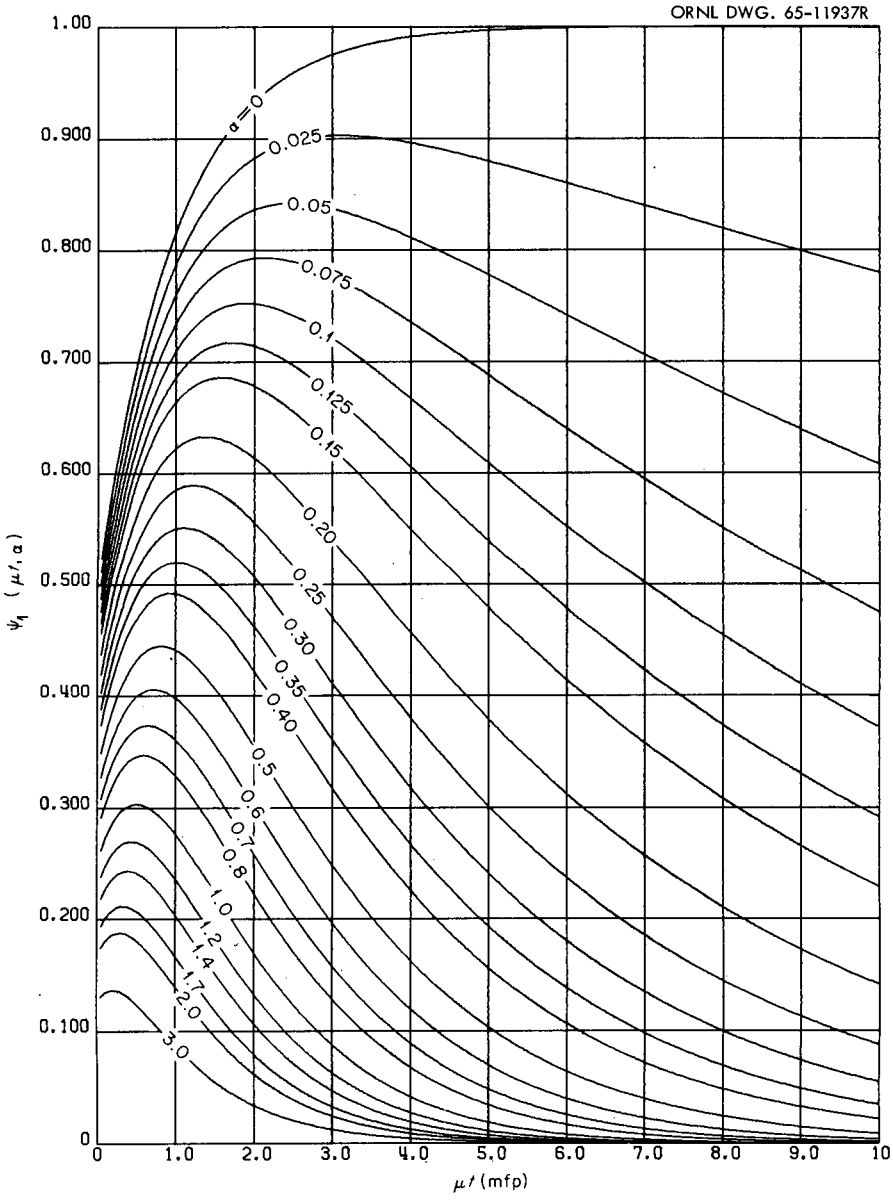

Fig. 3J.8. The Function $\Psi_1(\mu t,\alpha)$ for a Semi-Infinite Shield. (From ref. 141.)

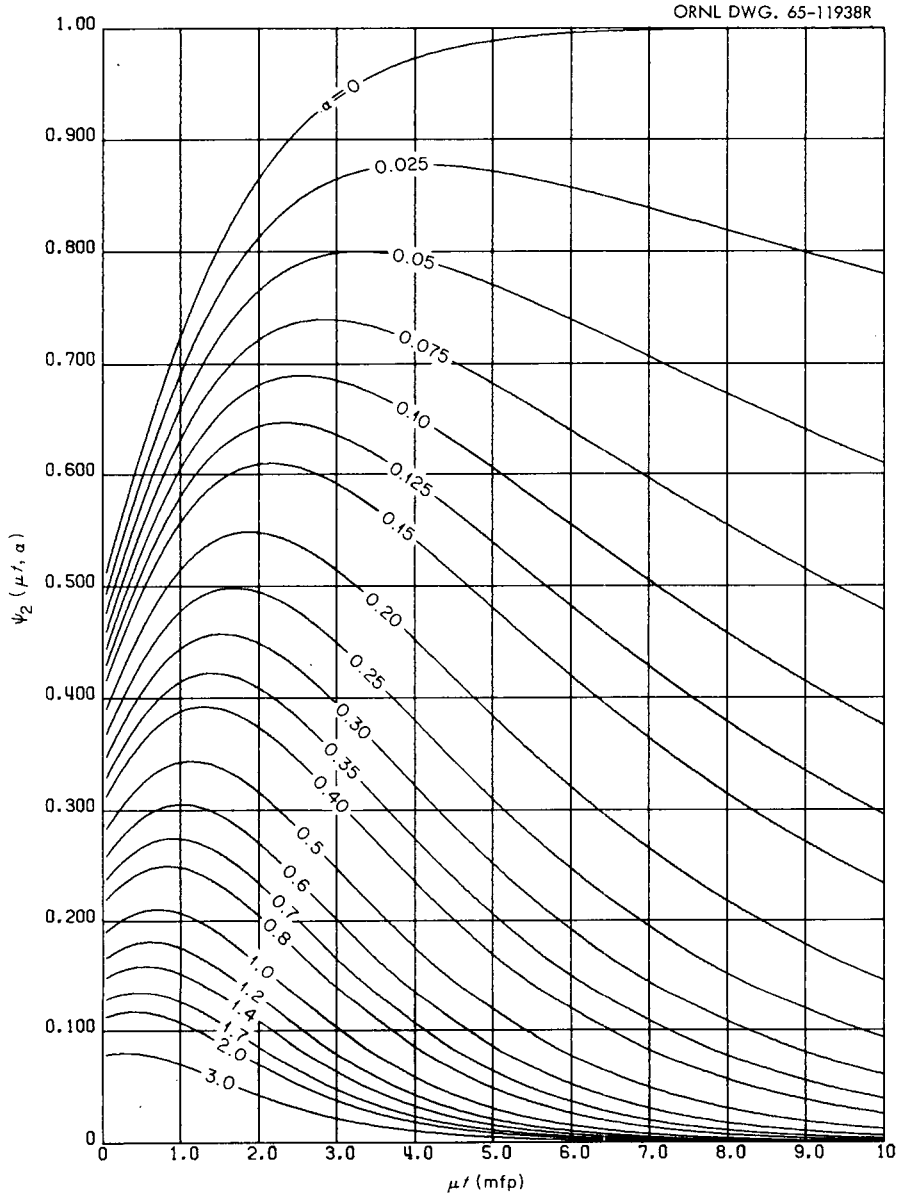

Fig. 3J.9. The Function $\Psi_2(\mu t,\alpha)$ for a Semi-Infinite Shield. (From ref. 141.)

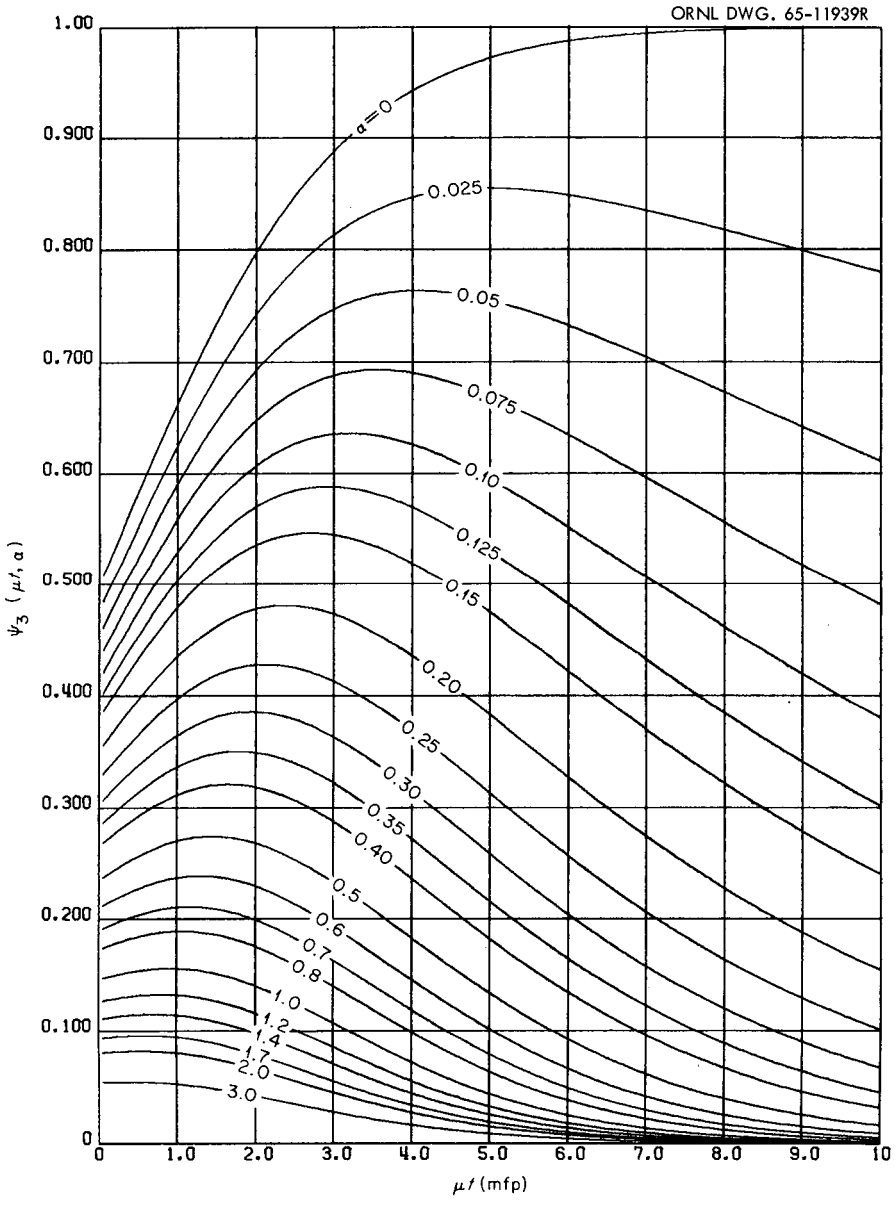

Fig. 3J.10. The Function $\Psi_3(\mu t,\alpha)$ for a Semi-Infinite Shield. (From ref. 141.)

References

[1] A. M. Weinberg and E. P. Wigner, *The Physical Theory of Neutron Chain Reactors,* University of Chicago Press, Chicago, 1958.

[2] K. Shure, "P-3 Multigroup Calculations of Neutron Attenuation," *Nucl. Sci. Eng.* **19**, 310 (1964).

[3] W. D. Lanning, "Application of the Spherical Harmonics Technique to Problems in Gamma Transport," *Nucl. Sci. Eng.* **15**, 259-267 (1963).

[4] G. C. Wick, "Uber ebene Diffusionprobleme," *Physick* **121**, 702 (1943).

[5] S. Chandrasekhar, *Radiative Transfer,* Clarendon Press, Oxford, 1950.

[6] B. G. Carlson, *Solution of the Transport Equation by the S_n Method,* Los Alamos Scientific Laboratory Report LA-1891 (1955).

[7] W. E. Engle, M. A. Boling, and B. W. Colston, *DTF II, A One-Dimensional Multigroup Neutron Transport Program,* North American Aviation, Los Angeles, Report NAA-SR-10951 (1966).

[8] K. D. Lathrop, *DTF-IV, A FORTRAN-IV Program for Solving the Multigroup Transport Equation with Anisotropic Scattering,* Los Alamos Scientific Laboratory Report LA-3373 (1965).

[9] W. W. Engle, Jr., *A User's Manual for ANISN, A One-Dimensional Discrete Ordinates Transport Code with Anisotropic Scattering,* Union Carbide Corp., Nuclear Division, K-25, Report K-1693 (1967).

[10] B. Carlson, C. Lee, and J. Worlton, *The DSN and TDC Neutron Transport Codes,* Los Alamos Scientific Laboratory Report LAMS-2346 (1960); C. E. Lee, *The Discrete S_n Approximation to Transport Theory,* Los Alamos Scientific Laboratory Report LA-2595 (1962).

[11] F. R. Mynatt, "A User's Manual for DOT, A Two-Dimensional Discrete Ordinates Transport Code with Anisotropic Scattering," informal notes included in RSIC Computer Code Collection CCC-89, Oak Ridge National Laboratory.

[12] F. R. Mynatt, F. J. Muckenthaler, and P. N. Stevens, *Development of Two-Dimensional Discrete Ordinates Transport Theory for Radiation Shielding,* Union Carbide Corp., Nuclear Division, Report CTC-INF-952 (1969).

[13] S. Preiser, G. Rabinowitz, and E. de Dufour, *A Program for the Numerical Integration of Boltzmann Transport Equation – NIOBE,* Nuclear Development Corp. of America, Aeronautical Research Laboratories, Report ARL-TR-60-314 (1960).

[14] H. Goldstein and J. E. Wilkins, Jr., *Calculations of the Penetration of Gamma Rays,* Final Report, Nuclear Development Associates Report NYO-3075 (1954) (also NDA-15C-41).

[15] U. Fano, L. V. Spencer, and M. J. Berger, "Penetration and Diffusion of X-Rays," *Handbuch der Physik (Encyclopedia of Physics),* Vol. 38, 660-817 (1959).

[16] H. Goldstein, *Fundamental Aspects of Reactor Shielding,* Addison-Wesley, Reading, Mass., 1959.

[17] J. Certaine, *A Solution of the Neutron Transport Equation. Introduction and Part I,* New York Operations Office Report NYO-3081 (Nuclear Development Associates Report NDA-15C-43) (1954); *Part II, NDA-UNIVAC Moments Calculation,* NYO-6268 (NDA-15C-53) (1955); and *Part III, Reconstruction of a Function from Its Moments,* NYO-6270 (NDA-15C-61) (1956).

[18] R. Aronson *et al., Penetration of Neutrons from a Point Isotropic Fission Source in Water,* New York Operations Office Report NYO-6267 (Nuclear Development Associates Report NDA-15C-42) (1954).

[19] R. Aronson, J. Certaine, and H. Goldstein, *Penetration of Neutrons from Point Isotropic Monoenergetic Sources in Water,* New York Operations Office Report NYO-6269 (Nuclear Development Associates Report NDA-15C-60) (1954).

[20] A. D. Krumbein, *Summary of NDA Unclassified Results of Moments Calculations for the Penetration of Neutrons Through Various Materials,* Nuclear Development Corp. of America, Report NDA-92-2 (Rev.) (1957).

[21] *Radiation Shielding. Analysis and Design Principles as Applied to Nuclear Defense Planning,* W. R. Kimel, Editor, prepared by Office of Civil Defense and Kansas State University, Report TR 40 (1966).

[22] L. V. Spencer, *Structure Shielding Against Fallout Radiation from Nuclear Weapons,* National Bureau of Standards Monograph 42 (1962).

[23] J. M. Hammersley and D. C. Handscomb, *Monte Carlo Methods,* Wiley, New York, 1964.

[24] N. P. Buslenko *et al., The Monte Carlo Method* (translated from the Russian), Pergamon, New York, 1966.

[25] H. Kahn, "Random Sampling (Monte Carlo) Techniques in Neutron Attenuation Problems - I and II," *Nucleonics* **6**(5), 27 and **6**(6), 60 (1950).

[26] G. Goertzel and M. H. Kalos, "Monte Carlo Methods in Transport Problems," p. 35 in *Progress in Nuclear Energy,* Series I, *Physics and Mathematics,* Vol. 2, Pergamon, New York, 1958.

[27] H. Kahn, *Applications of Monte Carlo,* Rand Corp. Report AECU-3295 (1954).

[28] E. D. Cashwell and C. J. Everett, *A Practical Manual on the Monte Carlo Method for Random Walk Problems,* Pergamon, New York, 1959.

[29] J. Spanier and E. M. Gelbard, *Monte Carlo Principles and Neutron Transport Problems,* Addison-Wesley Publishing Co., Reading, Mass., 1969.

[30] B. E. Watt, "Energy Spectrum of Neutrons from Thermal Fission of U^{235}," *Phys. Rev.* **87**, 1037 (1952).

[31] R. R. Coveyou, V. R. Cain, and K. J. Yost, "Adjoint and Importance in Monte Carlo Application," *Nucl. Sci. Eng.* **27**, 219 (1967).

[32] F. H. Clark, *The Exponential Transform as an Importance-Sampling Device - A Review,* Oak Ridge National Laboratory Report ORNL-RSIC-14 (1966).

[33] V. R. Cain, "Application of S_N Adjoint Flux Calculations to Monte Carlo Biasing," *Trans. Am. Nucl. Soc.* **10**, 399 (1967).

[34] F. H. Clark, "Variance of Certain Flux Estimators Used in Monte Carlo Calculations," *Nucl. Sci. Eng.* **27**, 235 (1967).

[35] D. C. Irving *et al., O5R, A General-Purpose Monte Carlo Neutron Transport Code,* Oak Ridge National Laboratory Report ORNL-3622 (1965).

[36] D. C. Irving *et al.,* Oak Ridge National Laboratory, unpublished report.

[37] E. A. Straker, P. N. Stevens, D. C. Irving, and V. R. Cain, *The MORSE Code - A Multigroup Neutron and Gamma-Ray Monte Carlo Transport Code,* Oak Ridge National Laboratory Report ORNL-4585 (1970).

[38] C. R. Greenhow, G. O. Mueller, and G. E. Sabian, *Use of Diffusion Theory Codes to Predict Gamma Heating,* Knolls Atomic Power Laboratory Report KAPL-M-DNA-5 (1963).

[39] V. A. Ambarzumian, "Diffusion of Light by Planetary Atmosphere," *Astron. Zh.* **19**, 30 (1942).

[40] R. Bellman, R. Kalaba, and G. M. Wing, "Invariant Imbedding and Mathematical Physics. I. Particle Processes," *J. Math. Phys.* **1**(4), 280 (1960).

[41] G. M. Wing, *An Introduction to Transport Theory,* Wiley, New York, 1962.

[42] A. Shimizu and H. Mizuta, "Application of Invariant Imbedding to the Reflection and Transmission Problem in Gamma Rays (I)," *J. Nucl. Sci. Technol. (Tokyo)* **3**, 2 (1966).

[43] A. Shimizu and H. Mizuta, "Application of Invariant Imbedding to the Reflection and Transmission Problems of Gamma Rays (II)," *J. Nucl. Sci. Technol. (Tokyo)* **3**, 10 (1966).

[44] D. R. Mathews, K. F. Hansen, and E. A. Mason, "Deep Penetration of Radiation by the Method of Invariant Imbedding," *Nucl. Sci. Eng.* **27**, 263 (1967).

[45] J. O. Mingle, "Applications of the Invariant Imbedding Method to Monoenergetic Neutron Transport Theory in Slab Geometry," *Nucl. Sci. Eng.* **28**, 177 (1967).

[46] André Mockel, "Invariant Imbedding and Polyenergetic Neutron Transport Theory - Part I: Theory," *Nucl. Sci. Eng.* **29**, 43 (1967).

[47] André Mockel, "Invariant Imbedding and Polyenergetic Neutron Transport Theory - Part II: Numerical Results," *Nucl. Sci. Eng.* **29**, 51 (1967).

[48] W. Pfeiffer and J. L. Shapiro, "Reflection and Transmission Functions in Reactor Physics," *Nucl. Sci. Eng.* **38**, 253 (1969).

[49] *Radiation Quantities and Units,* International Commission on Radiation Units and Measurements, ICRU Report 11 (1968).

[50] D. K. Trubey, *Use of ICRU-Defined Quantities and Units in Shielding,* Oak Ridge National Laboratory Report ORNL-RSIC-16 (1968).

[51] R. L. Walker and M. Grotenhuis, *A Summary of Shielding Constants for Concrete,* Argonne National Laboratory Report ANL-6443 (1961).

[52] T. Rockwell, editor, *Reactor Shielding Design Manual,* Van Nostrand, Princeton, 1956.

[53] A. Honig, *Dose Build-Up Factors for Concrete,* Oak Ridge National Laboratory Report ORNL-tr-502 [translated from *Kerntechnik* **6**(9), 393 (1964)].

[54] F. H. Clark and D. K. Trubey, "Energy and Dose Buildup Factors for Various Concretes," *Nucl. Appl.* **4**, 37 (1968).

[55] Francis H. Clark, "Gamma-Ray Buildup Factors for Sand, Air, and Wood (Cellulose)," *Nucl. Appl.* **6**, 588 (1969).

[56] Francis B. K. Kam and Francis H. S. Clark, "Fission Neutron Attenuation and Gamma-Ray Buildup Factors for Lithium Hydride," *Nucl. Appl.* **3**, 433 (1967).

[57] A. B. Chilton, "Buildup Factors for Point Isotropic Gamma Ray Sources in Infinite Medium of Ordinary Concrete," *Nucl. Eng. Des.* **6**, 205 (1967).

[58] L. A. Bowman and D. K. Trubey, *Stratified Slab Gamma-Ray Dose Rate Buildup Factors for Lead and Water Shields,* Oak Ridge National Laboratory Report ORNL CF 58-1-41 (1958).

[59] L. A. Bowman and D. K. Trubey as reported by U. Fano *et al.,* in *Reactor Handbook,* E. P. Blizard and L. S. Abbott, editors, Sec. Ed., Vol. III, *Part B, Shielding,* p. 118, Interscience, New York, 1962.

[60] J. H. Hubbell, "A Power-Series Buildup Factor Formulation Application to Rectangular and Off-Axis Disk Source Problems," *J. Res. Natl. Bur. Std.* **67C**, 291 (1963).

[61] See ref. 16, p. 218.

[62] J. J. Taylor, *Application of Gamma Ray Buildup Data to Shield Design,* Westinghouse Electric Corp., Atomic Power Division, Report WAPD-RM-217 (1954).

[63] G. L. Strobel, "Additional Exponential Representations of Gamma-Ray Buildup Factors," *Nucl. Sci. Eng.* **11**, 450 (1961).

[64] S. Buscaglione and R. Manzini, *Build-Up Factors: Coefficients of the Equation of J. J. Taylor,* Oak Ridge National Laboratory Report ORNL-tr-80 (Rev.) [translated from Comitato Nazionale per l'Energia Nucleare Report RT/FI(65)7 (1965)].

[65] M. Capo, *Polynomial Approximation of Gamma Ray Buildup Factors for a Point Isotropic Source,* General Electric Co., Atomic Products Division, Report APEX-510 (1959).

[66] S. Buscaglione and R. Manzini, *On the Build-up Factors of Concrete: Coefficients of the Polynomial Representation,* Oak Ridge National Laboratory Report ORNL-tr-349 [translated from Comitato Nazionale per l'Energia Nucleare Report CEC-94 (1964)].

[67] D. K. Trubey, *A Survey of Empirical Functions Used to Fit Gamma-Ray Buildup Factors,* Oak Ridge National Laboratory Report ORNL-RSIC-10 (1966).

[68] M. J. Berger, p. 47 in *Proceedings of Shielding Symposium Held at the U. S. Naval Radiological Defense Laboratory, October 17-19, 1956,* U. S. Naval Radiological Defense Laboratory Reviews and Lectures No. 29.

[69] A. B. Chilton, D. Holoviak, and L. K. Donovan, *Interim Report, Determination of Parameters in an Empirical Function for Build-Up Factors for Various Photon Energies,* Naval Civil Engineering Laboratory Report NCEL-TN-389 (AD-249195) (1960).

[70] A. Rudloff, "The Use of Buildup Factors in Calculating Gamma Radiation from Plane Sources Behind Absorber of Finite Extension," *Atomkernergie* **9**, 451 (1946).

[71] A. B. Chilton, "Two-Parameter Formula for Point Source Buildup Factors," *Nucleonics* **23**(8), 119 (1965).

[72] L. A. Bowman and D. K. Trubey, *Deposition of Gamma-Ray Heating in Stratified Lead and Water Slabs,* Oak Ridge National Laboratory Report CF-58-7-99 (1958); see also as reported by C. N. Klahr in *Reactor Handbook, op cit.* p. 176 (refer to ref. 59).

[73] M. H. Kalos as reported in ref. 16, p. 225; also reported in *Reactor Handbook, op. cit.,* p. 120 (refer to ref. 59).

[74] D. L. Broder, Yu. P. Kaywin, and A. A. Kutrezov, *Sov. J. Atomic Energy* **12**, 26 (1962); also reported in *Engineering Compendium on Radiation Shielding,* R. G. Jaeger *et al.,* Editors, Vol. I, Springer-Verlag, New York, 1968.

[75] M. Kitazume, "Some Considerations of Buildup Factors in Gamma-Ray Penetration for Multiple Layers," *J. Atomic Energy Japan* **7**(9), 496 (1965).

[76] Y. Harima and Y. Nishiwaki, "An Approximate Transmission Dose Buildup Factor for Stratified Slabs," *J. Nucl. Sci. Tech. Japan* **6**(12), 711 (1969).

[77] R. D. Albert and T. A. Welton, *A Simplified Theory of Neutron Attenuation and Its Application to Shield Design,* Westinghouse Electric Corp., Atomic Power Division, Report WAPD-15 (1950).

[78] G. T. Chapman and C. L. Storrs, *Effective Neutron Removal Cross Sections for Shielding,* Oak Ridge National Laboratory Report ORNL-1843 (AECD-3978) (1955).

[79] See ref. 16, pp. 310-316.

[80] E. P. Blizard and J. M. Miller, *Radiation Attenuation Characteristics of Structural Concrete,* Oak Ridge National Laboratory Report ORNL-2913 (1958).

[81] P. B. Hemmig, in *Second Semiannual ANP Shielding Information Meeting, November 14–15, 1956,* Convair Report NARF 56-41T (Vol. 4) (classified); and J. M. Miller in *Applied Nuclear Phys. Div. Ann. Prog. Rept. Sept. 2, 1957,* Oak Ridge National Laboratory Report ORNL-2389, p. 187.

[82] J. M. Miller in *Neutron Phys. Div. Ann. Prog. Rept. Sept. 1, 1959,* Oak Ridge National Laboratory Report ORNL-2842, p. 168.

[83] L. K. Zoller, "Fast-Neutron-Removal Cross Sections," *Nucleonics* **22** (8), 128 (1964).

[84] D. K. Trubey and G. T. Chapman, *Effective Neutron Removal Cross Sections for Carbon and Oxygen in Continuous Mediums,* Oak Ridge National Laboratory Report ORNL-2197 (1958).

[85] D. K. Trubey, Oak Ridge National Laboratory, later unpublished analysis of the homogeneous-medium data.

[86] D. J. Dudziak and J. E. Schmucker, *Hydrogeneous-Material-Dependent Removal Cross Section of Lead for Fast Neutron Biological Dose,* Westinghouse Electric Corp., Report WAPD-TM-662 (1968).

[87]H. Bohl, Jr., E. M. Gelbard, B. L. Anderson, A. P. Hemphill, and B. P. Peterson, *P3MG1, A One-Dimensional Multigroup P-3 Program for the Philco-200 Computer,* Westinghouse Electric Corp., Report WAPD-TM-272 (1963).

[88]W. J. Price and W. L. Dunn, *Dose Attenuation of Polonium-Beryllium Neutrons by Iron, Aluminum, and Lead,* Air Force Institute of Technology, Tech. Report 57-7 (1967); see also ORNL-2497, Vol I (1957).

[89]D. J. Dudziak, "Fast-Neutron Biological Dose Attenuation by Lead and Polyethylene Shields," *Nucl. Appl.* **6**, 63 (1969).

[90]K. Shure, J. A. O'Brien, and D. M. Rothberg, "Neutron Dose Rate Attenuation by Iron and Lead," *Nucl. Sci. Eng.* **35**, 371 (1969).

[91]A. W. Casper, *Modified Fast Neutron Attenuation Functions,* General Electric Co., Atomic Products Division, Report XDC-60-2-76 (1960).

[92]E. P. Blizard, *On the Disk to Point or Infinite Plane Shielding Transformation,* Oak Ridge National Laboratory Report ORNL-2882 (1959).

[93]E. P. Blizard, "Analytical Methods of Shield Design," in *Reactor Handbook, op. cit.,* p. 128 (refer to ref. 59).

[94]See ref. 20.

[95]E. Solomito and J. R. Stockton, *Modifications of the Point-Kernel Code QAD-P5A: Conversion to the IBM-360 Computer and Incorporation of Additional Geometry Routines,* Oak Ridge National Laboratory Report ORNL-4181 (1968).

[96]F. H. Clark, N. A. Betz, and J. Brown, *Monte Carlo Calculations of the Penetration of Normally Incident Neutron Beams Through Concrete,* Oak Ridge National Laboratory Report ORNL-3926 (1967).

[97]*Reactor Physics Constants,* Argonne National Laboratory Report ANL-5800, 2d ed. (1963).

[98]D. K. Trubey and M. B. Emmett, *Some Calculations of the Fast-Neutron Distribution in Ordinary Concrete from Point and Plane Isotropic Fission Sources,* Oak Ridge National Laboratory Report ORNL-RSIC-4 (1965).

[99]R. W. Roussin and F. A. R. Schmidt, "Adjoint S_n Calculations of Coupled Neutron and Gamma-Ray Transport Through Concrete Slabs," accepted for publication in *Nuclear Engineering and Design.*

[100]F. J. Allen and A. T. Futterer, "Neutron Transmission Data," *Nucleonics* **21**(8), 120 (1963).

[101]D. K. Trubey, "The Single-Scattering Approximation to the Solution of the Gamma-Ray Air-Scattering Problem," *Nucl. Sci. Eng.* **10**, 102 (1961).

[102]W. Lowen, *A Build-Up Corrected Single Collision Model for Gamma-Ray Backscattering,* Eidgenossisches Institut fur Reaktorforschung, Wurenlingen, Report EIR-53 (1963).

[103]H. Yamakoshi, *An Examination of Several Calculational Models for Use in Computing Gamma-Ray Penetration of Structures,* Oak Ridge National Laboratory Report ORNL-TM-2520 (1969).

[104]J. Moteff, *Proposed Two-Component Method of Nuclear Shield Analysis,* General Electric Co., Cincinnati, Report DC-60-4-87 (1960).

[105]J. Moteff and H. W. Osgood, "Two-component Method of Neutron Shield Analysis for Space Application," *Trans. Am. Nucl. Soc.* **5**, 403 (1962).

[106]S. N. Cramer and M. Solomito, *SPACETRAN: A Code to Calculate Dose at Detectors at Various Distances from the Surface of a Cylinder,* Oak Ridge National Laboratory Report ORNL-TM-2592 (1969).

[107]D. G. Lindstrom and A. D. Wilcox, "Leakage Tracing from Boundaries of Low-Order S_N Solutions," *Trans. Am. Nucl. Soc.* **12**, 401 (1969).

[108]H. J. Amster and R. C. Gast, "The Analysis of Foil Activation Experiments in Infinite Homogeneous Media," *Nucl. Sci. Eng.* **11**, 167 (1961).

[109]M. J. Berger and J. Doggett, "Reflection and Transmission of Gamma Radiation by Barriers: Semi-analytic Monte Carlo Calculations," *J. Res. Natl. Bur. Std.* **56**, 89 (1956).

[110]S. N. Cramer, V. R. Cain, R. R. Coveyou, P. N. Stevens, and E. A. Straker, *The Use of Kernels in Studying Neutron Transport Problems,* Oak Ridge National Laboratory Report ORNL-TM-2508 (1969).

[111]M. O. Cohen, *AIRTRANS: A Time-Dependent Monte Carlo System for Radiation Transport in a Variable Density Atmosphere and the Ground,* United Nuclear Corp., Elmsford, N. Y., Report UNC-5179 (1967).

[112]D. E. Bendall and A. K. McCracken, "McBEND - A Prototype Code Utilizing Both Removal-Diffusion and Monte Carlo Methods," in *Proceedings of the Conference on the Physics Problems of Reactor Shielding, September, 1967,* Atomic Energy Research Establishment, Harwell, AERE-R-5773, Vol. 1, p. 41 (1968).

[113]T. W. Armstrong and P. N. Stevens, "A V^0 Importance Function for the Monte Carlo Calculation of the Deep Penetration of Gamma Rays," *J. Nucl. Energy* **23**, 331 (1969).

[114]J. H. Hubbell, R. L. Bach, and R. J. Herbold, "Radiation Field from a Circular Disk Source," *J. Res. Natl. Bur. Std.* **65C**, 249 (1961).

[115]D. K. Trubey, Oak Ridge National Laboratory, unpublished calculations.

[116]J. H. Hubbell, R. L. Bach, and J. C. Lamkin, "Radiation Field from a Rectangular Source," *J. Res. Natl. Bur. Std.* **64C**, 121 (1960).

[117]R. J. Burnside and D. Grim, "Nuclear Rocket Radiation," *Trans. Am. Nucl. Soc.* **12**, 377 (1969).

[118]M. A. Capo, L. D. Stephenson, and J. R. Magaw, "Analysis of the NRX-A6 Radiation Measurements," *Trans. Am. Nucl. Soc.* **12**, 379 (1969).

[119]R. G. Soltesz, V. S. Oblock, J. R. Magaw, L. D. Stephenson, and W. D. Rankin, "Comparison of Experimentally Measured and Calculated Radiation Environments Internal to Nuclear Rocket Shield Experiments," *Trans. Am. Nucl. Soc.* **12**, 380 (1969).

[120]Private communication by E. A. Warman to D. K. Trubey of Aerojet-General Corporation Report RN-PA-0020, *Seminar/Workshop Material on Kernel Techniques for Nuclear Rocket Propellant Tank Geometry/Shielding Analyses* (1929).

[121]M. Solomito and H. C. Claiborne, "Shipping Cask Shielding Requirements," *Neutron Phys. Div. Ann. Prog. Rept. for Period Ending May 31, 1967,* Oak Ridge National Laboratory Report ORNL-4134, p. 73 (1967).

[122]A. P. Fraas, Oak Ridge National Laboratory, private communication.

[123]R. L. French, *Reactor Shield Heating Calculations for Gamma Rays,* Convair, Ft. Worth, Texas, Report NP-9354 (also FZM-1076) (1960).

[124]F. R. Mynatt and L. R. Williams, "Some Characteristics of Secondary Gamma-Ray Transport in Asymmetric Shields," *Proceedings of the Special Sessions on Gamma-Ray Production and Transport and on Civil Defense Shielding, November 1967,* ANS-SD-7, p. 113-135 (1969).

[125]F. R. Mynatt, "Some Characteristics of Secondary Gamma-Ray Transport in Asymmetric SNAP Shields," *Trans. Am. Nucl. Soc.* **10**, 542 (1967).

[126]J. W. Haffner, "Neutron Energy Spectrum Calculations in Reactor Shields," Preprint V-84, *Nuclear Engineering and Science Conference, April 6-9, 1959, Cleveland, Ohio,* Engineers Joint Council, New York.

[127]D. C. Anderson and K. Shure, "Thermal Neutron Flux Distributions in Metal-Hydrogenous Shields," *Nucl. Sci. Eng.* **8**, 260 (1960).

[128]K. Shure, "Few-Group and Multigroup Calculations of Neutron Penetration," *Nucl. Sci. Eng.* **27**, 468 (1967).

[129]A. F. Avery *et al., Methods of Calculation for Use in the Design of Shields for Power Reactors,* United Kingdom Atomic Energy Authority Report AERE-R-3216 (1960).

[130]D. E. Bendall, *RASH D - A Mercury Programme for Neutron Shielding Calculations,* United Kingdom Atomic Energy Authority Report AEEW-M-261 (1962).

[131]J. Butler, *The Status of Theoretical Methods for Reactor Shield Design,* United Kingdom Atomic Energy Authority Report AEEW-R-361 (1964).

[132]E. G. Peterson, *MAC - A Bulk Shielding Code,* Hanford Atomic Products Operation Report HW-73381 (1962).

[133]U. Canali *et al., MAC-RAD, A Reactor Shielding Code,* European Atomic Energy Community Report EUR-2152.e (1964).

[134]L. Hjarne, editor, *A User's Manual for the NRL Shield Design Method,* Aktiebolaget Atomenergia Report AE-145 (1964).

[135]L. Hjarne and M. Leimdorfer, "A Method for Predicting the Penetration and Slowing Down of Neutrons in Reactor Shields," *Nucl. Sci. Eng.* **24**, 165 (1966).

[136]C. Ponti, H. Preusch, and H. Schubart, *SABINE: A One Dimensional Bulk Shielding Program,* European Atomic Energy Community, Ispra, Italy, Report EUR 3636.e (1967).

[137]R. Nicks, G. Perline, and C. Ponti, "SABINE: A One-Dimensional Shielding Programme Which Employs Experimental Removal Cross Sections," in AERE-R-5773 *op. cit.*, Vol. 1, pp. 5-40 (1968); see ref. 112.

[138]W. D. Collier and G. C. Curtis, *ATTOW, A Two-Dimensional Shielding Program,* United Kingdom Atomic Energy Authority, Risley, Report TRG-1466(R) (1967).

[139]A. F. Avery and C. C. Curtis, "Neutron Attenuation Studies in Fast Reactor Shielding," in AERE-R-5773 *op. cit.*, Vol. 2, pp. 515-553 (1968); see ref. 112.

[140]"Sixth Period Discussion," AERE-R-5773 *op. cit.*, Vol. 2, pp. 598-599 (1968); see ref. 112.

[141]H. C. Claiborne, "Analytical Solutions for Heat Generation Distributions in Regular Geometries," in *Engineering Compendium on Radiation Shielding,* R. G. Jaeger *et al.*, editors, Vol. I, p. 441, Springer-Verlag, New York, 1968.

[142]J. H. Renken, *Use of Solutions to the Adjoint Transport Equation for the Evaluation of Radiation Shield Designs,* Sandia Laboratories Report SC-RR-70-98 (1970).

[143]M. H. Kalos, "Monte Carlo Integration of the Adjoint Gamma-Ray Transport Equation," *Nucl. Sci. Eng.* **33**, 284-290 (1968).

[144]B. F. Maskewitz, *Abstracts of Digital Computer Code Packages Assembled by the Radiation Shielding Information Center,* Oak Ridge National Laboratory Report ORNL-RSIC-13, Vol. I.

[145]K. D. Lathrop, *GAMLEG - A FORTRAN Code to Produce Multigroup Cross Sections for Photon Transport Calculations,* Los Alamos Scientific Laboratory Report LA-3267 (1967).

[146]B. G. Carlson *et al., DTF Users Manual,* United Nuclear Corp. Report UNC Phys/Math-3321, Vols. I and II (1963).

[147]J. H. Renken and K. G. Adams, *An Improved Capability for Solution of Photon Transport Problems by the Method of Discrete Ordinates,* Sandia Laboratories, Albuquerque Report SC-RR-69-739 (1969).

[148]H. Penkuhn, *A Numerical Solution of the Gamma Transport Boltzmann Equation Applied to Concrete Slabs,* European Atomic Energy Community, Ispra, Italy, Reports EUR 2488.e (1965); see also EUR 1643.e, p. 92 (1964); and Argonne National Laboratory Report ANL-7050, p. 113 (1965).

[149]H. Penkuhn, *User's Manual for the Gamma Transport Codes BIGGI 4P and BIGGI 4T,* European Atomic Energy Community, Ispra, Italy, Report EUR 3555.e (1967).

[150]R. G. Soltesz, R. K. Disney, and G. Collier, *User's Manual for the DOT-IIW Discrete Ordinates Transport Computer Code,* Westinghouse Astronuclear Laboratory Report WANL-TME-1982 (1969).

[151]N. M. Greene and C. W. Craven, Jr., *XSDRN: A Discrete Ordinates Spectral Averaging Code,* Oak Ridge National Laboratory Report ORNL-TM-2500 (1969).

[152]N. M. Greene, *XLACS: Cross Section Production Package for XSDRN,* Oak Ridge Computing Technology Center Report (to be published).

[153]W. W. Engle, Jr., *A Users Manual for ASOP, ANISN Shield Optimization Program,* Oak Ridge Computing Technology Center Report CTC-INF-941 (1969).

[154]F. R. Mynatt *et al., Neutron Phys. Div. Ann. Prog. Rept. May 31, 1967,* Oak Ridge National Laboratory Report ORNL-4134, p. 55.

[155]W. W. Engle, Jr., and F. R. Mynatt, *Neutron Phys. Div. Ann. Prog. Rept. May 31, 1968,* Oak Ridge National Laboratory Report ORNL-4280, p. 61.

[156]K. D. Lathrop, *TWOTRAN, A FORTRAN Program for Two Dimensional Transport,* Gulf General Atomic Report GA-8747 (1968).

[157]K. D. Lathrop and F. W. Binkley, *Theory and Use of the General-Geometry TWOTRAN Program,* Los Alamos Scientific Laboratory Report LA-4432 (1970).

[158]K. D. Lathrop, *User's Guide for the TWOTRAN (x,y) Program,* Los Alamos Scientific Laboratory Report LA-4058 (1968).

[159]W. E. Kinney, *Program STATEST, An Application of the Method of Statistical Estimation to the Calculation of Neutron Flux in Anisotropically Scattering Media by Monte Carlo,* Oak Ridge National Laboratory Report ORNL-3715 (1964).

[160]F. B. K. Kam and K. D. Franz, *ACTIFK, A General Analysis Code for O5R,* Oak Ridge National Laboratory Report ORNL-3856 (1966).

[161]H. Steinberg and R. Aronson, *TRG-SGD, A Monte Carlo Program to Calculate Secondary Gamma Ray Dose from a Nuclear Weapon Detonation,* Kirtland Air Force Base, Weapons Laboratory, Report WL-TDR-64-46, Vols. I and II (1964).

[162]D. J. Raso and S. Woolf, *Monte Carlo Program for Calculating Doses Resulting from an Isotropic Point Source in an Exponential Atmosphere,* Technical Operations Research Report TO-B 64-12 (1964).

[163]S. K. Penny, D. K. Trubey, and M. B. Emmett, *OGRE, A Monte Carlo System for Gamma-Ray Transport Studies, Including an Example (OGRE-P1) for Transmission Through Laminated Slabs,* Oak Ridge National Laboratory Report ORNL-3805 (1966).

[164]D. K. Trubey and M. B. Emmett, *OGRE-G, An OGRE System Monte Carlo Code for the Calculation of Gamma-Ray Dose Rate at Arbitrary Points in an Arbitrary Geometry,* Oak Ridge National Laboratory Report ORNL-TM-1212 (1966).

[165]B. Eisenman and E. Hennessy, *Adonis: An IBM-7090 Monte Carlo Shielding Code Which Solves for the Transport of Neutrons or Gamma Rays in Three-Dimensional Rectangular Geometry,* United Nuclear Corp. Report UNUCOR-635 (1963).

[166]B. Eisenman and F. R. Nakache, *UNC-SAM: A FORTRAN Monte Carlo System for the Evaluation of Neutron or Gamma-Ray Transport in Three-Dimensional Geometry,* United Nuclear Corp. Report UNC-5093 (1964).

[167]E. S. Troubetzkoy, *UNC-SAM-2: A FORTRAN Monte Carlo Program Treating Time-Dependent Neutron and Photon Transport Through Matter,* United Nuclear Corp. Report UNC-5157 (1966).

[168]E. S. Troubetzkoy, *Modification of UNC-SAM-2 to UNC-SAM-3,* Defense Atomic Support Agency Report DASA-2338 (UNC-5157 Supplement) (1970).

[169]S. Kelman, *ENDT: A FORTRAN Program to Prepare Cross-Section Data for UNC-SAM-3 from ENDF/B Tapes,* Defense Atomic Support Agency Report DASA-2337 (UNC-5243) (1970).

[170]See ref. 167.

[171]W. Guber, R. Nagel, R. Goldstein, P. S. Mittleman, and M. H. Kalos, *A Geometrical Description Technique Suitable for Computer Analysis of Both the Nuclear and Conventional Vulnerability of Armored Military Vehicles,* Mathematical Applications Group, Inc., Report MAGI-6701 (1967).

[172]R. E. Maerker and V. R. Cain, *AMC: A Monte Carlo Code Utilizing the Albedo Approach for Calculating Neutron and Capture Gamma-Ray Distributions in Rectangular Concrete Ducts,* Oak Ridge National Laboratory Report ORNL-3964 (1967).

[173]T. M. Jordan, *FASTER, A FORTRAN Analytic Solution of the Transport Equation by Random Sampling,* Westinghouse Astronuclear Laboratory Report WANL-PR-(LL)-010, Vol. 9 (1967).

[174]M. A. Capo, *Basic Geometry for the Nuclear Rocket Reactor Sample Problem,* Westinghouse Astronuclear Laboratory Report WANL-PR-(LL)-014, Vol. 1 (1967).

[175]M. A. Capo and T. M. Jordan, *Sample Nuclear Rocket Reactor Problem for the FASTER Code,* Westinghouse Astronuclear Laboratory Report WANL-PR-(LL)-014, Vol. 8 (1967).

[176]G. L. Case, *Utilization Manual, Computer Program 2M5300, AIRTRANS,* Lockheed Missile and Space Company Report LMSC-5234 (1968).

[177]M. O. Cohen, *AIRTRANS: A Time-Dependent Monte Carlo System for Radiation Transport in a Variable Density Atmosphere and the Ground,* United Nuclear Corp. Report, Elmsford, N. Y., UNC-5179 (1967).

[178]E. R. Friedman, M. H. Kalos, S. Preiser, G. Rabinowitz, and J. G. Beckerley, *The Numerical Solution of the Adjoint Transport Equation for Gamma Rays by the GADJET Code,* Naval Radiological Defense Laboratory Report NRDL-TRC-68-27 (1968).

[179]S. Preiser, M. Kalos, A. Stathoplos, J. G. Beckerley, E. R. Friedman, G. Rabinowitz, H. Sadowski, and L. A. Willis, *Calculation of Gamma Exposure Rates in an Open or Covered Basement in Fallout Fields Using the GADJET Code,* Naval Radiological Defense Laboratory Report NRDL-TRC-68-25 (1968).

[180]M. O. Cohen, *ANTE-2 - A Fortran Computer Code for the Solution of the Adjoint Neutron Transport Equation by the Monte Carlo Technique,* Defense Atomic Support Agency Report DASA-2396 (1970).

[181]M. J. Berger and S. M. Seltzer, *Electron and Photon Transport Programs (I. Introduction and Notes on Program DATAPAC 4),* National Bureau of Standards Report NBS-9836 (1968).

[182]M. J. Berger and S. M. Seltzer, *Electron and Photon Transport Programs (II. Notes on Program ETRAN 15),* National Bureau of Standards Report NBS-9837 (1968).

[183]T. M. Jordan, *BETA, A Monte Carlo Computer Program for Bremsstrahlung and Electron Transport Analysis,* Air Force Weapons Laboratory Report AFWL-TR-68-111 (1968).

[184]R. E. Malenfant, *QAD: A Series of Point Kernel General-Purpose Shielding Programs,* Los Alamos Scientific Laboratory Report LA-3537 (1967).

[185]G. P. Lahti, *QAD-HD Point Kernel Radiation Shielding Computer Code to Evaluate Propellant Heating and Dose to Crew,* National Aeronautics and Space Administration Report NASA-TM-X-1397 (1967).

[186]E. D. Arnold and B. F. Maskewitz, *SDC, A Shielding-Design Calculation Code for Fuel-Handling Facilities,* Oak Ridge National Laboratory Report ORNL-3041 (1966).

[187]E. D. Arnold, *PHOEBE - A Code for Calculating Beta and Gamma Activity and Spectra for ^{235}U Fission Products,* Oak Ridge National Laboratory Report ORNL-3931 (1966).

[188]R. L. Engle, J. Greenborg, and M. M. Hendrickson, *ISOSHLD - A Computer Code for General Purpose Isotope Shielding Analysis,* Pacific Northwest Laboratory Richland, Report BNWL-236 (1966).

[189]R. O. Gumprecht, unpublished data on Code RIBD (*R*adio *I*sotope *B*uildup and *D*ecay).

[190]H. H. Van Tuyl, *BREMRAD - A Computer Code for External and Internal Bremsstrahlung Calculations,* Hanford Atomic Products Operations Report HW-83784 (1964).

[191]G. L. Simmons, J. J. Regimbal, J. Greenborg, E. L. Kelly, Jr., and H. H. Van Tuyl, *ISOSHLD-II: Code Revision to Include Calculations of Dose Rate from Shielded Bremsstrahlung Sources,* Pacific Northwest Laboratory, Richland, Report BNWL-236 Suppl. (1967).

[192]C. A. Mansius, *A Revised Photon Probability Library for Use with ISOSHLD-III,* Pacific Northwest Laboratory, Richland, Report BNWL-236, Suppl. 2 (1969).

[193]L. D. O'Dell and W. L. Bunch, *Revised Fast Reactor Library for Use with RIBD,* Pacific Northwest Laboratory, Richland, Report BNWL-962 (1969).

[194]F. T. Binford, F. B. K. Kam, and J. Barish, *Estimation of Radiation Doses Following a Reactor Accident,* Oak Ridge National Laboratory Report ORNL-4086 (1968).

[195]R. K. Disney and M. A. Capo, *KAP-V: The Point Kernel Attenuation Program,* Westinghouse Astronuclear Laboratory Report WANL-PR-(LL)-010, Vol. 4 (1967).

[196]M. A. Capo, R. K. Disney, T. M. Jordan, and H. C. Woodsum, *Synopsis of Methods and Results of Analyses,* Westinghouse Astronuclear Laboratory Report WANL-PR-(LL)-010, Vol. 1 (1967).

[197]M. A. Capo, *Sample Nuclear Rocket Reactor Problem for the KAP V Code,* Westinghouse Astro-

nuclear Laboratory Report WANL-PR-(LL)-014, Vol. 7 (1967).

[198]J. Greenborg, *Two Cross Section Libraries for Use with MAC Shielding Code,* Hanford Atomic Products Operation Report HW-73381, Supp. 1 (1964).

[199]H. Preusch and H. Ilsemann, *MAC-RAD, A Multigroup Attenuation Code for Plane Geometry,* Oak Ridge National Laboratory Report ORNL-tr-610 (1963) (translated from Allgemeine Elektricitats-Gesellschaft, Kernenergieanlagen, Hochhaus, Germany, Report AEG-KEA-116).

[200]Kj. Nyman *et al., A Preliminary User's Manual for the NRL Shield Design Method in FORTRAN Language,* Aktiebolaget Atomenergia, Stockholm, Report AE-FFA-673-RFN-213 (1965).

[201]E. Aalto, R. Fraki, and K. Malen, "The Fine Adjustment of the Neutron Penetration in the NRN Method," *Nucl. Sci. Eng.* **22**, 443 (1965).

[202]A. F. Avery, J. Clarke, and A. Hartley, *COMPRASH (A Preliminary User's Guide Prepared for the ENEA Seminar-Workshop on Shielding Programmes Held at Ispra, April 1966),* United Kingdom Atomic Energy Authority Report AEEW-M648 (1966).

[203]C. Ponti, *SABINE, A One-Dimensional Bulk Shielding Program,* European Atomic Energy Community - EURATOM, Report EUR 3636.e Addendum (1969).

[204]W. B. Henderson and W. E. Edwards, *NSP Kernel-Diffusion Library, KDLIBE, NSO910 (User's Manual),* Nuclear Systems Program, General Electric Co., Cincinnati, Report GESP-226 (n.d.).

[205]W. E. Edwards, *Shield Kernel-Diffusion Analysis,* Nuclear Technology Department, General Electric, Report GEMP-599 (1968).

[206]W. D. Collier and G. C. Curtis, *A Two-Dimensional Shielding Program,* United Kingdom Atomic Energy Authority, Report TRG-1466 (R).

[207]W. W. Engle, Jr., and F. R. Mynatt, "One-Dimensional Time-Dependent Discrete Ordinates," *Trans. Am. Nucl. Soc.* **12**, 400 (1969).

[208]E. P. Blizard, "Geometrical Transformations," in *Engineering Compendium on Radiation Shielding,* R. G. Jaeger *et al.,* Editors, Vol. I, pp. 403-411, Springer-Verlag (1968).

[209]G. Placzek, *The Functions* $E_n(x) = \int_1^\infty e^{-xu} u^{-n}\, dx$, National Research Council of Canada, Division of Atomic Energy, Report NRC-1547 (1946).

[210]D. K. Trubey, *A Table of Three Exponential Integrals,* Oak Ridge National Laboratory Report ORNL-2750 (1959).

[211]Federal Works Agency, Works Project Administration, *Tables of Sine, Cosine, and Exponential Integrals,* Vols. I and II, under sponsorship of National Bureau of Standards, 1940.

[212]F. Clark, *Approximation to All Orders of the Exponential Integral,* Wright Air Development Center Report WADC-TR-57-771 (1958).

[213]M. Abramowitz and I. A. Stegun, editors, *Handbook of Mathematical Functions with Formulas, Graphs, and Mathematical Tables,* National Bureau of Standards, Applied Mathematics Series 55, GPO, Washington, 1964.

[214]F. A. Schmidt, *The Attenuation Properties of Concrete for Shielding of Neutrons of Energy Less than 15 MeV,* Oak Ridge National Laboratory Report ORNL-RSIC-26 (1970).

[215]D. K. Trubey, "Gamma-Ray Buildup Factor Coefficients for Concrete and Other Materials," *Nucl. Appl. Tech.* **9**, 439 (1970).

Unclassified

Security Classification

DOCUMENT CONTROL DATA - R & D

(Security classification of title, body of abstract and indexing annotation must be entered when the overall report is classified)

1. ORIGINATING ACTIVITY *(Corporate author)*

Oak Ridge National Laboratory
Oak Ridge, Tennessee

2a. REPORT SECURITY CLASSIFICATION
Unclassified

2b. GROUP

3. REPORT TITLE

"Methods for Calculating Neutron and Gamma-Ray Attenuation,"
Chapter 3 of Weapons Radiation Shielding Handbook

4. DESCRIPTIVE NOTES *(Type of report and inclusive dates)*
Handbook

5. AUTHOR(S) *(First name, middle initial, last name)*

Authors: Paul N. Stevens and David K. Trubey
Editors: Lorraine S. Abbott, H. Clyde Claiborne, Charles E. Clifford

6. REPORT DATE	7a. TOTAL NO. OF PAGES	7b. NO. OF REFS
April 1971	182	215

8a. CONTRACT OR GRANT NO.	9a. ORIGINATOR'S REPORT NUMBER(S)
Interagency Agreement: 40-36-64	DNA-1892-3 Rev. 1 (Formerly DASA-1892-3)
b. PROJECT NO.	
c. IACRO EO 71-804-0	9b. OTHER REPORT NO(S) *(Any other numbers that may be assigned this report)*
d. RMSS Subtask PE033-01	

10. DISTRIBUTION STATEMENT

Approved for public release; distribution unlimited

11. SUPPLEMENTARY NOTES	12. SPONSORING MILITARY ACTIVITY
	Director, Defense Nuclear Agency Washington, D.C. 20305

13. ABSTRACT

Calculations of the attenuation of neutrons and gamma rays in shields can be performed by several techniques, the best technique for a particular problem depending on the type of problem to be solved and the degree of accuracy required. This chapter of the Handbook surveys the calculational methods used most frequently and provides summaries of digital computer codes based on the various methods. The methods covered are those of spherical harmonics, discrete ordinates, moments, Monte Carlo, diffusion theory, invariant imbedding, and kernels, plus a method which combines a removal kernel with diffusion theory. Except for the invariant imbedding method, all these techniques are either approximate solutions to the well-known Boltzmann equation or are based on kernels obtained from solutions to the equation. A discussion of the Boltzmann equation is also included in the chapter. (U)

DD FORM 1 NOV 65 1473

Unclassified

Security Classification

Unclassified
Security Classification

14. KEY WORDS	LINK A		LINK B		LINK C	
	ROLE	WT	ROLE	WT	ROLE	WT
Neutron attenuation						
Gamma-ray attenuation						
Secondary gamma-ray attenuation						
Radiation transport methods						
Boltzmann transport equation						
Spherical harmonics method						
Discrete ordinates S_n method						
Moments method						
Monte Carlo method						
Diffusion theory						
Invariant imbedding						
Point kernels						
Empirical kernels						
Buildup factors						
Removal cross sections						
Albert-Welton kernel						
Removal-diffusion method						
Spinney method						
Attenuation functions						

Unclassified
Security Classification

DISTRIBUTION

Department of Defense

1. Director, Advanced Research Projects Agency, Washington, D.C. 20301, ATTN: Technical Information Officer
2–13. Director, Defense Nuclear Agency, Washington, D.C. 20305, ATTN: RARP (4 copies); Technical Library (APTL, 2 copies); APSI (archives); DDST; APSI for transmittal to Assistant to the Secretary of Defense (Atomic Energy); APSI for transmittal to Director of Defense Research and Engineering [ATTN: Assistant Director (Strategic Weapons), Deputy Director (Strategic and Space Systems), and Assistant Director (Defensive Systems)]
14–25. Administrator, Defense Documentation Center, Cameron Station – Bldg. 5, Alexandria, Virginia 22314, ATTN: TC (12 copies)
26. Commandant, Industrial College of the Armed Forces, Ft. Lesley J. McNair, Washington, D.C. 20315, ATTN: Document Control
27. Commandant, National War College, Washington, D.C. 20305, ATTN: Class Rec. Library
28. Director, Weapons Systems Evaluation Group, Washington, D.C. 20305, ATTN: Capt. Donald E. McCoy, USN
29. Commander, Field Command, Defense Nuclear Agency, ATTN: FCWS-5C, Kirtland AFB, Albuquerque, New Mexico 87115

Department of the Army

30. Director of Civil Defense, Department of the Army, Washington, D.C. 20310, ATTN: RE (Assistant Director for Research)
31. Chief of Engineers, U.S. Army, Washington, D.C. 20315
32–33. Chief of Research and Development, Department of the Army, Washington, D.C. 20310, ATTN: Nuclear, Chemical-Biological Division; ABMDA-00
34. Director, Advanced Ballistic Missile Defense Agency, Department of the Army, Washington, D.C. 20310
35. Commandant, Army Command and General Staff College, Fort Leavenworth, Kansas 66027, ATTN: Acquisitions, Library Division
36. Superintendent, U.S. Military Academy, West Point, New York 10996, ATTN: Document Library
37. Commandant, Army War College, Carlisle Barracks, Pennsylvania 17013
38–44. Commanding Officer, Army Combat Developments Command, Nuclear Agency, Fort Bliss, Texas 79916, ATTN: Technical Library; Charles N. Davidson, LTC Fraser; CDINS-E
45. Commanding Officer, Atmospheric Sciences Laboratory, USAECOM, White Sands Missile Range, New Mexico 88002
46–47. Commanding General, Army Electronics Command, Ft. Monmouth, New Jersey 07703, ATTN: Technical Documents Center, Evans Area; AMSEL-XL-D
48. Commanding Officer Army Electronic Proving Ground, Fort Huachuca, Arizona 85613, ATTN: Technical Library
49. Commanding Officer, Army Engineer Explosive Excavation Research Office, Lawrence Livermore Laboratory, Livermore, California 94550, ATTN: Document Control
50. Director, Army Engineer Waterways Experiment Station, Box 631, Vicksburg, Mississippi 39180, ATTN: Library
51. Commanding General, Army Materiel Command, Washington, D.C. 20315, ATTN: AMCRD-BN-RE, N. Stulman
52–54. Department of the Army, Harry Diamond Laboratories, Washington, D.C. 20433, ATTN: Chief, Nuclear Vulnerability Branch; Technical Reference Branch; AMXDO-NP

55–57. Commanding Officer, Army Nuclear Effects Laboratories, Edgewood Arsenal, Maryland 21010, ATTN: Technical Library; Dr. Eccleshall; AMXRD-BNL, Mr. David Rigotti
58. Director, U.S. Army Advanced Ballistic Missile Defense Agency, Huntsville Office, P.O. Box 1500, Huntsville, Alabama, 35807
59. Commanding Officer, Army SAFEGUARD System Command Field Office, Bell Telephone Laboratories, Whippany Road, Whippany, New Jersey 07981, ATTN: SENSC-DTF-B, J. Turner
60–63. Commanding Officer, Army Ballistic Research Laboratories, Aberdeen Proving Ground, Maryland 21005, ATTN: Technical Library; Mr. Thomas Jeter; Mr. J. Bock; AMXRD-BNL
64. Chief, Army Research Office (Durham), Box CM, Duke Station, Durham, North Carolina 27706, ATTN: Dr. R. Mace/Herman Robl

Department of the Navy

65. Superintendent, Naval Academy, Annapolis, Maryland 21402
66. Commanding Officer, Naval Applied Science Laboratory, Flushing and Washington Avenues, Brooklyn, New York 11251
67. Commanding Officer, Naval Civil Engineering Laboratory, Port Hueneme, California 93041, ATTN: Code L31
68. Commander, Naval Oceanographic Office, Washington, D.C. 20390, ATTN: Library (Code 1640)
69–70. Commander, Naval Ordnance Laboratory, Silver Spring, Maryland 20910, ATTN: Code 121, Navy Nuclear Program Office; Code 1-315, Technical Library
71–72. Superintendent, Naval Postgraduate School, Monterey, California 93940, ATTN: Technical Library; Code 0384
73–75. Director, Naval Research Laboratory, Washington, D.C. 20390, ATTN: Technical Library; Code 7633, Dr. Wayne D. Jones; Code 7680, Mr. Laverne S. Birks
76. Commanding Officer, Naval Schools Command, Treasure Island, San Francisco, California 94130, ATTN: NBCD Department (Technical Library)
77. Commanding Officer, Naval School, Civil Engineer Corps Officers, Naval Construction Battalion Center, Port Hueneme, California, 93041, ATTN: Librarian
78. Commander, Naval Ship Research and Development Center, Washington, D.C. 20007, ATTN: Library
79. President, Naval War College, Newport, Rhode Island 02840
80–81. Commanding Officer, Naval Weapons Evaluation Facility, Kirtland Air Force Base, Albuquerque, New Mexico 87117, ATTN: Document Control; Mr. J. Abbott
82. Chief of Naval Research, Department of the Navy, Arlington, Virginia 22217

Department of the Air Force

83. Headquarters, USAF, Washington, D.C. 20330, ATTN: AFGOA (Chief, Operations Analysis), Dr. Ray
84–87. Headquarters, Air Force Systems Command, Andrews AFB, Washington, D.C. 20331, ATTN: SCPSL, Technical Library; SCTSW (Weapons & Weapons Effects Div.); SCTS (Director, Science & Tech.); Mr. A. J. Chiota
88. Headquarters, Office of Aerospace Research, 1400 Wilson Blvd., Arlington, Virginia 22209
89. AF Office of Scientific Research, OAR, 1400 Wilson Blvd., Arlington, Virginia 22209, ATTN: Documents Branch
90. AF Aero-Propulsion Laboratory, AFSC, Wright-Patterson AFB, Ohio 45433
91. AF Cambridge Research Laboratories, OAR, L. G. Hanscom Field, Bedford, Massachusetts 01730, ATTN: SUOL, Research Library, STOP 29
92. AF Director of Nuclear Safety, Kirtland AFB, New Mexico 87117
93. AF Institute of Technology, AU, Wright-Patterson AFB, Ohio 45433, ATTN: Technical Library
94. AF Materials Laboratory, AFSC, Wright-Patterson AFB, Ohio 45433, ATTN: Library
95–102. AF Weapons Laboratory, AFSC, Kirtland AFB, New Mexico 87117, ATTN: WLOL, Technical Library; WLRET (TREE Group Leader); WLTH; Chief, WLBR (Biophysics Br.); SR; WLC; SRE; SRR
103. Air University Library, AU, Maxwell Air Force Base, Alabama 36112
104. Electronic Systems Division, AFSC, L. G. Hanscom Field, Bedford, Massachusetts 01730, ATTN: ESTI, Science and Technical Info. Division
105. Foreign Technology Division, AFSC, Wright-Patterson AFB, Ohio 45433, ATTN: TD-BTA, Library

106–107. Rome Air Development Center, AFSC, Griffiss Air Force Base, New York 13440, ATTN: Documents Library (EMLAL-1); EMTLD (Documents Library)
108. Space and Missile Systems Organization, AFSC, AF Unit Post Office, Los Angeles, California 90045, ATTN: Library
109. Space and Missile Systems Organizations, AFSC, Norton AFB, Calif. 92409, ATTN: Library

Atomic Energy Commission

110. Sandia Laboratories, Livermore Laboratory, P.O. Box 969, Livermore, California, ATTN: Library
111–329. U.S. Atomic Energy Commission, Division of Tech. Info. Ext., P.O. Box 62, Oak Ridge, Tennessee 37830, ATTN: Document Control and given distribution as shown in TID-4500 under Reactor Technology category (25 copies – NTIS)
330. U.S. Atomic Energy Commission, New York Operations Office, 376 Hudson Street, New York, New York 10014, ATTN: Document Control
331. Argonne National Laboratory, 9700 South Cass Avenue, Argonne, Illinois 60440, ATTN: Document Control For – Library Services Dept./Report Sec.
332. Battelle Memorial Institute, Pacific Northwest Laboratory, P.O. Box 999, Richland, Washington 99352, ATTN: Document Control For: K. H. Larson
333–334. Brookhaven National Laboratory, P.O. Box 150, Upton, Long Island, New York 11973, ATTN: Document Control For – Document Section; NCSC
335–341. University of California, Lawrence Livermore Laboratory, Technical Information Division, P.O. Box 808, Livermore, California 94550, ATTN: Technical Library; Dr. R. Howerton; Dr. John Anderson; Dr. Lawrence S. Germaine (L-18); Mr. Robert Kuckuck (L-18); Mr. J. Watson; Mr. P. Ebert
342–348. Los Alamos Scientific Laboratory, P.O. Box 1663, Los Alamos, New Mexico 87544, ATTN: Document Control For: R. Taschek; Dr. Diven; Dr. Young; Dr. Stewart; Mr. W. A. Biggers; Mr. Westervelt; Mr. Thayer
349–352. Sandia Laboratories, P.O. Box. 5800, Albuquerque, New Mexico 87115, ATTN: Document Control For: C. R. Mehl; Dr. Jim Plimpton; Dr. Jack Walker; Dr. Frank Biggs
353–404. Union Carbide Corporation, Nuclear Division, Oak Ridge National Laboratory, P.O. Box X, Oak Ridge, Tennessee 37830, ATTN: Document Control For: Radiation Shielding Info. Ctr. (3 copies); C. E. Clifford, (2), L. S. Abbott (5), D. K. Trubey (5), H. C. Claiborne (2), P. N. Stevens (25), J. Auxier (1), Civil Defense Library (1), Central Research Library (3), Document Reference Section (1), Laboratory Records, ORNL R.C. (1), ORNL Patent Office (1), R. B. Parker (1), A. M. Weinberg (1)
405. Assistant General Manager for Military Application, U.S. Atomic Energy Commission, Washington, D.C. 20545

Other Government

406–407. National Bureau of Standards, Washington, D.C. 20234, ATTN: R. B. Schwartz; Mr. C. M. Eisenhauer

Department of Defense Contractors

408. National Academy of Sciences, 2101 Constitution Avenue, N.W., Washington, D.C. 20418
409. The Trustees of Boston College, Chestnut Hill Campus, Chestnut Hill, Massachusetts 02167, ATTN: Dr. I. J. Russell
410. California Institute of Technology, Jet Propulsion Laboratory, 4800 Oak Grove Drive, Pasadena, California 91103, ATTN: Document Control Office
411. University of California, San Diego, P.O. Box 109, La Jolla, California 92038, ATTN: Keith A. Brueckner
412. University of Illinois, Urbana Campus, 112 English Bldg., Urbana, Ill. 61801, ATTN: Classified Information Supervisor For – Dr. Arthur Chilton
413. University of New Mexico, Albuquerque, New Mexico 87106, ATTN: Library
414. Eric H. Wang Civil Eng. Research Facility, University of New Mexico, Box 188, University Station, Albuquerque, New Mexico 87106
415. Pennsylvania State University, University Park, Penn. 16802, ATTN: Dr. A. Forderaro
416. Aerospace Corporation, P.O. Box 95085, Los Angeles, California 90045, ATTN: Off. of Tech., Surviv. Dir. (V. Josephson)
417–418. Aerospace Corporation, P.O. Box 5866, San Bernardino, California 92408, ATTN: Mr. Greenhow; Library

419–420. Battelle Memorial Institute, 505 King Avenue, Columbus, Ohio 43201, ATTN: Radiation Effects Information Center; Library
421–423. Bell Telephone Laboratories, Inc., Whippany Road, Whippany, New Jersey 07981, ATTN: Tech. Rpt. Ctr., Rm 2A-165B/Dr. Benedict; Tech. Rpt. Ctr., Rm 2A-165B/Dr. McAfee; Tech. Rpt. Ctr., Rm 2A-165B/E. Oberer
424. The Boeing Company, P.O. Box 3707, Seattle, Washington 98124, ATTN: G. Keister
425. EG&G, Inc., Santa Barbara Division, P.O. Box 98, 130 Robin Hill Road, Goleta, California 93017, ATTN: Technical Library
426. Fairchild, Space & Defensive Systems Division, 30 Space Park, Paramus, New Jersey 07652, ATTN: J. D. O'Neill
427. General Electric Company, TEMPO-Center for Advanced Studies, 816 State Street, Santa Barbara, California 93102, ATTN: DNA Information and Analysis Center
428. Gulf General Atomic, Inc., P.O. Box 1111, San Diego, California 92112, ATTN: Chief, Tech. Information Services For – Dr. V. A. J. Van Lint
429. Institute for Defense Analysis, 400 Army-Navy Drive, Arlington, Virginia 22202, ATTN: Technical Information Office
430. IIT Research Institute, 10 West 35th Street, Chicago, Illinois 60616, ATTN: Library
431. ION Physics Corporation, South Bedford Street, Burlington, Mass. 01803
432. Kaman Sciences Corporation, Kaman Nuclear Division, 1700 Garden of the Gods Road, Colorado Springs, Colorado 80907, ATTN: Dr. Frank Shelton
433. LFE, Inc., Trapelo/West Division, 2030 Wright Avenue, Richmond, California 94804
434. Lockheed Missiles and Space Company, A Division of Lockheed Aircraft Corporation, P.O. Box 504, Sunnyvale, California 94088, ATTN: Library
435–436. Lockheed Missiles and Space Co., 3251 Hanover St., Palo Alto, California, 94304, ATTN: Technical Library; Dr. Lloyd Chase
437. Lovelace Foundation for Medical Education and Research, 5200 Gibson Blvd., S.E., Albuquerque, New Mexico 87108, ATTN: Dr. Clayton White
438. Mathematical Applications Group, Inc., 180 S. Broadway, White Plains, New York 10605
439. MITRE Corporation, Route 62 and Middlesex Turnpike, Bedford, Massachusetts 01730, ATTN: Technical Library
440. North American Rockwell Corp., Autonetics Division, 3370 Miraloma Avenue, Anaheim, California 92803, ATTN: Technical Library
441. Physics International Company, 2700 Merced Street, San Leandro, California 94577, ATTN: Technical Library
442–445. Radiation Research Associates, Inc., 3550 Hulen Street, Fort Worth, Texas 76107 (N. M. Schaeffer, M. B. Wells, L. G. Mooney, R. French)
446–450. R & D Associates, P.O. Box 3580, Santa Monica, California 90403, ATTN: Mr. William R. Graham; Mr. William Wright; Dr. William Karzas; Dr. Harold Brode; Dr. Robert Lelevier
451. Stanford Research Institute, 333 Ravenswood Avenue, Menlo Park, California 94025, ATTN: Library
452. System Development Corporation, 2500 Colorado Avenue, Santa Monica, California 90406, ATTN: Technical Library
453. Systems, Science and Software, Inc., P.O. Box 1620, La Jolla, California 92037, ATTN: Dr. L. Schalit
454. Technical Operations, Inc., South Avenue, Burlington, Massachusetts 01804, ATTN: Dr. Eric Clarke
455. Texas Nuclear Corporation, Box 9267, Allendale Station, Austin, Texas 78756
456. TRW Systems Group, San Bernardino Operations, P.O. Box 1310, San Bernardino, California 92402, ATTN: Library
457. TRW Systems Group, One Space Park, Redondo Beach, California 90278, ATTN: STL Technical Library
458. United Nuclear Corporation, Grasslands Road, Route 100C, Elmsford, New York 10523
459. Westinghouse Electric Corporation, Defense and Space Center, P.O. Box 1693, Baltimore, Maryland 21203, ATTN: Dr. Pan/Eng. Dir. of Sci. and Tech.
460. Dr. M. H. Kalos, Courant Institute of Mathematical Sciences, 251 Mercer Street, New York, New York 10012
461. Dr. Reed Johnson, Department of Nuclear Engineering, University of Virginia, Charlottesville, Virginia 22901
462. Physics International Company, 2700 Merced Street, San Leandro, California 94577, ATTN: Dr. W. E. Kreger

463. Department of the Army, USAMC Main Battle Tank Engineering Agency, 28150 DeQuindre, Warren, Michigan 48092
464. McDonnell Douglas Corp., 3000 Ocean Park Blvd., Santa Monica, California 90406
465. McDonnell Douglas Corp., 5301 Bolsa Ave., Huntington Beach, California 92647, ATTN: A3-328-Technical Library Services
466. Science Applications Inc., P.O. Box 2351, La Jolla, California 92037, ATTN: Dr. S. Robert Beyster